

**PEPTIDE OR PEPTIDOMIMETIC RANDOMIZATION OF
PRIVILEGED STRUCTURES: A NOVEL GREEN
MULTICOMPONENT SYNTHETIC ROUTES
TO DRUG LEADS**

*Thesis submitted
to the University of Calicut for the
award of the degree of*

DOCTOR OF PHILOSOPHY IN CHEMISTRY

RAJEENA PATHOOR



**DEPARTMENT OF CHEMISTRY
UNIVERSITY OF CALICUT
KERALA**

FEBRUARY 2018

DECLARATION

I, Rajeena Pathoor, hereby declare that the thesis entitled “**PEPTIDE OR PEPTIDOMIMETIC RANDOMIZATION OF PRIVILEGED STRUCTURES: A NOVEL GREEN MULTICOMPONENT SYNTHETIC ROUTES TO DRUG LEADS**” is the report of the original research work carried out by me under the supervision of Dr. D. Bahulayan, Professor, Department of Chemistry, University of Calicut for the award of the degree of Doctor of Philosophy in Chemistry of the University of Calicut and further that this thesis contains no material previously submitted for a degree, diploma, associateship, fellowship or other similar title of any other University or Society.

University of Calicut
February 2018

Rajeena Pathoor

ACKNOWLEDGEMENTS

It's has been a long journey up to finishing this thesis for my PhD, which would not have been as feasible and doable as it seems now without the help and support of so many individuals and institutions that have been instrumental in the completion of it. It is an irony that you begin to formally acknowledge those individuals only at the end of your work, though one has to depend on them throughout. It is very difficult to mention all those names here, as such an exercise will end up missing so many other names; but mentioning some of them here is not just necessary but a pleasure. And hence, "now" is the time to express my pleasure and privilege in acknowledging the roles of those individuals without whose help this thesis would not have been this thesis.

First and foremost, I praise and thank Allah, the Almighty, for showering His blessings on me throughout which have helped me immensely, particularly during the difficult times of my research.

It's a genuine pleasure to express my deep sense of gratitude to my mentor and research supervisor Prof. D. Bahulayan, Department of Chemistry, University of Calicut, for his guidance and support in shaping this work to what it is now. His supervision and timely advice as well as his professional approach to research have helped me greatly to complete my thesis. Sir, you have taught me that nothing can substitute hard work; I can only thank you enough by working harder.

I am also grateful to Dr. P. Raveendran, the Head, Department of Chemistry, University of Calicut; and former heads of the department, Dr. K. Muraleedharan and Dr. V.M. Abdul Mujeeb, for providing me the necessary facilities. I also acknowledge the support provided by Dr. K. Mulareedharan, Director, CSIF, for my research.

Any prolonged research work will naturally become dry and dull, if the research environment does not provide you the additional impetus in the form of friends and co-researchers. Thanking them for the help they have rendered in various ways is not just a duty but a pleasure. My heartfelt gratitude is extended to all my dear friends, especially from my lab, P. Jithin Raj, T. Jency Mohan, Soumya T. V, Thasnim, P Shyam Shankar, E. Shamsiya, Muhammed Salim K. M, as well as to other lab members, especially Vijisha and Shameera.

I cannot thank enough those whose help has come from outside the University—Dr. Arun kumar, Dr. Lakshmi, Jithin, Divya and Dijo Prasannan (NIT) and Dr.K.Vimala (Periyar University).

I also take this opportunity to thank all other teachers and non-teaching staff of the Department of Chemistry, University of Calicut, for their valuable help and support.

Above all, I am grateful to my parents—especially my mother who had to raise us all since our father left us—and my husband, and my brother Jamsheer, as well as my in-laws, for their kindness and support throughout. I fondly remember the pleasant moments and laughter provided by my beloved daughter Isha (sorry molu for not being able to pay as much attention to your needs as you might have expected from me), which have enabled me immensely to forget the otherwise difficult times and worries of the research work. I also extend my sincere gratitude to other family members for their constant support and love throughout. Without the prayers and encouragement of this family, I could not have completed this thesis.

Finally, I acknowledge the financial assistance provided by the CSIR throughout my research .

Rajeena Pathoor

To
Allah, the Almighty

PREFACE

Privileged structures are molecular scaffolds with trustful binding properties, so that a single scaffold can impart potent and selective ligands for a range of diverse biological targets through their functional group modification. Numerous heterocycles have been identified and reinvestigated as privileged scaffolds, of which Indole ring is a prominent privileged scaffold and were reported in various bioactive molecular synthesis. The literature reveals that the indole functionalized scaffolds can provide ligands for diverse receptors and can be able to interact with unrelated and undruggable targets. Instead of indole scaffold Coumarins, dihydropyrimidinones another important privileged scaffolds, hence we tried to functionalise indole heterocycle with Coumarin and Dihydropyrimidinone via a novel-green multicomponent synthetic strategy. Also we tried to evaluate the anticancer activity and photophysical activities. The Click reaction yields a 1,2,3-triazole which can mimic the peptide bond and also mimic the natural processes, since nature generates substances by joining small molecular units.

The thesis has been divided into nine chapters. The first chapter presents an overview of the importance of indole derivatives in drug discovery and their biological and photophysical applications. Instead of indole scaffold, coumarin and dihydropyrimidinone are discussed with their biological properties. Various aspects of these three privileged structures has been summarized in this chapter, including the applications of new synthetic methodologies for their

functionalization and the evaluation of biological properties. The chapter 2 discusses the chemistry and synthesis of a new series of indole-triazole-peptidomimetics based on Click with MCR synthetic strategy. These synthesised peptidomimetics are resembles to recently reported indoline-2- carboxamide derivative as potential curing agent for stage 1 human African trypanosomiasis (HAT). Here we introduced Ugi azides as the pairable functionality with alkyne functionalized indole derivatives. The 3rd chapter is the continuation of the second chapter to evaluate the molecular docking interactions and the cytotoxicity study against the human breast cancer cell lines.

Chapter 4 is the peptidomimetic modification with another privileged scaffold Coumarin to the indole derivative. This coumarin functionalized pairable functionality was synthesised via alternate Mannich reaction protocol. The 5th chapter is the continuation of the second chapter to evaluate the molecular docking interactions and the cytotoxicity study against the human breast cancer cell lines. Chapter 6 is the synthesis of indole-pyrimidinone peptidomimetics, here the dihydropyrimidinones were synthesised via biginali reaction. These synthesised peptidomimetics were evaluated for their molecular docking and cytotoxicity.

Chapter 7 presents the progress of the work from linear peptidomimetics to indole based macrocyclic peptidomimetics using an intra molecular MCR-Click strategy. A discussion on the biological properties of the molecules as well as the molecular docking with CDK2 enzyme was also presented. Chapter 8 presents the photophysical studies of the all the synthesised peptidomimetics and

discussed their stoke shift values. Besides photophysical study, the chemosensing behavior of indole-coumarine peptidomimetics was also presented in chapter 8.

Chapter 9 presents the conclusion and future aspects of the work presented in the thesis. As highlighted in chapters 2-8, this study has made significant advancement in the chemistry, chemical biology and photophysics of large number of indole based peptidomimetics. However, further in-depth study based on computational techniques and in vitro and in vivo biological assay is necessary to push this field further ahead to achieve the goal of cost effective and green synthesis of therapeutic agents.

CONTENTS

	<i>Page No</i>
Chapter 1	1-49
Indole derivatives as a promising scaffold in drug discovery.	
Chapter 2	50-125
The synthesis of Indole-Triazole Carboxamide peptidomimetics via MCR-Click strategy.	
Chapter 3	126-141
Computational and Biological Evaluation of Indole-Triazole Carboxamide peptidomimetics against CDK 2 proteins and human breast cancer cell line MCF-7.	
Chapter 4	142-186
Structure alterations of Indole-Triazole-Carboxamides with Coumarin moieties: Synthesis of a new series of Indole-Triazole-Coumarin hybride peptidomimetics.	
Chapter 5	187-202
Biological evaluation of Indole-Triazole-Coumarin hybride peptidomimetics	
Chapter 6	203-237
Structure alterations of Indole-Triazole-Carboxamides with a Pyrimidine sub unit: Synthesis and cytotoxicity evaluation of a new series of Indole-Triazole-Pyrimidinone Hybride.	
Chapter 7	238-274
Structure alteration of Indole-Triazole-Carboxamides via Macrocyclization: Synthesis and <i>in vitro</i> cytotoxicity evaluation of Indole-Triazole-Amide macrocycles.	
Chapter 8	275-293
Photophysical and chemosensing behavior of Indole peptidomimetics	
Chapter 9	294-302
Conclusion and Future Perspectives	
Research Publication	

CHAPTER 1

**Indole derivatives as a promising scaffold
in drug discovery**

Contents

1.1. Indole as privileged scaffold.....	1
1.2. Coumarin as a privileged scaffold.....	30
1.3. Pyrimidinone as a privileged scaffold.....	31
1.4. Peptides and Peptidomimetics as Drug Leads	32
1.5. Strategies for the synthesis of linear and cyclic peptidomimetics	34
1.5. Conclusion	41
References	42

1.1. Indole as privileged scaffold

Privileged structures are molecular scaffolds with trustful biological properties and can provide potent and selective ligands for a range of diverse biological targets through their functional group modification. By definition it is a “single molecular framework with the ability to provide ligands for diverse receptors”.¹ After benzodiazepine, a large number of privileged scaffolds such as purine,² indole,³ benzimidazoles,⁴ benzofurans,⁵ coumarins,⁶ and dihydropyrimidinones⁷ have been reported of which Indole scaffolds are more prominent with frequent recurring in various therapeutic systems.

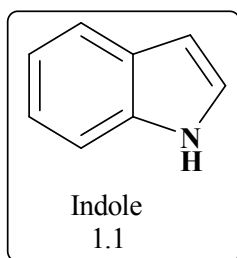


Fig. 1.1. Structure of indole

Indole chemistry began with the study of the indigo dye. The indole was first isolated through the treatment of the indigo dye with oleum and therefore the name indole is a portmanteau of the words *indigo* and *oleum*. Indole is a benzopyrrole ring system in which the benzene and pyrrole rings are merged through the 2- and 3-positions of the pyrrole nucleus. Indole is wide spread in the natural environment and can be produced by a variety of bacteria. The amino acid tryptophan is an indole derivative and the precursor of the neurotransmitter serotonin.⁸ Several natural alkaloids with indole as

basic ring are therapeutically active. Indole is solid and smells the odour of manure, but when highly diluted, it smells like jasmine.

1.1.1. Chemical and Biological Importance

Indole is the parent substance of a large number of important compounds that occur in nature. Tryptophan (2-amino-3-(3'-indolyl) propionic acid) **1.2**, is one of the naturally occurring essential amino acids. In higher plants this tryptophan degrades into heteroauxin (indole-3-acetic acid)**1.3**, a plant hormone. Serotonin **1.4**, is an indole derivative with a hydroxyl group on the benzene ring which is a vasoconstrictor hormone that plays an important role in conducting impulses to the brain.⁹ Bufotenine **1.5** and psilocybin **1.6**, are indole derivatives that are found in the skins of toads, toxic mushrooms, and West Indian snuff.¹⁰

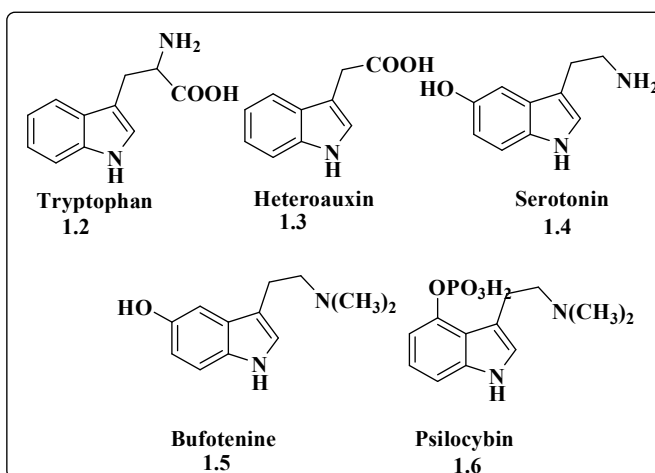


Fig. 1.2. Derivatives of indoles

Some indole alkaloids exert considerable pharmacological activity. Of the clinically useful alkaloids, three groups are notable: (a)

the ergot alkaloids—ergometrine with its direct action on the contraction of uterine muscle (b) the rauwolfia alkaloids, which is specifically reserpine, and is used as the forerunner of the tranquillisers; (c) the dimeric anti-leukemic alkaloids of catharanthus are vinblastine and vincristine. Tryptophan is an essential amino acid and one of the constituent of most proteins.¹¹

The study and classification of 5-hydroxy-tryptamine receptors resulted in the design and synthesis of sumatriptan **1.7**¹² For the treatment of migraine and ondansetron **1.8**, for the suppression of the nausea and vomiting caused by cancer chemotherapy and radiotherapy¹³.

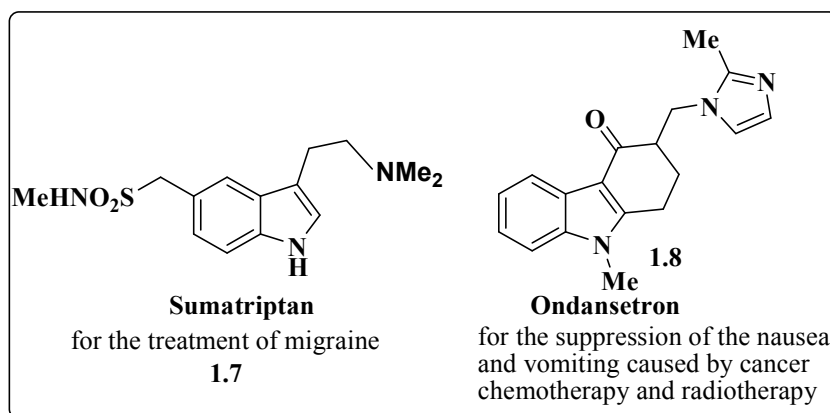


Fig. 1.3. Structure of Indoles used in Chemotherapy

1.1.2. Biological activities of synthetic molecules containing indole nucleus.

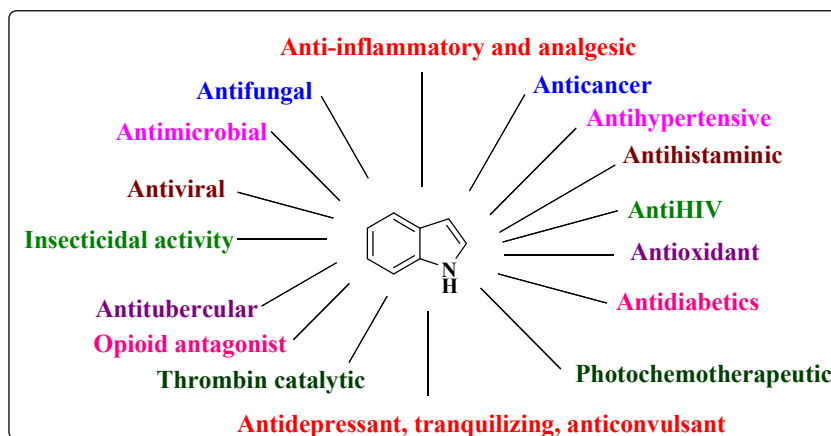


Fig. 1.4. Graphical representation of the biological activity of indole derivatives

1.1.2.1. Anti-inflammatory and analgesic activity.

Inflammation is a complex biological response of body tissues due to the hurtful stimuli such as pathogens, irritants and damaged cells. The literature survey has showed that only a few indole based natural anti-inflammatory agents have been reported. A series of bis-indole derivatives were synthesized and evaluated for the anti-inflammatory activity by Singh *et al.* From the study it was confirmed that the bis-indole derivative **1.11**, was the most active compound (53.3% at 50 mg/kg dose) of the synthesized series, which showed higher percent of inhibition of oedema, lower ulcerogenic liability and acute toxicity than phenyl butazone (38.8% at 50 mg/kg dose).¹⁴

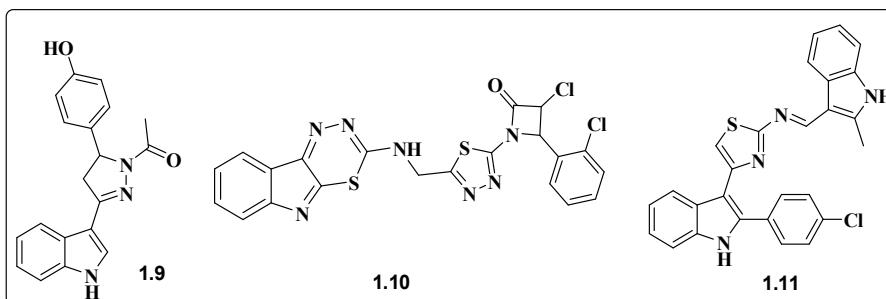


Fig. 1.5. Bis Indole derivatives with potent anti-inflammatory activity.

Similarly, indole oximes, exhibit analgesic and anti-inflammatory activities. Indole oxime **1.12** was found to be the most active analgesic and anti-inflammatory agent.¹⁵

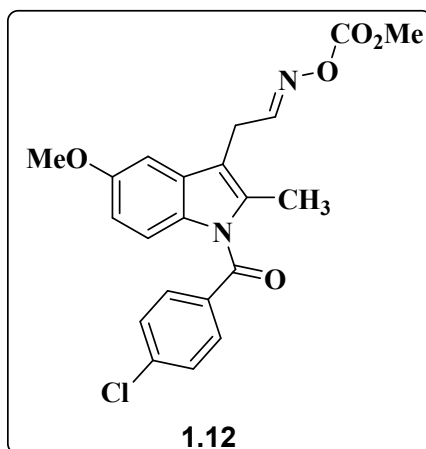


Fig.1.6. Indole oxime as anti-inflammatory agent.

Indole-3-acetic acids were synthesized and evaluated for their *in vivo* anti-inflammatory activity. It was reported that the compound 1,2-disubstituted-5-methoxy-indole/benz(g)indole-3-acetic acid **1.13**, showed significant *vivo* anti-inflammatory activity.¹⁶

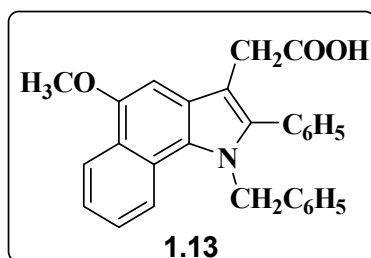


Fig. 1.7. 1, 2-disubstituted-5-methoxy-indole/benz(g) Indole-3-acetic acid

Indole triazole derivatives have been reported as potent analgesic and anti-inflammatory agent. The compounds 2-Phenyl-3-(20-carboxyphenyliminomethyl)- indole **1.14** and 2-phenyl 1-3-(20-carboxy phenyl imino methyl) -indol-1-acetic acid **1.15** are found to be most potent.¹⁷

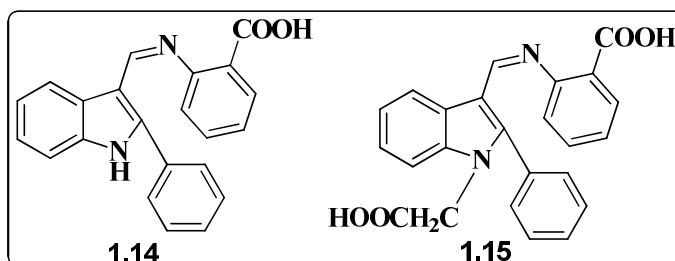


Fig.1.8.2 -Phenyl-3-(20- carboxy phenyl imino methyl) and indole and 2-phenyl-3-(20-carboxy phenyl imino methyl)-indol-1-acetic acid

1.1.2.2. Anti-microbial and Anti-fungal activity

Microbial infections are due to the activity of a range of microbes, including bacteria and fungi, such as, enterococcus, aspidosperma, plasmodium, staphylococcus and seudomonas. Resisting such microbes has become a global concern and structurally novel molecules with new mode of action are required for the

treatment of bacterial infections. Some substituted 3-(aryl) and 3-(heteroaryl) indoles were synthesized by Hiari et al and were evaluated for antibacterial activity. Of the synthesized compounds, the most active compound was 3-(4-trifluoromethyl-2-nitrophenyl) indole **1.16** exhibiting MIC $\sim 7 \mu\text{g}/\text{cm}^3$ against *Escherichia coli* and *Staphylococcus aureus*.¹⁸

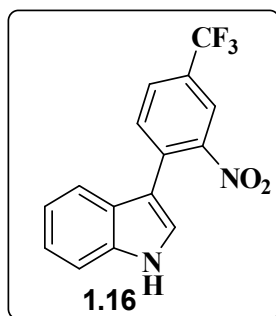


Fig. 1.9. 3-(4-trifluoromethyl-2-nitrophenyl) indole

Substituted azetidonyl and thiazolidinonyl-1,3,4-thiadiazino [6,5-b]indoles were reported as promising antimicrobial agents. Of the synthesized compounds the compounds **1.17** and **1.18** were found to exhibit most inhibitory effect against *E. coli* and *S. aureus*.¹⁹

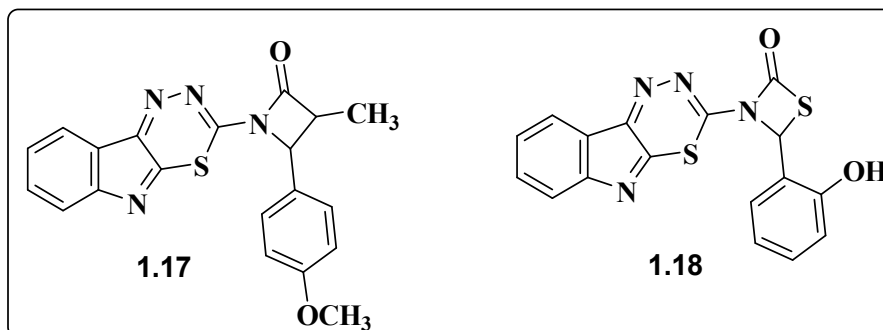


Fig. 1.10. Substituted azetidonyl and thiazolidinonyl- 1,3,4-thiadiazino[6,5-b]indoles

1.1.2.3. Anticancer activity

Cancer, otherwise known as malignancy, is an extraordinary growth of the cells. There are different varieties of cancer such as breast cancer skin cancer, lung cancer, colon cancer, prostate cancer and lymphoma. Breast cancer is commonly found in women and is one of the causes for the increased female death rate.²⁰ The high mortality rate is also an indication of the limited efficacy of the various cancer treatments available now, such as radiation, chemotherapy and surgery.²¹ Increasing interest has been shown by scientists and researchers to invent more effective medicine for curing the disease without side effects.²²

Indole has become, owing to its excellent cytotoxic activities, an ideal choice for the development of new anticancer drugs. Hong et al. synthesized a series of various tricyclic and tetracyclic indoles and evaluated their anticancer activity where the compounds **1.19**, **1.20**, **1.21** and **1.22** were found to exhibit highest in vitro activity against human nasopharyngeal carcinoma (HONE-1) and gastric adenocarcinoma (NUGC-3) cell lines.²³

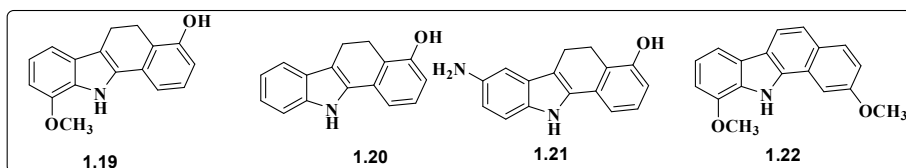


Fig. 1.11. Tricyclic and tetracyclic indoles with potent anti-cancer activity.

Garcia and coworkers reported pyrrolo [2,3-e] indole derivatives and evaluated the in vitro cytotoxic activity. The compound **1.23** was found to be the potent one in PC-3 (prostate) cell line.²⁴

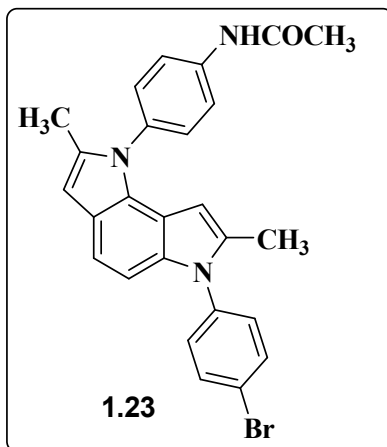


Fig. 1.12. Pyrrolo [2,3-e] indole derivatives as potent one in PC-3 (prostate) cell line.

A series of halogenated indole-3-acetic acids were reported for targeted cancer therapy and of the synthesized compounds, the halogenated indole-3-acetic acid **1.24** was found to possess highest cytotoxicity suitable for targeted cancer therapy.²⁵

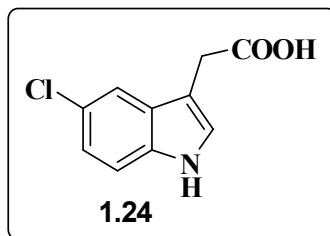


Fig.1.13.Halogenated indole-3-acetic acids with highest cytotoxicity

The synthesis and inhibitory activity of the heteroaryl indoles on the inhibition of human tumor cell lines, MCF-7 (breast

adenocarcinoma), NCI-H460 (non-small cell lung cancer), and SF-268 (CNS cancer) were reported by Queiroz et al. From the study it was observed that methyl 3-(dibenzothien-4-yl) indole-2-carboxylate **1.25** had the most potent growth inhibitory activity in all the tumour cell lines tested (with GI50 values ranging from 1 to 17 μ M).²⁶

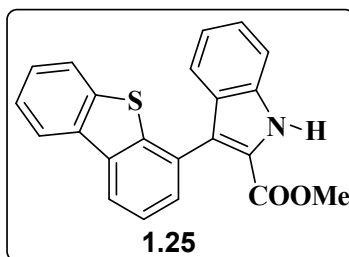


Fig. 1.14. Hetero-aryl indoles as most potent growth inhibitory activity in all the tumor cell lines tested.

Enzastaurin **1.26**, is an indole based drug, which is currently under clinical evaluation, for the treatment of lymphoma, breast cancer, prostate cancer, NSCLC, leukemia, colorectal cancer, ovarian cancer, renal cell carcinoma and pancreatic cancer.²⁷

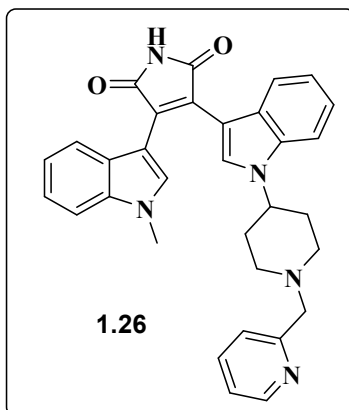


Fig. 15. Enzastaurin

Sotrastaurin **1.27**, was developed by Novartis and has been evaluated for effectiveness in the treatment of lymphocytic leukemia, lymphoma, melanoma and kidney transplantation.²⁸

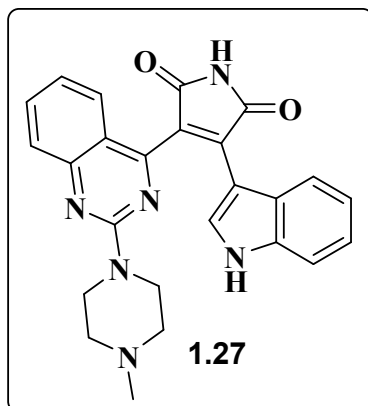


Fig. 16. Sotrastaurin

Similarly, Agouron pharmaceuticals reported Rucaparib **1.28**, which is an investigational candidate for advanced solid tumor, breast and ovarian cancer with BRCA1 and BRCA2 mutation.²⁹

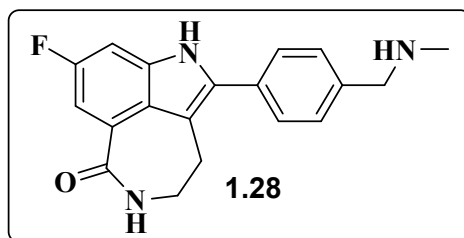


Fig. 17. Rucaparib

1.1.2.4. Antiviral Activity

Viruses are the main agents responsible for various disease classes like influenza (seasonal, pandemic), smallpox, dengue, chikungunya etc. they are also involved in chronic diseases in the form of human immunodeficiency virus (HIV), hepatitis B and C viruses (HBV and HCV, respectively), coronaviruses (Middle east respiratory Syndrome), MERS; severe acute respiratory syndrome, (SARS), viral hemorrhagic fevers (Ebola) etc. Most anti-virals are used for specific viral infections, while a broad-spectrum antiviral is effective against a wide range of viruses. Unlike most antibiotics, antiviral drugs do not destroy their target pathogen; instead they inhibit their development. The literature on this has revealed that the indole scaffolds, by virtue of their high affinity and specificity to bind with different molecular targets, are considered as efficient antiviral agents.

Arbidol (Umifenovir) **1. 29**, exhibits broad-spectrum antiviral activity against a number of enveloped and non-enveloped viruses by inhibiting the fusion of viral capsid with the host cell membrane. The drug possesses high potency against influenza A, B and C viruses, respiratory syncytial virus, hepatitis B virus, hepatitis C virus, human rhinovirus type 14, coxsackie B3 virus, adenovirus type 7.³⁰ Delavirdine (Rescriptor) **1.30**, acts as non-nucleoside reverse transcriptase inhibitor (NNRTI) and is used for the treatment of human immunodeficiency virus (HIV). It is also an inhibitor of cytochrome P450 enzyme CYP3A4 and interacts with many medications.³¹ Ateviridine (U-87201E) **1.31**, is a bis-heteroaryl piperazine with in-vitro activity against human immunodeficiency virus (HIV-1).³² GSK2248761 (Fosdevirine) is another NNRTI that is under Phase 2 clinical evaluation. This compound has been reported to have sub

nano-molar activity against NNRTI resistant mutant HIV.³³ Golotimod (SCV-07) **1.32**, is an orally bio-available synthetic peptide containing the amino acids D-glutamine and L-tryptophan connected by a gamma-glutamyl linkage with potential immune-stimulating, antimicrobial and anti-neoplastic activities.³⁴ Panobinostat (LBH589) **1.33**, is a non-selective histone deacetylase inhibitor (HDACinhibitor) for treatment of Multiple Myeloma (Phase III) and Acute Myeloid Leukemia (Phase II).³⁵

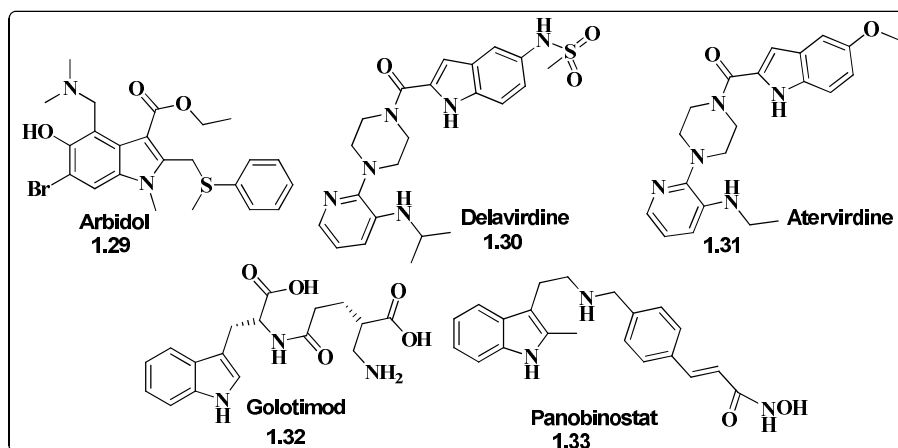


Fig.18. Some Indole derived antiviral compounds

1.1.3. Indole Ring Containing Important Marketed Drug Molecules

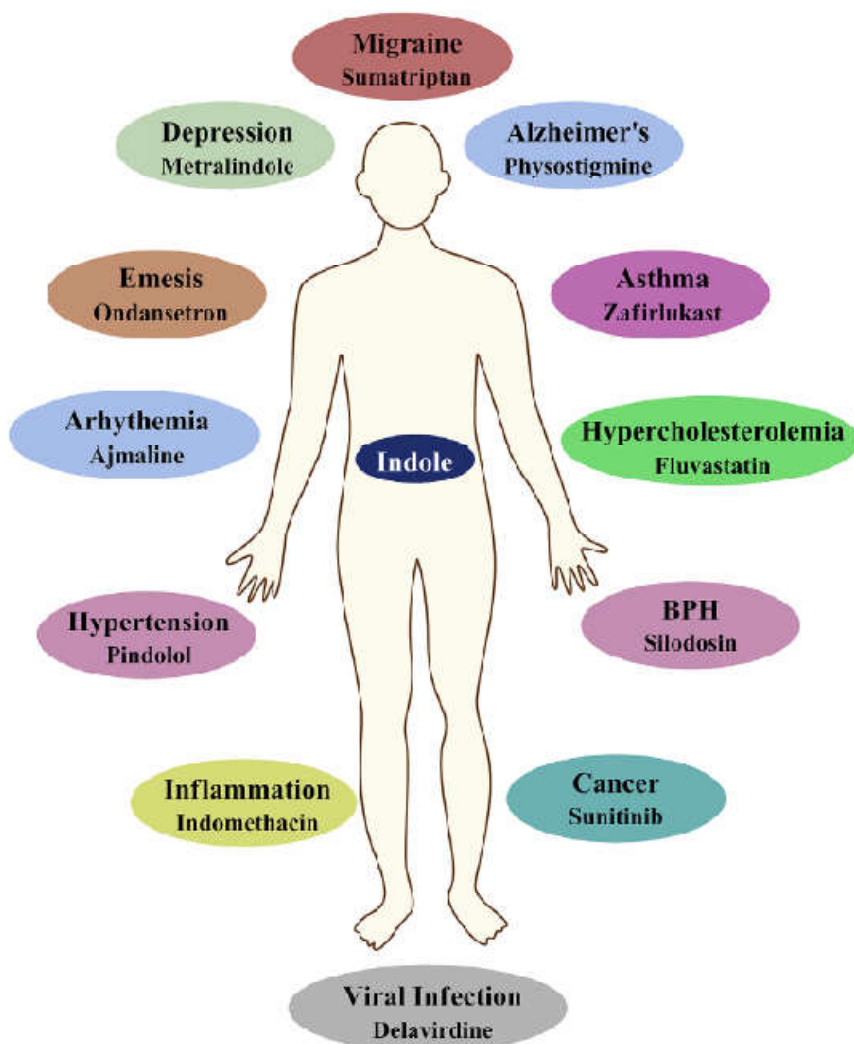


Fig.1.19. Indole possessing polypharmacological activity

The list of important indole ring-containing marketed drugs with their biological activities are listed in table 1.2.

Table1.2. Indole ring containing drug molecules

Drug	Application	Drug	Application	Drug	Application
Vincristine	Anticancer	Vincamine	Vasodilator	Roxindole	Schizophrenia
Vinblastine	Anticancer	Reserpine	Antihypertensive	Delavirdine	Anti-HIV
Vinorelbine	Anticancer	Peridopril	Antihypertensive	Atevirdine	Anti-HIV
Vindesine	Anticancer	Pindolol	Antihypertensive	Arbidol	Antiviral
Mitraphylline	Anticancer	Binedaline	Antidepressant	Zafirlukast	Anti-Asthmatic
Cediranbin	Anticancer	Amedalin	Antidepressant	Bucindolol	b-Blockers
Panobinostat	Anti-leukemic	Oxypertine	Antipsychotic	Pericine	Opioid agonist
Apaziqone	Anticancer	Siramesine	Antidepressant	Mitragynine	Opioid agonist
Tropisetron	Antiemetic	Indalpine	Antidepressant	Pravadoline	Analgesic
Doleasetron	Antiemetic	Yohimbine	Sexual disorder	Bufotenidine	Toxin
Oglufanide	Immunomodulatory	Indomethacine	Anti-inflammatory	Proamanullin	Toxin

Recently, the indole ring-containing compound yohimbine (17 α -Hydroxy-yohimban-16 α -carboxylic acid methyl ester) **1.34**, has been proven to be effective for the treatment of sexual dysfunction.³⁶ Yohimbine was also explored as a remedy for type-2 diabetes in animal and human models, carrying polymorphisms of the α 2A-adrenergic receptor gene.³⁷

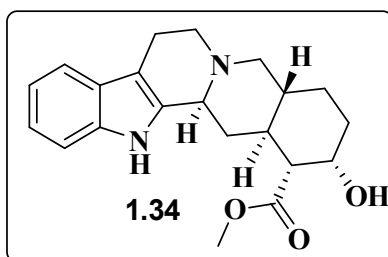


Fig. 1.20. Yohimbine: Drug for male impotency

Delavirdine **1.35**, an inhibitor of cytochrome P450 isozyme CYP3A4, is also a drug with an indole ring developed for the treatment of HIV type 1.³⁸

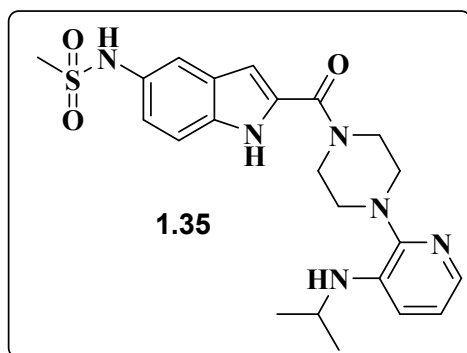


Fig. 1.21.Delavirdine:anti-HIV drug

Many existing pharmaceuticals can be replaced by indole based pharmaceuticals with enhanced biological profile. Apaziquone **1.36**, is an indole quinone, which is a chemical analog and prodrug of the older mitomycin C. Apaziquone is converted to active metabolites by intracellular reductases by a hypoxic environment, such as those on the inner surface of the urinary bladder.³⁹Oxypertine **1.37**, is an indole derivative similar to molindone which is an anti-psychotic and anti-depressant used in the treatment of schizophrenia.⁴⁰One of the most important inhibitors of angiotensin converting enzyme is perindopril. This enzyme is used in patients with hypertension, diabetes mellitus type 2, coronary heart disease and chronic heart failure.⁴¹

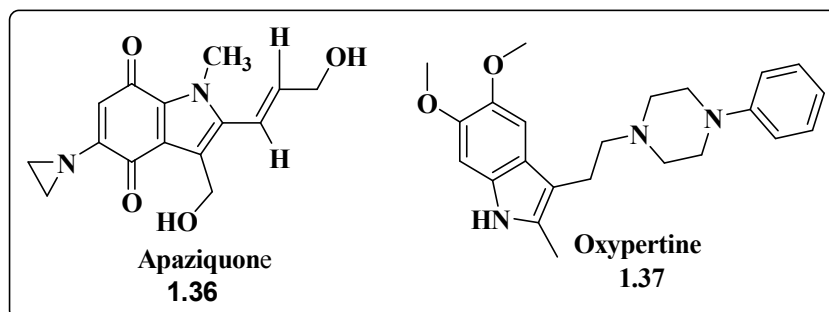


Fig. 1.22. Apaziquone as anticancer and Oxypertine as antipsychotic

Mitraphylline **1.38**, is an oxiindole derivative, and the current research on mitraphylline focuses on its anti-proliferative effects and its *in-vivo* efficacy to induce apoptosis in human breast cancer, sarcoma and leukemia cell lines.⁴² Panobinostat **1.39**, is also an indole based drug for the treatment of various cancers.⁴³ Amedalin **1.40** is one of the antidepressant, synthesized in the early 1970s, it is a selective norepinephrine reuptake inhibitor, but was never marketed. Pinodolol **1.41**, is added to standard antidepressant therapy as a beta blocker, if the patient fails to respond to the standard therapy alone.⁴⁴ Oglufanide **1.42** its immune modulatory properties, have been extensively studied as an agent that enhances the immune function. This compound is currently undergoing clinical trials in patients infected with the hepatitis C virus.⁴⁵

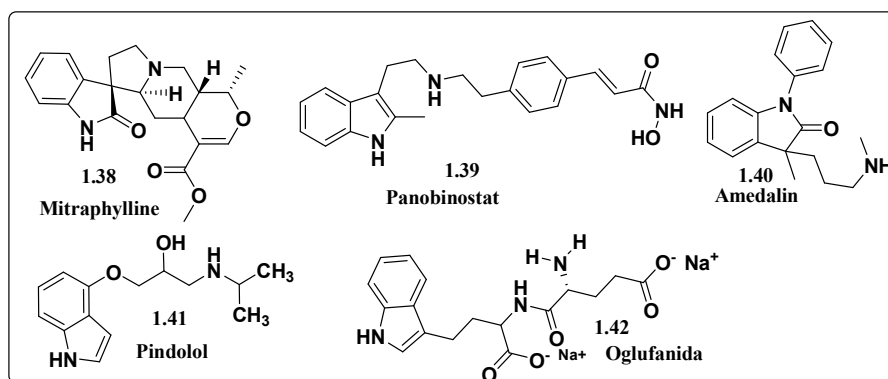


Fig. 1.23. Mitraphylline as anticancer, panobinostat as antileukemic, amedalin as antidepressant, pindolol as antihypertensive, oglufanide as Immunomodulator.

Roxindole **1.43**, was mainly developed for the treatment of schizophrenia, but it was unexpectedly found to produce potent

and rapid anti-depressant and anxiolytic effects. It has also been investigated as a therapeutic for Parkinson's disease and prolactinoma.⁴⁶ Tropisetron **1.44**, can work as both a selective 5-HT₃ receptor antagonist and α 7-nicotinic receptor agonist.⁴⁷ Ateviridine **1.45** is a non-nucleoside reverse transcriptase inhibitor and it has been studied for the treatment of HIV.⁴⁸ Indometacin or indomethacin **1.46** is a non-steroidal anti-inflammatory drug (NSAID) commonly used for the medication to reduce fever, pain, stiffness, and swelling. It also shows an analgesic and antipyretic activity. However, the continuous usage is harmful to the upper gastrointestinal system of patients.⁴⁹ Zafirlukast **1.47**, is mainly used as an oral leukotriene receptor antagonist (LTRA) for the maintenance treatment of asthma. Pericine **1.48**, is an indole alkaloid used as traditional medicine throughout West Africa. Pericine shows an IC₅₀ of 0.6 μ mol, around 6 times more potent than codeine.⁵⁰ Pravadoline **1.49** was displayed unexpectedly strong analgesic effects, and it is the first compound from a novel class of cannabinoid agonists, the aminoalkylindoles.⁵¹ Vincamine **1.50**, is an indole alkaloid found in the *Vinca minor* and *Catharanthus roseus*, it can be synthesized in the lab from related alkaloids.⁵² Indole-3-methanol is used in breast cancer treatment and can be applied at each stage of the disease, because it inhibits the development of cancer cells. As the breast cancer cells grow in the presence of estrogen the only way to stop that process is to inhibit the production of estrogen. Indole-3-methanol has an ability to inhibit the secretion of estrogen in the glands up to 70%, as a result, the growth of cancer cells is stopped.⁵³

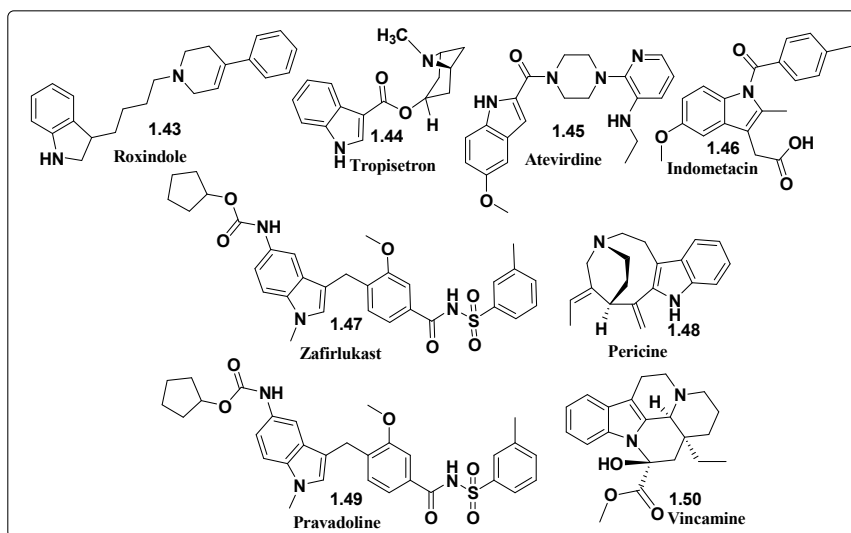


Fig. 1.24. Important indole ring-containing drugs

1.1.4. Indole scaffold as enzyme inhibitors

Enzyme inhibition is one of the most used approaches in drug discovery and many diseases can be successfully resolved by interrupting an enzymatic pathway intrinsically associated with the expressed physiopathology.⁵⁴ In recent years, the discovery of enzyme inhibitors has not only provided an increased number of potent therapeutically useful agents for the treatment of diseases, but has also significantly contributed to the better comprehension of the role of a determined biochemical pathway and a target enzymatic transformation in the development of some physiopathological states.⁵⁵

1.1.4.1. HMG-CoA Reductase Inhibitors

3-hydroxy-3-methylglutaryl-coenzyme A (HMG-CoA) reductase, is a key enzyme in cholesterol biosynthesis, which is responsible for conversion of HMG-CoA to mevalonate.⁵⁶ All statin drugs (a group of

cholesterol-lowering agents that have become some of the largest selling drugs worldwide) *e.g.* atorvastatin **1.51**, function through binding to the active site of HMG-CoA reductase and thus inhibiting the enzyme.

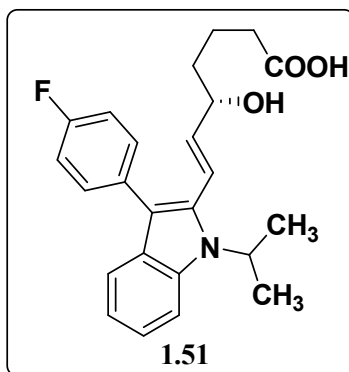


Fig. 1.25. Atorvastatin-HMG-CoA reductase inhibitor

1.1.4.2. Cyclooxygenase Inhibitors

Non-steroidal anti-inflammatory drugs (NSAIDs) are one of the most widely used groups of therapeutic agents for the treatment of pain, inflammation and fever associated to some diseases. Their pharmacological effect is by the common ability to inhibit the cyclooxygenase (COX), a key enzyme that catalyzes the conversion of arachidonic acid to prostaglandin H₂ (PGH₂), the immediate precursor to prostaglandins, thromboxane A₂ and prostacyclin.⁵⁷

Hu and co-workers showed that the indole ring proved to be an effective scaffold for the design of new COX-2 inhibitors, belonging to the terphenylic class. This study led to the discovery of two compounds, *i.e.* 2-phenyl-3-sulfonylphenyl-indole derivatives **1.52**,

which possess higher COX-2 inhibitory activity than celecoxib on cellular assay.⁵⁸

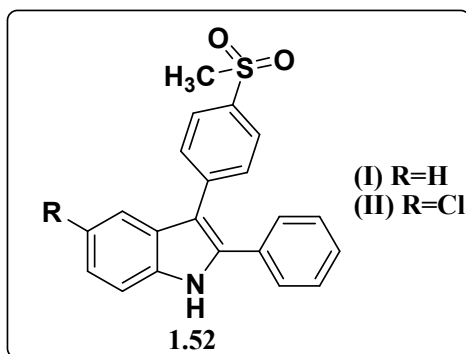


Fig. 1.26. Indole containing anti-inflammatory drug that acts as COX inhibitor

1.1.4.3. Phosphodiesterase (PDE) Inhibitors

PDEs are recognized as good drug targets due to the fact that there are so many different isoforms, with particular and prevalent tissue distributions. Currently, it is widely accepted that there are 11 different families of PDEs comprising of 21 different gene products.⁵⁹ Tadalafil **1.53**, a potent and selective indole containing PDE-5 inhibitor, was selected as clinical development candidate for the treatment of hypertension and congestive heart failure and in 2003 it was approved for the treatment of male erectile dysfunction in the U.S.⁶⁰

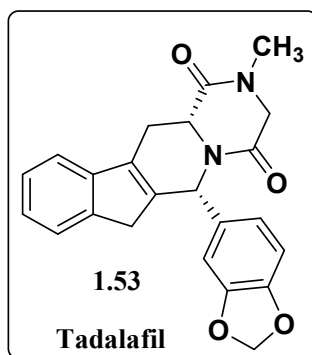


Fig.1.27. Structure of indole containing PDE inhibitor Tadalafil

1.1.4.4. CDK Inhibitors

Cyclin-dependent kinases (CDK/Cyclins) form a family of heterodimeric kinases that play prominent roles in regulation of cell cycle progression, transcription and other major biological processes including neuronal differentiation and metabolism. Constitutive or deregulated hyperactivity of these kinases due to amplification, overexpression or mutation of cyclins or CDK, contributes to proliferation of cancer cells, and aberrant activity of these kinases has been reported in a wide variety of human cancers.⁶¹ These kinases therefore constitute biomarkers of proliferation and attractive pharmacological targets for development of anticancer therapeutics. The structural features of several of these kinases have been elucidated and their molecular mechanisms of regulation characterized in depth, providing clues for development of drugs and inhibitors to disrupt their function. However, like most other kinases, they constitute a challenging class of therapeutic targets due to their highly conserved structural features and ATP-binding pocket. Notwithstanding, several

classes of inhibitors have been discovered from natural sources, and small molecule derivatives have been synthesized through rational, structure-guided approaches or through identifying it in high throughput screens.⁶² The larger part of these inhibitors target ATP pockets, but a growing number of peptides targeting protein/protein interfaces are being proposed, and a small number of compounds targeting allosteric sites have been reported. Structure of Indole based CDK2 inhibitors are shown in fig.1.28.

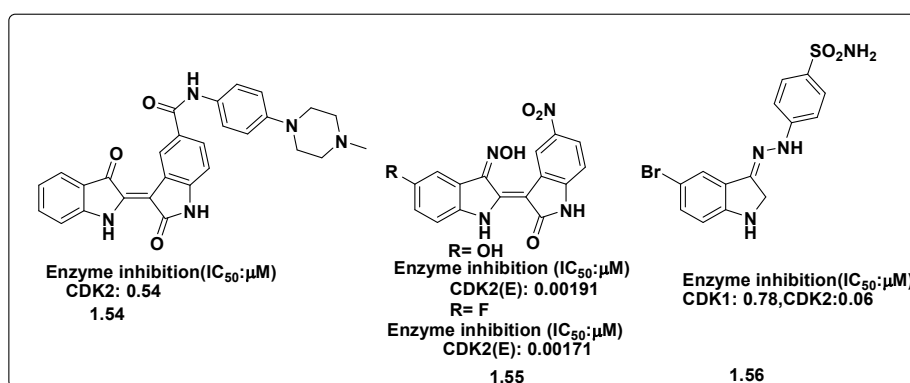


Fig. 1.28. Structure of indole based CDK2 inhibitors

1.1.5. Indole in Macrocycles

Macrocyclic compounds have unique physicochemical and topological properties that allow them to exhibit unusual biological properties.⁶³ These scaffolds are considered as privileged structures with the ring structures containing 12 or more atoms with a wide range of biological activities.⁶⁴ Compared to linear scaffolds, macrocycles are conformationally restricted molecules with high affinity, selectivity bioavailability towards biological targets.⁶⁵ Many methods have been reported in literature for the synthesis of macrocycles, such as

macrolactomization, macrolactonization, transition metal catalyzed cross coupling reactions and ring closing metathesis⁶⁶ Compared to these cyclization techniques, CuAAC reaction is unique for the efficient cyclization of peptide scaffolds in close to natural mode or for the triazole modification of a peptide macrocycle to the corresponding peptidomimetic version with increased biological profile.⁶⁷The indole heterocyclic system is found in several natural and synthetic macrocyclic structures and many of them possess excellent biological functions. Nowadays Indole-based macrocyclic systems attract increasing interest by virtue of their conformational and self-association properties, stacking interactions, spectroscopic features, cavity shape, and performance as ligands or ion-sensing scaffolds.

A series of macrocyclic compounds intended to display activity against blood coagulation Factor Xia were reported by Stephen Hanessian *et al.* This macrocyclic chloroindole **1.57**, displayed a promising activity against thrombin and good selectivity against APC.⁶⁸

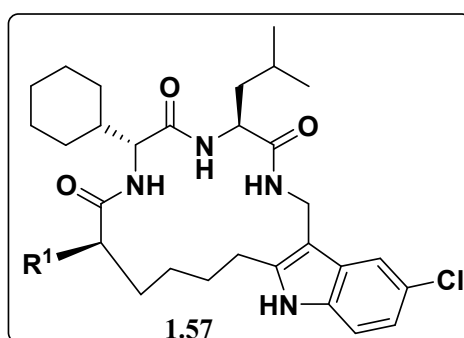


Fig. 1.29. Macrocyclic Chloroindole

Macrocyclic indoles **1.58**, were reported in which a tether connects a carboxylic acid bio-isostere in the 6-position to either the

indole nitrogen or 2-aryl position. These macrocycles afforded potent allosteric inhibitors of the HCV NS5b enzyme, reduction of sub-genomic HCV RNA replication in Huh-7 cells, and bioavailability in rats.⁶⁹

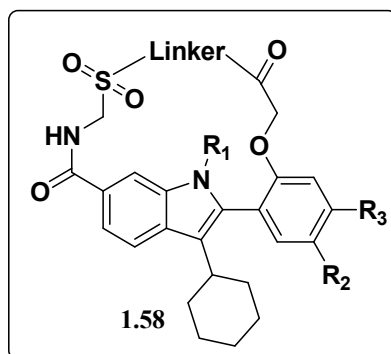


Fig. 1.30. Macrocyclic indole as potent allosteric inhibitor

An efficient method was developed for the synthesis of a novel series of macrocyclic bisindolyl maleimides **1.59**, containing linkers with multiple hetero-atoms. Potent inhibitors (single digit nanomolar IC₅₀) for PKC- β and GSK-3 β were pointed, and it was found that all these compounds showed good selectivity over PKC- α , - γ , - δ , - ϵ , and - ζ .⁷⁰

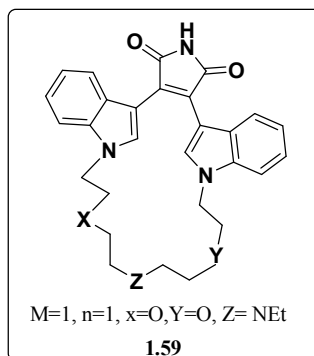


Fig. 1.31. Macrocyclic bisindolyl maleimide

5,6-dihydroxyindole macrocycle **1.60**, was obtained by biomimetic oxidative cross-coupling of the 2,2'-biindole and triindole. A putative reaction intermediate, 2-quinone, was detected and it was characterized by pulse radiolysis and DFT calculations.⁷¹

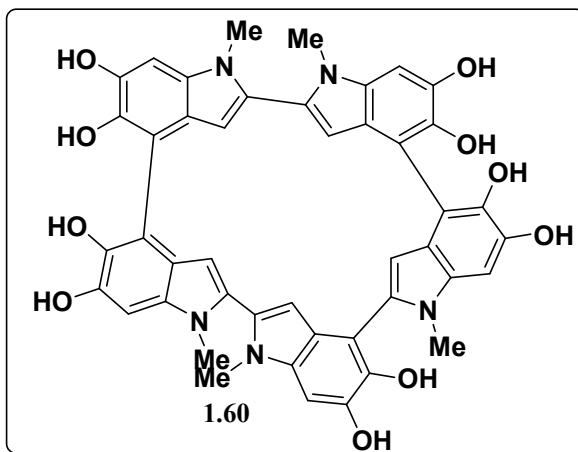


Fig.1. 32. 5,6-dihydroxyindole

A. Bertholet *et al* reported the synthesis of three constrained macrocyclic peptide analogues TMC-95A **1.61** which can be used as potential proteasome inhibitors. Here the main step of the synthesis involves a Ni(0)-mediated macrocyclization of tripeptides bearing halogenated aromatic side chains for the formation of the biaryl junction.⁷²

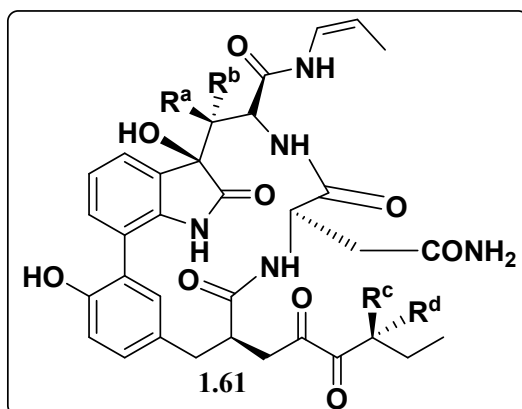


Fig. 1.33. Macrocyclic peptide analogues TMC-95A

A practical synthesis of novel tryptamine-based macrocycles **1.62**, using an Ugi 4-CR/click-cycloaddition sequential reaction protocol was reported by Luis D. Miranda *et al.* The main structural features of this macro-cyclic scaffolds are mainly the presence of a peptoid moiety, a 1,3-substituted indole nucleus, and a triazole ring. This protocol offered the opportunity to explore structural diversity by varying the isonitriles and carboxylic acids in the four-component set in the Ugi reaction.⁷³

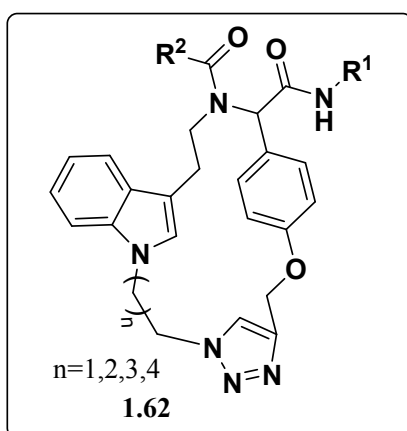


Fig. 1.34. tryptamine-based macrocycles

David StC. Black et al reported the formation of C-Amido-calix [3]indoles **1.63**, from 20- and 70-indolyglyoxylamides. A range of 20- and 70-indolyglyoxylic amides derived from 3-(40-chlorophenyl)-4,6-dimethoxy indole have been reduced to the corresponding alcohols, which on treatment with acid, underwent trimerization to give the calyx [3]indoles.⁷⁴

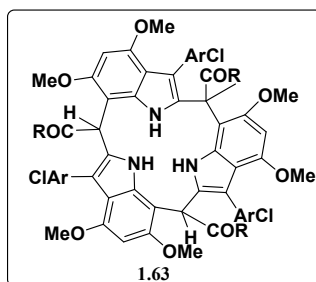


Fig. 1.35. C-Amidocalix[3]indoles

The bis-indoles were successfully formylated at C3 and the resulting dicarbaldehydes were combined with diamines to generate indole based imine macrocyclic systems **1.64**.⁷⁵

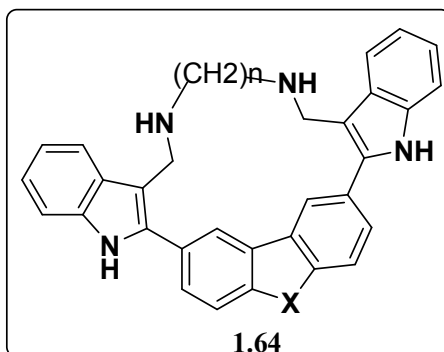


Fig.1.36. Indole based imine macrocyclic system

1.1.6. Photophysical properties of indole derivatives.

Fluorescent labeling of biologically active molecules is widely employed to study their functions within cells and whole organisms.⁷⁶ For the intracellular visualization and identification of the potential targets, the fluorescent tagging of a pharmacophore is very important in drug discovery.⁷⁷ Although fluorescent labels are relatively small, their embodiment can change the properties of the pharmacophore, thereby limiting their application. The ideal pharmacophore should exhibit its own specific fluorescent signature to allow “label-free” visualization. Such an association of molecular-recognition and fluorescent properties within one molecule would generate a relevant source of imaging probes for biomarker discovery. One way to achieve this goal is to explore the chemical space around the known fluorophore cores to search for fluorescent drug-like molecules with specific recognition properties.⁷⁸

Similarly, the fluorescent chemosensors can sense biologically important analytes by different signal transduction mechanisms. In this regard, sensing of certain alkaline earth metal ions (such as Ca^{2+} and Mg^{2+}) and transition metal ions (such as Cu^{2+} , Fe^{2+} , Fe^{3+}) are important owing to their involvements in various biological processes. Chemosensors are generally composed of a receptor unit, which is selective for a specific analyte and covalently bound to a signaling unit. The changes due to the receptor–analyte binding in the form of output signals are to be generally probed through changes in either spectral (^1H NMR, electronic, or fluorescence) or redox behavior.⁷⁹ For a system, where receptor and analyte are separated by a saturated

spacer, photo-induced electron transfer (PET)⁸⁰ process is reported to be one of the dominant processes; while for an integrated system, having an amino functionality conjugated to an electron-withdrawing functionality, ICT process, usually is the dominant one.⁸¹The main feature of the PET process is the appreciable change in the luminescence intensity on metal ion binding and ICT process is generally associated with spectral shift. One of the indole derivative **1.65**, as a chemosensor for copper and fluorinet is shown in figure 1.37.

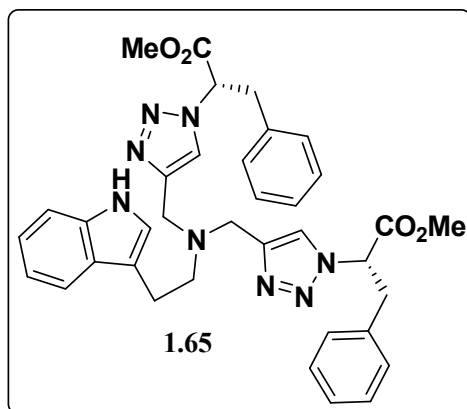


Fig. 1.37 Bis-triazolyl Indole amine as a Chemosensor for copper and fluorinet.

1.2. Coumarin as a privileged scaffold

Coumarin constitutes a highly interesting privileged scaffold to access a broad variety of biologically active compounds.⁸²The coumarin scaffold represents one of the key structural subunits for the discovery of new drug candidates⁸³. Recent decades have witnessed the emergence of coumarins (either fused or linked with heterocycle derivatives) as an efficient privileged scaffold in both medical and

materials chemical research reflecting the importance of these compounds. Their structural variability enables them to achieve a special place in the realm of natural products and synthetic organic chemistry⁸⁴ and as a consequence, many research groups worked on coumarin chemistry to develop fused or heterocycle linked coumarin moieties as privileged scaffolds. They belong to a large family of heterocycles and have been extensively studied both in biochemical and pharmaceutical field because of their broad spectrum of pharmacological activities. Various interactions like hydrogen bonding, electrostatic, van der Waals, π - π , hydrophobic and metal coordination with active sites in the body are responsible for its huge biological⁸⁵ properties such as anticancer, antibacterial, anti-tumor and antimicrobial activities. Selected examples are shown in fig. 1. 38.

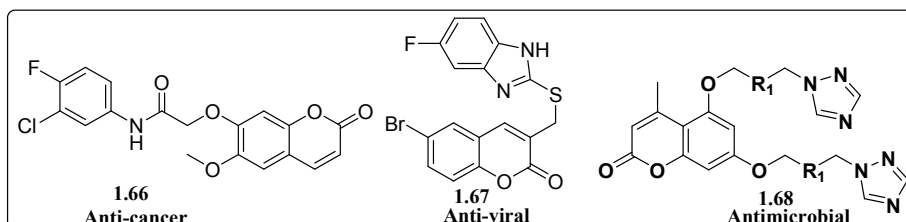


Fig.1. 38. Selected examples of coumarins as privileged scaffolds

1.3. Pyrimidinone as a privileged scaffold

In 1893, Italian chemist Pietro Biginelli reported on the acid catalyzed cyclo- condensation reaction of ethyl acetoacetate, benzaldehyde, and urea.⁸⁶ The reaction was carried out by simply heating a mixture of the three components dissolved in ethanol with a catalytic amount of HCl at reflux temperature. Biginelli identified the

product of this novel one-pot, three-component synthesis as 3,4-dihydropyrimidin-2(1*H*)-one. Nowadays a broad range of biological effects, including anti-viral, anti-tumor, anti-bacterial, and anti-inflammatory activities, have been ascribed to these partly reduced pyrimidine derivatives.⁸⁷ Some of the drugs with DHPM are given in figure 1.39.

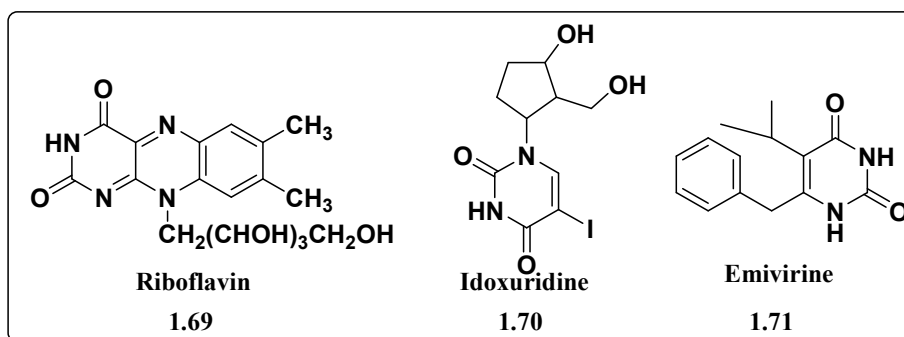


Fig. 1.39. Dihydropyrimidinone skeleton containing drugs.

1.4. Peptides and Peptidomimetics as Drug Leads

Peptides are the biological switches which modulate the biological functions in organisms including complex interaction with targets⁸⁸. The molecules which mimic peptides are known as Peptidomimetics⁸⁹. Even though many natural product based drugs are available, the area remains still underexplored. Natural products have complex molecular structures, with cyclic semi-rigid scaffolds, several chiral centers, more than five H-bond donors, more than ten H-bond acceptors, more than five rotatable C-C bonds, a large polar surface area, and a molecular weight above 500. The combined effect of all these factors may lead to moderate levels of bioavailability. The main

problem associated with natural peptides is their poor stability. The peptide backbone should be sufficiently stable until it reaches the target. But in many cases, it easily gets hydrolyzed by peptidases in the gastrointestinal tract. Those one which can resist this hydrolysis will fail to cross the blood-brain barrier due to poor transport properties. In most cases, this will happen if the peptide is having a large size or high molecular weight. Another problem is the flexibility of peptide backbone. A more flexible structure causes interaction with multiple receptors in addition to the targeted protein which eventually causes unwanted side effects⁹¹. Therefore, modifications are necessary to improve the bioavailability, receptor selectivity and other pharmacokinetic properties. Structure activity relationship studies reveals that the biological activity can be altered by chemical modifications.⁹²

In recent years, researchers have paid more attention to design the natural product mimetics and have optimized these mimetics to get the best pharmacokinetic properties⁹⁰. As a result, small molecules are designed to get a peptide like structural feature which could mimic the complex interaction of natural peptides with biological targets. These modified structural moieties with improved bioactivity are known as peptidomimetics. The design and development of peptidomimetics involves the introduction of structural features analogues to that of original peptides to make it favorable for biological action. The design of a peptidomimetic structure needs the understanding of basic idea about peptide-target interaction. This interaction mainly depends on the nature of ligands used in

peptidomimetic. While designing a new peptidomimetic molecule, the weak points of natural peptide which causes the inefficiency of the drug action must be known. At the same time, the key structural part responsible for the biological action should also be identified. The weak points are replaced with appropriate functionality like hydroxyl group, amino group or sometimes some heterocyclic functionality. Literature reviews suggest that the incorporation of heterocyclic functionality to the peptidic structure could improve the biological properties⁹³. Such side chain activation will improve the binding affinity as well as selectivity at the same time reducing the unwanted side effects which will eventually lead to better therapeutic effects. Examples for peptidomimetic drugs are shown in figure 1.40.

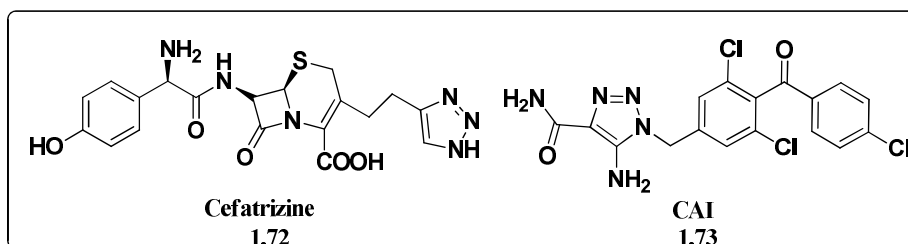


Fig. 1.40. Peptidomimetics as drug leads.

1.5. Strategies for the synthesis of linear and cyclic peptidomimetics

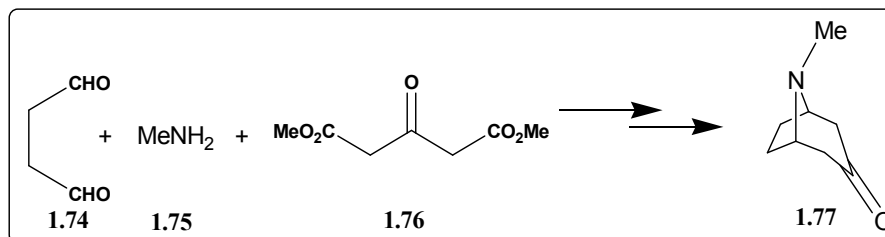
During the past few decades great efforts have been made to develop more efficient methods for the synthesis of linear and cyclic peptidomimetics as potential drug leads.⁹⁴ Several strategies have been established for the synthesis of peptidomimetics from the readily and

commercially available reagents. In expanding the molecular diversity along with the improvement in biological and physicochemical properties of the compound libraries, Schreiber and coworkers have introduced the concept of diversity-oriented synthesis (DOS) in 2010.⁹⁵ Molecules obtained through diversity oriented synthesis can interact with surrounding space in three dimensions and are characterized by high complexity content. An important property of DOS is that the final products, even though they are derived from a common starting material, are structurally and functionally different. There are several tools to introduce diversity oriented synthesis. Out of which the multicomponent reactions are considered as a near perfect tool for scaffold development through the efficient construction of functionally diverse structural scaffolds. The development of newer methods to carry out MCRs is a challenging endeavor. Through the MCR method, many heterocyclic drug-like molecules with structural diversity and complexity can be generated with minimum number of steps thereby facilitating lead identification in drug discovery programme. The straight forward approach of MCRs favors the synthesis of drug molecules to proceed through an easy and cost effective path way avoiding complex strategies.

1.5.1. Multicomponent reactions

By definition, Multicomponent reactions are reactions in which two or more starting materials reacts to form a product in which the majority of the atoms of the starting materials are incorporated in the product.⁹⁶ The history of the MCR begins with the strecker synthesis of α -amino acids in 1850. The first important application of MCRs in

natural product synthesis was Robinson's tropinone synthesis from succinic dialdehyde, methylamine, and dimethyl acetonedicarboxylate (scheme. 1.1)



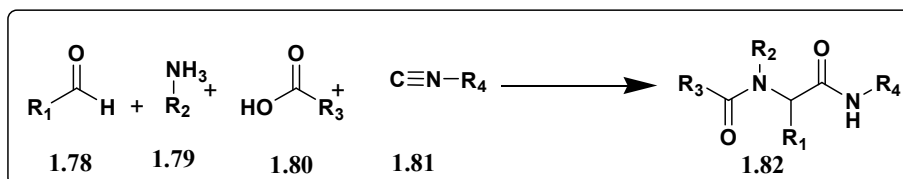
Scheme.1.1. Robinson's tropinone synthesis

MCRs are the best tool for the synthesis of hetrocyclic or non-hetrocyclic scaffolds. The Biginelli reaction for the synthesis of 3, 4-dihydropyrimidin-2(1H)-ones, Ugi 4 component reaction, Mannich reaction for β -amino carbonyl compounds, etc. are important for the synthesis of privileged scaffolds. There are various multicomponent reactions, of which isocyanide based MCRs are particularly useful for scaffold development. The molecules described in the coming chapters are mainly derived from Ugi, Mannich-type and Bigineli reactions.

1.5.1.1. Ugi reaction

In 1959, Ugi *et al.* described the most important variants of the four-component condensation using an isocyanide, acid, aldehyde and amine to afford α -acylamino carboxamide.⁹⁷ The chemical diversity of Ugi products are originating from their four substitutable diversity points. Since large number of aldehydes, amines, carboxylic acids, and isonitriles are available, it is possible to construct large collections of

carboxamides via solid phase or solution phase combinatorial synthesis (scheme.1.2)

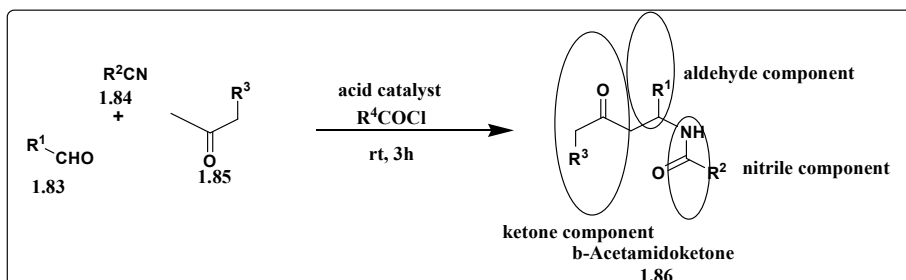


Scheme 1.2. Representation of Ugi 4 component reaction

1.5.1.2. Mannich type four component reaction

We have optimized a Mannich type four component reaction to construct the β -amidoketone type small peptide like structure (scheme1.3)⁹⁸ which is an important building block for the synthesis of 1,3-amino alcohols and β -lactams. The former is a structural part of peptidyl nucleoside antibiotics such as nikkomycins and polyoxins⁹⁹ and the latter is found in β -lactamase inhibitors such as 6- β -bromopenicillanic acid.¹⁰⁰ In this reaction an aldehyde, a nitrile component and an enolizable ketone reacts in presence of catalyst and small amount of an acid chloride to get the β -amidoketones. The reaction is initiated by the complexation of the carbonyl oxygen of the ketone to the metal atom of the catalyst to produce a sterically hindered enolate anion with a more nucleophilic α carbon. Subsequent reactions of this metal enolate with aldehyde component and acid chloride resulted in the carbon-carbon bond formation to produce a β -acyloxy ketone derivative. The acyloxy group then displaced by nucleophilic nitrogen of the nitrile component to produce a stable cation intermediate. Addition of water or other reactive species like

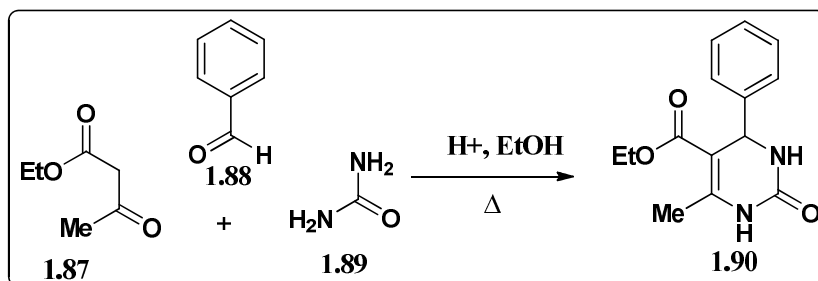
HOCl formed during the reaction leads to the formation of β -amido ketone scaffold and closes the catalytic cycle.



Scheme.1.3. Representation Mannich type 4 component reaction

1.5.1.3. Biginelli reaction

The Biginelli reaction is a three component reaction between aldehyde, β ketoester and urea to afford dihydropyrimidinone (DHPM) (scheme.1.4).¹⁰¹ The pyrimidinone derivatives are present in various fields and which displays a wide range of biological activities. These have led to the development of a number of therapeutics including calcium channel blockers, anti-viral, anti-cancer, anti-bacterial, anti-inflammatory and antihypertensive agents and they have been used as potent inhibitors of HIV integrase and poly(ADP-ribose) polymerase-1 (PARP-1).¹⁰²



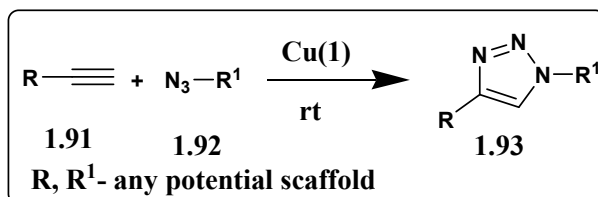
Scheme.1.4. Dihydropyrimidinone(DHPM).

1.5.2. Click Chemistry as a tool for fragment assembly

“The Nature generates substances by joining small molecular units”. Inspiring from this natural truth, in 2001 K. Barry Sharpless¹⁰³ introduced click chemistry as a chemical philosophy and described it as chemistry tailored to generate substances quickly and reliably by joining small units together. Click chemistry is not a specific reaction; it is a concept that mimics nature. A click reaction must be modular, wide in scope, give very high yields, generate only inoffensive byproducts that can be removed by nonchromatographic methods, and be stereo-specific (but not necessarily enantio-selective). The required process characteristics include simple reaction conditions (ideally, the process should be insensitive to oxygen and water), readily available starting materials and reagents, the use of no solvent or a solvent that is benign (such as water) or easily removed, and simple product isolation. Purification- if required- must be by non-chromatographic methods, such as crystallization or distillation, and the product must be stable under physiological conditions.

Click chemistry can be classified as cycloaddition reaction, nucleophilic substitution reaction, carbonyl chemistry reaction, addition reaction, thiol-ene click reaction etc. Out of these one of the best click reaction to date is copper catalysed azide alkyne cycloaddition and which is the modified Huisgen 1,3-dipolar cycloaddition of an alkyne and an azide. The active Cu (I) catalyst can be generated from Cu (I) or Cu (II) salt using sodium ascorbate as reducing agent. Addition of slight excess of sodium ascorbate prevents the formation of oxidative homo-coupling products. This Cu (I)

catalysed cyclo-addition results a region-selective 1, 4-disubstituted 1,2,3-triazole derivative as product which is a prominent privileged scaffold in drug discovery (scheme.1.5)



Scheme. 1.5. General Synthetic scheme for Cu(1) catalyzed azide-alkyne [3+2] cycloaddition reaction

1, 2, 3-Triazoles are important class of target molecules because of their interesting biological properties such as anti-allergic, anti-bacterial, and anti-HIV activity¹⁰⁴. Additionally, due to the resemblance in physiochemical properties such as planarity, dipole moment, C α distance and H-bond acceptor properties (of the lone pairs in nitrogen atoms), 1,2,3-triazoles are considered as peptide bond isosteres.¹⁰⁵ In addition to this, 1,2,3-triazole ring is highly chemically stable under hydrolytic as well as reductive and oxidative conditions. Consequently, amide-to-triazole substitutions are now common in drug-like molecules whose amide bonds are known to be crucial for biological activity. Representative drug examples of 1,2,3-triazole derivatives are shown in figure 1.41.

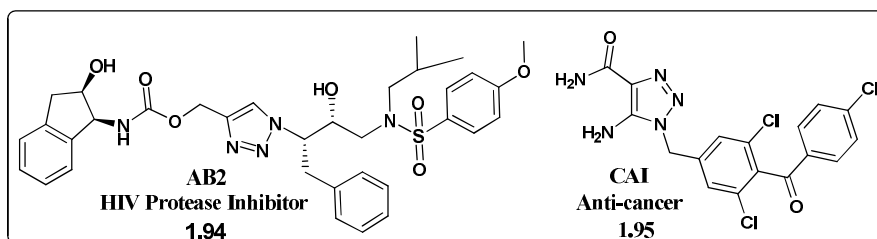


Fig. 1.41. Representative drug examples of 1,2,3-triazole derivatives.

1.6. Conclusion

The wide range of biological and drug like properties makes indole an attractive privileged scaffold. The literature survey has revealed the importance of indole scaffold in drug discovery, however, a lot more remains to be explored regarding this scaffold. Hence it was decided to undertake a study on the synthesis of indole based peptidomimetics tagged with coumarin and dihydropyrimidinone through a triazole. Similarly the indole based macrocycles are also an underexplored area in drug discovery. The study presented in the subsequent chapters are mainly focus on the development of indole derived peptidomimetic scaffolds as new potential lead compounds for drug discovery and as fluorescent probes for bio-imaging and metal ion sensing. A schematic representation of the summary of the work presented in chapters 2-9 are shown in the scheme below.

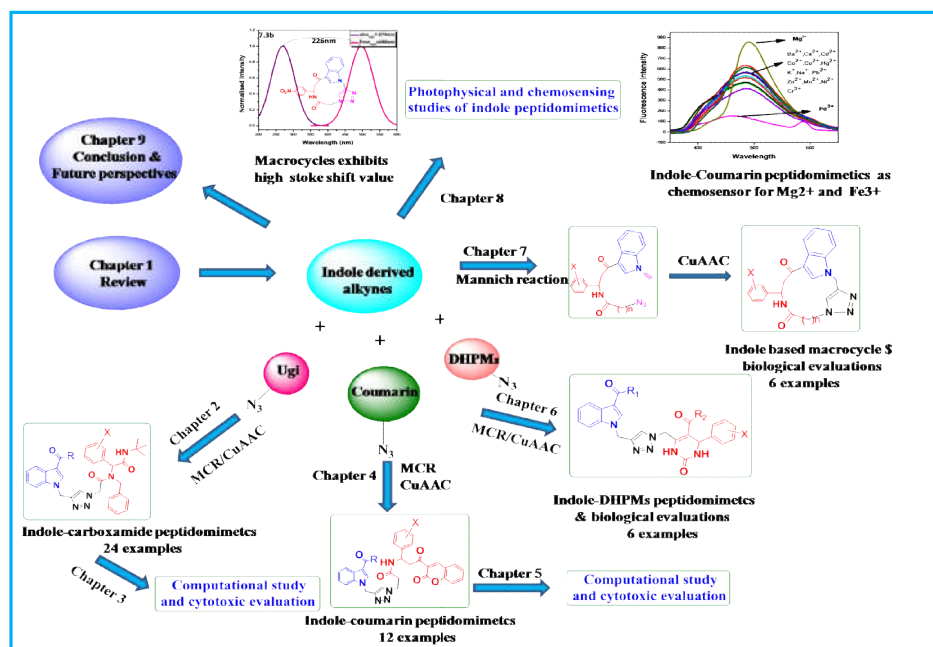


Fig. 1.42. Summary of the work

Reference

1. R.W. D. Simone, K.S. Currie, S.A. Mitchell, J.W. Darrow and D.A. Pippin, *Comb Chem High Throughput Screen.*, 2004, **7**, 473-493.
2. A.Y. Hassan, M.T. Sarg, A. H. Bayoumi and F. G. A. Kalaf, *Heterocyclic Chem.*, 2017, **54**, 3458-3470.
3. F. R. de Sá Alves, E. J. Barreiro and C. A. M. Fraga, *Mini-Reviews in Medicinal Chemistry*, 2009, **9**, 782-793.
4. R. Sharma, A. Bali and B. B. Chaudhari, *Bioorg Med Chem*, 2017, **27**, 3007-3013.
5. Z. W Mao, X. Zheng, Y. P. Lin C. Y. Hu, X. L. Wang, C. P. Wan and G. X. Rao, *Bioorg Med Chem.*, 2016, **26**, 3421-3424.
6. B. M. Chougala, S. Samundeeswari, M. Holiyachi, N. S. Naik, L. A. Shastri, S. Dodamani, S. Jalalpure, S, R. Dixit, S. D. Joshi and V. A. Sunagar, *Eur. J. Med. Chem.*, 2018, **143**, 1744-1756.
7. R. Kaur, S. Chaudhary, K. Kumar, M. k. Gupta and R.K. Rawal, *Eur. J. Med. Chem.*, 2017, **132**, 108-134.
8. L. Palego, L. Betti, A. Rossi and G. Giannaccini, *Journal of Amino Acids*, 2016.
9. M. Berger, J.A. Gray and B.L. Roth, *Annu. Rev. Med.* 2009, **60**, 335-366.
10. W.S. Chilton, J. Bigwood and R.E. Gensen, *J. Psychedelic Drugs*, 1979, **11**, 61-69.
11. N. K. Kaushik, N. Kaushik, P. Attri, N. Kumar, C.H. Kim, A. K. Verma and E. H. Choi, *Molecules*, 2013, **18**, 6620-6662.
12. E.F. Mueschenborn and A. Fox, *Headache*, 2005, **45**, 632-637.
13. J.A. Generali and D.J. Cada, *Hospital Pharmacy*, 2009, **44**, 670-671.
14. P. Singh, P. Prasher, P. Dhillon and R. Bhatti, *Eur. J. Med. Chem.* 2015, **97**, 104 - 123.
15. E. Abele, R. Abele, O. Dzenitis and E. Lukevics, *Chem Heterocycl Compd.* 2003, **39**, 3.

16. G.P.Kalaskar, M. Girisha, M.G. Purohit, B.S. Thippeswamy and B.M. Patil, *Indian J Heterocycl Chem.* 2007, **16**, 325.
17. M. Amir, N. Dhar and S.K. Tiwari, *Indian J Chem* .1997,**36B**, 96.
18. H. Panwar, R. S. Verma and V. K. Srivastava, Kumar, A. *Indian J Chem.* 2006, **45B**, 2099
19. Y. M. A Hiari, A. M Qaisi, M. M. Abadelah and W. Voelter, *Monatshefte Fur Chemie*; 2006, **137**, 243.
20. P. Singh, , *Eur. J. Med. Chem.* 2014, **74**, 440–450.
21. J. Khazir, I. Hyder, J.L. Gayatri, L. Prasad, N. Nalla, G. Chasoo, A. Mahajan, A.K. Saxena, M.S. Alam, G.N. Qazi and H.M. Sampath, *Eur. J. Med. Chem.*, 2014, **82**, 255–262.
22. N. Panathur, U. Dalimba, P. Venkat, M. Alvala, P. Yogeewari, D. Sriram and V. Kumar, *Eur. J. Med. Chem.*, 2013, **69**, 125–138.
23. B. C Hong, Y. Jiang, Y. Chang and S. Lee, *J Chin Chem. Soc.*, 2006, **53**, 647.
24. L. C. Garcia and R. Martinez, *Eur J Med Chem* 2002, **37**, 261.
25. S. Rossiter, L. K. Folkes, P. Wardman, *Bioorg Med Chem.*, 2002, **12**, 2523.
26. M. R. P. Queiroz, A. S. Abreu, M. S. D. Carvalho, P. M. T. Ferreira, N. Nazareth and M. S. Nascimento, *Bioorg Med. Chem.*, 2008, **16**, 5584.
27. a) M.J. Robertson, B.S. Kahl, J.M. Vose, S. de Vos, M. Laughlin, P.J. Flynn, K. Rowland, J.C. Cruz, S.L. Goldberg and L. Musib, *J. Clin. Oncol.*, 2007, **25** , 1741-1746. b) M. Crump, S. Leppä, L. Fayad, J.J. Lee, A. Di Rocco, M. Ogura, H. Hagberg, F. Schnell, R. Rifkin, and A. Mackensen, *J. Clin. Oncol.*, 2016, **34** ,2484-2492.
28. a) T.L. Naylor, H. Tang, B.A. Ratsch, A. Enns, A. Loo, L. Chen, P. Lenz, N.J. Waters, W. Schuler and B. Dörken, *Cancer Res.*, 2011, **71** ,2643-2653. (b) S. Friman, W. Arns, B. Nashan, F. Vincenti, B. Banas, K. Budde, D. Cibrik, L. Chan, J. Klempnauer and S. Mulgaonkar, *Am. J. Transpl.* , 2011, **11**, 1444-1455.

29. M. Ihnen, C. zu Eulenburg, T. Kolarova, J.W. Qi, K. Manivong, M. Chalukya, J. Dering, L. Anderson, C. Ginther, A. Meuter, *Mol. Cancer Ther.* 2013, **12**, 1002-1015.
30. Y. Boriskin, I. Leneva, E.I. Pecheur and S. Polyak, *Curr. Med. Chem.*, 2008, **15**, 997-1005.
31. J.R. Palmer, D.L. Romero, P.A. Aristoff, R.C. Thomas, H.W. Smith, in: Google Patents, 1996. US5563142. b) D.L. Romero, R.A. Morge, M.J. Genin, C. Biles, M. Busso, L. Resnick, I.W. Althaus, F. Reusser, R.C. Thomas and W.G. Tarpley, *J. Med. Chem.*, 1933, **36**, 1505-1508.
32. G.D. Morse, R.C. Reichman, M.A. Fischl, M. Para, J. Leedom, W. Powderly, L.M. Demeter, L. Resnick, Y. Bassiakos, J. Timpone, *Antivir. Res.*, 2000, **45** 47-58.
33. S. Castellino, M.R. Groseclose, J. Sigafos, D. Wagner, M. de Serres, J.W. Polli, E. Romach, J. Myer, B. Hamilton, *Chem. Res. Toxicol.*, 2012, **26**, 241- 251.
34. J. Aspinall and P.J. Pockros, *Curr. Opin. Investig. Drugs.*, 2006, **7**, 180-185.
35. P. Atadja, *Cancer Lett.*, 2009, **280**, 233-241.
36. K. E. Andersson. *Pharmacol. Rev.*, 2001, **53**, 417– 450
37. A. H. Rosengren R. Jokubka, D. Tojjar, C. Granhall, O. Hansson, D.Q. Li, V. Nagaraj, T. M. Reinbothe, J. Tuncel, Eliasson, L.; *Science*, 2009, **327**, 217–220.
38. L.J. Scott, C.M Perry, Delavirdine, *Drugs.*, 2000, **60**, 1411–1444.
39. V. Yutkin and J. Chin, *Expert Opin. Investig. Drugs.*, 2012, **21**, 251–260.
40. H. Chapman and P. H. Rhodes, *Dictionary of Organic Compounds*; Chapman & Hall: London, UK, 1996
41. D. A. Napalkov, *Kardiologiia.*, 2012, **52**, 80–83
42. a) N. Bacher, M. Tiefenthaler, S. Sturm, H. Stuppner, M. J. Ausserlechner, R. Kofler, G. Konwalinka, *J. Haematol.*, 2006, **132**, 615–622. (b) G. D. Giménez, G. E. García Prado, S. T. Rodríguez, F. A. Arche and R. de la Puerta, *Planta Med.*, 2010, **76**, 133–136.

43. a) H.M Prince and M.Bishton, Panobinostat (LBH589): *Hematol. Meet. Rep.*, 2009, **3**, 33–38.b) G. S. Mack, *Nat. Biotech.*, 2010, **28**, 1259–1266.
44. M.T. Isaac,*Evid. Based Ment. Health.*, 2004, **7**, 107.
45. D. Lednicer,*The Organic Chemistry of Drug Synthesis*; A John Wiley & Sons, Inc.: Hoboken, NJ, USA, 2007, **7**, 141–154.
46. A Klimke, E Klieser. *Pharmacopsychiatry.*, 1991, **24**, 107–112.
47. a) J.E. Macor, D Gurley, T. Lanthorn, J. Loch,. R.A. Mack, G Mullen,O Tran, N Wright and J.C. Gordon, *Bioorg. Med. Chem. Lett.*,2001, **11**, 319–321.(b) R.Cui, K. Suemaru, B. Li, S. Kohnomi and H. Araki, *Eur. J.Pharma.*, 2009, **609**, 74-77.
48. G.D.Morse, R.C.Reichman, M.A.Fischl, M.Para, J.Leedom, W.Powderly, L.M. Demeter, L. Resnick, Y.Bassiakos, J.Timpone, S.Cox and D.Batts,*Antiviral Res.*, 2010, **45**, 47–58.
49. C. Dejaco, C. Duftner and M. Schirmer *M.Rheumatol Int.*, 2007, **27**, 351-5.
50. (a) H.Arens, H.O.Borbe,B.Ulbrich and J .Stöckigt,*PlantaMed.*,1982, **46**, 210–214. (b) M.F Roberts and M. Wink, *Alkaloids: Biochemistry, Ecology, and Medicinal Applications*; Plenum Press: New York, NY, USA, 1998.
51. a) D.R Haubrich, S.J Ward, E.Baizman,M.R. Bell, J.Bradford, R Ferrari, M. Miller, M.Perrone, A.K.Pierson and J.K. Saelens,*J. Pharmacol. Exp. Ther.*,1990, **255**, 511–522.(b) M.R.Bell, T.E D'Ambra, V.Kumar, M.A Eissenstat, J.L.Herrmann, J.R Wetzal, J.D. Rosi, R.E. Phillion, S.J.Daum and D.J. Hlasta, *J. Med. Chem.*, 1991, **34**, 1099–1110.
52. a) P. Cook, I. James, *N. Engl. J. Med.* 1981, **305**, 1560–1564.(b) H. J Arpe and F. Ullmann, Indole Alkaloids. In *Ullmann's Encyclopedia of Industrial Chemistry*, 5th ed.; Wiley- VCH: Weinheim, Germany, 1985.
53. a)M. B. Arnao, J. Sanchezbravo and M.Acosta,*Biochem. Mol. Biol. Int.*, 1996, **39**,1125-34.(b) A. Podsèdek, *Lwt- Food Sci. Technol.* 2007, **40**, 1-11.(c) J. J. Michnovicz, *Nutr. Cancer* 1991, **16**, 59-66.(d) J. J. Michnovicz,*Natl. Cancer Inst*, 1997, **89**, 718-24.
54. . R. E. Dolle,. *Mol.Divers.*, 1997, **2**, 223-36.

55. M. J. G. L. McLeish and Kenyon, In *Approaches to the Rational Design of Enzyme Inhibitors*, Abraham, D. J., Ed.; John Wiley and Sons: New Jersey, 2003; Vol. **1**, p. 716.
56. R. S. Blumenthal, *Am. Heart J.*, 2000, **139**, 577-83.
57. W.L. Smith, D. L. DeWitt and R. M. Garavito, *Annu. Rev. Biochem.*, 2000, **69**, 145-82.
58. W. Hu, Z. Guo, X. Yi, C. Guo, F. Chu and G. Cheng, *Bioorg. Med. Chem.*, 2003, **11**, 5539-44.
59. A. T. Bender, J. Beavo, *Pharmacol. Rev.*, 2006, **58**, 488-520.
60. A. Daugan, P. Grondin, C. Ruault, A. C. Le Monnier de Gouville, H. Coste, J. M. Linget, J. Kirilovsky, F. Hyafil and R. Labaudiniere, *J. Med. Chem.*, 2003, **46**, 4533-42.
61. G. Mariaule and P. Belmont, *Molecules*, 2014, **19**, 14366-14382.
62. R. S. Finn, A. Aleshin and D. J. Slamon, *Breast cancer research*, 2016, **18**, 17
63. (a) E. Marsault and M. L. Peterson, *J. Med. Chem.*, 2011, **54**, 1961–2004. (b) M. Madsen and C. M. H. Clausen, *Eur. J. Org. Chem.*, 2011, 3107–3115.
64. (a) A. James and Wisner, *Nature chemistry*, 2013, **5**, 646. (b) Y. Xufen and S. Dianqing Sun, *Molecules*, 2013, **18**, 6230-6268.
65. J. Mallinson and I. Collins, *Future Med. Chem.*, 2012, **4**, 11, 1409–1438.
66. A. K. Yudin, *Chem. Sci.* 2015, **6**, 30-49. (b) M. E. Maier, *Org. Biomol. Chem.*, 2015, **13**, 5302-5343.
67. (a) A. Isidro-Llobet, T. Murillo and P. Bello, *Proc. Natl. Acad. Sci.*, 2011, U.S.A., **108**, 6793. (b) T. E. Nielsen, and S. L. Schreiber, *Angew. Chem., Int. Ed.*, 2008, **47**, 48.
68. M. G. David, V. Sandrine, I. L. Tse, T. Abdellah, H. Lili, D. C. Maxwell, A. Katie J. M. Berke, M. Canard, E. Cleiren, P. Dehertogh, L. Stefaan, E. Fransen, V. D. H. Elisabeth, I. V. Steen, L. Vijgen, M. C. Rouan, G. Fanning, O. Nyanguile, K. V. Emelen, K. Simmen and P. Raboisson, *Bioorg. Med. Chem. Lett.*, 2010, **20**, 6925–6928.

69. M.G. David, V. Sandrine, I.L.Tse, T. Abdellah, H. Lili, D.C. Maxwell, A. Katie J.M. Berke, M. Canard, E. Cleiren, P. Dehertogh, L. Stefaan, E. Fransen, V.D.H. Elisabeth, I. V. Steen, L. Vijgen, M. C. Rouan, G. Fanning, O. Nyanguile, K. V. Emelen, K. Simmen and P. Raboisson, *Bioorg. Med. Chem. Lett.*, 2012, **22**, 4431–4436.
70. H.C. Zhang, K. B. White, Y. Hong, F.M. David, K.D. Claudia, F.A. Michael, P.A. Gordon, A.J. Eckardt, B.R. Conway, L. Westover, J.Z. Xu, L. Richard, K. T. Demarest, S. Emanuel and B. E. Maryanoffa, *Bioorg. Med. Chem. Lett.* 2003, **13**, 3049–3053.
71. M. Arzillo, A. Pezzella, O. Crescenzi, A. Napolitano, E. J. Land, V. Barone and M. Ischia, *Org. Lett.*, 2010, **12**, 14.
72. A. Berthelot, S. Piguel, G. L. Dour and J. Vidal, *J. Org. Chem.*, 2003, **68**, 9835–9838.
73. L. C. Acevedo and L. D. Miranda, *Org. Biomol. Chem.*, 2015, **13**, 4408–4412
74. S. B. David, N. Kumar and D. B. McConnell, *Tetrahedron*, 2000, **56**, 8513–8524.
75. I. F. Sengul, K. Wood, N. Kumar and S.B. David, *Tetrahedron*, 2012, **68**, 9050–9055.
76. L. D. Lavis and R. T. Raines, *ACS Chem. Biol.*, 2008, **3**, 142.
77. O. N. Burchak, L. Mughherli, M. Ostuni, J. J. Lacap and M. Y. Balakirev. *J. Am. Chem. Soc.*, 2011, **133**, 10058–10061.
78. (a) G.R. Rosania, J. W. Lee, L. Ding, H.S. Yoon and Y.T. Chang, *J. Am. Chem. Soc.*, 2003, **125**, 1130. (b) M. Vendrell, J. S. Lee and Y.T. Chang, *Curr. Opin. Chem. Biol.*, 2010, **14**, 383.
79. M. Suresh and A. Das, *Tetrahedron Lett.*, 2009, **50**, 5808–5812.
80. Y. Wang, L. Anthony, Y. Ding, C. Brückner and Y. Lei, *RSC*, 2012.
81. S. Arimori, L. I. Bosch, C. J. Ward and T. D. James, *Tetrahedron Lett.*, 2001, **42**, 4553–4555.
82. C. E. Gaudino, S. Tagliapietra, K. Martina, G. Palmisano, and G. Cravotto, *RSC Adv.*, 2016, **6**, 46394–46405.

83. M.E. Riveiro, N. De Kimpe, A. Moglioni, R. Vázquez, F. Monczor, C. Shayo, and C. Davio, *Curr. Med. Chem.*, 2010, **17**, 1325-1338.
84. (a) D. Viña, M. J. Matos, M. Yáñez, L. Santana, and E. Uriarte, *Med. Chem. Commun.*, 2012, **3**, 213, (b) R. L. Mueller, *Best Practice & Research Clinical Haematology*, 2004, **17**, 23–53.
85. E. Jameel, T. Umar, J. Kumar, N. Hoda. *Chem Biol Drug Des.* 2016, **87**, 21–38.
86. P. Biginelli, *Gazz. Chim. Ital.*, 1893, **23**, 360–413.
87. L. H. S. Matos, F. T. Masson, L. A. Simeoni and M. H. de-Mello, *Eur. J. Med. Chem.*, 2018, **143**, 1779-1789.
88. V. J. Hruby and M. Cai, *Annu. Rev. Pharmacol. Toxicol.*, 2013, **53**, 557–580.
89. (a) R. Breinbauer, I. R. Vetter and H. Waldmann, *Angew. Chem. Int. Ed.*, 2000, **41**, 2878–2890 (b) K. Kumar, and H. Waldmann, *Angew. Chem. Int. Ed.*, 2009, **48**, 3224–3242.
90. A. Abell, A. (Ed.), *Advances in Amino Acid Mimetics and Peptidomimetics*, JAI Press, Greenwich, 1997, 1. (b) Abell, A. (Ed.), *Advances in Amino Acid Mimetics and Peptidomimetics*, JAI Press, Greenwich, 1999, 2.
91. Li Di, *AAPS J.*, 2015, **17**, 134–143.
92. *Pure & Appl. Chem.*; 1996, Vol. 68, No. 6, 1303-1308.
93. a) A. D. Abell, *Letters in Peptide Science*, 2002, **8**, 267-272, (b) I. Cerminara, L. Chiummiento, M. Funicello, A. Guarnaccio, P. Lupattelli, *Pharmaceuticals*, 2012, **5**, 297-316.
94. A. Abell, (Ed.), *Advances in Amino Acid Mimetics and Peptidomimetics*, JAI Press, Greenwich, 1997, 1.
95. (a) R. J. Spandl, A. Bender and D. R. Spring, *Org. Biomol. Chem.* 2008, **6**, 1149–1158. (b) T. E. Nielsen and S. L. Schreiber, *Angew. Chem., Int. Ed.*, 2008, 4748–4756; (c) S. L. Schreiber, *Science*, 2000, **287**, 1964–1969. (d) R. J. Spandl, A. Bender and D. R. Spring, *Org. Biomol. Chem.*, 2008, **6**, 1149–1158. (e) W. R. J. D. Galloway, A. Isidro-Llobet and D. R. Spring, *Nat. Commun.*, 2010, **1**, 80–92. (f) H. Eckert, *Molecules*, 2012, **17**, 1074-1102.
96. A. Dömling and I. Ugi, *Angew. Chem. Int. Ed.*, 2000, **39**, 3168
97. P. A. Tempest, *Curr Opin Drug Discov Devel.*, 2005, **8**, 776-788.

98. D. Bahulayan, S. K. Das, J. Iqbal, *J. Org. Chem.*, 2003, **68**, 5735-5738; (b) R. Ghosh, S. Maiti, A. Chakraborty, S. Chakraborty, A. K. Mukherjee, *Tetrahedron.*, 2006,**62**, 4059-4064; (c) V. Shinu, B. Sheeja, E. Purushothaman, D. Bahulayan, *Tetrahedron Lett.* 2009, **50**, 4838-4843.
99. (a) C. Bormann, W. Huhn and H. Zahner, *J. Antibiot.*,1985, **38**, 9-16; (b) S. Suzuki, K. Isono, J. Nagatsu, T. Mizutani, Y. Kawashima and T. Mizuno, *J. Antibiot.*,1965,**18**, 131.
100. R. Pratt and M. Loosemore, *Proc. Natl. Acad. Sci.*, 1978, **75**, 4145-4149.
101. X. H. Chen, X. Y. Xu, H. Liu, L. F. Cun and L. Z. Gong, *J. Am. Chem. Soc.*, 2006,**128**, 14802-14803.
102. a)J. Ishida, K. Hattori, H. Yamamoto, A. Iwashita, K. Miharab and N. Matsuoka, *Bioorg. Med. Chem. Lett.*, 2005, **15**, 4221 (b) D. J. Hazuda, P. Felock, M. Witmer, A. Wolfe, K. Stillmock, J. A. Grobler, A. Espeseth, L. Gabryelski, W. Schleif, C. Blau and M. D. Miller, *Science.*, 2000, **287**, 646(c) . A. Bernhart, F. B. Haudricourt, J. L. Assens, J. Gougat, C. Lacour, A. Roccon, C. Cazaubon, J. C. Brelie`re, G. Le Fur and D. Nisato, *Bioorg. Med. Chem. Lett.*, 1994, **4**, 157–162. (d) R. Dudhe, P. K. Sharma, P. Verma and A. Chaudhary, *J. Adv. Sci. Res.*, 2011, **2**.
103. (a) H. C. Kolb, M. Finn and K. B. Sharpless, *Angew. Chem. Int. Ed.*, 2001,**40**, 2004-2021.
104. (a) D. R.Buckle and C. J. M. Rockell, *J. Chem. Soc.,Perkin Trans.*, 1982, **1**, 627; (b) D. R. Buckle, D. J. Outred, C. J. M. Rockell, H. Smith and B.A. Spicer, *J. Med. Chem.*,1983, **26**, 251.(c) M. J. Genin et al. *J. Med. Chem.*,2000, **43**, 953.(d) R. Alvarez, S. Velazquez, A. San-Felix, S. Aquaro, E. De Clercq, C.F.Perno, A. Karlsson, J. Balzarini and M. J. Camarasa, *J. Med. Chem.*, 1994, **37**, 4185.
105. H. C. Kolb andK. B. Sharpless, *Drug Discov. Today.*, 2003, **8**, 1128.

CHAPTER 2

**The synthesis of Indole-Triazole
Carboxamide peptidomimetics via MCR-
Click strategy.**

Contents

2.1 Introduction.....	50
2.2 Result and discussion.....	53
2.3. Structure elucidation by spectroscopy	60
2.4. Conclusion.....	70
2.5. Experimental Section.....	70
References	87
Supplementary Material	89

2.1 Introduction

As explained in the previous chapter, indoles, triazoles, and carboxamides are the three potential structural scaffolds frequently occurring in natural as well as synthetic therapeutics¹. For example, 3-substituted indole derivatives are potentially useful for the development of enzyme inhibitors,² bioreceptormodulators,³ cannabinoid receptors⁴ etc. N-acyl or N-alkyl indole derivatives are also present in numerous biologically active molecules.⁵ Carboxamides are another interesting moiety present in many drug molecules.⁶ Telaprevir, used for the treatment of hepatitis C, bortezomib—a threonine protease inhibitor—and praziquantel used for the treatment of schistosomiasis, are some of the examples of this category. Similarly, triazole derivatives also possess valuable clinical profiles like anti-HIV,⁷ anti-allergic,⁸ antifungal,⁹ or anti-viral properties.¹⁰ Figure 2.1 shows selected drug molecules with one of these moieties as privileged scaffold.

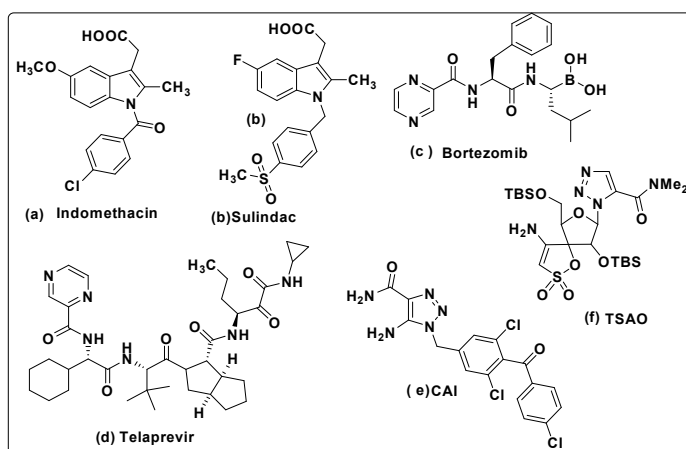


Fig. 2.1. Representative examples of commercial drug molecules with: (a, b): indole as structural part, (c, d): α -acylaminoamide as core structure, (e, f): 1,2,3-triazole as core structure.

Recently, indoline-2-carboxamide derivative A (Fig.2.2a) has been reported as a therapeutic agent for stage 1 Human African Trypanosomiasis (HAT).¹¹ However, it fails to produce positive results for the treatment of stage 2 HAT due to the lack of tolerability in biological environment. Stage 2 is more fatal because at this stage the parasites cross the blood–brain barrier and attack the central nervous system leading to medical conditions such as confusion, sleep disorders, coma or even death. No effective vaccine is available till date for the treatment of stage 2 HAT and therefore it is important to develop more bio-compatible molecules that can cross the blood–brain barrier to provide better bioavailability at the HAT infected sites. The failure of A to produce better results for type 2 HAT may be the poor stability of the molecule due to the vulnerability of the indole amide moiety and the ether oxygen toward protease action. Similarly, lipophilicity affects both blood–brain barrier permeation and brain distribution. It has been recognized that lipophilic molecules have greater access to the brain than hydrophilic molecules. Lipophilicity could bring the inhibitor into closer proximity with a brain target and exists in a highly lipophilic environment.¹² One of the methods to improve the stability, lipophilicity and bio-availability of a peptide like drug molecule is the design of its peptidomimetic version by substituting its protease unstable amide bonds with more stable isosteres.¹³ Many functionalities like 1,2,3-triazole, $-\text{CH}_2\text{-O-}$, $-\text{CH}_2\text{-CO-}$ and $-\text{CH}=\text{CH-}$ etc. are identified as amide bond isosteres.¹⁴ Among the various amide bond isosteres, 1,2,3-triazole is the more prominent one due to its close similarity with amide bonds in terms of physicochemical properties such as planarity, dipole moment, $\text{C}\alpha$ distance, and a

number of H-bonding sites.¹⁵ A 1,2,3-triazole can be easily linked between two subunits of a single drug via copper (I) catalyzed [3+2]azide-alkyne click cycloaddition (CuAAC)¹⁶ which has now emerged as a waste-free and chemoselective ligation tool for the fragment coupling of small molecule segments to produce conformationally restricted drug-like molecules.¹⁷ As part of the research work on peptidomimetic small molecules,¹⁸ we decided to investigate the possibility of designing new peptidomimetic versions of **A** via structural as well as isosteric modification to create various indole-triazole-carboxamide derivatives (ITC) as shown in Figure 2.2. Chapter 2 presents the development of the simple carboxamide versions of indole as shown in figure 2.2 and the methodology adopted for the same is presented in figure 2.3.

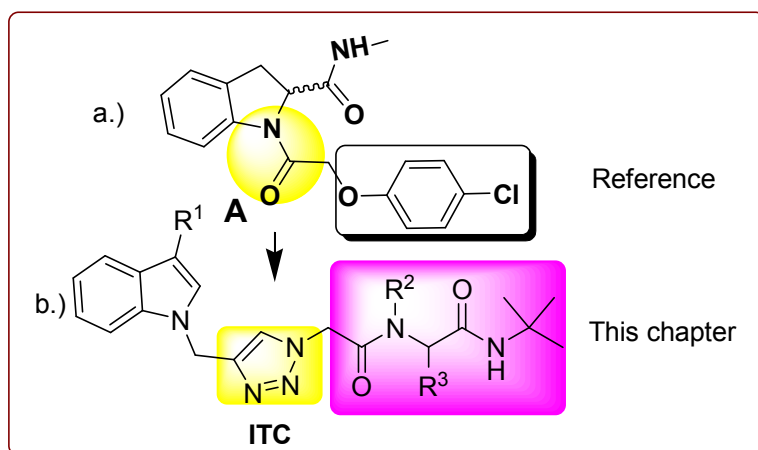


Fig. 2.2 a). Recently reported indoline-2- carboxamide derivative as potential curing agent for stage 1 human African trypanosomiasis (HAT). **b)** General structure of the indole-triazole-carboxamide (ITC) obtained via isosteric substitution.

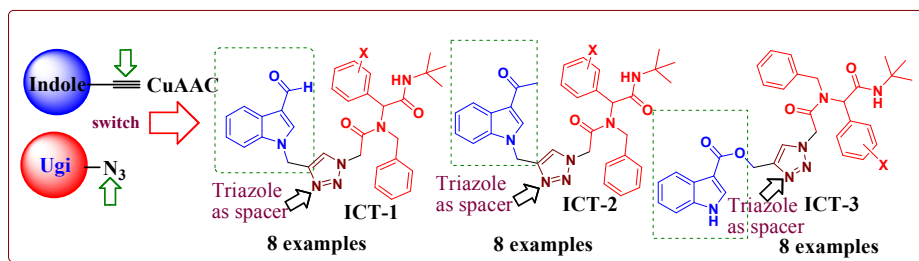


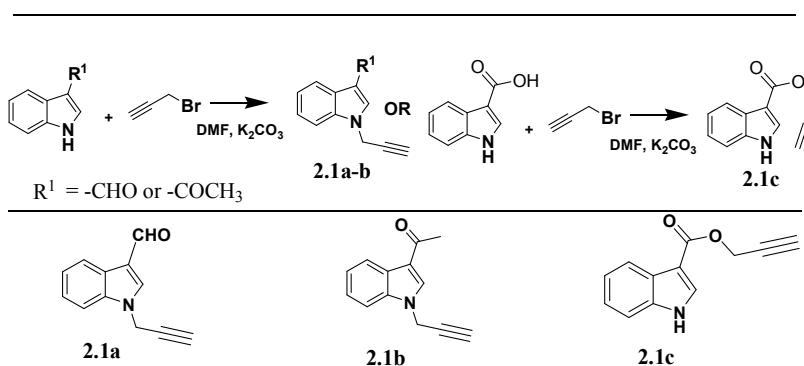
Fig. 2.3. A schematic representation of the “MCR-click” strategy for the synthesis of Indole-Triazole-Carboxamide peptidomimetic discussed in this chapter.

2.2 Result and discussion

A build/pair strategy¹⁹ based on multicomponent reactions (MCRs)²⁰ and click chemistry was used for the synthesis of the indole peptidomimetics ITC-1, ITC-2, and ITC-3.

2.2.1 Synthesis of Indole based alkyne and Ugi azides

The studies began with the synthesis of the starting alkynes and azides. The alkynes **2.1a–2.1c** was obtained via the base catalyzed propargylation of the corresponding 3-substituted indole with propargyl bromide in DMF as shown in Scheme 2.1.



Scheme 2.1. List of alkyne functionalized indole scaffolds.

The second fragment in the form of carboxamide azide (Fig. 2.4) was synthesized via the post reaction modification of the corresponding carboxamide chlorides which were obtained from an Ugi 4component reaction. The Ugi four-component condensation (U-4CC) between an aldehyde, an amine, a carboxylic acid and an isocyanide allows the rapid synthesis of α -aminoacyl amide derivatives. The Ugi Reaction products can exemplify a wide variety of substitution patterns, and can form a wide variety of peptidomimetics that have potential pharmaceutical applications. The carboxamide scaffold as shown in Fig. 2.4 is selected by virtue of its unique structural features comprising of at least four substitutable diversity points. Since a large number of aldehydes, amines, carboxylic acids and isonitriles are available, it is possible to construct large collections of carboxamides via solid phase or solution phase combinatorial synthesis. As shown in table 2.1, the carboxamide chloride intermediates were obtained by mixing equimolar amount of aldehyde, amine, chloroacetic acid and *tert*-butylisocyanide in methanol at room temperature by following Ugi reaction protocol. The carboxamide chlorides thus obtained were subsequently converted to the carboxamide azides by treating with sodium azide in the presence of potassium carbonate in DMF at room temperature.

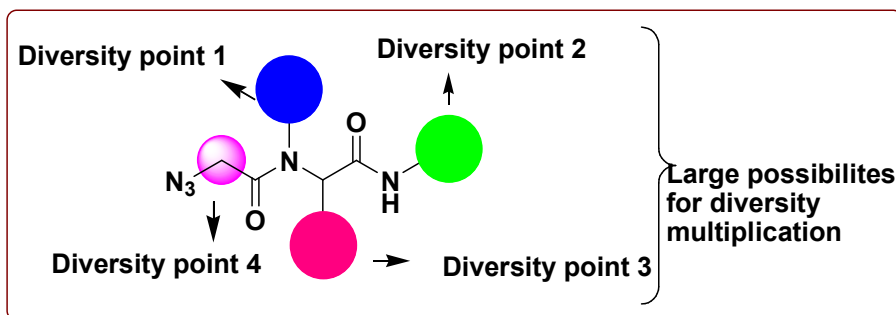
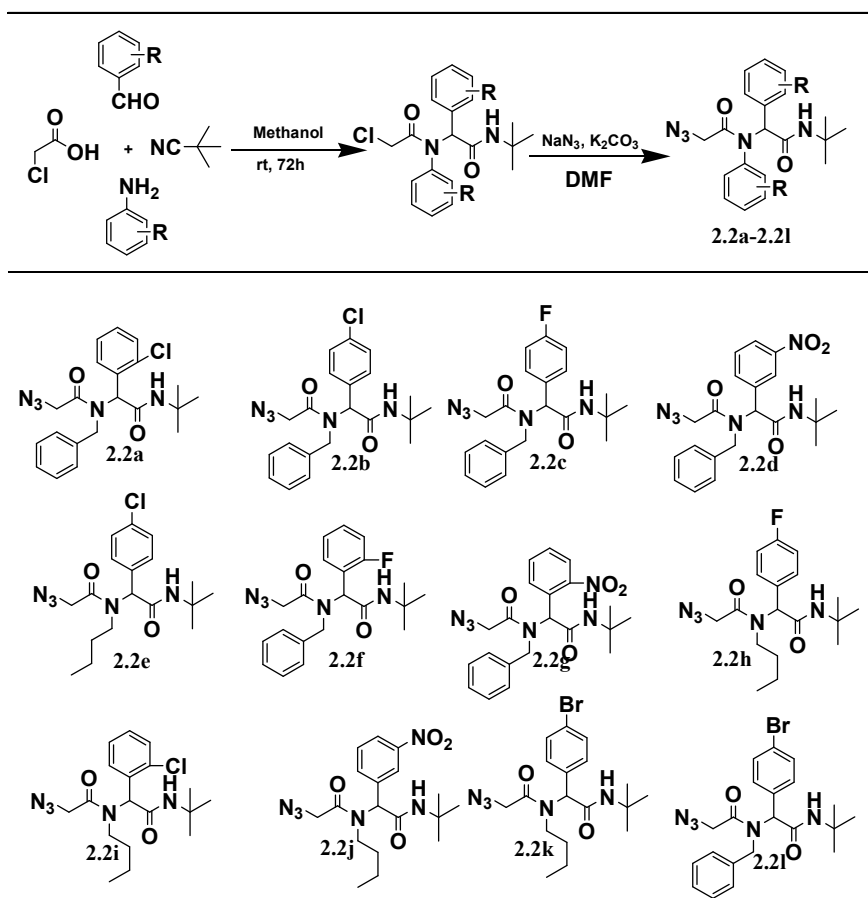


Fig. 2.4. General Structure of the carboxamide scaffolds in the azide form.

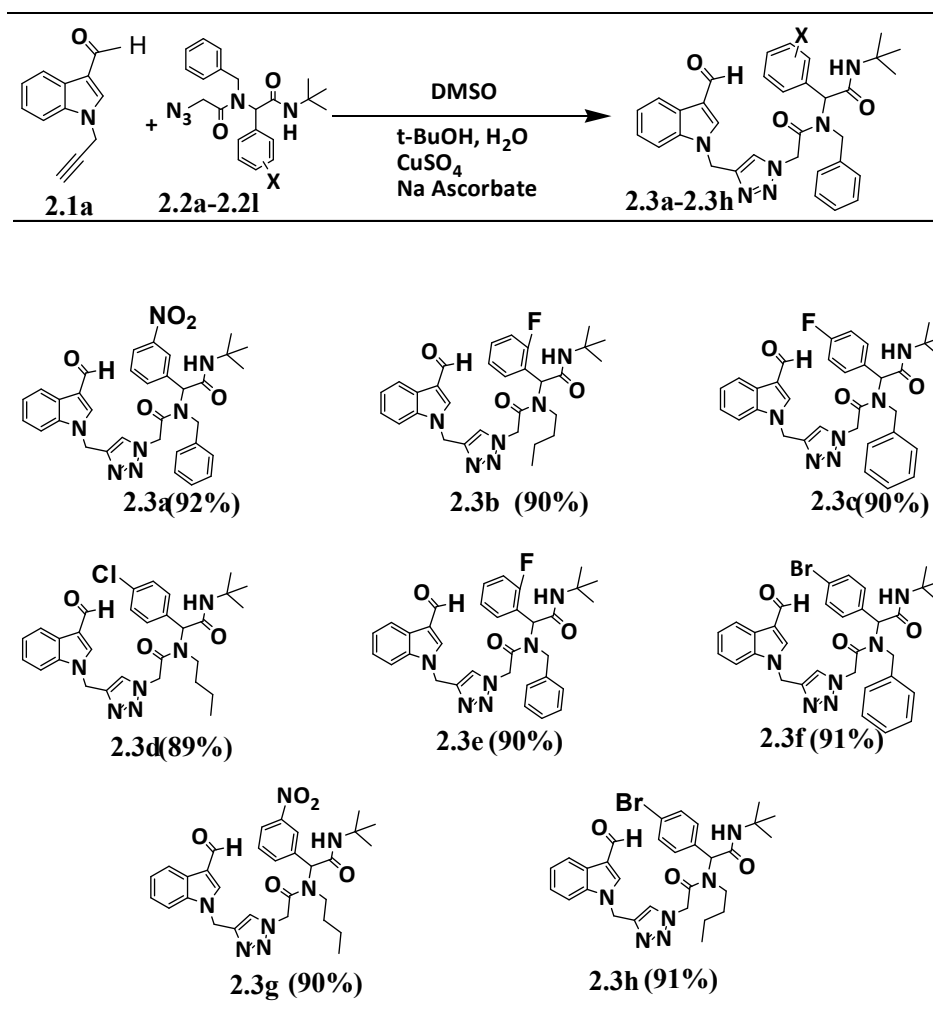
Table 2.1. List of carboxamide azides **2.2a-2.2l** synthesized for the ligation with indole alkynes **2.1a-2.1c**



2.2.2 Synthesis of Indole –Triazole peptidomimetics

Having synthesized the indole alkynes and carboxamide azides, we proceed to the synthesis of indole peptidomimetics by Copper catalysed azide alkyne cyclo-addition between these two entities. Eight peptidomimetics were prepared from each category of alkynes with selected azides from table 2.1. For example, for the synthesis of ICT-1 series, we have reacted alkyne 2.1a with azides 2.2c-f, 2.2h, 2.2j, 2.2k and 2.2l to obtain 2.3a-2.3h. In a representative reaction, an equimolar mixture of alkyne functionalized indole and the carboxamide azide were mixed with 0.2 equivalent of sodium ascorbate in a mixed solvent system containing tert-butanol, water and DMSO (4:2:1) at room temperature for 48h. The subsequent aqueous work-up followed by solvent wash afforded the peptidomimetics in pure form. The peptidomimetics and their starting scaffolds were thoroughly characterized by ¹H NMR, ¹³C NMR, FT-IR and Mass spectral studies. The structure of various peptidomimetics belonging to the ICT-1 series is presented in table 2.2.

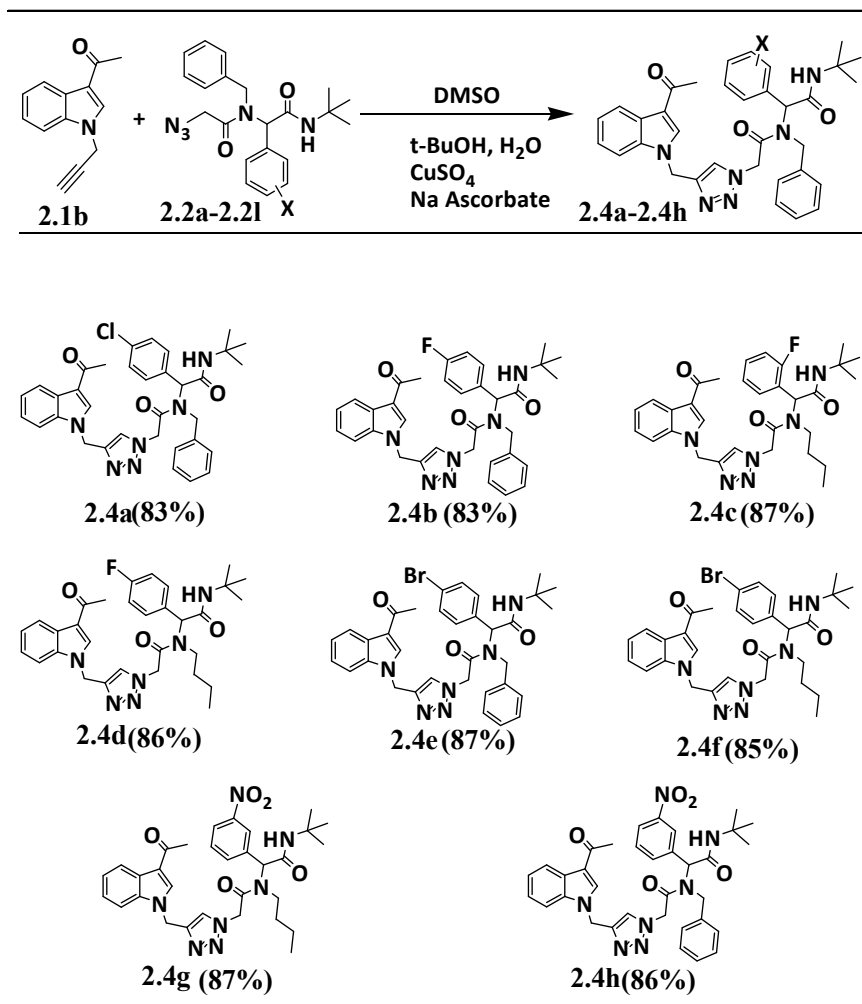
Table 2.2. List of ICT-1 series 1,4- substituted triazolyl-3-formyl indole scaffolds substituted with carboxamide residues.



The synthesis of the peptidomimetics in the ICT-2 series was also done in the same way and the details are presented in table 2.3 and 2.4, respectively. In the case of ICT-2, we synthesised eight indole-triazole carboxamide peptidomimetics, via the Click reaction between 2.1b alkyne with selected Ugi Azides. All the ICT-2 series formed in

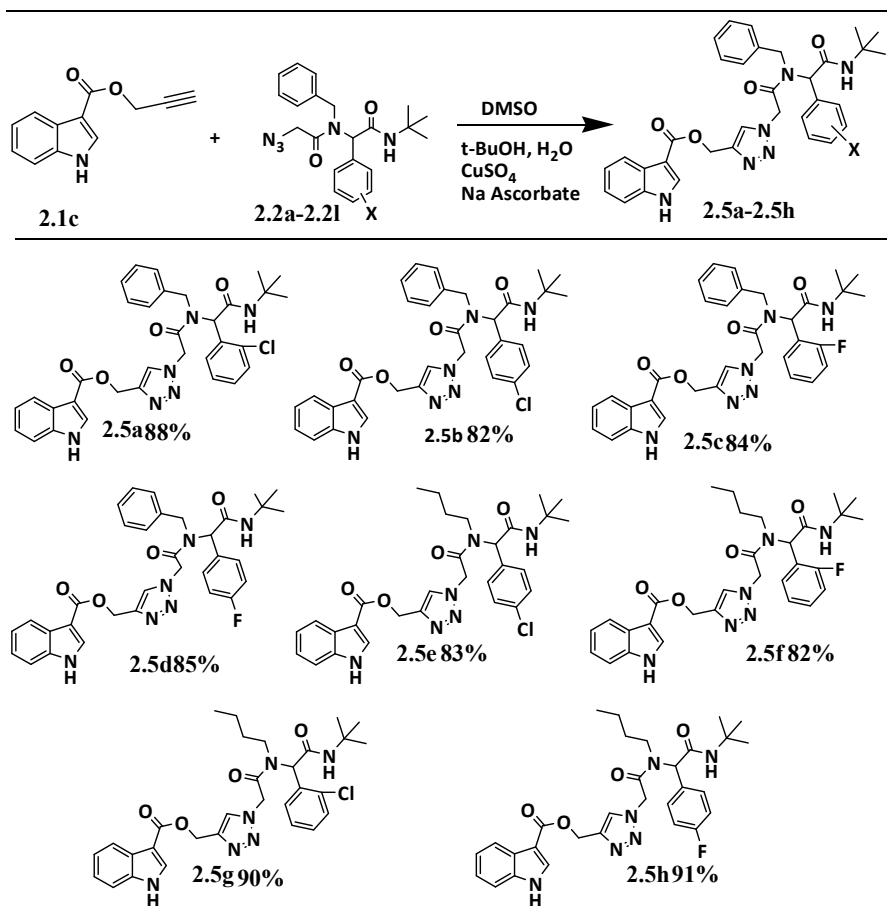
good to excellent yield with a maximum of 87% irrespective of the nature of the skeletal substitution patterns. The structure of various peptidomimetics belong to the ICT-2 series are presented in table 2.3.

Table 2.3. List of ICT-2 series 1,4- substituted triazolyl-3-acetyl indole scaffolds substituted with carboxamide residues



The synthesis of the peptidomimetics in the ICT-3 series was also done in the same way and the details are presented in table 2.4. In the case of ICT-3, we synthesised eight indole-triazole carboxamide peptidomimetics, via the Click reaction between 2.1c alkyne with selected Ugi Azides. All the ICT-3 series formed in good to excellent yield with a maximum of 91% irrespective of the nature of the skeletal substitution patterns. The structure of various peptidomimetics belonging to the ICT-3 series are presented in table 2.4.

Table 2.4. List of ICT-3 series indole peptidomimetics.



2.3. Structure elucidation by spectroscopy

2.3.1 Structure identification of 1-(prop-2-yn-1-yl)-1H indole-3-carbaldehyde 2.1a

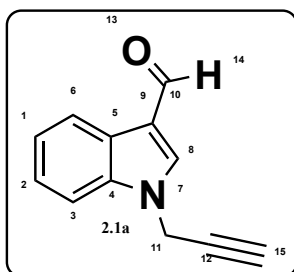
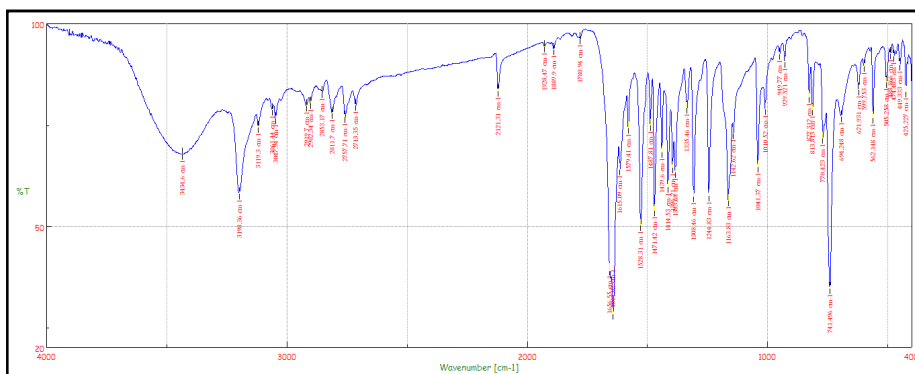


Fig.2.5. structure of **2.1a**

The alkyne functionalized Indole **2.1a** is taken as a representative example for a general discussion on structure elucidation. The compound is numbered as shown in fig.2.5. The FT-IR spectrum of the compound shows major absorptions at 3198, 2121, 1656, 1615 cm^{-1} . The presence of propargylated group was confirmed by the bands at 3198 and 2121 cm^{-1} . The peak due to the $\text{C}\equiv\text{C}-\text{H}$ stretching vibration appeared at 3198 cm^{-1} and the $\text{C}\equiv\text{C}$ stretching vibration occurred at 2121 cm^{-1} . The absorption at 1656 cm^{-1} is due to the $\text{C}=\text{O}$ stretching vibration of the ketone group (Fig.2.6).



The initial information obtained from the FT-IR spectrum about the formation of the product is further confirmed by the ^1H NMR spectrum (Fig. 2.7). The aldehydic proton is observed as a singlet at δ 9.94. The CH_2 protons at position 11 is observed as a singlet at δ 5.24 and the CH proton (alkyne CH) at position 15 is observed as another singlet at δ 3.43. The four aromatic protons were observed as three sets of multiplets at δ 8.15-8.12, δ 7.66-7.64 and δ 7.38-7.28.

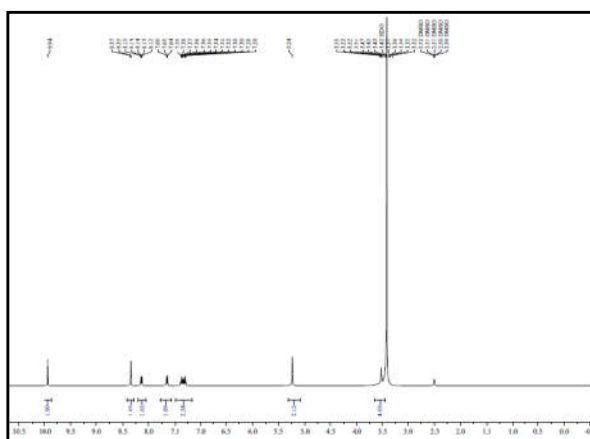


Fig.2.7. ^1H - NMR spectrum of compound 2.1a

The functional group absorptions observed in the FT-IR spectrum and ^1H NMR spectrum are in well agreement with the information obtained from its ^{13}C NMR spectrum. The down field peak at δ 185 is due to the carbonyl peak at position C10. The values at 140 and 137 are attributed to the carbons at position C4 and C8 respectively. The signals at δ 125, 124, 127, 123, 121, 118 and 111 are due to the aromatic carbons. The propargyl groups absorb at δ 78, 77 and 40 corresponding to C12, C15 and C11 carbon atoms (Fig. 2.8).

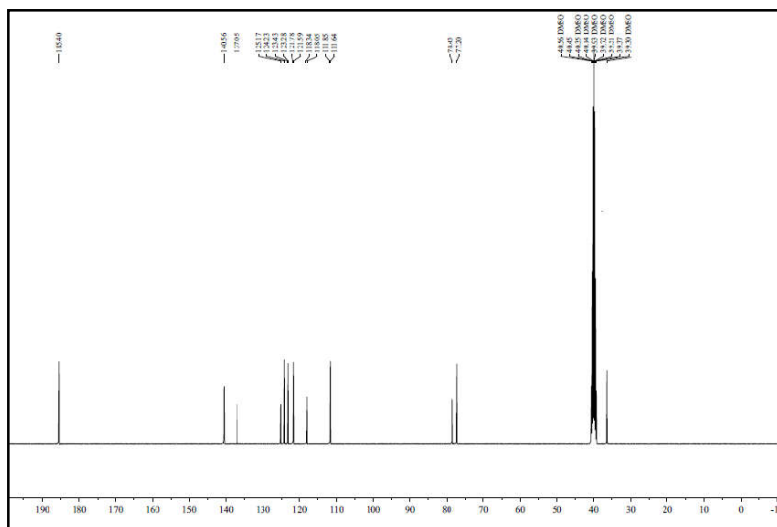


Fig. 2.8. ^{13}C NMR spectrum of compound **2.1a**

The structure of the compound is further confirmed by its mass spectral analysis. The molecular ion peak at 184 (m/z) obtained in MS (ESI) further confirms the structure of the compound **2.1a** (Fig. 2.9).

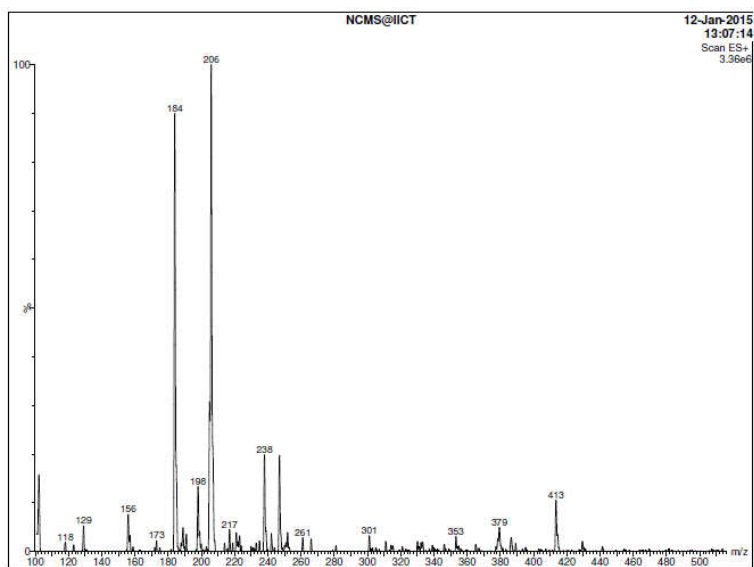


Fig. 2.9: ESI-MS of compound **2.1a**

2.3.2 Structure identification of 2-azido-N-benzyl-N-(2-tert-butylamino)-1-(4-chlorophenyl)-2-oxo ethyl acetamide 2.2a

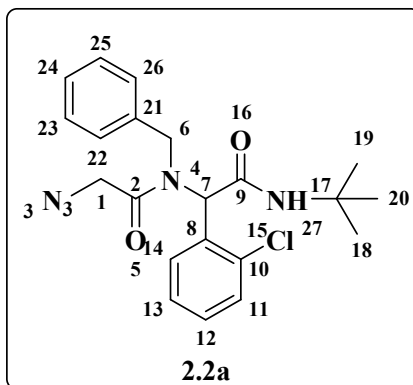


Fig.2.10.structure of **2.2a**

The α -acyl amino acetamide **2.2a** was taken as the representative example for the structure elucidation. The compound is numbered as shown in figure **2.10**. The FT-IR spectrum of the compound showed major absorptions at 3304, 2100, 1659, 1648, 1552. The band observed at 3304 cm^{-1} is due to the NH stretching vibration of the acetamido group. The amide I band, i.e., band due to the C=O stretching vibration observed at 1659 cm^{-1} and the amide II band which arises from the interaction between the N-H bending and the C-N stretching of the C-N-H group is obtained at 1552 cm^{-1} . The absorption at 1648 cm^{-1} is due to the C=O stretching vibration of the ketone group (Fig.2.11).

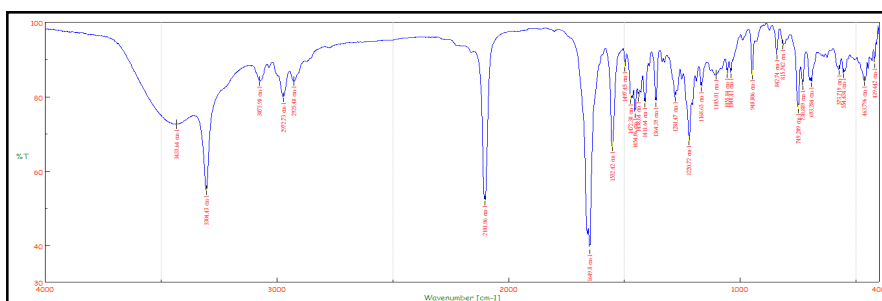
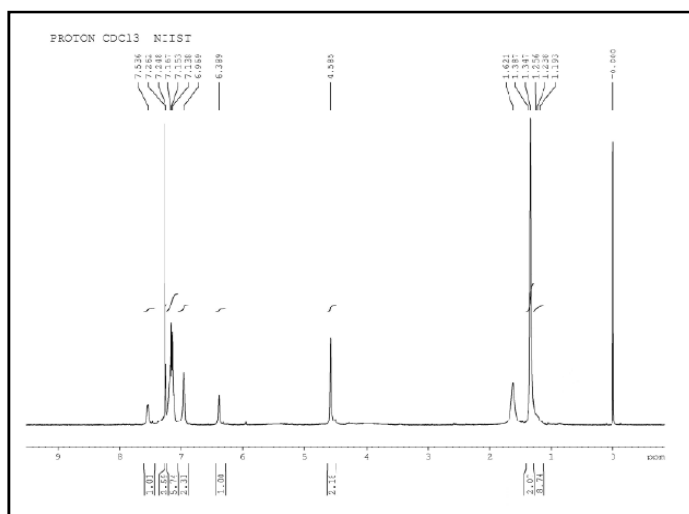


Fig. 2.11. FTIR spectrum of compound **2.2a**

The preliminary information obtained from FT-IR spectrum was further confirmed by ^1H NMR analysis. The 9 proton singlet observed at δ 1.15 corresponds to the three $-\text{CH}_3$ group present at position at 18, 19 and 20. The singlet at δ 1.62 is due to the $-\text{CH}_2$ group at the position 1. The singlet observed at δ 4.58 is attributed to $-\text{CH}_2$ protons at position 6. The singlet at δ 6.38 is attributed to $-\text{CH}$ proton at position 7. The aromatic protons were observed between δ 6.95-7.26. The NH proton singlet observed was observed at δ 7.53 (Fig. 2.12).



The structure was further confirmed by ^{13}C NMR analysis. The peaks observed at δ 30.6, 30.8, 31.1 corresponds the carbons at position 18, 19 and 20. The peak observed at δ 42.7 corresponds to the carbon at position 6. The peak observed at δ 48.3 corresponds to the carbon at position 17. The peak observed at δ 51.7 corresponds to the carbon at position 1. The peak at δ 52.2 corresponds to the carbon at position 7. The aromatic protons were observed at δ 126.8-129.7, and at 130.1-137.9. The peak observed at δ 167.0 corresponds to the carbon at position 9 and the signal due to carbon at position 9 was observed at δ 167. 2 (Fig. 2.13).

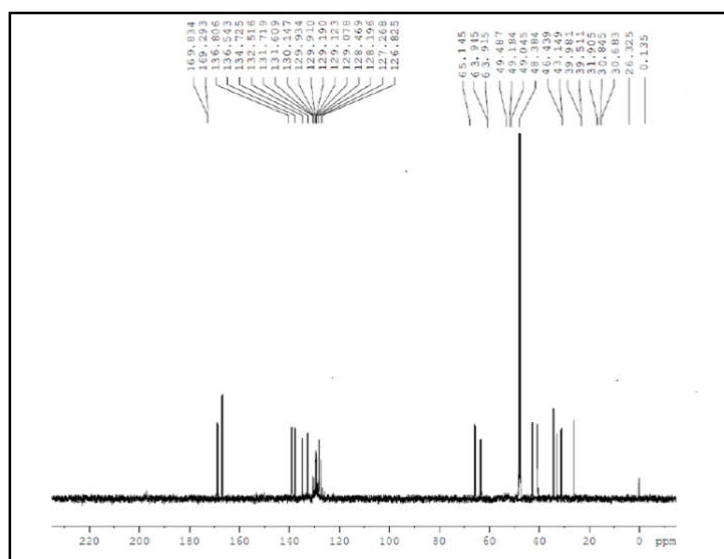


Fig. 2.13. ^{13}C NMR spectrum of compound 2.2a

The structure of the compound is further confirmed by its mass spectral analysis. The molecular ion peak at 414.4 (m/z) obtained in MS (ESI) further confirms the structure of the compound 2.2a (Fig. 2.14).

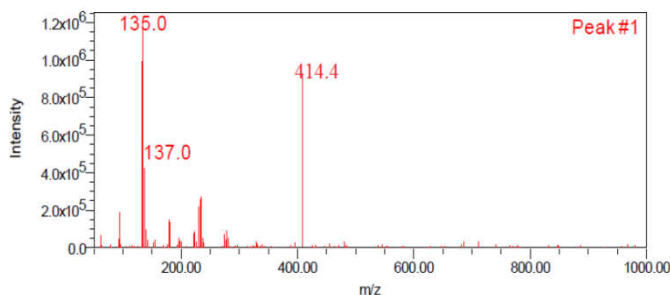


Fig. 2.14. ESI-MS of compound 2.2a

2.3.3. Structure identification of *N*-benzyl-*N*-(2-(*tert*-butylamino)-1-(3-nitrophenyl)-2-oxoethyl)-2-(4-(3-formyl-1*H*-indole-1-yl)methyl)-1*H*-1,2,3-triazol-1-yl)acetamide 2.3a

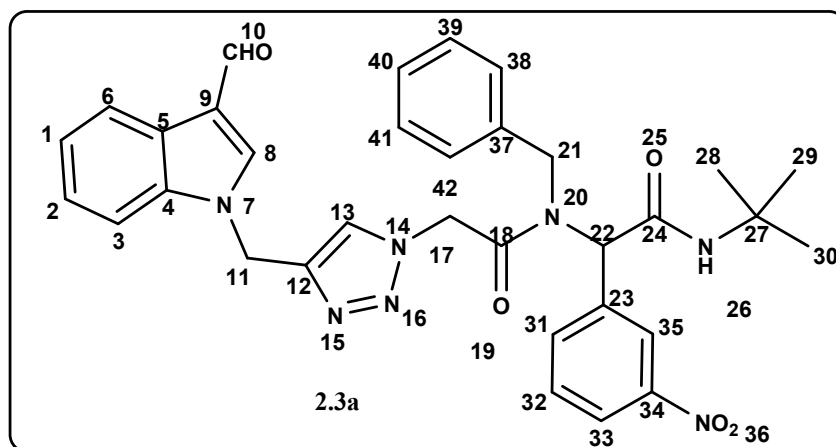


Fig. 2.15. structure of 2.3a

The Indole-triazole-carboxamide **2.3a** is taken as a representative example of this library for the structure elucidation. The compound is numbered as shown in figure **2.15**. The FT-IR spectrum of the compound shows major absorptions at 3422, 1664, 1650, 1582, 1532, 1508 cm^{-1} . The band at 3422 cm^{-1} is due to the NH stretching

vibration of the acetamido group. The amide I band, i.e., band due to the C=O stretching vibration occurs at 1650 cm^{-1} and the amide II band which arises from the interaction between the N-H bending and the C-N stretching of the C-N-H group is obtained at 1582 cm^{-1} . The absorption at 1664 cm^{-1} is due to the C=O stretching vibration of the aldehydic part (Fig. 2.16).

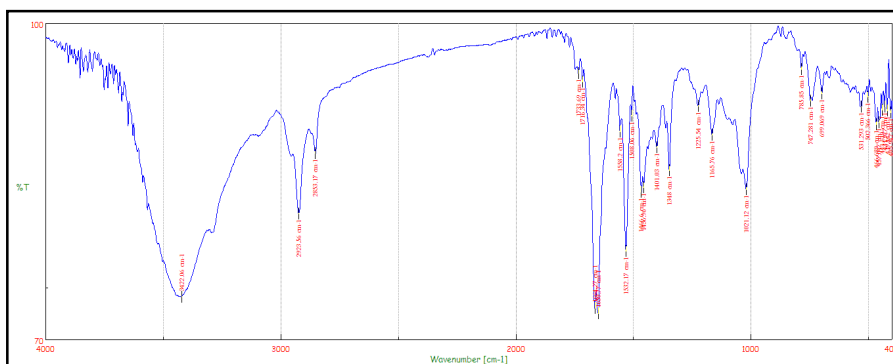


Fig. 2.16. FTIR spectrum of compound 2.3a

The initial information obtained from FT-IR spectrum was further confirmed by ^1H NMR studies (Fig. 2.17). The 9 proton singlet observed at δ 1.24 corresponds to the three $-\text{CH}_3$ group at the position at 28, 29 and 30. The singlet observed at δ 5.37 due to the CH_2 proton at position 21. The singlet at δ 5.63 is due to the CH_2 proton at position 17. The singlet proton observed at δ 5.84 was attributed to $-\text{CH}$ proton at position 14. The singlet proton at δ 5.33 is due to the $-\text{CH}_2$ proton at C-11. The singlet proton at δ 6.14 is due to the $-\text{CH}$ proton at position 22. The aromatic protons were observed as five set of signals. 5 proton multiplet at δ 7.52-7.04, a singlet at δ 7.54, four proton multiplet between δ 7.99-7.67, five proton multiplet between 8.38-8.03 and a

singlet at δ 8.40. The singlet observed at δ 9.94 is attributed to aldehydic proton at position 10.

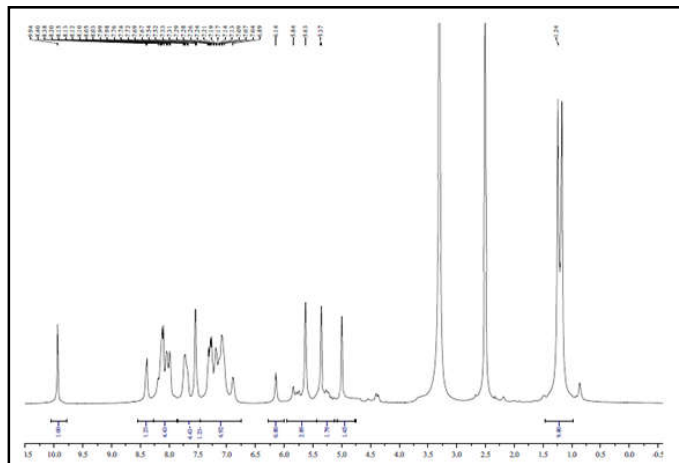


Fig. 2.17. ¹H- NMR spectrum of compound **2.3a**

The structure was further confirmed by ¹³C NMR. The peak at δ 28.5 corresponds to the carbon at 28, 29 and 30th position. The peak observed at 48.5 corresponds to the carbon atom at positions 21. The peak at δ 51.08 corresponds to the carbon at position 11. The peak observed at δ 51.68 corresponds to the carbon at position 17. The peak at 61.0 corresponds to the carbon at position 27. The aromatic carbons are observed at δ 111.8-117.8, 121.4-128.6, 130.1-137.3, 141.0-147.8, 167.6 and 167.7. The signal at δ 185.1 corresponds to the carbon at position 10 (Fig. **2.18**).

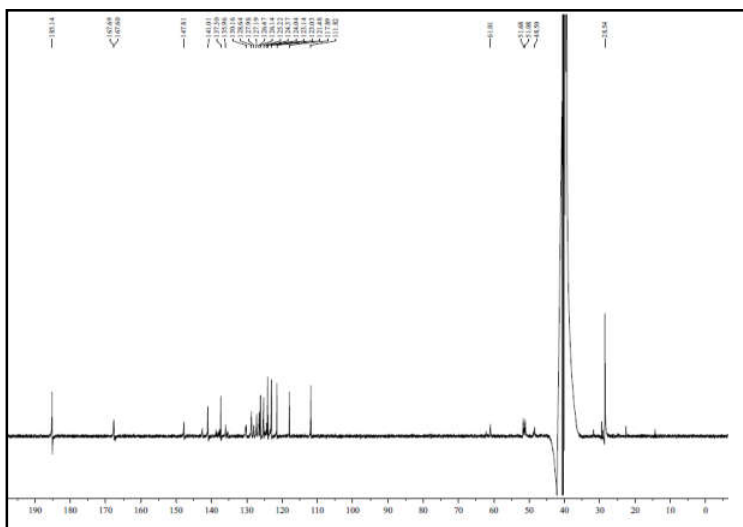


Fig. 2.18. ^{13}C NMR spectrum of compound **2.3a**

The peak at m/z 631 $[\text{M}+\text{Na}]^+$ in the mass spectrum (Fig. 2.19) further confirms the structure of the compound.

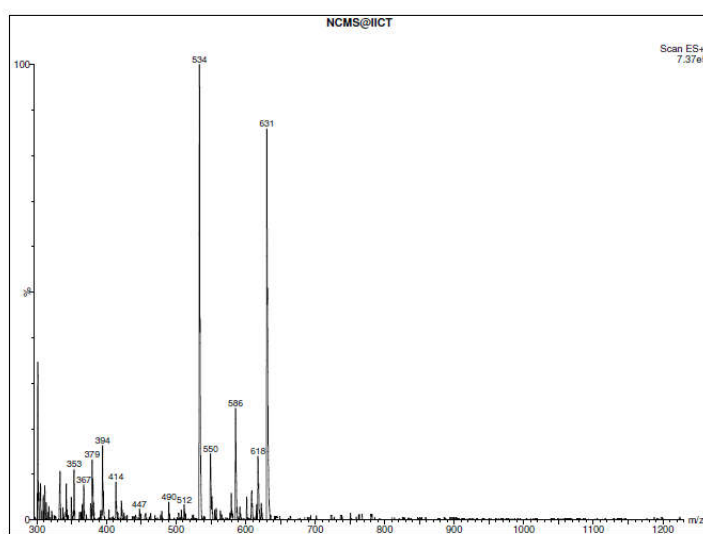


Fig. 2.19: EI-MS of compound **2.3a**

2.4. Conclusion

In conclusion, in this chapter we have discussed the development of a convenient methodology for the synthesis of a series of indole based bifunctional peptidomimetics using a build-pair concept. The structural scaffolds were derived from the readily available building blocks based on multicomponent coupling strategy and the fragments thus generated were assembled by copper (I) catalysed [3+2] azide -alkyne cycloaddition. Three series of Indole triazole carboxamide peptidomimetics (ICT-1, ICT-2 and ICT-3) were synthesised in good to excellent yield. The *invitro* screening of the biological properties of the molecules via experimental and computational methods are discussed in chapter 3.

2.5. Experimental Section

2.5.1 Materials and methods

All solvents and reagents were of reagent grade quality from Aldrich Chemical Company, Fluka, or Merck and used without any further purification. Reactions were monitored by thin-layer chromatography (TLC) using plates prepared with Merck silica gel G by irradiation with UV light and/or treatment with iodine. Fourier transform infrared (FT-IR) spectra were recorded on a Jasco FTIR-4100 spectrometer. The ¹H- and ¹³C-nuclear magnetic resonance (NMR) spectra operating at the frequencies of 400 and 100 MHz respectively were measured with Varian NMR (VNMRS-400) spectrometer and the ¹H- and ¹³C-nuclear magnetic resonance (NMR) spectra operating at the frequencies of 300 and 75 MHz respectively were measured with

Bruker ACF 300 MHz spectrometer in dimethylsulphoxide-*d* (DMSO-*d*₆). The ¹H NMR Chemical shifts are reported in parts per million (ppm) relative to TMS as internal standard (δ= 0 ppm). The coupling constants are reported in hertz (Hz). Mass (FAB) spectra are recorded on a JEOL JMS600H spectrometer. Absorption spectra of the compounds were recorded on JASCO V 550 UV/Vis spectrophotometer and Fluorescence measurements were carried out on Perkin Elmer LS 55 spectrophotometer.

2.5.2. Typical experimental procedure for the synthesis of -(prop-2-yn-1-yl)-1H indole-3-carbaldehyde 2.1a : Commercially available indole-3-carbaldehyde (145.15mg, 1mmol) and potassium carbonate (414.63mg, 3mmol) were dissolved in minimum amount of DMF, and stirred at 50⁰C for 10 min and then cooled to room temperature. To this, propargyl bromide (118.96mg, 1mmol) was added and stirred for another 4 h. After completion of the reaction (monitored by TLC), the reaction mixture was poured into ice cold water. The solid product obtained was filtered and dried under vacuum to afford (prop-2-yn-1-yl)-1H indole-3-carbaldehyde **2.1a**

1-(prop-2-yn-1-yl)-1H indole-3-carbaldehyde 2.1a: white solid ; 159mg (yield 87%); Mp 90-93⁰C ; IR (KBr) ν_{\max} :3198, 2121, 1656, 1644, 1615, 1579, 1528, 1471, 1441, 1308, 1244, 1163, 1041, 770, 741, 562 cm⁻¹. ¹H NMR (DMSO-*d*₆, 400 MHz) δ_{H} (ppm): 9.94 (1H,s), 8.37-8.35(1H, d=8Hz), 8.15-8.12(1H, m),7.66-7.64(1H,m),7.38-7.28(2H,m), 5.24(2H,s), 3.43(1H,s).¹³CNMR(DMSO-*d*₆,100MHz) δ_{C} (ppm):185.4, 140.5,137.0, 125.1,124.2, 123.4, 121.7, 118.3, 111.8, 78.4,77.2, 40.4; MS(ESI): m/z =184 [M+1]⁺.

1-(1-(prop-2-yn-1-yl)-1H-indol-3-yl)ethanone 2.1b: White solid; 167mg (yield 85%);Mp 103-105°C ; IR (KBr) ν max : 3218, 2125, 1676, 1628, 1578,1523, 1388, 1211, 932, 762, 747 cm^{-1} ; ^1H NMR (DMSO- d_6 , 500 MHz) δ_{H} (ppm): 8.40(1H,s), 7.91(1H,s), 7.35-7.32(1H,m), 7.26(2H,s), 4.92(2H,s), 2.17(1H,s), 1.56(3H,s); ^{13}C NMR (DMSO d_6 , 125MHz) δ_{C} (ppm):195.4, 140.5, 137.0, 125.1, 124.2, 123.2, 121.5, 118.0, 111.6, 78.4,77.2, 40.4, 25.1. MS (HRMS): m/z = 221.0739 [M+Na] $^+$.

Prop-2-yn-1-yl 1H-indole-3- carboxylate 2.1c: White solid ; 163mg (yield 82%) ;Mp 80-82°C; IR (KBr) ν max :3298, 3282, 2120,1698, 1698, 1619, 1539, 1271, 1245, 1183, 1149, 1095, 916, 774, 749, 626 cm^{-1} . ^1H NMR (DMSO- d_6 , 400 MHz) δ_{H} (ppm):12.00 (1H,S); 8.05-8.00 (2H, m); 7.66-7.64 (1H, d j=8Hz); 7.35-7.27 (2H,m), 5.23 (2H,S); 3.56 (1H,S). ^{13}C NMR (DMSO- d_6 , 100 MHz) δ_{C} (ppm): 163.8,136.8,126.6,122.9,121.9,121.1,120.7,112.9,111.7,79.6,76.9,51.4 ; MS(ESI): m/z = 222 [M+Na] $^+$.

2.5.3. Typical experimental procedure for the synthesis of 2-azido-N-benzyl-N-(2-tert-butylamino)-1-(4-chlorophenyl)-2-oxo ethyl acetamide 2.2a: An equimolar amount of 2-chlorobenzaldehyde (140 mg, 1 mmol), and benzyl amine (107 mg, 1 mmol), was taken in dichloromethane (8 ml), and stirred at room temperature for 20 min to form the Schiff-base. To this, 1 equivalent of tertiary -butyl isocyanide (94 mg, 1 mmol) and chloroacetic acid (83 mg, 1 mmol) were added and stirring was continued at room temperature. The reaction was monitored by TLC and found to complete after 72 h. The solvent was

evaporated under vacuum and the residue obtained was washed with petroleum ether (5 -15 ml) to afford the chloro derivative of the Ugi product. In a subsequent step, the Ugi chloride (407 mg, 1 mmol), K_2CO_3 (414 mg, 3 mmol), and NaN_3 (65 mg, 1 mmol) were stirred at room temperature for 4 h in dimethyl formamide. After completion of the reaction, the reaction mixture was poured into ice cold water. The solid product obtained was filtered and dried under vacuum to afford 2- $\{[N\text{benzyl-(N-1-azidopropan-2-one)-N-tert-butyl-2-(2-chlorophenyl)}]\}$ acetamide **2.2a**.

2-azido-N-benzyl-N-(2-tert-butylamino)-1-(4-chlorophenyl)-2-oxoethyl acetamide 2.2a : White solid ; 0.335 g (yield 81%) ; IR (KBr) ν_{max} : 3304, 3073, 2972, 2925, 2100, 1659, 1648, 1552, 1497, 1472, 1454, 1438, 1411, 1365, 1282, 1220, 1168, 1055, 1040, 994, 842, 816cm^{-1} . ^1H NMR ($CDCl_3$, 500 MHz) δ_{H} (ppm): 1.25 (s, 9H), 1.62 (s, 2H), 4.58 (s,2H), 6.38 (s, 1H), 6.95–7.26 (m, 9H), 7.53 (s, 1H). ^{13}C NMR (DMSO-(d6), 125 MHz); δ_{C} (ppm): 31.1, 42.7, 48.3, 51.7, 52.2, 126.8, 127.2, 128.4, 129.6, 129.7, 130.1, 132.5, 134.7, 137.7, 137.9, 167.0, 167.2;MS(EI):m/z= 414.4 $[M]^+$.

2-azido-N-benzyl-N-(2-tert-butylamino)-1-(2-chlorophenyl)-2-oxoethyl acetamide 2.2b: White solid; 0.368 g (89 %) ; IR (KBr) ν_{max} : 3294, 2102,1660, 1650, 1560,1491, 1455, 1409, 1364, 1223, 1092, 949, 818, 724, 694 cm^{-1} . ^1H NMR ($CDCl_3$, 500 MHz) δ_{H} (ppm): 7.97(1H,s), 7.26-6.9(9H,m), 6.20(1H,s), 4.88 (2H,s), 2.42 (2H,s), 1.20 (9H,s), ^{13}C NMR (DMSO-(d6),125MHz) δ_{C} (ppm): 169.9, 168.8, 136.7, 132.4,131.0,130.1,128.5,128.0,127.2,126.7,70.1, 56.7, 51.8, 48.5, 28.5.

2-azido-N-butyl-N-(2-tert-butylamino)-1-(4-chlorophenyl)-2-oxo ethyl acetamide 2.2e: White solid; 0.303g(80%); IR(KBr) ν_{\max} : 3300, 2960, 2933, 2104, 1654, 1544, 1491, 1420, 1365, 1274, 1219, 1196, 1132, 1089, 1017, 930, 837, 609, 479 cm^{-1} ; ^1H NMR (CDCl_3 , 500 MHz) δ_{H} (ppm): 8.48 (1H,s), 7.68 (1H,d=1Hz), 7.12 (1H,d=1.5Hz), 4.42(1H,s), 3.37(2H,t), 2.12(1H,s), 1.58(2H,q), 1.37(9H,s), 1.07(2H,m), 0.71(3H,t); ^{13}C NMR (DMSO-(d₆), 125 MHz) δ_{C} (ppm): 168.5, 168.6, 134.0, 133.0, 131.0, 129.0, 61.0, 51.0, 50.0, 45.0, 32.0, 28.0, 20.0, 13.0.

2-azido-N-benzyl-N-(2-tert-butylamino)-1-(2-fluorophenyl)-2-oxo ethyl acetamide 2.2f: White solid; 0.337g (85%); IR (KBr) ν_{\max} : 3351, 2102, 1685, 1647, 1547, 1490, 1454, 1225, 759 cm^{-1} ; ^1H NMR (CDCl_3 , 500MHz) δ_{H} (ppm): 8.75(1H,s); 7.57-6.79(10H,m); 5.80(1H,s); 4.94(2H,s); 2.171(2H,s); 1.253(9H,s); ^{13}C NMR(DMSO(d₆), 125MHz) δ_{C} (ppm): 169.0, 168.0, 161.0, 136.0, 131.0, 128.0, 127.0, 127.5, 127.2, 124.0, 122.0, 116.0, 65.0, 55.0, 50.0, 48.0, 29.0.

2-azido-N-butyl-N-(2-tert-butylamino)-1-(4-fluorophenyl)-2-oxo ethylacetamide 2.2h: White solid; 0.312g(86%) IR(KBr) ν_{\max} : 3308, 2966, 2107, 1674, 1651, 1542, 1509, 1455, 1421, 1362, 1278, 1221, 1192, 1160, 1130, 871, 847, 795, 598, 527, 513, 460 cm^{-1} ; ^1H NMR(CDCl_3 , 500 MHz) δ_{H} (ppm): 8.11(1H,s), 7.26 (2H,m), 7.24-7.23 (2H,d, J=9Hz), 6.11 (1H,s), 3.49(2H,t), 2.17(2H,s), 1.61(2H,m), 1.31(9H,s), 1.29(2H,m), 0.97 (3H, t), ^{13}C NMR (DMSO-(d₆), 125MHz) δ_{C} (ppm): 169.9, 168.8, 161.6,

132.4,131.0,116.4,70.1,56.7,51.8,46.1,28.5,19.9,13.3.MS(HRMS): m/z =386.1969 [M+Na]⁺.

2-azido-N-butyl-N-(2-tert-butylamino)-1-(2-chlorophenyl)-2-oxoethyl acetamide 2.2i: White solid; IR(KBr)_{max} :3321, 2963, 2931, 2106, 1680, 1644, 1553, 1508, 1457, 1418, 1365, 1277, 1223,1 121,1 052, 936, 856, 761, 603, 554cm⁻¹. ¹HNMR (CDCl₃,500MHz) δ_H(ppm): 8.02, (1H,s), 7.55 (1H,s), 7.38-7.37 (1H,d=6.5Hz), 7.19 (1H,t), 7.11(1H,t), 6.02(1H,s) 4.04(2H,t), 2.19 (2H,s), .64 (9H,s), 1.40 (2H,m), 1.07(2H,m), 0.71 (3H,t), ¹³CNMR (DMSO-(d₆), 125MHz) δ_C(ppm): 169.0, 168.1, 136.1, 132.5, 130.8, 124.5, 122.5, 122.4, 56.7, 51.8, 46.1, 31.6, 28.5, 19.9, 13.3.

2.5.4. Typical experimental procedure for the synthesis of N-benzyl-N-(2-(tert-butylamino)-1-(3-nitrophenyl)-2-oxoethyl) -2-(4-(3-formyl-1H-indole-1-yl)methyl)-1H-1,2,3-triazol-1-yl)acetamide 2.3a: The alkyne functionalized indole-3-carbaldehyde **2.1a**(183mg, 1 mmol) and the Ugi azide **2.2d** (424mg, 1 mmol) were dissolved in minimum amount of DMSO. To this, 2 ml of *t*-BuOH, 1 ml of water, CuSO₄ 5H₂O (11 mg), and sodium ascorbate (50 mg) were added and stirred at room temperature for 12 h. After 12 h, the mixture was poured in to cold water. The precipitated solid was collected and washed with water and dried. The dried product was washed with diethyl ether (3.5 ml) to afford **2.3a**.

N-benzyl-N-(2-(tert-butylamino)-1-(3-nitrophenyl)-2-oxoethyl)-2-(4-(3-formyl-1H-indole-1-yl)methyl)-1H-1,2,3-triazol-1-yl)

Acetamide 2.3a: White solid; 559mg (92%); Mp 145-150°C; IR(KBr) ν_{\max} : 292, 2853, 1664, 1650, 1582, 1532, 1508, 1466, 1401, 1348, 1225, 1165, 1021, 785, 747, 699, 531, 502 cm^{-1} ; ^1H NMR (CDCl_3 , 400 MHz) δ_{H} (ppm): 9.94(1H, s), 8.40 (1H,s), 8.38-8.03(5H,m), 7.99-7.67(4H,m); 7.54 (1H,s), 7.52-7.04 (5H,m), 6.14 (1H,s), 5.84(2H,s), 5.63(2H,s), 5.37(2H,s), 1.24 (9H,s); ^{13}C NMR (DMSO-(d₆), 100MHz) δ_{C} (ppm): 185.1, 167.6, 167.6, 147.8, 141.0, 137.3, 135.9, 130.1, 128.6, 127.9, 127.1, 126.4, 125.2, 124.3, 124.0, 123.1, 123.0, 121.4, 117.8, 111.8, 61.0, 51.6, 51.0, 48.5, 28.5; MS (ESI):m/z= 631 [M+Na]⁺.

N-(tert-butyl)-2-(N-butyl-2-(4-(3-formyl-1H-indole-1-yl)methyl)-1H-1,2,3-triazol-1-yl)acetamido)-2-(2-fluorophenyl)acetamide 2.3b:

White solid; 492mg (90%); Mp 173-176°C; IR(KBr) ν_{\max} : 2962, 2931, 2814, 1659, 1613, 1579, 1531, 1489, 1364, 1336, 1283, 1228, 1169, 1135, 1111, 1098, 1052, 1038, 973, 938, 897, 838, 786, 751, 671, 599, 576 cm^{-1} , ^1H NMR(CDCl_3 , 400MHz) δ_{H} (ppm): 9.90 (1H,s), 8.49(1H,s), 8.15(1H,s), 7.75-7.73(1H,d=8Hz), 7.5(1H,s), 7.49-7.25(6H,m), 5.91(1H,s), 5.64(2H,s), 5.42(2H,s), 3.67-3.44(2H,t), 1.48-1.33(2H,m), 1.32(9H,s), 1.23-0.98(2H,m), 0.69-0.66(3H,t), ^{13}C NMR (DMSO-(d₆), 100MHz) δ_{C} (ppm): 185.1, 168.4, 167.8, 166.6, 142.4, 137.3, 136.1, 135.7, 133.0, 131.2, 130.6, 129.1, 128.8, 126.0, 125.2, 124.0, 123.0, 121.4, 117.8, 111.8, 62.2, 60.2, 51.2, 50.9, 45.8, 28.7, 20.0, 19.8, 13.9.

N-benzyl-N-(2-(tert-butylamino)-1-(4-fluorophenyl)-2-oxoethyl)-2-(4-(3-formyl-1H-indole-1-yl)methyl)-1H-1,2,3-triazol-1-yl)acetamide

2.3c: White solid; 522mg (90%); Mp 180-185^oC; IR(KBr) ν_{\max} :3288,3080, 2973, 2924, 1653, 1608, 1578,1556, 1532, 1509, 1466, 1403, 1364, 1340, 1300, 1224, 1160, 1136, 1050, 950, 786, 747 699, 644, 602, 508cm⁻¹; ¹HNMR(CDCl₃, 00MHz) δ_{H} (ppm): 9.93(1H,s), 8.38(1H,s),8.11(1H,S), 7.88(1H,s), 7.30-6.93(13H,m), 6.09(1H,s), 5.69(2H,s), 5.62(2H,s), 5.33(2H,s), 1.18(9H,s)¹³CNMR (DMSO(d₆), 100MHz) δ_{C} (ppm):185.1, 168.6, 67.4, 140.9, 138.0, 137.2, 131.6, 131.5, 128.6, 128.0, 127.3, 127.1, 126.3, 126.1, 125.2, 124.0, 123.0, 121.4, 117.8, 115.5, 115.3, 111.8, 60.7, 51.6, 50.9, 48.1, 28.5.MS(ESI):m/z= 604[M+Na]⁺.

N-(tert-butyl)-2-(N-butyl-2-(4-(3-formyl-1H-indole-1-yl)methyl)-1H-1,2,3-triazol-1-yl)acetamido)-2-(4-chlorophenyl)acetamide

2.3d: White solid; 501mg(89%); Mp175-180^oC; IR(KBr) ν_{\max} :3289, 3106, 2961, 2930, 2870, 1652, 1558, 1530, 1490, 1467, 1448, 1410, 1364, 1338, 1298, 1223, 1172, 1134, 1051, 937, 844, 751cm⁻¹. ¹HNMR(CDCl₃,400MHz) δ_{H} (ppm):9.94(1H,s),8.40(1H,s), 8.13(1H,s), 8.11(1H,s), 7.51-7.25(7H,m), 7.75(1H,s), 5.91(1H,s), 5.64(2H,s), 5.42(2H,s), 1.23-0.66(9H,m), 1.32(9H,s); ¹³CNMR(DMSO(d₆), 100MHz) δ_{C} (ppm):185.1, 168.4, 167.8, 142.4, 140.9, 137.3, 136.1, 135.7, 133.0, 131.2, 130.6, 129.1, 128.8, 126.0, 125.2, 124.0, 123.0, 121.4, 117.8, 111.8, 62.2, 60.6, 51.7, 51.2, 50.9, 45.8, 28.7,78.6, 20.0, 19.8, 13.9, 13.7; MS(ESI):m/z= 586[M+Na]⁺.

N-benzyl-N-(2-(tert-butylamino)-1-(2-fluorophenyl)-2-oxoethyl)-2-(4-(3-formyl-1H-indole-1-yl)methyl)-1H-1,2,3-triazol-1-yl)

Acetamide(3e): White solid; 522mg(90%); Mp 158-163°C; IR(KBr) ν_{\max} : 2966, 2925, 1655, 1579, 1531, 1490, 1465, 1402, 1364, 1230, 1166, 1136, 1098, 1039, 946, 786, 751, 699, 508 cm^{-1} ; ^1H NMR (CDCl_3 , 400 MHz) δ_{H} (ppm): 9.93(1H,s), 8.37(1H,s), 8.12(1H,s), 7.93(1H,s), 7.45-69.5 (13H,m), 6.06(1H,s), 5.73(2H,s), 5.55(2H,s), 4.92(2H,s); ^{13}C NMR (DMSO-(d₆), 100MHz) δ_{C} (ppm): 185.1, 168.1, 167.2, 162.3, 138.1, 137.6, 137.3, 131.1, 131.0, 130.7, 130.6, 130.3, 129.4, 128.6, 127.9, 127.1, 127.0, 126.6, 126.3, 126.2, 126.0, 125.2, 125.0, 124.6, 124.0, 123.8, 123.7, 123.0, 121.0, 121.4, 117.8, 115.8, 115.6, 115.4, 111.8, 67.3, 57.7, 55.8, 51.6, 51.4, 51.1, 50.9, 48.7, 48.4, 28.6, 28.4.

N-benzyl-N-(2-(tert-butylamino)-1-(4-bromophenyl)-2-oxoethyl)-2-(4-(3-formyl-1H-indole-1-yl)methyl)-1H-1,2,3-triazol-1-yl)acetamide 2.3f:

white solid; 584mg(91%); Mp; 190-195°C; IR (KBr) ν_{\max} : 2916, 2849, 1652, 1559, 1464, 1403, 1165, 1025, 512, 467 cm^{-1} ; ^1H NMR(CDCl_3 , 400MHz) δ_{H} (ppm): 9.93(1H,s), 8.37(1H,s), 8.12(1H,s), 8.10(1H,s), 7.93(1H,s), 7.45-6.95(12H,m), 6.06(1H,s), 5.73(2H,m); 5.55 (2H,s), 4.5(2H,s), 1.2(9H,s); ^{13}C NMR (DMSO-(d₆), 100 MHz) δ_{C} (ppm): 185.2, 168.2, 167.5, 140.9, 137.2, 131.7, 131.5, 128.7, 128.0, 127.3, 127.2, 126.3, 126.1, 125.2, 124.0, 123.0, 121.5, 121.4, 117.8, 111.8, 60.9, 51.6, 50.9, 28.6; MS(ESI): m/z=665[M+Na]⁺.

N-(tert-butyl)-2-(N-butyl-2-(4-(3-formyl-1H-indole-1-yl)methyl)-1H-1,2,3-triazol-1-yl)acetamido)-2-(3-nitrophenyl)acetamide 2.3g:

White solid; 516mg(90%); Mp 160-165°C; IR(KBr) ν_{\max} : 2957, 2928,

2870, 1657, 1561, 1535, 1468, 1448, 1410, 1382, 1348, 1299, 1221, 1171, 1134, 1101, 1051, 937, 838, 751, 700, 612 cm⁻¹. ¹H NMR (CDCl₃, 400 MHz) δ_H (ppm): 9.94 (1H, s), 8.40 (1H, s), 7.91 (1H, s), 8.22-8.07 (4H, m), 7.75-7.69 (3H, m), 7.33-7.26 (2H, m), 6.01 (1H, s), 5.64 (2H, s), 5.52 (2H, s), 3.67 (2H, t), 1.48 (2H, m), 1.33 (12H, m), 0.68 (2H, m); ¹³C NMR (DMSO-d₆, 100 MHz) δ_C (ppm): 185.1, 167.8, 166.8, 148.1, 142.5, 140.9, 139.5, 137.2, 135.9, 130.4, 126.0, 125.2, 124.0, 123.7, 123.2, 123.0, 112.4, 117.8, 111.8, 60.8, 51.0, 48.1, 29.4, 28.6, 19.8, 19.8, 13.7.

N-(tert-butyl)-2-(N-butyl-2-(4-(3-formyl-1H-indole-1-yl)methyl)-1H-1,2,3-triazol-1-yl)acetamido)-2-(4-bromophenyl) acetamide

2.3h: white solid; 553 mg (91%); Mp 185-190 °C; IR (KBr) ν_{max}: 2960, 2932, 2873, 1655, 1605, 1580, 1487, 1455, 1420, 1384, 1364, 1322, 1294, 1258, 1221, 1195, 1132, 1111, 1072, 1036, 1012, 972, 929, 897, 865, 838, 808, 763 cm⁻¹. ¹H NMR (CDCl₃, 400 MHz) δ_H (ppm): 9.93 (1H, s), 8.40 (1H, s), 8.13 (1H, s), 8.10 (1H, s), 7.75 (1H, s), 7.51-7.25 (7H, m), 6.06 (1H, s), 5.64 (2H, s), 5.42 (2H, s), 1.32 (9H, s), 1.23-0.66 (9H, m); ¹³C NMR (DMSO-d₆, 100 MHz) δ_C (ppm): 185.2, 168.3, 167.0, 137.3, 136.1, 135.7, 133.0, 131.2, 130.6, 126.0, 125.2, 124.0, 123.0, 121.4, 117.8, 111.8, 105.8, 70.7, 62.2, 51.7, 45.8, 28.7, 28.6, 20.0, 13.7.

2-(4-((3-acetyl-1H indol-1-yl)methyl)-1H-1,2,3-triazol-1-yl)-N-benzyl-N-(2-(tert-butylamino)-1-(4-chlorophenyl)-2-oxoethyl) acetamide

2.4a: White solid; 507 mg (83%); Mp: 180-185 °C; IR (KBr) ν_{max}: 3294, 3087, 2970, 2926, 1660, 1652, 1559, 1525, 1491, 1454, 1409, 1390, 1364, 1265, 1223, 1206, 1170, 1091, 1015, 951, 873, 841,

818, 745, 724,694,; ¹H NMR(CDCl₃, 400MHz) δ_H(ppm):8.38(1H,s), 8.11(1H,s), 7.88(1H,s), 7.72(2H,s), 7.306.93(10H,m), 6.09(1H,s), 5.69(2H,s), 5.29(2H,s), 4.95(2H,s),2.11(3H,s), 1.18(9H,s); ¹³C NMR(DMSO(d₆),100MHz)δ_C(ppm):195.1, 168.6, 167.4, 140.9, 138.0, 137.2, 131.6, 131.5, 128.6, 128.0, 127.3, 127.1, 126.3, 126.1, 125.2, 124.0, 123.0, 121.4, 117.8, 115.5, 115.3, 111.8, 68.6, 60.7, 51.6, 50.9, 48.1, 28.5, 28.0.

2-(4-((3-acetyl-1H indol-1-yl)methyl)-1H-1,2,3-triazol-1-yl)-N-benzyl-N-(2-(tert-butylamino)-1-(4-fluorophenyl)-2-oxoethyl)

Acetamide 2.4b: white solid; 507mg (83 %); Mp;170-175⁰C;IR(KBr)ν_{max}:3291, 2971, 1659, 1651, 1559, 1526, 1510, 1454,1391, 1365, 1224, 1159, 1029, 952, 847;¹H NMR (CDCl₃, 400 MHz) δ_H(ppm):9.58(1H,s),8.64-8.54(1H,m), 8.38(1H,s), 7.88(1H,s), 7.72-6.93(12H,m), 6.09(1H,s), 5.62(2H,s), 5.29(2H,s), 4.91(2H,s), 4.91(2H,s), 2.18(3H,s),1.18(9H,s); ¹³C NMR(DMSO-(d₆), 100MHz) δ_C(ppm): 195.7, 168.6, 167.4, 160.7, 140.9, 138.0, 137.2, 131.6, 131.5, 128.6, 128.0, 127.3, 127.1, 126.3, 126.1, 125.2, 124.0, 123.0, 121.4, 117.8, 115.5, 115.3, 111.8, 70.9, 60.7, 51.6, 50.9, 48.1, 28.5, 28.3.

2-(4-((3-acetyl-1H indol-1-yl) methyl)-1H-1,2,3-triazol-1-yl)-N-butyl-N-(2-(tert-butylamino)-1-(2-fluorophenyl)-2-oxoethyl)

Acetamide 2.4c: white solid;487mg(87%);Mp;162-165⁰CIR(KBr) ν_{max};3329,3070,2963,2873,2106,1653,1527,1490,1455,1390,1365,1228,1190,1127,1096,1051,932,757cm⁻¹; ¹H NMR (CDCl₃, 400 MHz) δ_H(ppm):9.32(1H,s),8.49(1H,s), 7.75-7.73(1H,d=8Hz),7.51(1H,s), 7.49-7.25(7H,m), 5.91(1H,s), 5.64(2H,s), 5.23(2H,s), 3.67-3.44(2H,t),

2.11(3H,s), 1.48-1.33(2H,m), 1.32(9H,s), 1.23-0.98(2H,m), 0.690-0.66(3H,t); ^{13}C NMR(DMSO(d6), 100MHz) δ_{C} (ppm):195.1, 168.4, 167.8, 166.6, 140.9, 137.3, 136.1, 135.7, 133.0, 131.2, 130.6, 129.1, 128.8, 126.0, 125.2, 124.0, 123.0, 121.4, 117.8, 111.8, 62.2, 60.6, 51.7, 51.2,50.9,45.8,44.9, 39.6, 39.4, 31.7, 31.3, 28.7, 28.6, 20.0,19.8,13.9,13.7.

2-(4-((3-acetyl-1H indol-1-yl)methyl)-1H-1,2,3-triazol-1-yl)-N-benzyl-N-(2-(tert-butylamino)-1-(4-bromophenyl)-2-oxoethyl)

Acetamide 2.4e: white solid ; 571mg (87 %); Mp;198-201 $^{\circ}\text{C}$; IR (KBr) ν_{max} ;3432, 2917, 2849, 1654, 1587,1530, 1466, 1439, 1400, 1387, 1168, 1091, 1038, 749, 420 cm^{-1} ; ^1H NMR (CDCl₃, 400 MHz) δ_{H} (ppm):9.12(1H,s), 8.37(1H,s), 8.12-8.10(1H,d=8 Hz), 7.72(1H,s), 7.45-6.95(12H,m), 6.06(1H,s), 5.55(2H,s), 5.25(2H,s), 4.92(2H,s), 2.12 (3H,s), 1.20(9H,s); ^{13}C NMR (DMSO-(d6), 100MHz) δ_{C} (ppm): 195.1, 168.2, 167.2, 137.2, 131.7, 131.5, 128.7, 128.0, 127.3, 127.2, 126.1, 125.2, 124.0, 123.0, 121.5, 121.4, 117.8, 111.8, 70.1, 60.9, 51.6, 50.9, 46.1, 28.6, 28.5.

2-(4-((3-acetyl-1H indol-1-yl)methyl)-1H-1,2,3-triazol-1-yl)-N-butyl-N-(2-(tert-butylamino)-1-(4-bromophenyl)-2-oxoethyl)

Acetamide 2.4f: White solid ;529mg (85 %); Mp;192-195 $^{\circ}\text{C}$ IR (KBr) ν_{max} ;3441, 2923, 2372, 1654, 1605, 1509, 1412, 1384, 1327, 1178, 1126, 1107, 989, 936, 865, 618 cm^{-1} ; ^1H NMR(CDCl₃,400MHz) δ_{H} (ppm):9.42 (1H,s), 8.40(1H,s), 8.13-8.10(1H,d,j=12Hz), 7.75(1H,s), 6.06(1H,s), 5.64(2H,s), 5.42(2H,s), 2.13(3Hs),1.32(9H,s),1.23-0.66 (9H,m), ^{13}C NMR(DMSO-(d6),100MHz) δ_{C} (ppm):195.2, 168.3, 167.0,

137.3, 136.1, 135.7, 133.0, 131.2, 130.6, 126.0, 125.2, 124.0, 123.0, 121.4, 117.8, 111.8, 105.8, 70.7, 62.3, 51.7, 45.8, 39.8, 39.6, 39.4, 31.7, 30.3, 28.7, 28.6, 20.0, 19.8, 13.9, 13.7.

2-(4-((3-acetyl-1H indol-1-yl)methyl)-1H-1,2,3-triazol-1-yl)-N-butyl-N-(2-(tert-butylamino)-1-(3-nitrophenyl)-2-oxoethyl)

acetamide (4g): white solid ; 512mg (87 %); Mp; 182-186⁰C IR (KBr) ν max;3422, 2961, 2929, 2872, 1662, 1532, 1487, 1455, 1395, 1365, 1339, 1224, 1171, 1124, 1075, 1047, 1012, 936, 750cm⁻¹; ¹HNMR (CDCl₃,400MHz) δ _H(ppm):9.40(1H,s), 8.40(1H,s), 8.228.07(1H,m), 7.91(1H,s), 7.757.69(3H,m), 7.337.26(4H,m), 6.01(1H,s), 5.64(2H,s), 5.48(2H,s), 3.673.44(2H,t), 2.12(3H,s),1.33(9H,s), 1.250.66(7H,m); ¹³CNMR(DMSO(d6),100MHz) δ _C(ppm):194.0, 167.8, 166.8, 148.1, 142.5, 140.9, 139.5, 137.2, 135.9, 130.4, 126.0, 125.2, 124.0, 123.7, 123.2, 123.0, 121.4, 117.8, 111.8, 70.4, 60.8, 55.0, 51.0, 48.1, 29.4, 28.6, 19.8, 19.8, 13.7.

2-(4-((3-acetyl-1H indol-1-yl)methyl)-1H-1,2,3-triazol-1-yl)-N-benzyl-N-(2-(tert-butylamino)-1-(3-nitrophenyl)-2-oxoethyl)

Acetamide 2.4h: White solid;534mg(86%); Mp;185-190⁰CIR(KBr) ν max; 3331, 3145, 3104, 2963, 2932, 2872, 1657, 1614, 1579, 1531, 1466, 1401, 1392, 1348, 1287, 1248, 1222, 1168, 1134, 1051, 1040, 939, 899,841, 786,750,700cm⁻¹; ¹HNMR (CDCl₃,400MHz) δ _H(ppm):9.12(1H,s);8.40(1H,s);8.38- 7.98(4H,m); 7.76-7.67(2H,m); 7.54(1H,s);7.33-7.04(7H,m); 6.14(1H,s); 5.84(2H,s); 5.63(2H,s);5.03(2H,s);2.15(3H,s); 1.24(9H,s); ¹³CNMR(DMSO(d6), 100MHz) δ _C(ppm):194.3, 167.6, 167.6, 147.8, 141.0, 137.3, 135.9,

130.1, 128.6, 127.9, 127.1, 126.4, 126.1, 125.2, 124.3, 124.0, 123.1, 123.0, 121.4, 117.8, 111.8, 71.0, 61.0, 51.0, 48.5, 28.6, 28.5.

(1-(2-benzyl(2-tert-butylamino)-1-(2-chlorophenyl)-2-oxoethyl)

amino)-2-oxoethyl)-1H-1,2,3-triazol-4-yl)methyl-1H-indole-3-

carboxylate 2.5a: White solid; 539mg (88%); Mp; 120-124⁰C;

IR(KBr) ν_{\max} : 2924, 1671, 1534, 1439, 1365, 1225, 1169, 1083, 1018,

751, 697, 506 cm⁻¹; ¹H NMR(CDCl₃, 400 MHz) δ_{H} (ppm): 11.99(1H, s);

8.16(1H, s) 8.01(1H, s); 8.00(1H, s) 7.71(1H, s); 7.707.05(12H, m);

6.30(1H, s); 5.88(2H, s); 5.50(2H, s); 4.93(2H, s); 1.14(3H, s);

¹³C NMR(DMSO(d₆), 100 MHz) δ_{C} (ppm): 168.0, 167.9, 164.0, 142.7,

137.9, 136.5, 135.9, 134.6, 133.8, 130.0, 129.8, 129.7, 128.5, 128.5,

127.9, 127.8, 127.4, 126.6, 126.3, 123.1, 122.9, 121.9, 120.9, 112.9,

64.0, 61.1, 59.9, 58.5, 48.5, 28.5; MS(ESI): m/z = 636[M+Na]⁺.

(1-(2-benzyl(2-tert-butylamino)-1-(4-chlorophenyl)-2-oxoethyl)

amino)-2-oxoethyl)-1H-1,2,3-triazol-4-yl)methyl-1H-indole-3-

carboxylate 2.5b: White solid; 503mg (82%); Mp; 113-

116⁰C; IR(KBr) ν_{\max} : 2966, 1671, 1535, 1458, 1402, 1361, 1229, 1175, 1087,

1024, 748 cm⁻¹; ¹H NMR(CDCl₃, 400 MHz) δ_{H} (ppm): 11.94(1H, s), 8.16

(1H, s), 8.12(1H, s), 8.08(1H, s), 8.05(1H, s), 8.00(1H, s), 7.94(1H, s),

7.92(1H, s), 7.69(1H, s), 7.64-6.95(8H, m), 6.10(1H, s), 5.73(2H, s),

5.38(2H, s), 4.95(2H, s), 1.19(9H, s); ¹³C NMR(DMSO(d₆),

100 MHz) δ_{C} (ppm): 168.3, 167.5, 164.0, 142.7, 137.9, 136.5, 135.2,

133.1, 130.7, 128.6, 128.0, 127.2, 127.0, 125.9, 122.9, 122.6, 121.1,

120.8, 112.8, 111.8, 106.4, 76.8, 62.4, 60.8, 56.9, 48.1, 28.5; m/z =

635[M+Na]⁺

(1-(2-benzyl(2-tert-butylamino)-1-(2-fluorophenyl)-2-oxoethyl)amino)-2-oxoethyl)-1H-1,2,3-triazol-4-yl)methyl-1H-indole-3-carboxylate 2.5c: White solid; 502mg (84%); Mp; 145-150⁰C; IR(KBr) ν_{max} : 2969, 1653, 1558, 1540, 1508, 1489, 1455, 1396, 1364, 1339, 1228, 1178, 1096, 754, 697, 618 cm^{-1} ; ¹H NMR(CDCl₃, 400MHz) δ_{H} (ppm): 11.93 (1H,s), 8.24(1H,s), 8.08(1H,s), 8.04(1H,s), 7.94(1H,s), 7.31-7.04(12H, m), 6.30(1H,s), 5.38(2H,s), 4.74(2H,s), 4.50(2H,s), 1.16(9H,s); ¹³C NMR (DMSO-(d₆), 100MHz) δ_{C} (ppm): 168.1, 167.5, 167.2, 164.0, 142.7, 137.5, 136.5, 131.1, 130.7, 128.6, 128.0, 127.8, 127.0, 125.0, 124.6, 122.6, 122.4, 122.2, 121.9, 121.0, 115.6, 112.9, 111.8, 105.8, 57.7, 55.8, 51.5, 50.9, 48.4, 28.6

(1-(2-benzyl(2-tert-butylamino)-1-(4-fluorophenyl)-2-oxoethyl)amino)-2-oxoethyl)-1H-1,2,3-triazol-4-yl)methyl-1H-indole-3-carboxylate 2.5d: White solid; 507mg (85%); Mp; 140-145⁰C; IR(KBr) ν_{max} : 2923, 2360, 1667, 1533, 1509, 1455, 1365, 1227, 1161, 1123, 1019, 751, 697 cm^{-1} ; ¹H NMR (CDCl₃, 400 MHz) δ_{H} (ppm): 11.41(1H,s), 8.23 (1H,s), 8.17(1H,s), 8.07(1H,s), 7.68(1H,s), 7.49-6.93(12H,m), 6.08(1H,s), 5.57(2H,s), 5.37(2H,s), 4.91(2H,s), 1.38(9H,s); ¹³C NMR(DMSO-(d₆), 100MHz) δ_{C} (ppm): 168.6, 167.5, 164.4, 160.8, 142.8, 138.0, 136.5, 132.3, 131.6, 128.6, 128.0, 127.3, 126.0, 122.9, 122.2, 121.9, 120.7, 115.8, 112.8, 111.7, 106.4, 77.6, 62.4, 60.8, 56.8, 48.1, 28.6.

(1-(2-butyl(2-tert-butylamino)-1-(4-chlorophenyl)-2-oxoethyl)amino)-2-oxoethyl)-1H-1, 2, 3-triazol-4-yl) methylindole-3-carboxylate 2.5e: White solid; 480mg(83%); Mp; 109-113⁰C; IR(KBr) ν_{\max} : 2961, 2932, 2873, 1652, 1534, 1491, 1455, 1394, 1365, 1339, 1223, 1169, 1125, 1090, 1044, 1016 cm⁻¹. ¹H NMR (CDCl₃, 400MHz) δ_{H} (ppm): 11.94(1H,s), 8.26(1H,s), 8.18(1H,s), 8.00(1H,s), 7.80(1H,s), 7.50-7.18(5H,m), 5.92(1H,s), 5.51(2H,s), 4.92(2H,s), 3.4(2H,t), 1.33-0.67 (16H,m); ¹³CNMR(DMSO-(d₆), 100MHz) δ_{C} (ppm): 168.5, 166.7, 164.4, 142.3, 136.8, 135.9, 133.4, 129.1, 128.8, 126.0, 122.9, 122.2, 121.8, 120.7, 112.9, 111.1, 106.5, 77.6, 62.2, 60.7, 56.8, 45.8, 29.4, 28.7, 20.0, 13.7.

(1-(2-butyl(2-tert-butylamino)-1-(2-fluorophenyl)-2-oxoethyl)amino)-2-oxoethyl)-1H-1,2,3-triazol-4-yl)methylindole-3-carboxylate 2.5f: White solid; 462mg(82%); Mp; 122-125⁰C; IR(KBr) ν_{\max} : 2961, 2926, 1654, 1531, 1490, 1455, 1365, 1339, 1232, 1168, 1124, 1039, 753 cm⁻¹. ¹H NMR(CDCl₃, 400MHz) δ_{H} (ppm): 11.93(1H,s), 8.28 (1H,s), 8.26(1H,s), 8.18(1H,s), 8.12(1H,s), 7.99(1H,s), 7.85 (1H,s), 7.71(1H,s), 7.49-7.21(4H,m), 6.42 (1H,s), 6.31(2H,s), 5.48 (2H,s), 4.91-4.83 (2H,t), 1.32(9H,s), 1.23-0.83(4H,m), 0.69-0.66(3H,t); ¹³CNMR(DMSO(d₆), 100MHz) δ_{C} (ppm): 168.2, 167.2, 164.4, 162.6, 142.7, 136.8, 131.5, 129.5, 125.1, 124.8, 122.9, 122.9, 122.2, 121.8, 120.7, 115.8, 112.8, 111.8, 106.4, 62.8, 61.4, 57.5, 55.7, 50.8, 28.7, 28.5, 20.0, 13.2.

(1-(2-butyl(2-tert-butylamino)-1-(2-chlorophenyl)-2-oxoethyl)amino)-2-oxoethyl)-1H-1,2,3-triazol-4-yl)methyl-1H-indole-3-carboxylate 2.5g: white solid; 521mg (90%); Mp; 111-115⁰C; IR(KBr) ν_{\max} : 3417, 2924, 1662, 1534, 1487, 1455, 1406, 1364, 1320, 1226, 1162, 1078, 1013, 823, 750, 699 cm^{-1} ; ¹H NMR(CDCl₃, 400MHz) δ_{H} (ppm): 11.94(1H,s), 8.26(1H,s), 8.17(1H,s), 8.09(1H,s), 7.70(1H,s), 7.50-7.19 (7H,m), 6.10(1H,s), 5.75(2H,s), 4.83(2H,s), 1.33(9H,s), 1.30-0.69(9H,m); ¹³C NMR(DMSO-(d₆), 100MHz) δ_{C} (ppm): 168.4, 166.3, 164.4, 139.8, 136.8, 134.0, 133.3, 130.8, 129.9, 129.8, 127.6, 126.0, 122.9, 122.2, 121.8, 120.7, 112.8, 111.7, 106.5, 62.8, 60.8, 56.8, 45.8, 29.9, 29.4, 20.0, 13.8.

(1-(2-butyl(2-tert-butylamino)-1-(4-fluorophenyl)-2-oxoethyl)amino)-2-oxoethyl)-1H-1,2,3-triazol-4-yl)methyl-1H-indole-3-carboxylate 2.5h: White solid; 489mg(87%); Mp; 110-115⁰C; IR(KBr) ν_{\max} : 2957, 2924, 2854, 1661, 1534, 1509, 1464, 1395, 1365, 1339, 1226, 1161, 1122, 1085, 1017, 851, 811, 750, 669 cm^{-1} . ¹H NMR (CDCl₃, 400 MHz) δ_{H} (ppm): 11.99(1H,s), 8.26(1H,s), 7.50-7.19(5H,m), 8.18(1H,s), 8.08(1H,m), 7.74(1H,s), 5.93(1H,s), 5.61(2H,s), 4.93(2H,s); 1.33-0.80(18H,m); ¹³C NMR (DMSO-(d₆), 100MHz) δ_{C} (ppm): 168.8, 166.6, 164.4, 161.0, 142.7, 136.8, 131.6, 131.0, 126.0, 122.5, 122.2, 121.8, 120.7, 116.0, 112.8, 111.8, 106.5, 76.8, 62.1, 60.6, 56.9, 44.8, 29.4, 28.7, 20.0, 13.7.

2.6. References

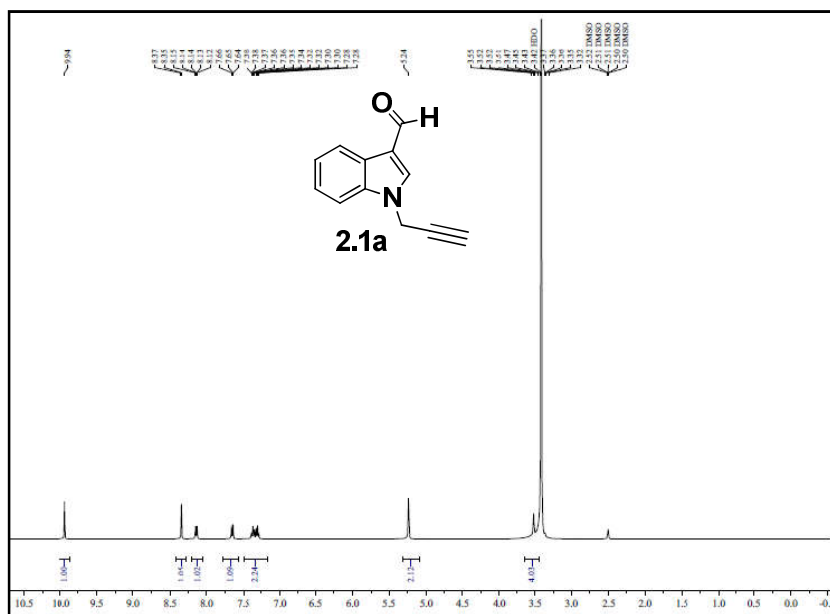
- 1 a) M.E. Welsch, S.A. Snyder and B.R. Stockwell, *Curr. Opin. Chem. Biol.* 2010, **14**, 347; (b) D.R. Spring, *Org. Biomol. Chem.* 2003, **1**, 3867; (c) Y. Gao, Q. Xu, Q. and M. Shi, *ACS Catal.*, 2015, **5**, 6608; (d) A. de Sa, R. Fernando, E. J. Barreiro, M. Fraga and C. Alberto, *Mini-Rev. Med. Chem.*, 2009, **9**, 782.
- 2 R. R. Ramsay and K. F. Tipton, *Molecules.*, 2017, **22**, 1192.
- 3 P.D. Leeson and L. L. Iversen, *J. Med. Chem.*, 1994, **37**, 24.
- 4 T.E. D'Ambra, K.G. Estep, M.R. Bell, M.A. Eissenstat, K.A. Josef, S.J. Ward, D. A. Haycock, E.R. Baizman, F.M. Casiano, N.C. Beglin, S.M. Chippari, J.D. Grego, R.K. Kullnig and G.T. Daley, *J. Med. Chem.*, 1992, **35**, 124.
- 5 (a) A. Lione, and A. R. Sciallia, *Reprod. Toxicol.* 1995, **9**, 7; (b) B. Liu and M. D. Barkely, *J. Phys. Chem. B.*, 2000, **104**, 1837; (c) K. Anil, S. Prasanta and K. Hota, *J. Photoscie.*, 2004, **1**, 107.
- 6 I. Antonini, P. Polucci, A. Magnano, B. Gatto, M. Palumbo, E. Menta, N. Pescalli and S. Martelli, *J. Med. Chem.*, 2003, **46**, 3109.
- 7 (a) R. Alvarez, S. Velazquez, A. San Felix, S. Aquaro, E.D. Clercq, C. Perno, A. Karlsson, J. Balzarini and M.J. Camarasa, *J. Med. Chem.* 1994, **37**, 4185; (b) D.R. Buckle, D.J. Outred, C.J.M. Rockell, H. Smith and B.A. Spicer, *J. Med. Chem.*, 1983, **26**, 251;
- 8 M. J. Genin, A.D. Allwine, D.J. Anderson, M.R. Barbachyn, D.E. Emmert, S. A. Garmon, D.R. Graber, K.C. Grega, J.B. Hester, D.K. Hutchinson, J. Morris, R. J. Reischer, C.W. Ford, G.E. Zurenko, J. C. Hamel, R. D. Schaadt, D. Stapert and B. H. Yagi, *J. Med. Chem.*, 2000, **43**, 953.
- 9 J. Ohwada, M. Tsukazaki, T. Hayase, N. Oikawa, Y. Isshiki, H. Fukuda, E. Mizuguchi, M. Sakaitani, Y. Shiratori, T. Yamazaki, S. Ichihara, I. Umeda and N. Shimma, *Bioorg. Med. Chem., Lett.* 2003, **13**, 191-196.
- 10 Y.A. Alsoud, M.N. Aldweri and N. Almasoudi, *IL FARMACO.*, 2004, **59**, 775.
- 11 L.A.T. Cleghorn et al. *J. Med. Chem.*, 2015, **58**, 7695.

- 12 E.H. Kerns and L.Di, *Academic Press*. 2008, *Drug-like properties: Concepts, structure design and methods: from ADME to toxicity optimization*.
- 13 (a) D.S.Pedersen and A. Abell,*Eur. J. Org. Chem.*2011, 2399; (b) T. Godballe, L.L.Nilsson,P.D. Petersen and H. Jenssen, *Chem. Biol. Drug. Des.*, 2011, **77**, 107.
- 14 A. Choudhary and R.T. Raines,*ChemBioChem.*,2011, **12**, 1801.
- 15 M. H. Justin and K. Kent, *Chem. Soc. Rev.* 2010, **39**, 1325.
- 16 (a)H. C. Kolb,M. G. Finn and K.B. Sharpless,*Angew. Chem. Int. Ed.*,2001, **40**, 2004.
- 17 S. G.Agalave, S.R. Maujan and V.S. Pore,*Chem. Asian. J.*, 2011, **6**, 2696.
- 18 (a)P. Pramitha and D. Bahulayan,*Bioorg.Med.Chem. Lett.*, 2012 , **22**, 2598.
- 19 (a)T. Luo and S.L. Schreiber,*J.Am. Chem. Soc.*2009, **131**, 5667;(b)H.S.G. Beckmann, F.Nie, F.C.E. Hagerman,H. Johansson, Y.S. Tan, D.Wilcke andD.R.Spring,*Nature Chem.* 2013, **5**,861; (c)S. L. Schreiber, *Science.*, 2000, **287**, 1964.
- 20 a) A. Dömling and I. Ugi, *Angew. Chem .Int. Ed.*, 2000, **39**, 3168.

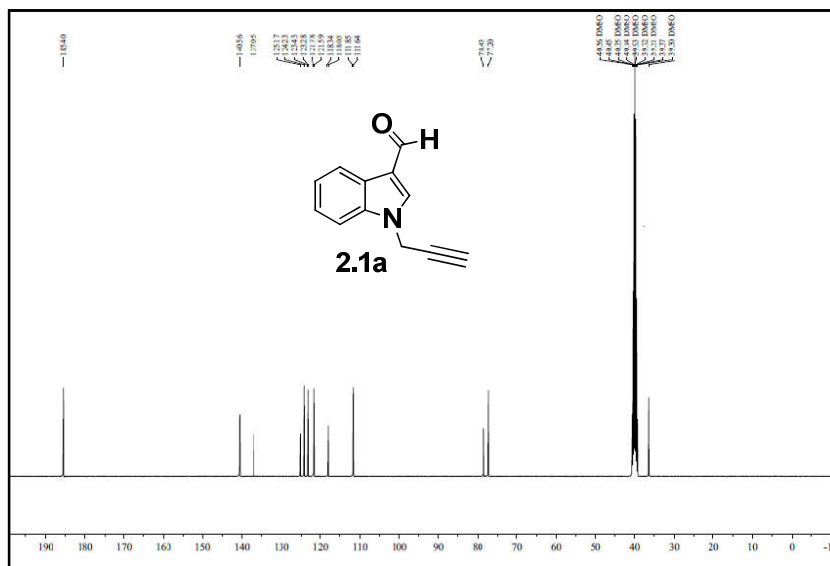
Supplementary Material

Copies of ^1H NMR, ^{13}C NMR and Mass spectra of selected compounds

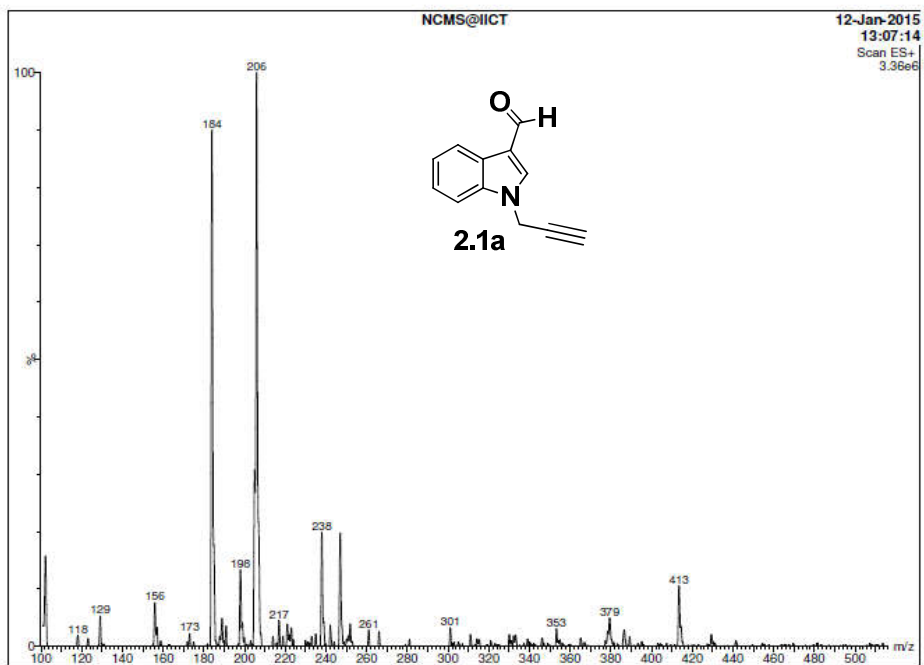
¹H NMR spectrum of the compound **2.1a**



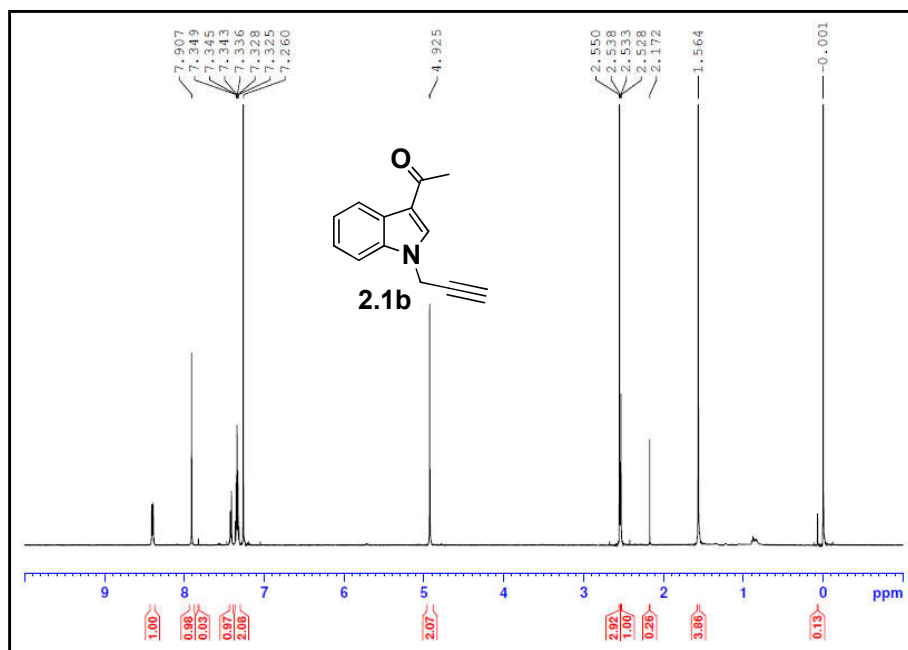
¹³C NMR spectrum of the compound **2.1a**



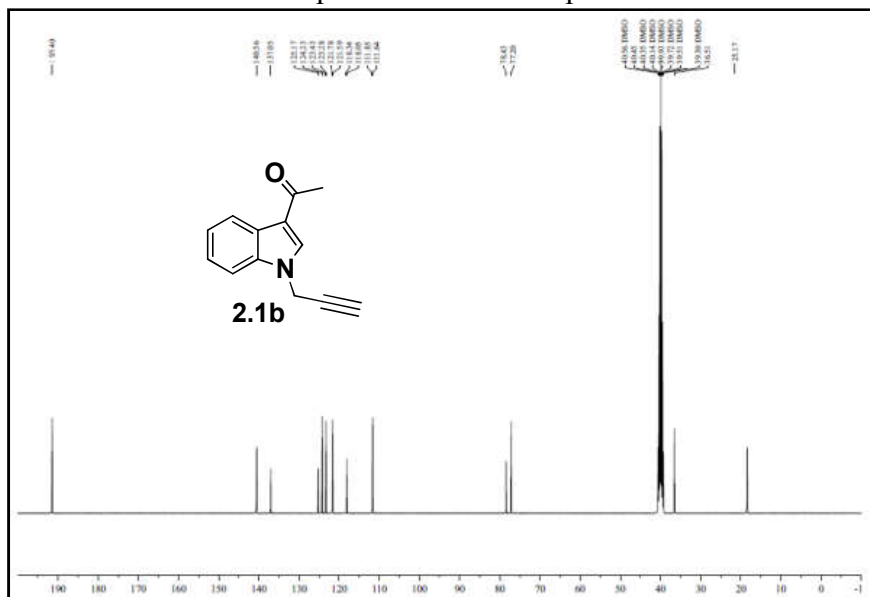
Mass spectrum of the compound 2.1a



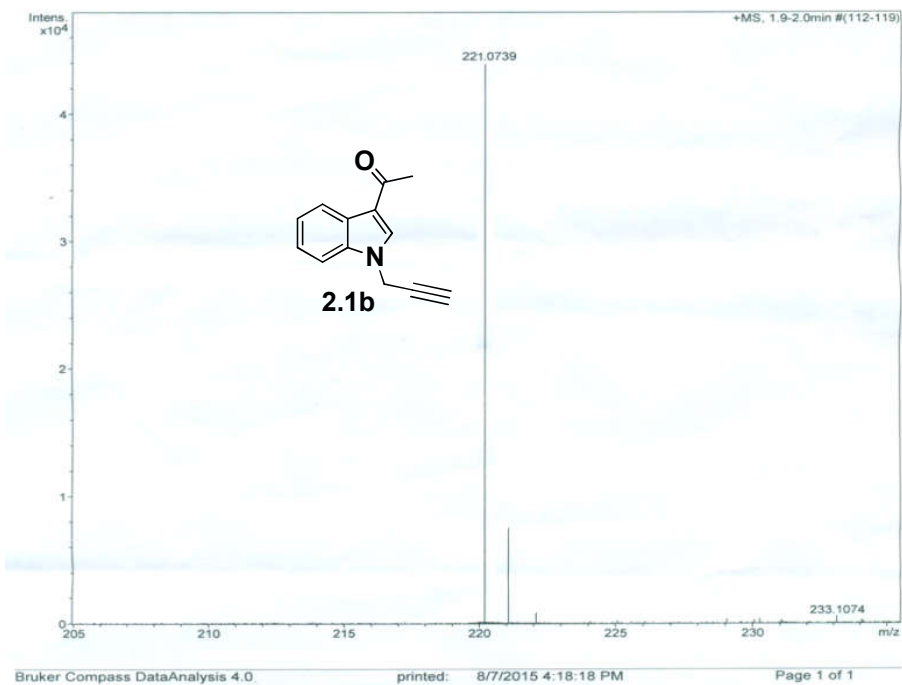
¹H NMR spectrum of the compound 2.1b



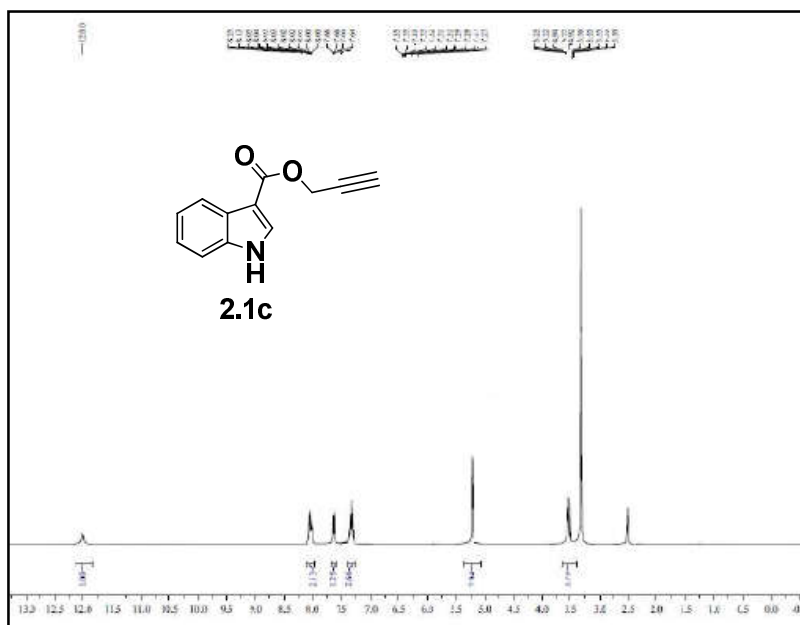
^{13}C NMR spectrum of the compound **2.1b**



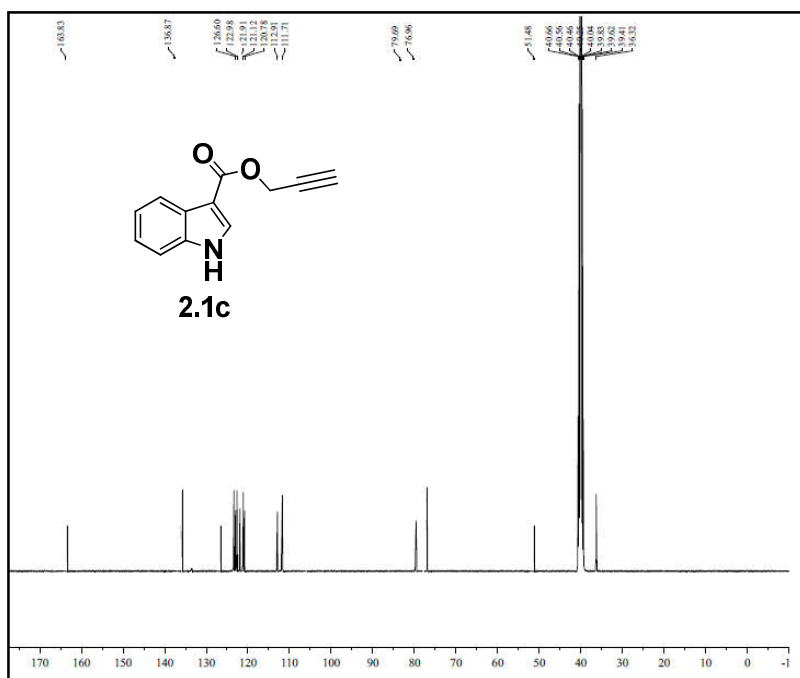
Mass spectrum of the compound **2.1b**



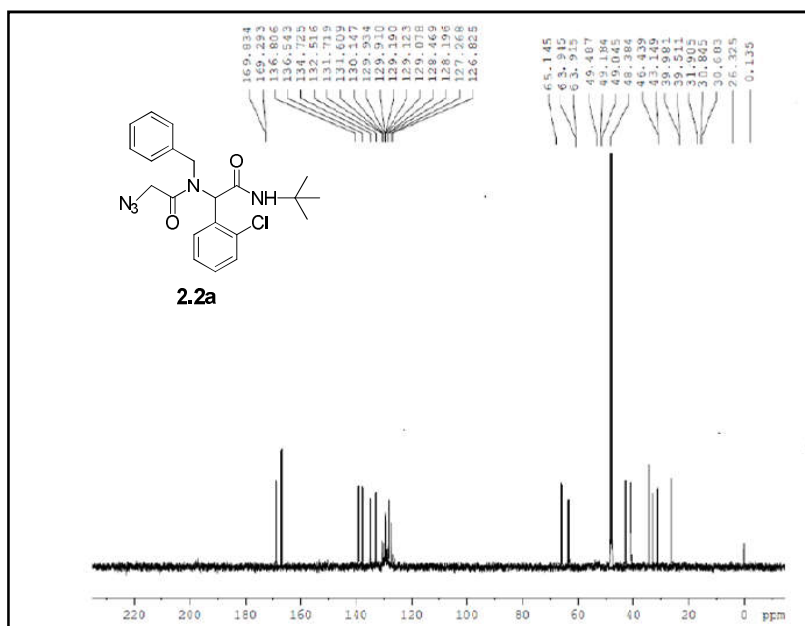
¹H NMR spectrum of the compound **2.1c**



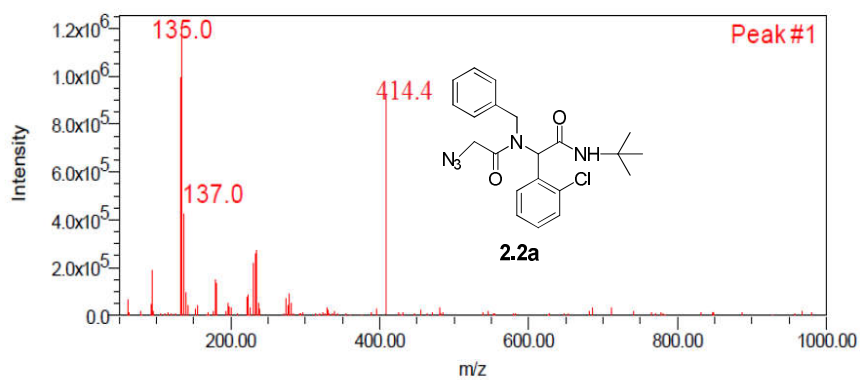
¹³C NMR spectrum of the compound **2.1c**



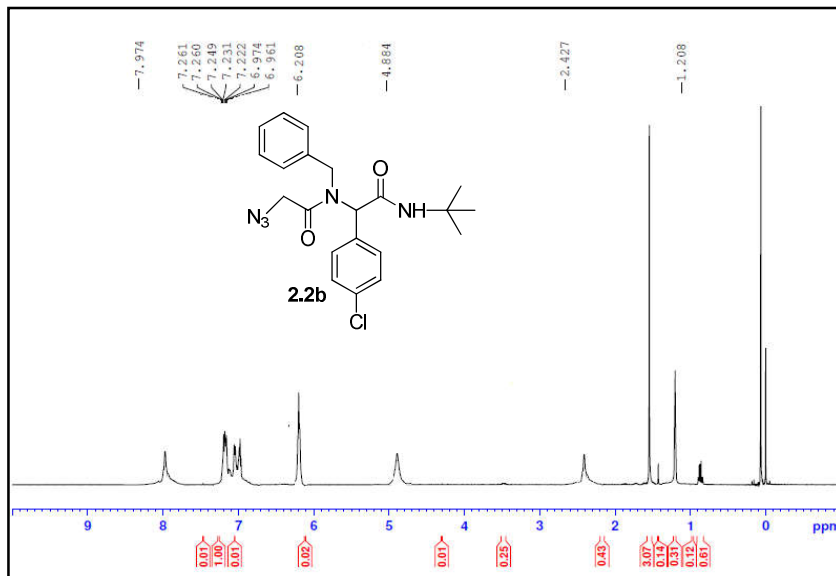
^{13}C NMR spectrum of the compound **2.2a**



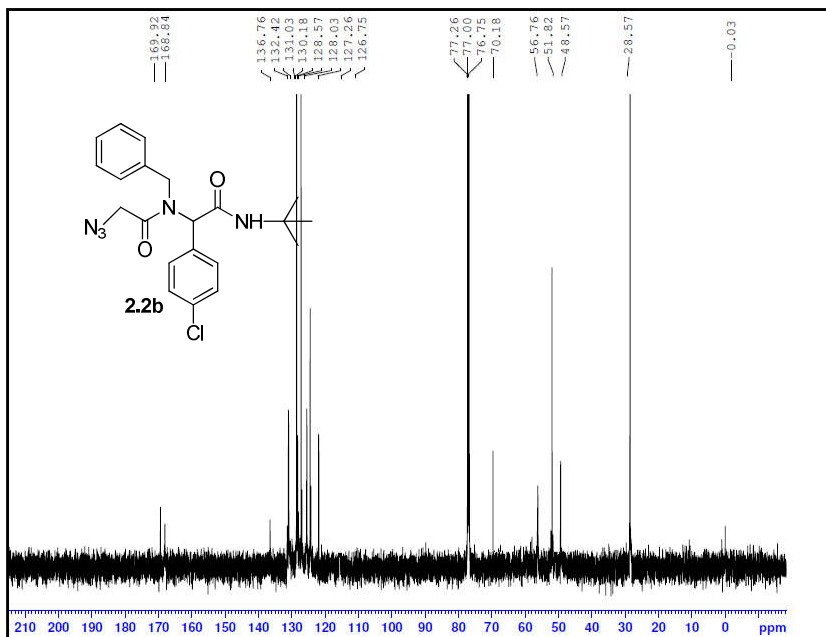
Mass spectrum of the compound **2.2a**



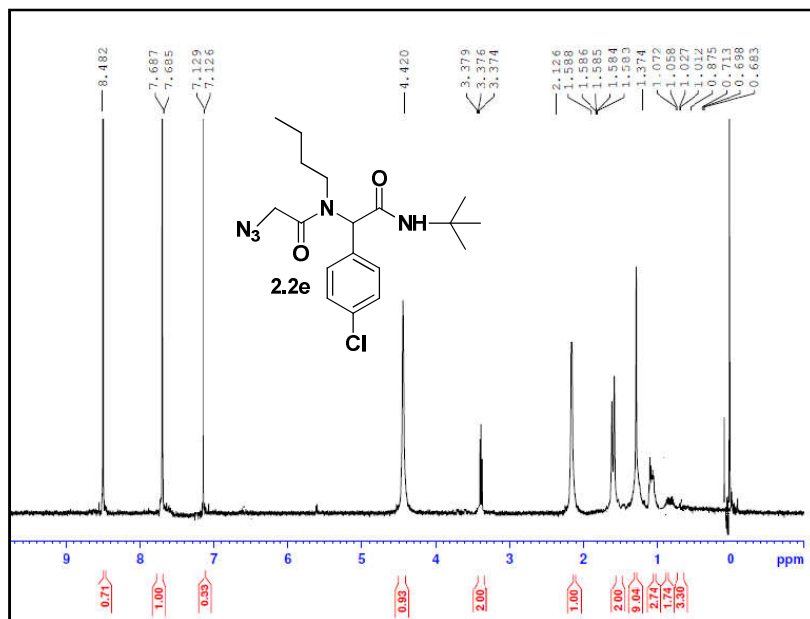
¹H NMR spectrum of the compound **2.2b**



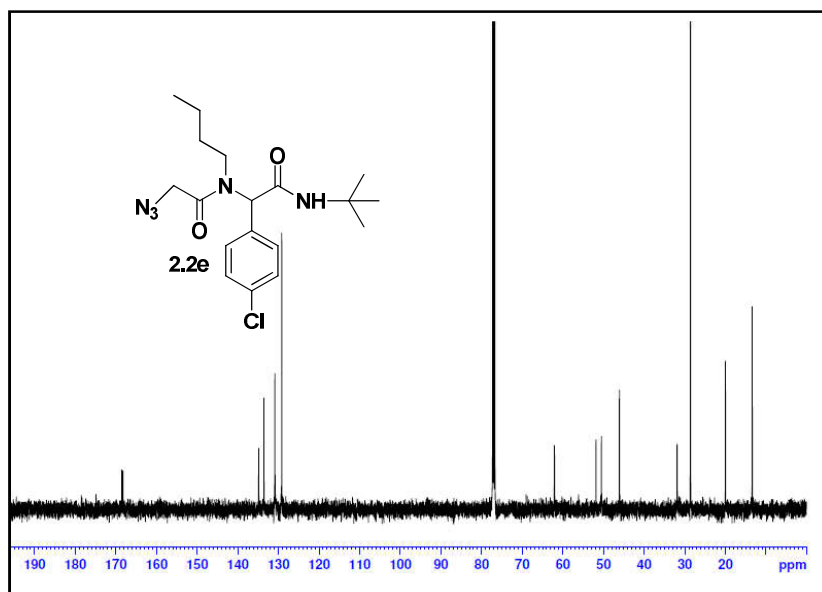
¹³C NMR spectrum of the compound **2.2b**



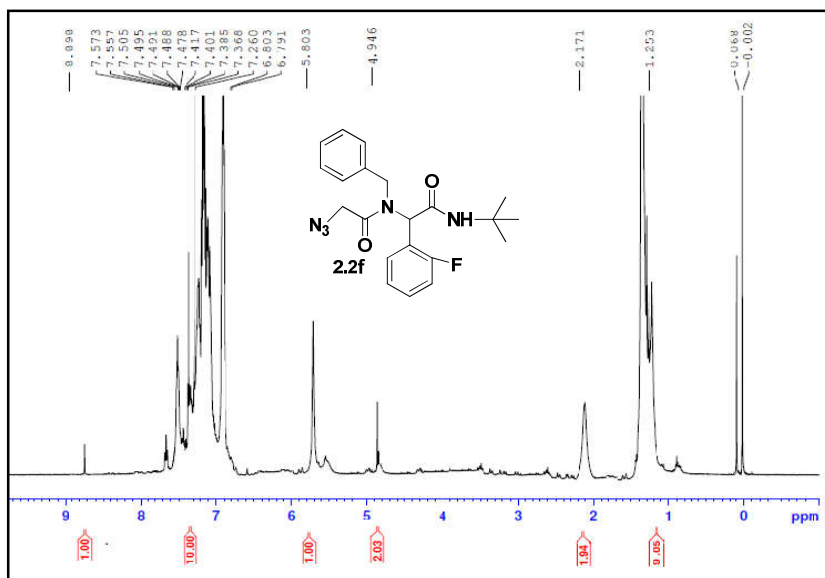
^1H NMR spectrum of the compound **2.2e**



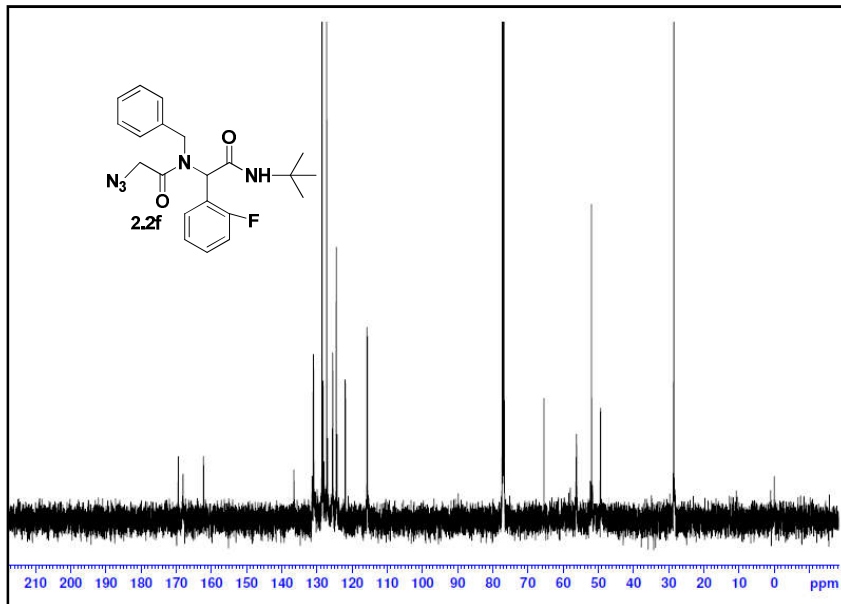
^{13}C NMR spectrum of the compound **2.2e**



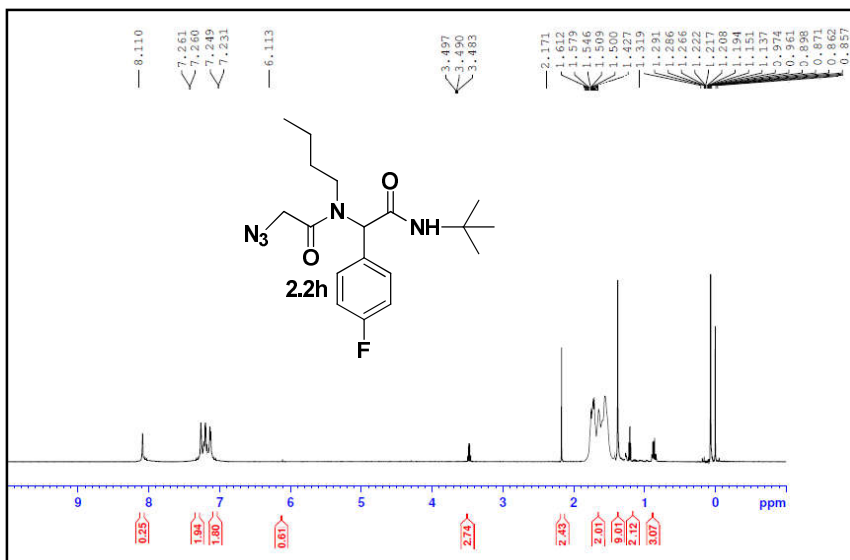
^1H NMR spectrum of the compound **2.2f**



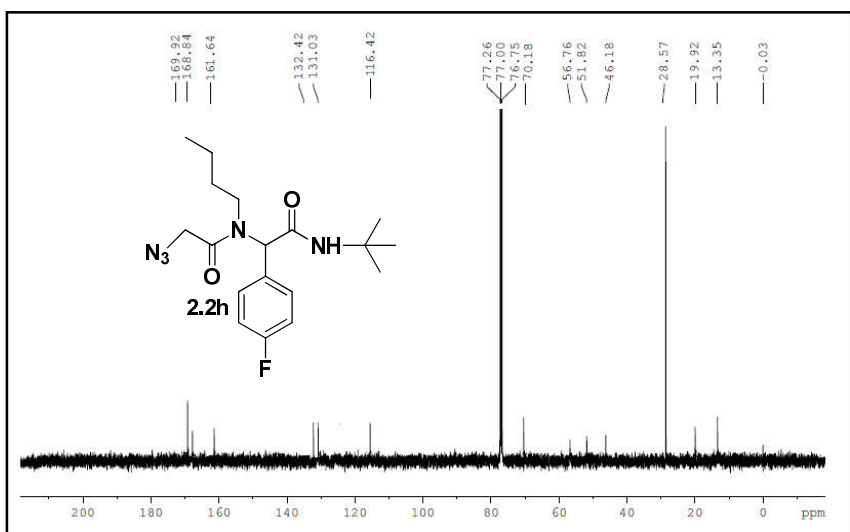
^{13}C NMR spectrum of the compound **2.2f**



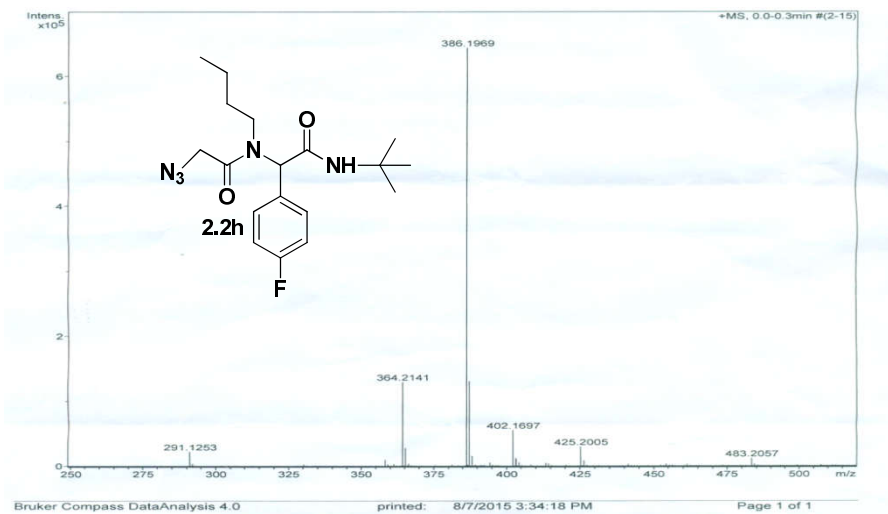
¹H NMR spectrum of the compound **2.2h**



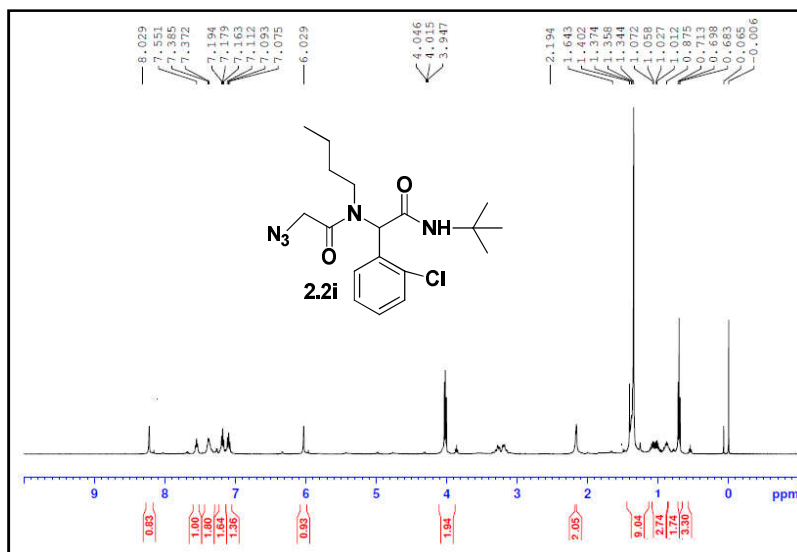
¹³C NMR spectrum of the compound **2.2h**



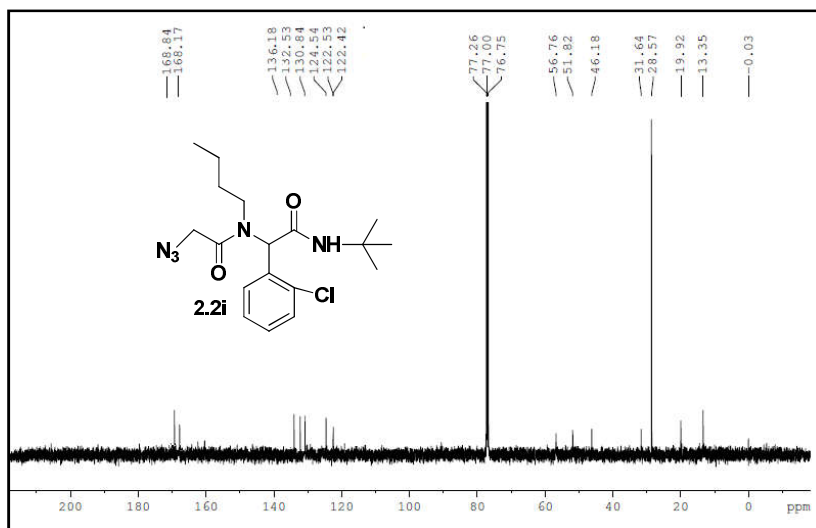
Mass spectrum of the compound **2.2h**



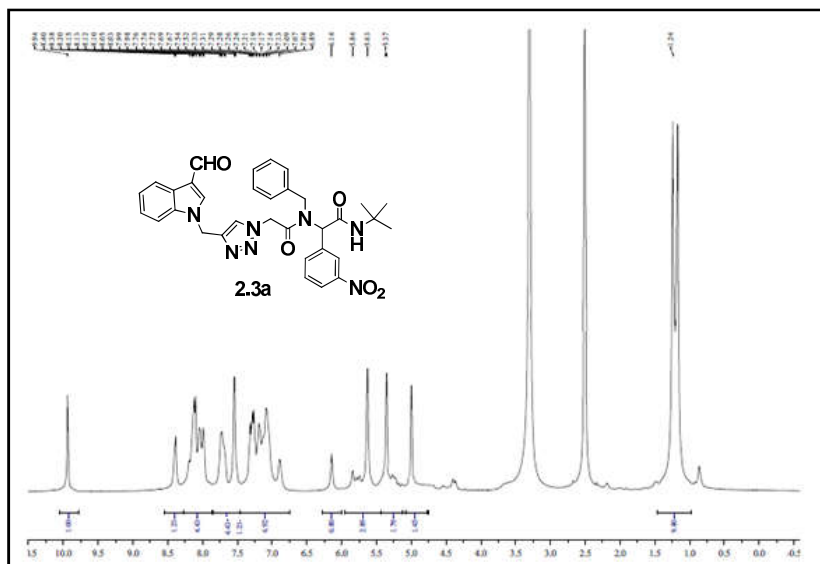
¹H NMR spectrum of the compound **2.2i**



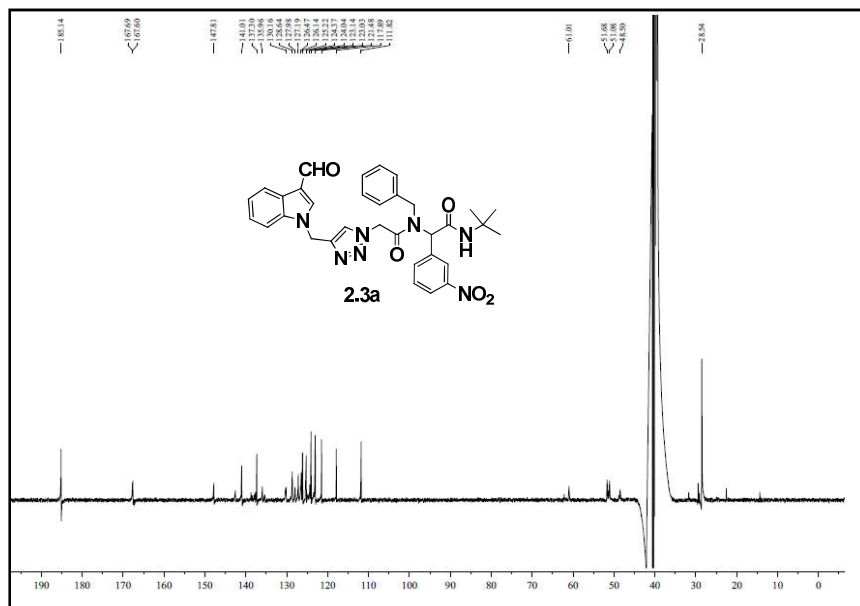
^{13}C NMR spectrum of the compound **2.2i**



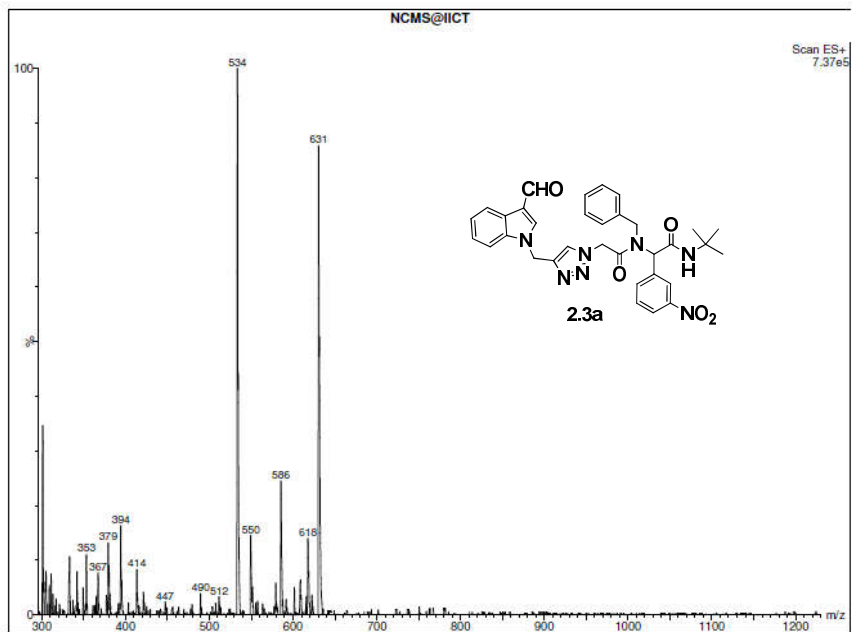
^1H NMR spectrum of the compound **2.3a**



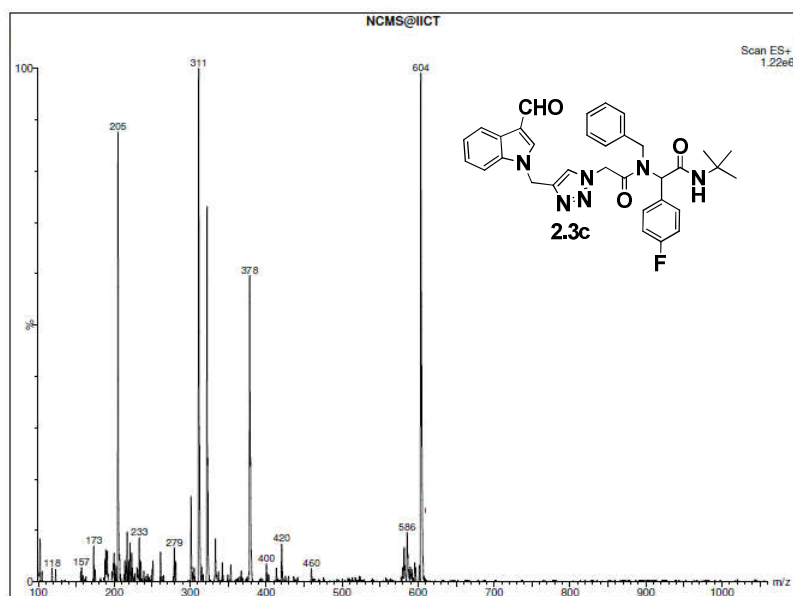
^{13}C NMR spectrum of the compound **2.3a**



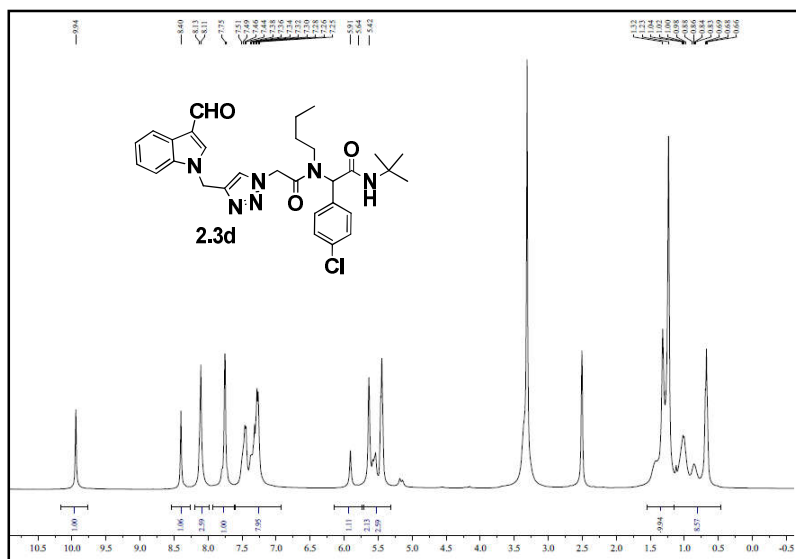
Mass spectrum of the compound **2.3a**



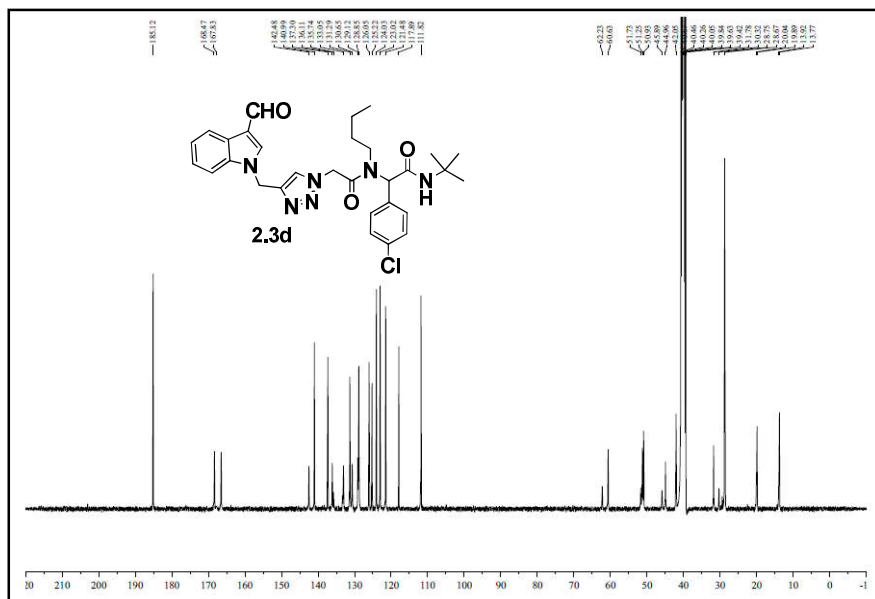
Mass spectrum of the compound 2.3c



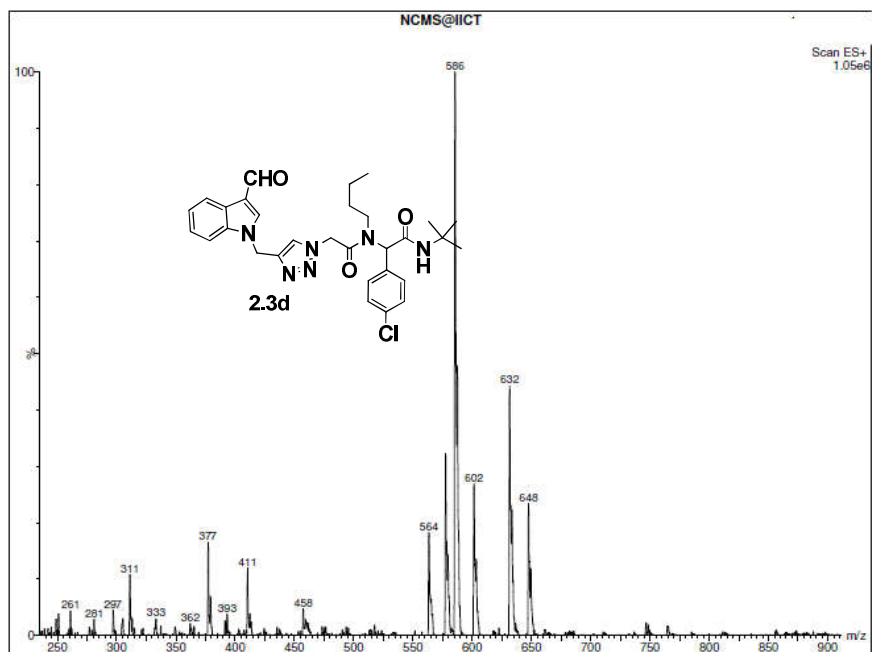
¹H NMR spectrum of the compound 2.3d



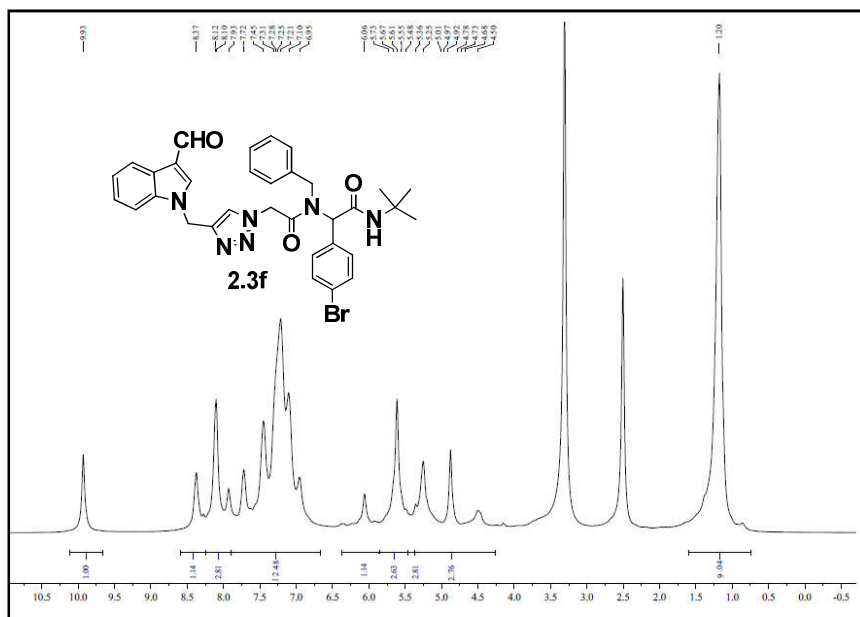
^{13}C NMR spectrum of the compound **2.3d**



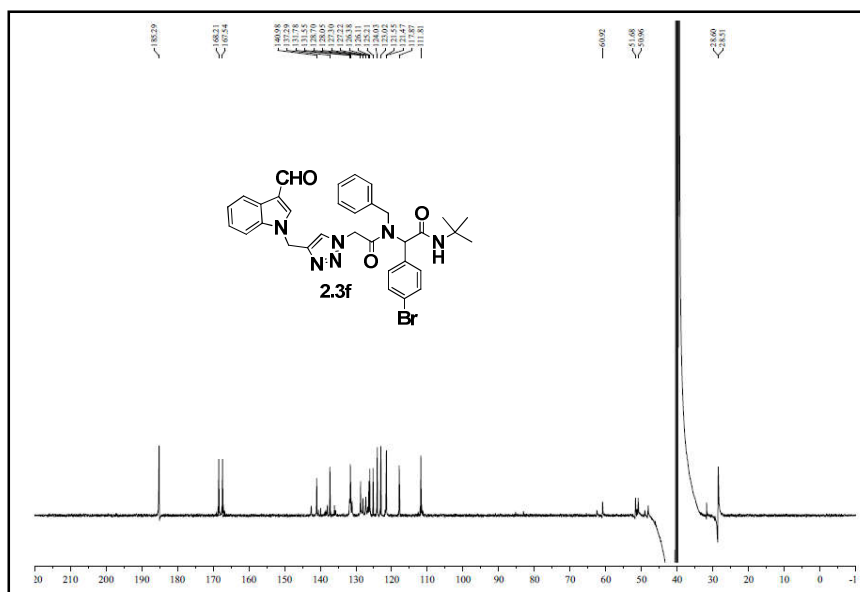
Mass spectrum of the compound **2.3d**



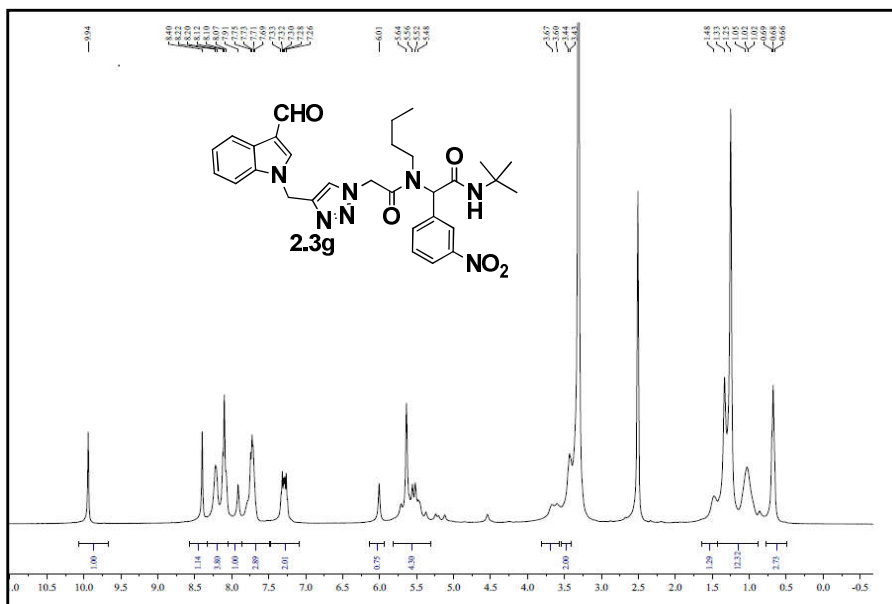
¹H NMR spectrum of the compound **2.1a**



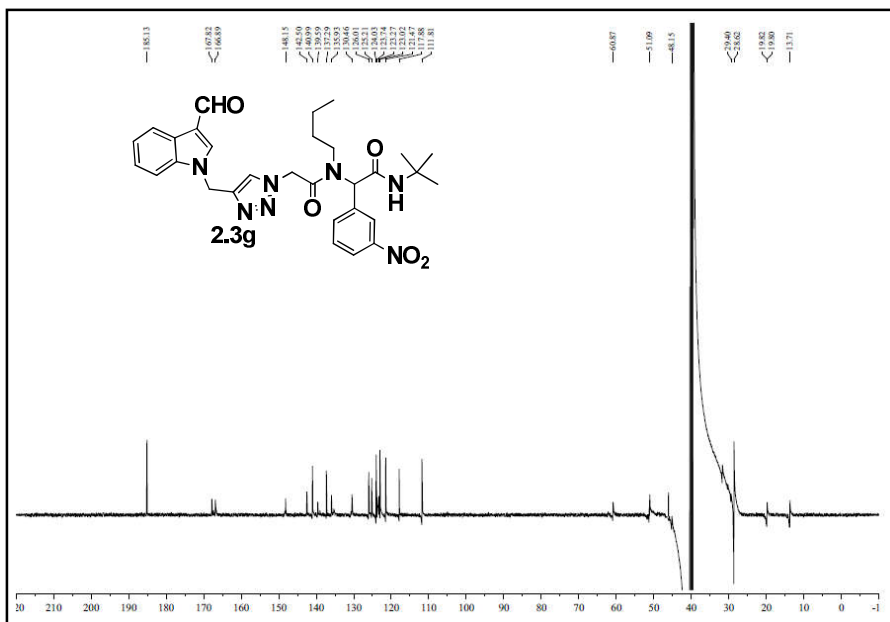
¹³C NMR spectrum of the compound **2.3f**

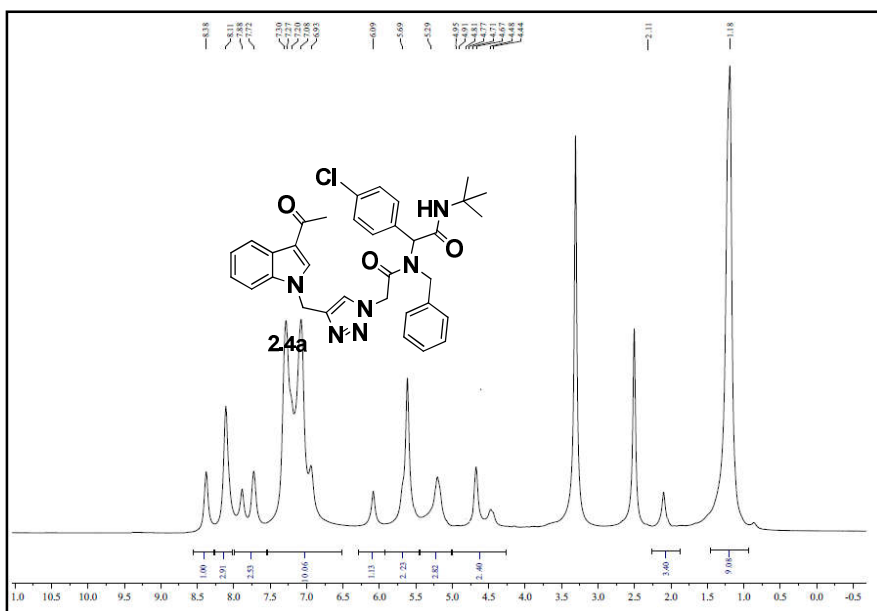


¹H NMR spectrum of the compound **2.3g**

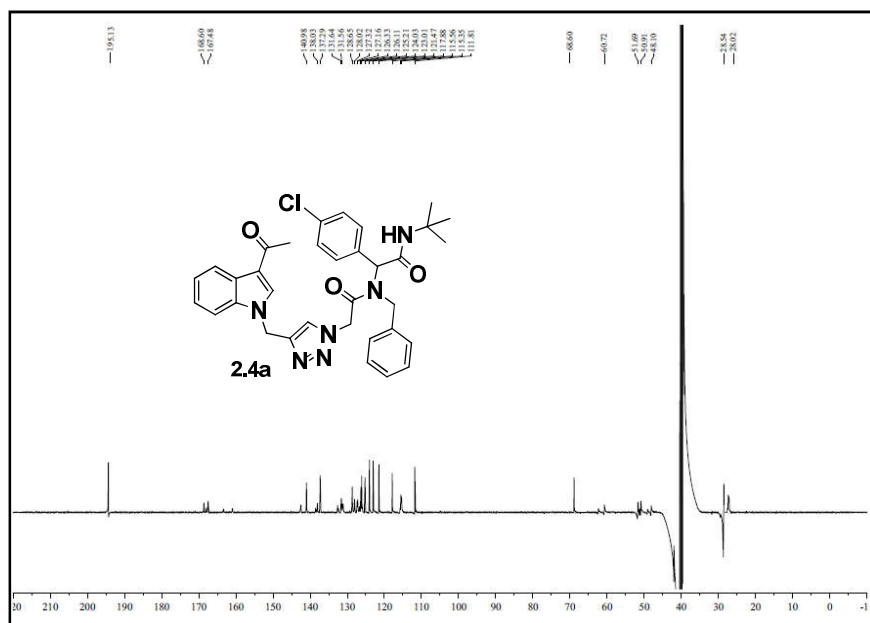


¹³C NMR spectrum of the compound **2.3g**

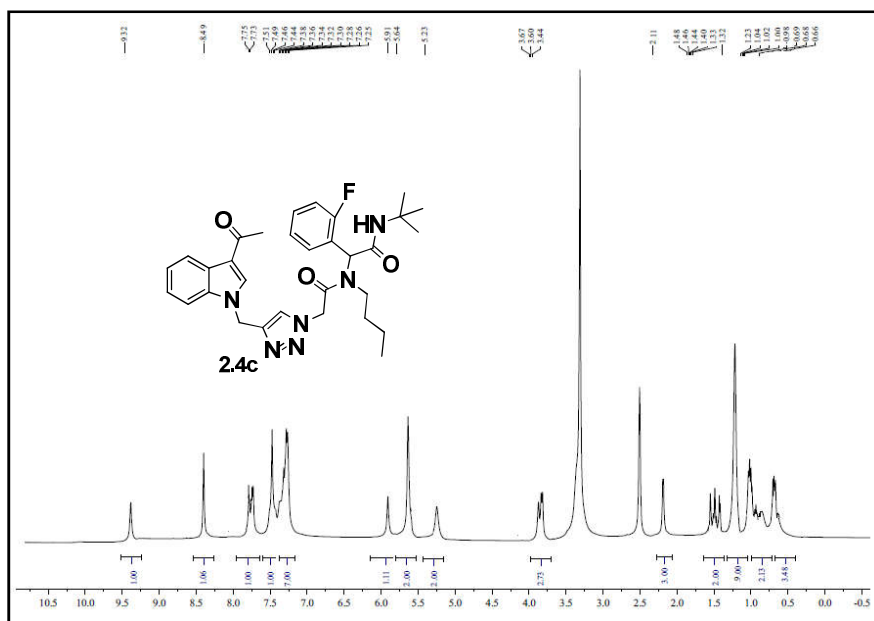




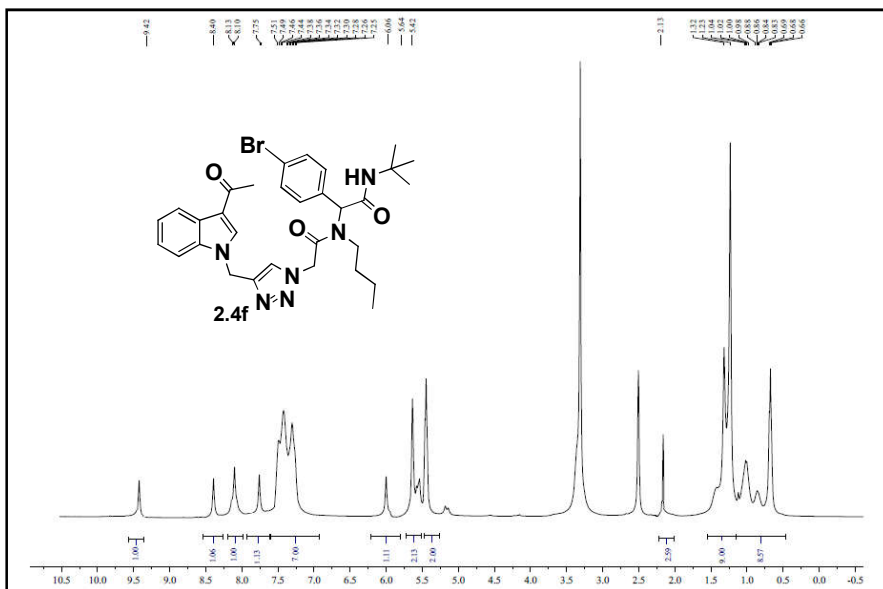
¹³C NMR spectrum of the compound 2.4a



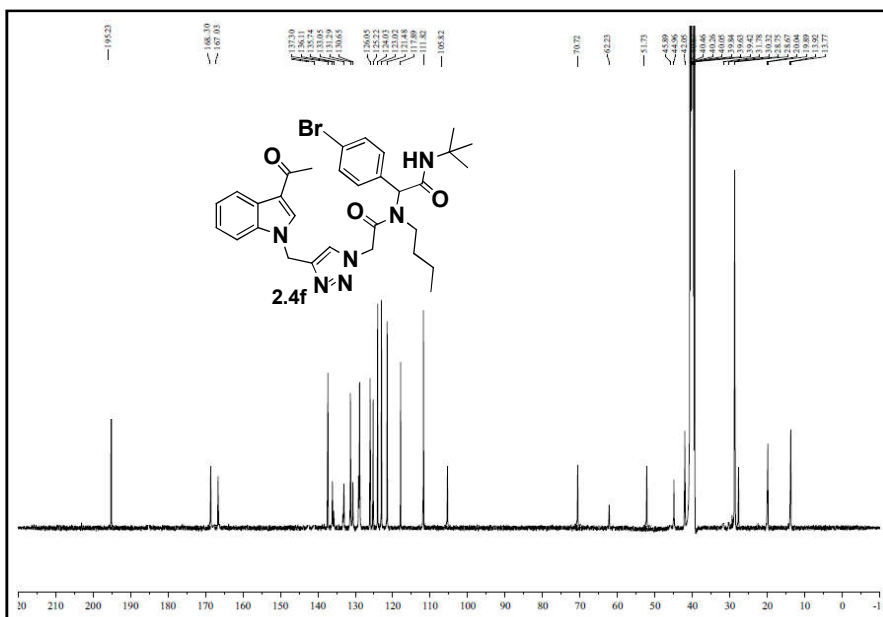
^1H NMR spectrum of the compound **2.4c**



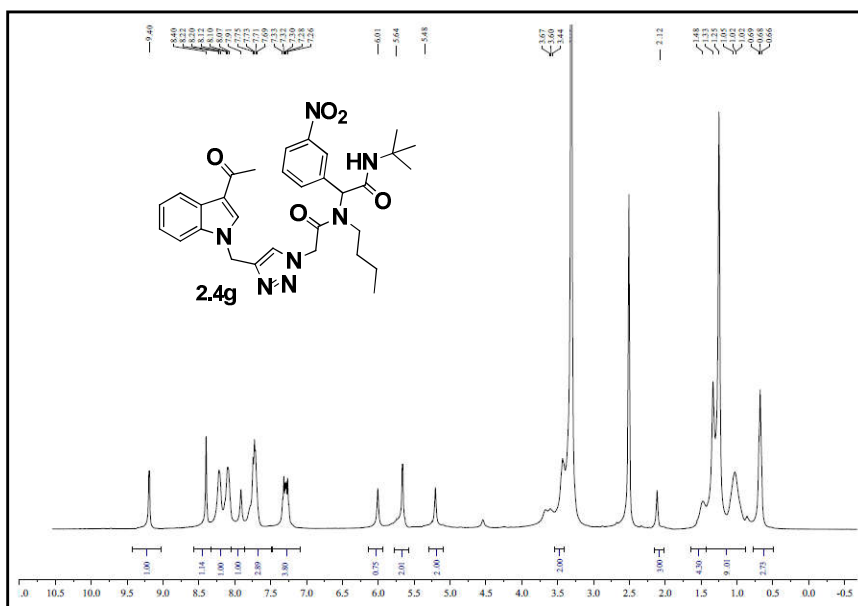
^1H NMR spectrum of the compound **2.4f**



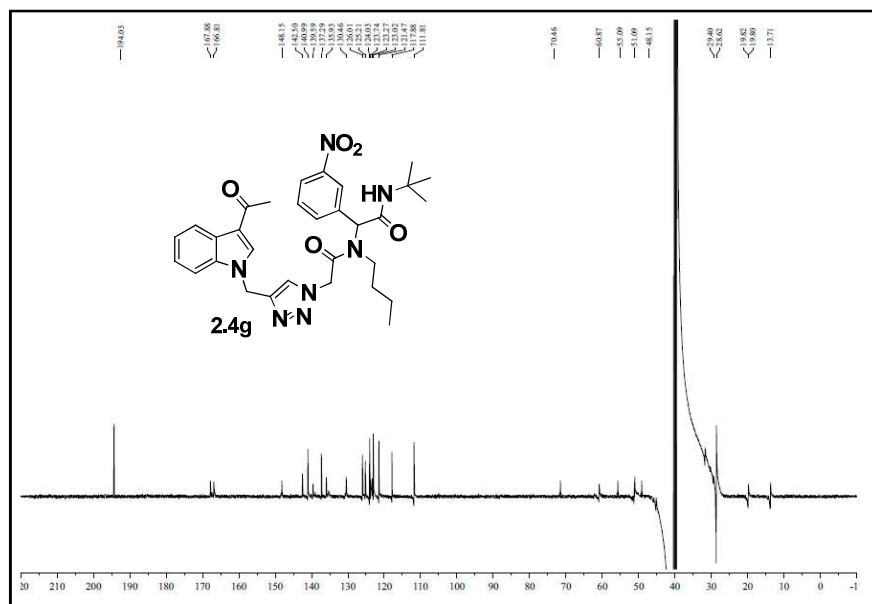
^{13}C NMR spectrum of the compound **2.4f**



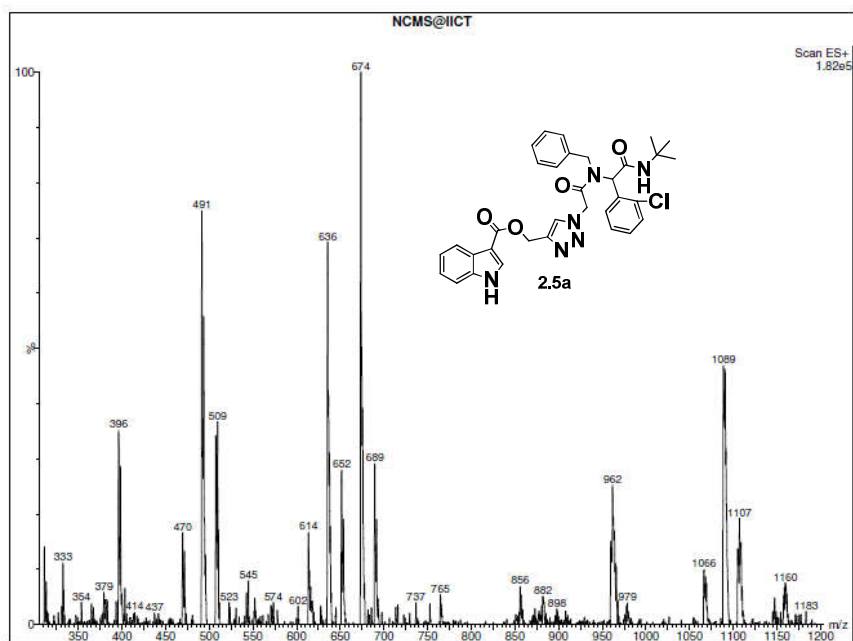
¹H NMR spectrum of the compound **2.4g**



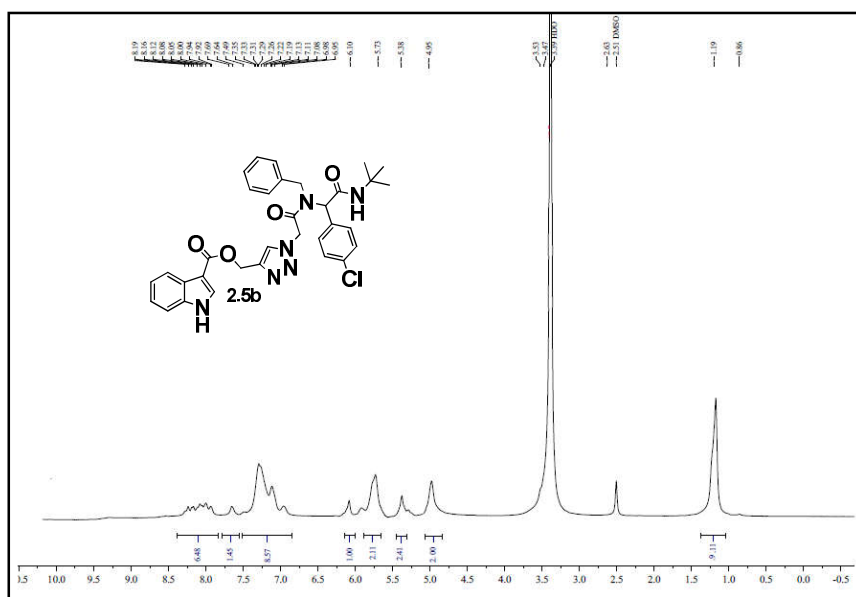
¹³C NMR spectrum of the compound **2.4g**



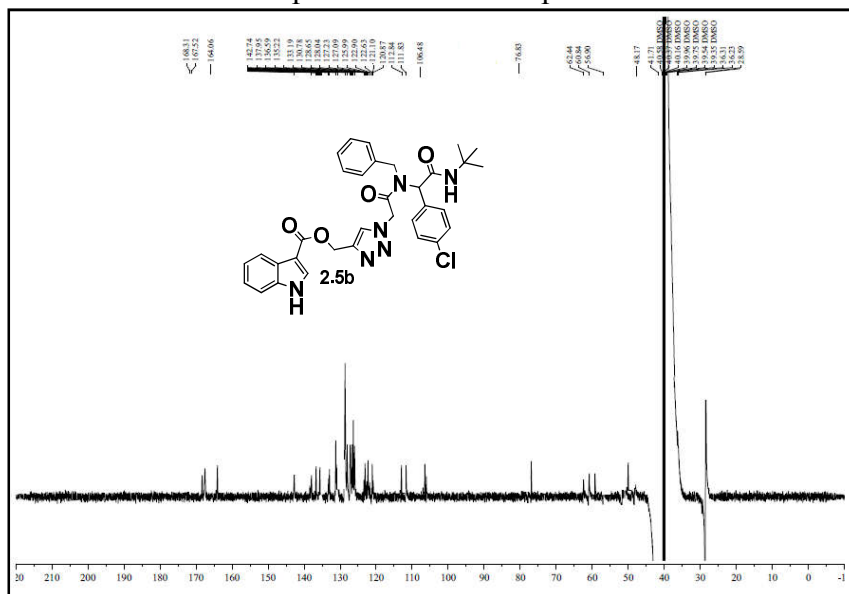
Mass spectrum of the compound **2.5a**



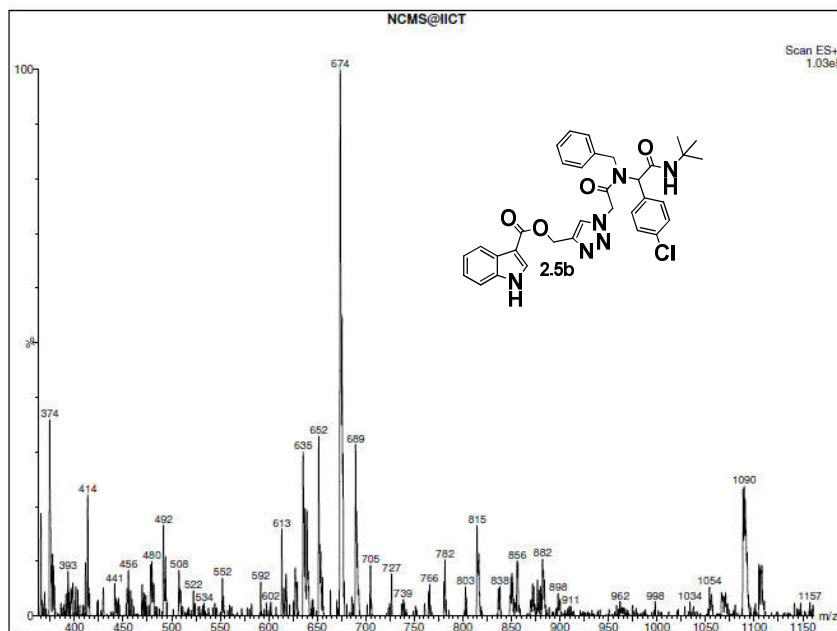
NMR spectrum of the compound **2.5b**



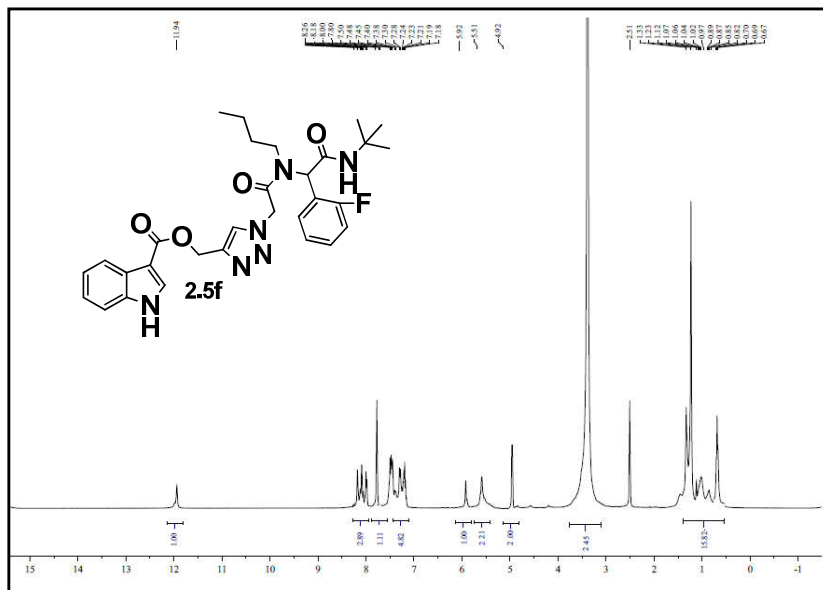
^{13}C NMR spectrum of the compound **2.5b**



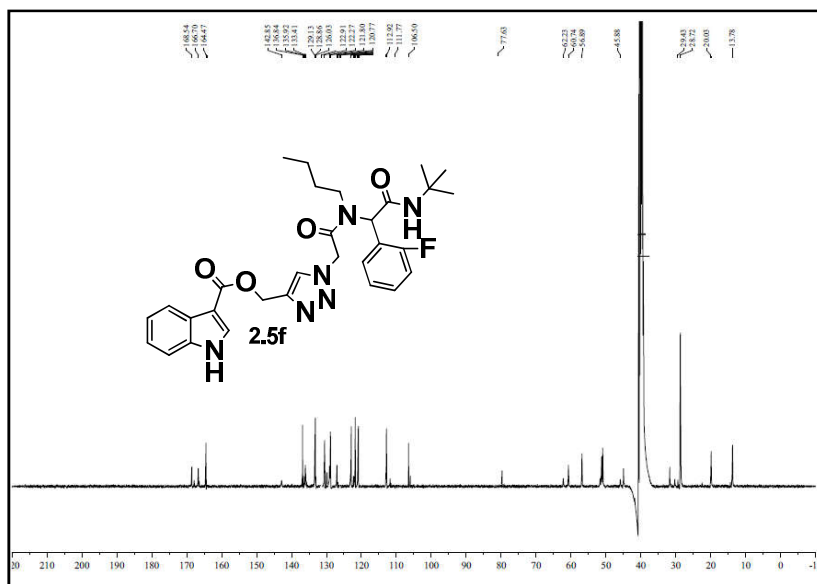
Mass spectrum of the compound **2.5d**



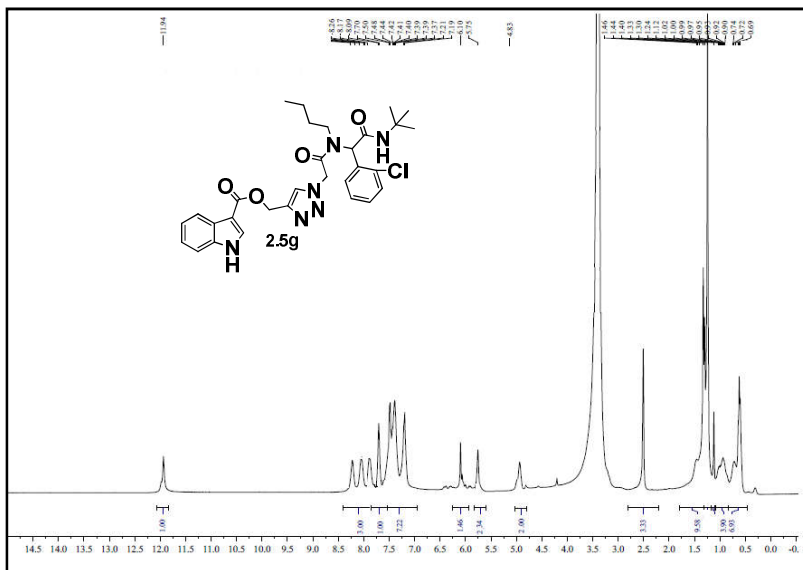
^1H NMR spectrum of the compound **2.5f**



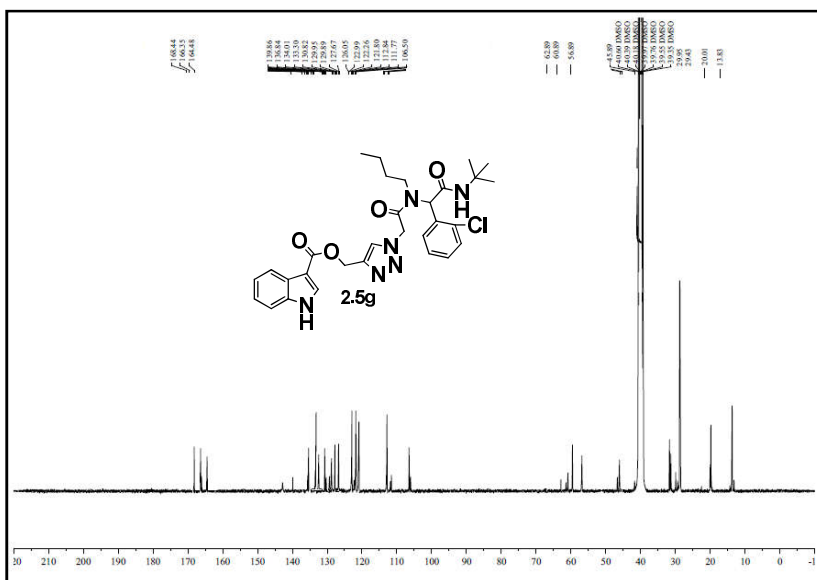
^{13}C NMR spectrum of the compound **2.5f**



¹H NMR spectrum of the compound **2.5g**



¹³C NMR spectrum of the compound **2.5g**



CHAPTER 3

**Computational and Biological evaluation of
Indole-Triazole Carboxamide
peptidomimetics against CDK 2 proteins
and human breast cancer cell line MCF-7.**

Contents

3.1 Introduction.....	126
3.2. Result and discussion.....	128
3.3. Conclusion.....	138
3.4. Experimental section	139
References	141

3.1 Introduction

The process involved in the discovery of a new anti-cancer agent is long, risky and expensive. However, the recent developments in computation chemistry and biological sciences have provided new paradigms that help researchers to model and understand drug targets and to discover drugs within a short time span. These drugs are less costly and safer than the existing ones. The use of structure-based drug design techniques has been made possible by the availability of crystal structures of target protein. These technologies involve virtual screening, pharmacophore development and structure based optimization.¹ The drug discovery process functions from the selection of target enzyme and the drug molecule interacts with target enzyme to inhibit it. The successful inhibition of enzyme with small drug molecule prevents the normal working of enzyme and hence the seizing of the normal enzyme functionality. The cell regulator enzymes are target enzymes in most cases of cancer treatment. The regulators of the timing and coordination of eukaryotic cell cycle events are the cyclin-dependent protein kinases (CDKs). As monomers, CDKs are inactive and their activation requires binding to cyclins with phosphorylation by CDK-activating kinase on a specific threonine residue. The cyclin is part of different family of proteins and their levels oscillate during cell cycle.² In the regulation of G1/S transition, a functional complex of Cdk2 with cyclin E plays a crucial role.³ However, CDK/Cyclins are dysregulated in many human cancers.⁴ These cyclones create damage in the coordinated cycle of cell growth and proliferation and contribute to the uncontrolled spreading characteristic of cancer cells.⁵ Hence, there is a clear need to develop target specific CDK inhibitors based on biocompatible privileged

scaffolds using robust synthetic methodologies. Since many of the CDK 2 inhibitors and other potential anti-cancer molecules contain either indole or 1, 2, 3-triazole as a structural component (Fig.3.1), we decided to carry out the computational and biological evaluation of the indole-triazole-carboxamide molecules discussed in chapter 2 against CDK 2 and human breast cancer cell line MCF-7, as shown in the graphical representation given in figure 3.2.

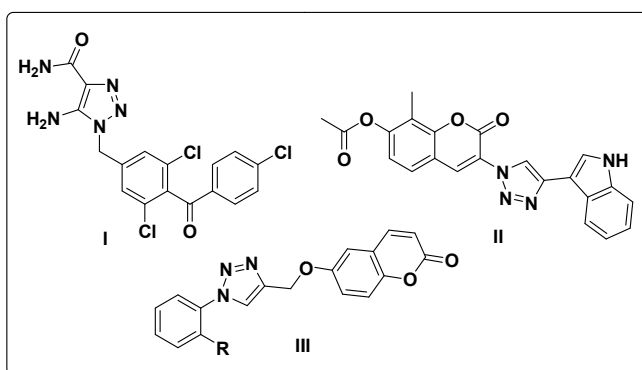


Fig. 3.1. The chemical Structure of some Triazole containing potent anticancer compounds.

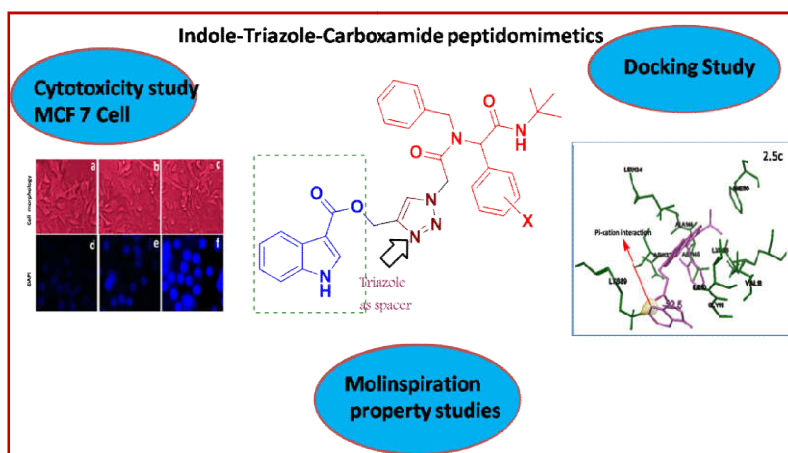


Fig. 3. 2. A schematic representation of the computational and biological evaluation of Indole-triazole-Carboxamide peptidomimetics.

3.2. Result and discussion

3.2.1. Primary evaluation of drug-likeness

The primary evaluation of the drug likeness has been carried out by calculating the drug property descriptors of all the three series of peptidomimetics (ICT-1, ICT-2 and ICT-3) using molinspiration property calculation service.⁶ Drug-likeness of the molecules mainly depends on their molecular size, lipophilicity, polarity (accessed by the polar surface area, tPSA) and the presence of optimal number of rotatable bonds.⁷ Drug like molecules usually have log P values in between -0.4 and 5.6.⁸ The calculated drug-property descriptors are presented in table **3.1**. These peptidomimetics have log P values in between 4.25 and 5.28 and are in the preferred range of antipsychotic (CNS) drugs. The enhanced log P values of the new peptidomimetics also shows that, these molecules have improved blood-brain barrier (BBB) permeation and brain distribution and the possibilities for further studies focused to stage 2 HAT inhibition.

Table 3.1. Calculated drug-property descriptors of Indole triazole peptidomimetics series

Compound	miLog p	TPSA	NO. of atoms	n O	n N	nOHNH	Nrot b	nViolation
2.3a	4.25	147.95	45	12	1	1	12	2
2.3b	4.47	102.13	40	9	1	1	12	1
2.3c	4.48	102.13	43	9	1	1	11	1
2.3d	5.04	102.13	40	9	1	1	12	2
2.3e	4.43	102.13	43	9	1	1	11	1
2.3f	5.13	102.13	43	9	1	1	11	2
2.3g	4.29	147.95	42	12	1	1	13	2
2.3h	5.17	102.13	40	9	1	1	12	2
2.4a	5.11	102.13	44	9	1	1	11	2
2.4b	4.59	102.13	44	9	1	1	11	1
2.4c	4.58	102.13	41	9	1	1	12	1
2.4d	4.63	102.13	41	9	1	1	12	1
2.4e	5.24	102.13	44	9	1	1	11	2
2.4f	5.28	102.13	41	9	1	1	12	2
2.4g	4.40	147.95	43	12	1	1	13	2
2.4h	4.36	147.95	46	12	1	1	12	2
2.5a	4.92	122.22	44	10	2	2	12	1
2.5b	4.97	122.22	44	10	2	2	12	1
2.5c	4.41	122.22	44	10	2	2	12	1
2.5d	4.46	122.22	44	10	2	2	12	1
2.5e	5.01	122.22	41	10	2	2	13	2
2.5f	4.45	122.22	41	10	2	2	13	1
2.5g	4.96	122.22	41	10	2	2	13	1
2.5h	4.50	122.22	41	10	2	2	13	1

3.2.2. Molecular docking studies

The promising results obtained from the drug-likeness calculations prompted us to perform the virtual screening of our molecules against CDK 2 based on molecular docking.⁹ Docking studies were carried out using the Auto Dock Vina 1.1.2. The active site of CDK2-2vv9 comprised of amino acid residues such as 31 Alanine, 144 Alanine, 145 Asparagine, 64 Valine, 83 Leucine, 134 Leucine, 10 Isoleucine, 85 Glutamine, 131 Glutamine, 89 Lysine, 80

Phenylalanine.¹⁰ Since most of the amino acid residues in the active site are hydrophobic and hence they are the main contributors for the receptor ligand interaction. PDB id 2vv9 was docked with **2.3a-2.5h** and the docking score obtained for the synthesized compounds are listed in table **3.2**. All the synthesized compounds showed higher binding affinity than the parent ligand (parent ligand exhibits binding affinity of -8.7 Kcal/mol). Of the synthesized compounds, **2.5b** and **2.5c** exhibits highest docking score of -12.5 Kcal/mol. As shown in Figure **3.4**, compound **2.5c** inserted into the binding cage surrounded by 31 Alanine, 144 Alanine, 145 Asparagine, 64 Valine, 83 Leucine, 134 Leucine, 10 Isoleucine, 85 Glutamine, 131 Glutamine, 89 Lysine and 80 Phenylalanine without any hydrogen bonding between the ligand and the receptor. At the same time the compounds **2.3a**, **2.3g**, **2.4g**, **2.4h**, and **2.5e** formed hydrogen bonds with the CDK 2 protein. In **2.3a**, the carbonyl group of the indole forms a hydrogen bond with leucine 83 of receptor whereas in **2.3 g**, the NO₂ group of the compound formed a hydrogen bond with the receptor. Similarly in the case of **2.4g** and **2.4h** the NO₂ group forms hydrogen bonding with Lysine 89. The indole carbonyl group of **2.5e** also forms hydrogen bonds with Lysine 89. In addition to this, all the compounds showed pi-cation interaction with the protein. Whereas the indole ring and other aromatic rings present in the ligand act as the pi system and NH₃⁺ part of the protein acts as the cation. As shown in figure **3.3**, the parent ligand and synthesized compounds are well embedded in the binding pocket of the CDK2 forming energetically stable drug receptor interaction.

Table 3.2. Docking score of the synthesized compounds

Compounds	Docking Score (Binding affinity) Kcal/mol	Compounds	Docking Score (Binding affinity) Kcal/mol
2.3a	-9.7	2.4e	-10.1
2.3b	-9.2	2.4f	-9.6
2.3c	-10.1	2.4g	-9.4
2.3d	-8.9	2.4h	-8.8
2.3e	-9.5	2.5a	-11.9
2.3f	-10.0	2.5b	-12.5
2.3g	-9.0	2.5c	-12.5
2.3h	-9.2	2.5d	-12.4
2.4a	-10.2	2.5e	-11.2
2.4b	-9.7	2.5f	-10.9
2.4c	-9.6	2.5g	-10.7
2.4d	-9.6	2.5h	-11.2

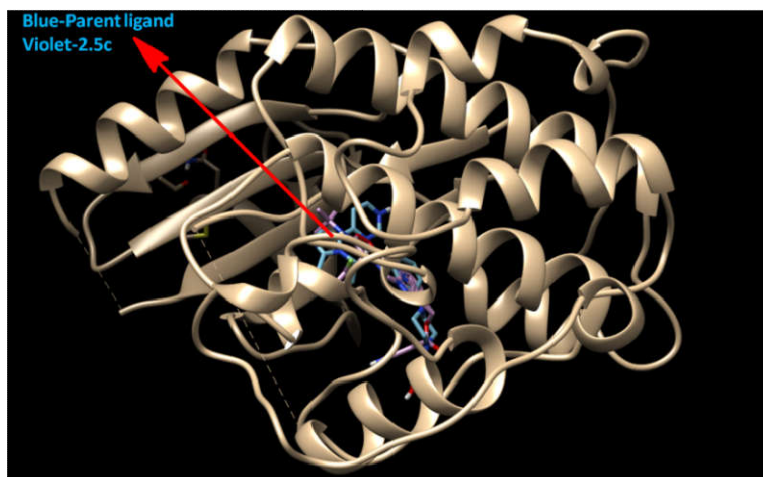


Fig. 3.3. The super imposition of the compounds **2.5C** (violet) with parent ligand (blue) in the active site of CDK2-2vv9

the cytotoxicity evaluation of representative samples against, Dalton's lymphoma ascites cells (DLA) or Ehrlich Ascites Carcinoma (EAC) cells by trypan blue exclusion and MTT reduction test in MCF-7 cell lines.

3.2.3.1. Trypan blue exclusion method

The test compounds were studied for short term in vitro cytotoxicity using Dalton's lymphoma ascites cells (DLA) or Ehrlich Ascites Carcinoma (EAC) cells. The tumour cells aspirated from the peritoneal cavity of tumour bearing mice were washed thrice with PBS or normal saline. The Cell viability was determined by trypan blue exclusion method. Viable cell suspension (1×10^6 cells in 0.1 ml) was added to tubes containing various concentrations of the test compounds and the volume was made up to 1 ml using phosphate buffered saline (PBS). Control tube contained only cell suspension. These assay mixture were incubated for 3 h at 37°C. Further cell suspension was mixed with 0.1 ml of 1% trypan blue and kept for 2-3 minutes and loaded on a haemocytometer. Dead cells take up the blue colour of trypan blue, while live cells do not take up the dye. The number of stained and unstained cells was counted separately.¹¹

$$\% \text{ cytotoxicity} = \frac{\text{No. of dead cells}}{\text{No. of live cell} + \text{No. of dead cell}} \times 100$$

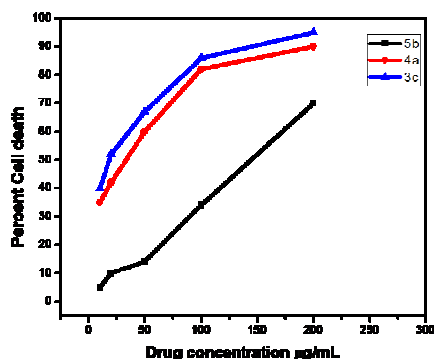


Fig. 3.5. Cytotoxic effects of **2.3c**, **2.4a** and **2.5b** on EAC cells.

Table 3.3. IC₅₀ Value of **2.3c**, **2.4a** and **2.5b** from Trypan blue exclusion method

Compound	IC ₅₀
2.3c	17 µg/Ml
2.4a	33 µg/Ml
2.5b	143 µg/Ml

IC₅₀ values (concentration that inhibited cell growth in 50% compared to untreated controls) were obtained from the graph (Fig. 3.5) and the IC₅₀ values are given in table.3.3. Of the three tested compounds, **2.3c** showed IC₅₀ value of 17µg/mL, **2.4a** 33µg/mL and **2.5b** 143 µg/mL. The literature review reveals that the presence of electron withdrawing groups enhances the cytotoxicity than the electron releasing group. Here the **2.3c** exhibits enhanced cytotoxicity due to the presence of aldehyde group than the ketonic and ester group.

3.2.3.2. Cytotoxicity evaluation against Human breast cancer cell line MCF-7: MTT Assay

(A): Cell culture and maintenance

Human breast cancer MCF-7 (purchased from National Centre for Cell Science, Pune, India) cells were maintained in RPMI medium 1640 supplemented with 10% fetal bovine serum as well as 100 µg/mL streptomycin, 100 U/mL penicillin, 2 mM L-glutamine and Earle's BSS adjusted to contain 1.5 g/l Na bicarbonate, 0.1 mM nonessential amino acids, and 1.0 mM of Na pyruate in a humidified atmosphere containing 5% CO₂ at 37 °C.

(B): In vitro cytotoxicity of synthesized 2.5c

MCF-7 cells were seeded in 96-well plates at a concentration of 1.0×10^4 cells/well and incubated overnight at 37°C in a 5% CO₂ humidified environment. Then the cells were treated with different concentrations of the sample **2.5c** like 10, 20, 30, 40, 50, 60, 70, 80, 90, and 100 µM/mL (dissolved with RPMI medium 1640), respectively. Controls were cultivated under the same conditions without addition of **2.5c**. The treated cells were incubated for 48 h for cytotoxicity analysis. The cells were then subjected for MTT assay. The stock concentration (5 mg/mL) of MTT-(3-(4,5-dimethylthiazol-2-yl)-2,5-diphenyltetrazolium bromide, a yellow tetrazole) was prepared and 100 µL of MTT was added in each wells and incubated for 4h. Purple color formazan crystals were observed and these crystals were dissolved with 100 µL of dimethyl sulphoxide (DMSO), and read at 620 nm in a multi well ELISA plate reader

(Thermo, Multiskan). The dose dependent cytotoxicity was observed in the case of indole-triazole peptidomimetics **2.5c** treated MCF-7 cells. Fifty percentage of cell death, which determines the inhibitory concentration (IC₅₀) value of **2.5c** against MCF-7 cells holds at 25 μM in 48 h (Fig.3.6). This indicates that these molecules exhibit increased bioavailability and have tremendous anticancer potential.

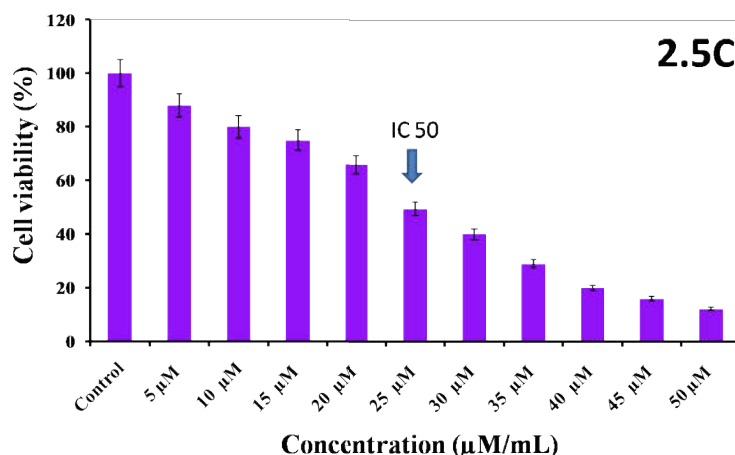


Fig. 3.6. MTT assay results confirming the in vitro cytotoxicity effect of **2.5c** against the MCF-7 cells. The detected IC₅₀ concentration was 25 $\mu\text{M/mL}$.

(C): DAPI (4, 6-diamidino-2-phenylindole, dihydrochloride) staining

MCF-7 cells were treated with **2.5c** at its IC₅₀ concentration (25 μM) for 48 h, and then fixed with methanol: acetic acid (3:1, v/v) prior to washing with PBS. The washed cells were then stained with 1 mg/mL DAPI (4, 6-diamidino-2-phenylindole dihydrochloride) for 20 min in the dark atmosphere. Stained images were recorded with fluorescent microscope with appropriate excitation filter. The bright filed and fluorescence microscopic images are shown in Fig.3.7. However, on treatment with **2.5c** a significant nuclei fragmentation

with condensed and apoptotic nuclei was observed and the total number of apoptotic cells were increasing when the incubation concentration increased. As shown in figure 3.7, strong bluish fluorescence and cellular uptake were observed in the imaging studies with 2.5c and which reveals that these molecules have high potency against breast cancer cell lines (MCF-7).

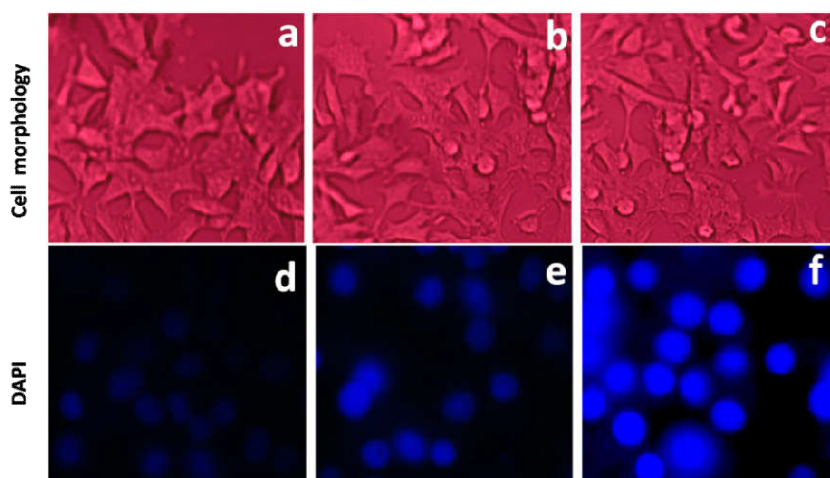


Fig. 3.7. Bright field inverted light microscopy images (a, b, c) and the DAPI nuclear staining (d, e, f) of control cells and 2.5C treated cells. The DAPI images exhibit condensed forms of nuclear materials in apoptotic cells

3.2.3.3. Western blot Analysis

Western blotting was performed to detect the proteins of CDK2 in MCF-7 using beta-actin as the internal standers. The MCF-7 cells (1×10^6) were seeded onto 100-mm culture dishes in the presence or absence of 2.5c were treated for 48 hrs. Cells were then washed twice with ice-cold PBS and incubated in lysis buffer. The lysates were centrifuged at $10,000 \times g$ for 5 min at 4 °C, and were used as the cell protein extracts. Each of the extracts

was applied to 12% SDS polyacrylamide gel electrophoresis after which the proteins were transferred onto a nitrocellulose membrane, and then blocked for 1 h using 10% skim milk in water. After washing in a PBS containing 0.1% Tween 20 for 3 times, the primary antibodies were added at a v/v ratio of 1:1000. After overnight incubation at 4 °C, the primary antibodies were washed away and the secondary antibodies were added for 1 h incubation at room temperature. Finally, the enhanced chemiluminescence detection reagents were used to develop the signal of the membrane.¹² As shown in figure 3.8, our findings demonstrate that the protein level of CDK2 is significantly down-regulated in the 2.5c treated cells when compared to control.

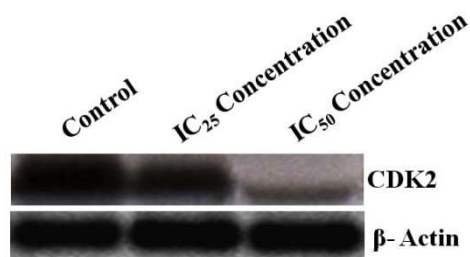


Fig. 3.8. Western blot Analysis of 2.5c from MCF-7 cell line

3.3. Conclusion

24 new indole-triazole-carboxamide peptidomimetics discussed in chapter 2 were subjected to in vitro cytotoxicity assay using computational and experimental methods. The drug property descriptors and the docking scores obtained are promising and based on that we have carried out the in vitro cytotoxicity evaluation of

selected compound against various cancer cell lines. The studies showed that, the molecules are potent against human breast cancer cell line MCF-7. In order to study the selectivity of the new compounds against CDK 2 in MCF-7, western blot analysis was carried out with selected molecules and that also afforded positive results showing the potential of these molecules to undertake further studies based on structure alterations.

3.4. Experimental section

3.4.1. Molecular docking study

Docking studies were carried out using the Auto Dock Vina 1.1.2 program. For this, the pdb structure of 2VV9 (protein structure) was retrieved from the Brookhaven protein database (<http://www.rcsb.org>). Subsequently, the water molecules and the original inhibitors were deleted from the protein structure. The 3D structure of the synthesized compounds was provided using Marvin Sketch 5.8.3, 2012, ChemAxon (<http://www.chemaxon.com>) and was converted to pdbqt coordinate by Autodock Tools (ADT; version 1.5.4). After removing all water molecules, polar hydrogens were added, and charges were assigned using the Kollman united atom library using Autodock Tools (ADT; version 1.5.4). To assign the docking site, all maps were calculated with 1 Å spacing between grid points by Auto grid. The center of the grid box was placed at the center of donepezil with coordinates $x = 2.05$, $y = 25.44$, $z = 10.05$ with exhaustiveness 8. The dimensions of the active site box were seated at 1

5 X17 X 11 Å, and these parameters were noted into conf file. After this, command prompt was opened to run the command followed by splitting the file using vinasplit. After finishing the vinasplit, docking interactions were analyzed using autodock tool.

References

1. (a) M.K.Susan, A. G. Jeanne, J.W. William,T.P. Sean, and C.W. Norman *Combinatorial Chem. and high throughput Screening.*, 2005, **8**, 27-38..
2. B.Bilgin, M.A. N. Sendur, D. S. Dede, M. B. Akinci and B. Yalcin, *Curr. Med. Res. Open.*, 2017, **33**, 1559-1569.
3. G. Mariaul, and P. Belmont.*Molecules.*, 2014, **19**, 14366-14382.
4. M. Malumbres and M. Barbacid, *Nat. Rev. Cancer.*, 2009, **9**, 153–166.
5. (a)D. Hanahan and R.A. Weinberg, *Cell.*, 2000, **100**, 57–70. (b)M. Hall, and G.Peters, *Adv. Cancer Res.* 1996, **68**, 67–108. (c)M. Malumbres, and M. Barbacid, *Nat. Rev. Cancer.*,2001, **1**, 222–231.
6. (a)M.Q. Zhang, *Methods Mol Biol.*, 2012, **803**, 297(b) R. K. Verma, V.K. Prajapati, G.K.Verma, D. Chakraborti, S. Sundar, M. Rai, V.K. Dubey and M. S. Singh, *ACS Med. Chem. Lett.*,2012, **3**, 243. (c) B. J. Al-Hourani, S. K. Sharma, M.Suresh and F. Wuest., *Bioorg. Med. Chem. Lett.*, 2012, **22**, 2235.
7. V. Giulio and P. Alessandro, *Drug Discov. Today.*, 2008, **13**, 285.
8. K.G. Arup, N. V. Vellarkad and J.W. John, *J. Comb. Chem.* 1999, **1**,55.
9. (a) V.S. Heena, H.G. Sunil and P. Rama, P, *J Comput Sci syst Biol.* 2012, **5**, 12–15; (b) P.F. Lamie, W.A.M. Ali, V. Bazgier and R. Lucie, *Eur. J. Med. Chem.*, 2016, **123**, 803-813.
10. M. R. V. Finlay, D. G. Acton, D. M. Andrews, A. J. Barker, M. Dennis, E. Fisher, M. A. Graham, C. P. Green, D. W. Heaton, G. Karoutchi, S. A. Loddick ,R.C. Morgentin , A. Roberts, J. A. Tucker, M. Hazel Weir. *Bioorg.Med.ChemLett.*, 2008 , **18**, 4442-4446.
11. M. F. D. Mota, P. L. Benficiaa, A. C. Batista, F. S. Martins, J.R.D. Paula, M.C. Valadares, *J. Ethnopharmacol.* 2012,**139**,319-329.
12. K. Vimala, S. Sundarraj,M. Paulpandi, S. Vengatesan, S. Kannan, *Process Biochem.*, 2014, **49**, 160-172.

CHAPTER 4

**Structure alterations of Indole-Triazole-
Carboxamides with Coumarin
moieties: Synthesis of a new series of
Indole-Triazole-Coumarin hybride
peptidomimetics.**

Contents

4.1. Introduction.....	142
4.2. Result and discussion.....	143
4.3. Structure elucidation by spectroscopy	149
4.4. Conclusion	161
References	170
Supplementary Material	171

4.1. Introduction

The promising results obtained from the biological screening of Indole-Triazole-Carboxamides (ITC) described in chapter 3 prompted us to undertake systematic structure alterations on it to attain better efficiency and selectivity. As shown in figure 4.1, we decided to substitute the carboxamide part of ITC with a coumarin carboxamide fragment.

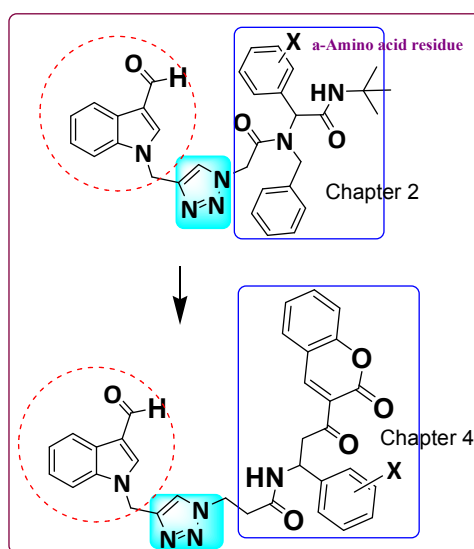


Fig. 4.1: Structure optimizations of Indole-triazole –coumarin peptidomimetics from Indole-triazole- carboxamide peptidomimetics.

Similar to indole, coumarin is another interesting privileged scaffold with repeated occurrence in a large variety of medicinally active natural molecules and drug candidates. Several therapeutically active compounds containing coumarin sub units were reported as anti-bacterials,¹ anti-fungals,² anti-coagulants³ and anti-HIV agents⁴. The pharmacological, biochemical and therapeutic properties of coumarin derivatives are strongly dependent on the nature as well as the position of their structural substituents.⁵ Some of these coumarin derivatives

also exert anticancer effects⁶ and can cause significant changes in the regulation of immune responses. The selected examples of such anticancer molecules are presented in figure 4.2.

As compounds with two or more heterocycles play a vital role in natural and synthetic bioactive compounds, we planned to link indole core with a coumarin moiety through a 1,2,3-triazole spacer using copper (I) catalyzed [3+2] azide-alkyne cycloaddition (CuAAC),⁷ reaction as the fragment assembly tool. The representative structures of the coumarin substituted ITCs are presented in figure 4.3

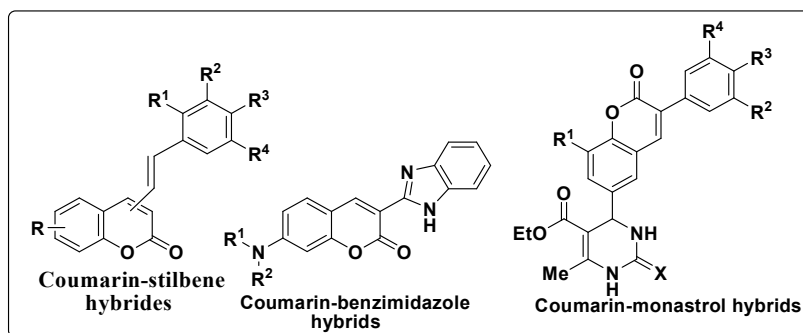


Fig. 4.2 Chemical structure of some Coumarin containing potent anticancer compounds.

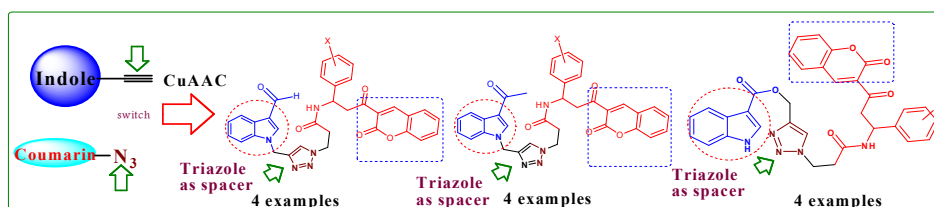


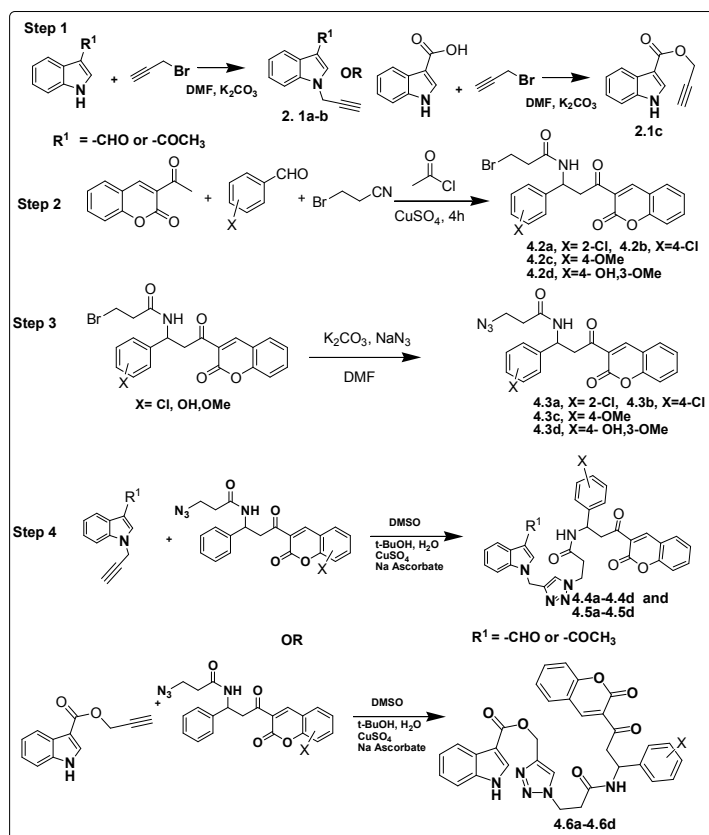
Fig. 4.3. A schematic representation of the “MCR-click” strategy for the synthesis of Indole-Triazole-Coumarin peptidomimetics.

4.2. Result and discussion

The overall sequence involved in the synthesis of the Indole-Triazole Coumarin hybrids are shown in scheme 4.1. As shown in

scheme 4.1, the concept of multicomponent coupling reactions and click chemistry were effectively utilized for the synthesis of these new molecules. The overall sequence involved three synthetic steps.

1. Synthesis of alkyne functionalized indole derivatives.
2. Synthesis of azide functionalized coumarins via an alternate Mannich reaction.
3. Coupling of alkyne and azide functionalities via Cu catalyzed(3+2) cycloaddition.

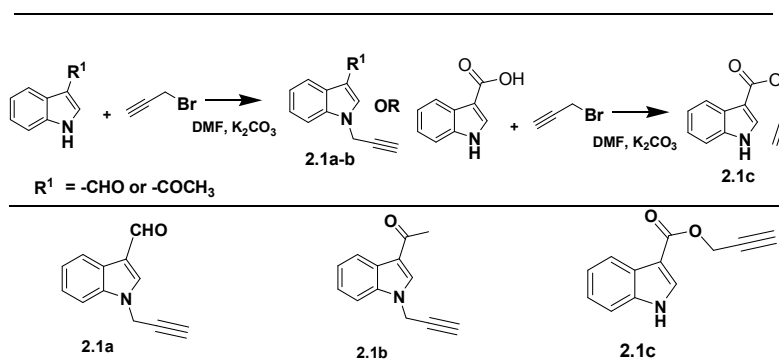


Scheme 4.1. Overall protocol for the synthesis of Indole-Triazole-Coumarin peptidomimetics

4.2.1. Synthesis of alkyne functionalized indole derivatives.

Indole derivatives such as indole-3- carbaldehyde, 3-acetyl indole and indole-3-carboxylic acid were converted to the corresponding alkyne derivatives **2.1a–2.1c** via the base catalyzed propargylation in DMF as shown in Table 4.1.

Table 4.1. List of alkyne functionalized indole derivatives.

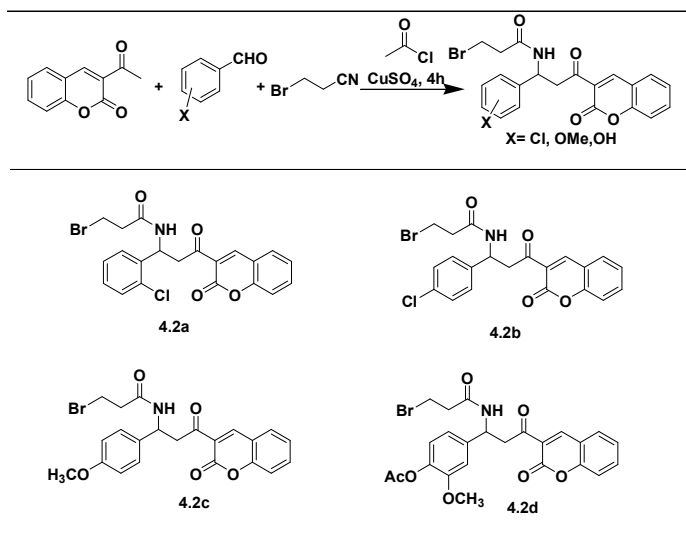


4.2.2. Synthesis of azide functionalized coumarins via alternate Mannich reaction.

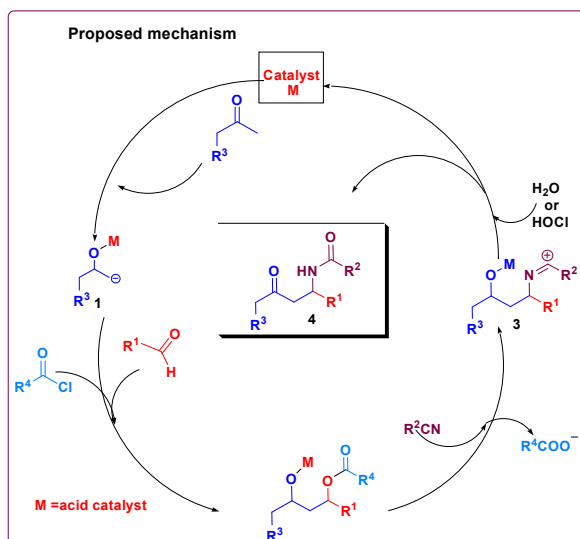
A Mannich type four component reaction as shown in table 4.2 was adopted for the synthesis of the coumarin azides **4.2a-d**. The Mannich reaction was conducted as a solvent free reaction by stirring an aldehyde derivative, 3-acetyl coumarin and bromopropionitrile with slight excess of acetyl chloride in the presence of catalytic amount of boron trifluoride etherate at room temperature for 3h. The subsequent aqueous workup followed by silica column chromatography afforded the bromoamidocoumarins **4.2a-d**(table 4.2)..Those aldehyde scaffolds substituted with an electron withdrawing group at the phenyl ring gave better yield compared to those with electron donating groups at the

same position. The proposed mechanism for the synthesis of compounds **4.2a-d** is given in scheme 4.2.

Table 4.2. List of bromo amido coumarins **4.2a-d** synthesized via alternate Mannich reaction



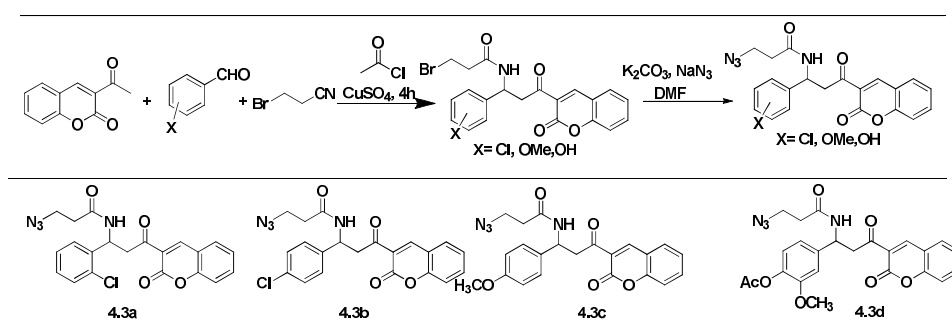
The general mechanism of alternate Mannich reaction is given below.



Scheme 4.2. The proposed Mechanism for the synthesis of compounds **4.2a-d**

The bromine present in **4.2a-d** was then replaced with an azide moiety by treating the bromo amido coumarins with sodium azide via a base catalyzed reaction in DMF at room temperature. The aqueous work of this reaction mixture afforded the azidoamidocoumarins **4.3a-d** in good to excellent yield (Table. **4.3**) and the structures were characterized via FT-IR, ^1H NMR, ^{13}C NMR and HRMS analysis.

Table 4.3. List of Coumarin azides **4.3a-4.3d** synthesized via alternate Mannich reaction.

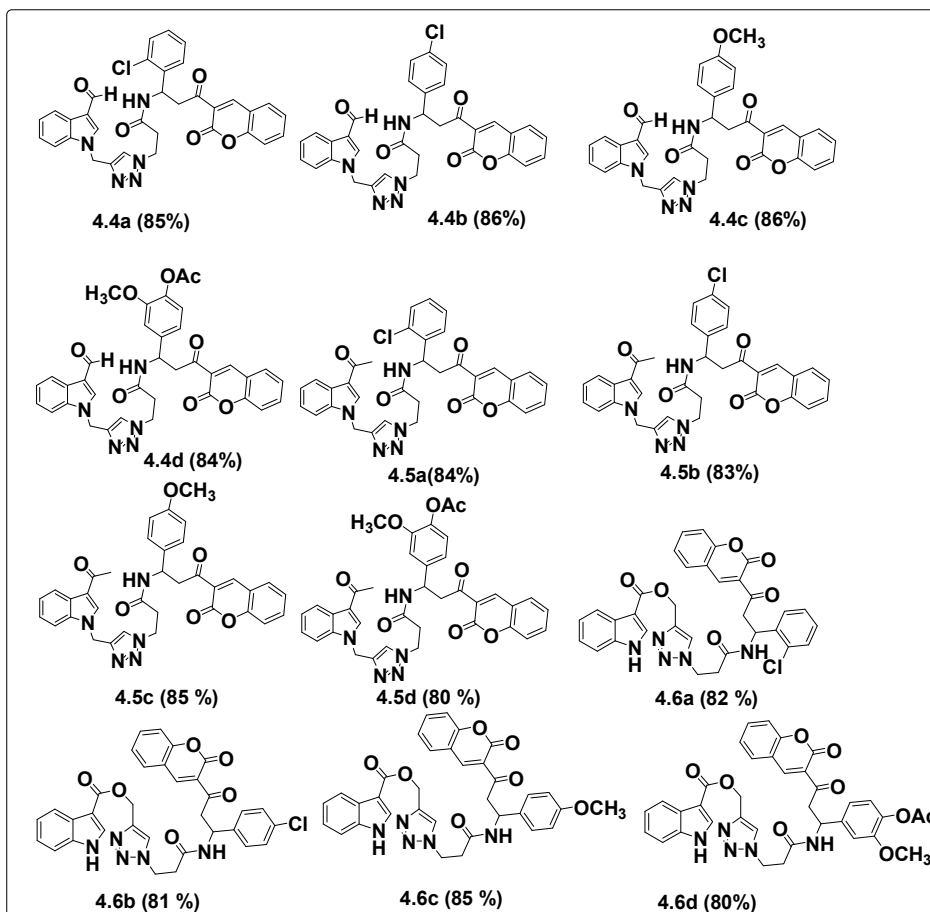


4.2.3. Synthesis of Indole-Triazole-Coumarin peptidomimetics via Copper(I) catalysed Azide Alkyne cycloaddition (CuAAC).

The fragments **2.1a-2.1c** and **4.3a-4.3d** were then assembled via CuAAC to obtain the peptidomimetic **4.4a-4.6d** spaced with a linker 1,2,3-triazole (scheme **4.1**, step **4**). The click reactions were done at room temperature in a mixed solvent system containing *t*-butanol, water and DMSO in the ratio 4:2:1 using CuSO₄ as Cu (I) source and sodium ascorbate as the reducing agent. The entire click reactions afforded excellent yield for **4.4a-4.6d** as shown in table **4.4** and the structures were characterized via FT-IR, ^1H NMR, ^{13}C NMR

and HRMS analysis. The cytotoxicity evaluation will be discussed in chapter 5.

Table 4.4. The List of Indole-Triazole-Coumarin hybrids synthesized via CuAAC reaction.



4.3. Structure elucidation by spectroscopy

Structure identification of 1-(1-(prop-2-yn-1-yl)-1H-indol-3-yl) ethanone 2.1b

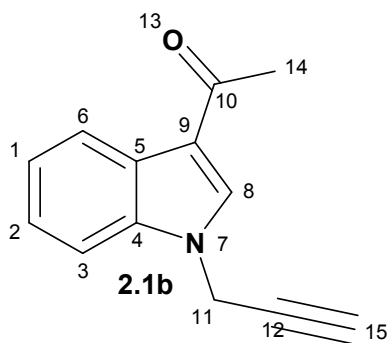


Fig.4.4.structure of **2.1b**

The alkyne functionalized indole **2.1b** is taken as a representative example for a general discussion on structure elucidation. The compound is numbered as shown in figure 4.4. The FT-IR spectrum of the compound shows major absorptions at 3218, 2125, 1676, 1628 cm^{-1} . The presence of propargylated group is confirmed by the bands at 3218 and 2125 cm^{-1} . The peak due to the $\text{C}\equiv\text{C}-\text{H}$ stretching vibration appeared at 3218 cm^{-1} and the $\text{C}\equiv\text{C}$ stretching vibration occurred at 2125 cm^{-1} . The absorption at 1676 cm^{-1} is due to the $\text{C}=\text{O}$ stretching vibration of the ketone group (Fig.4.5).

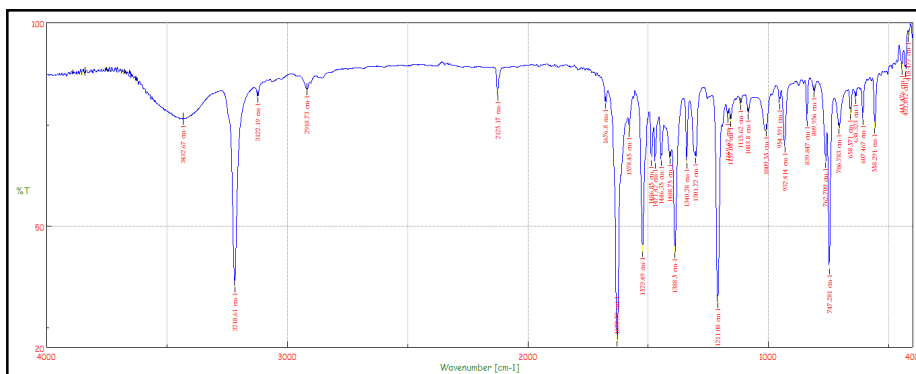


Fig.4.5. FTIR spectrum of compound **2.1b**

The initial structure information obtained from the FT-IR spectrum is further confirmed by the ^1H NMR spectrum (Fig.4.6). In the ^1H NMR spectrum, the $-\text{CH}_3$ proton at position 14 is observed as a singlet at δ 1.56 ppm. The aromatic proton at position 8 is observed at δ 8.40. The CH_2 proton at position 11 is observed as a singlet at δ 4.92 and the CH proton (alkyne CH) at position 15 is observed as another singlet at δ 2.17. The four aromatic protons were observed as three sets, as two protonsinglet at δ 7.26 , one proton as singlet at δ 7.91 and one proton multiplet between δ 7.35-7.3 and three sets of multiplets at δ 8.15-8.12 , δ 7.66-7.64 and δ 7.38-7.28.

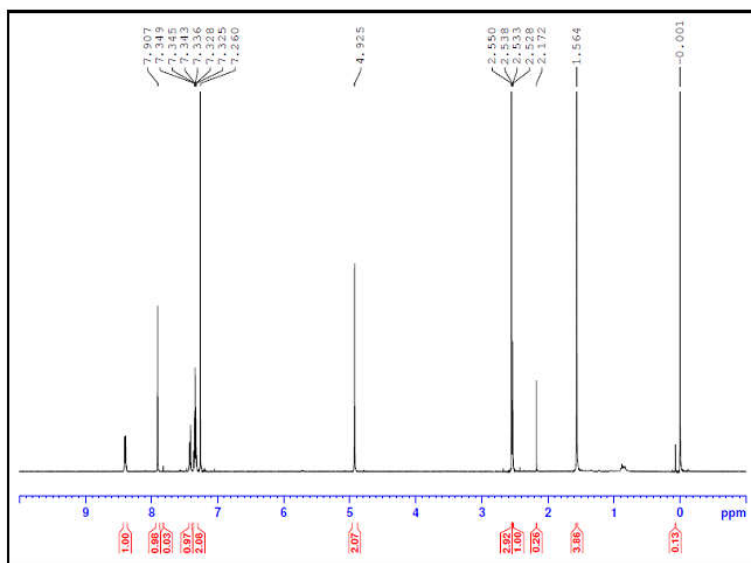


Fig.4.6. ^1H - NMR spectrum of compound **2.1b**

The functional group absorptions observed in the FT-IR spectrum and ^1H NMR spectrum are in well agreement with the information obtained from its ^{13}C NMR spectrum. The down field peak at δ 195.4 is due to the carbonyl carbon at position C10. The peaks at δ 140.5 and δ 137.05 are attributed to the carbons at position C4 and C8 respectively. The signals at δ 125.1, 124.2, 123.2, 121.5, 118.0 and 111 are due to the aromatic carbons. The propargyl group carbons at C12, C15 and C11 were observed at δ 78.4, 77.2 and δ 40.2. The $-\text{CH}_3$ carbon at position 14 is observed at δ 25.1 (Fig. 4.7).

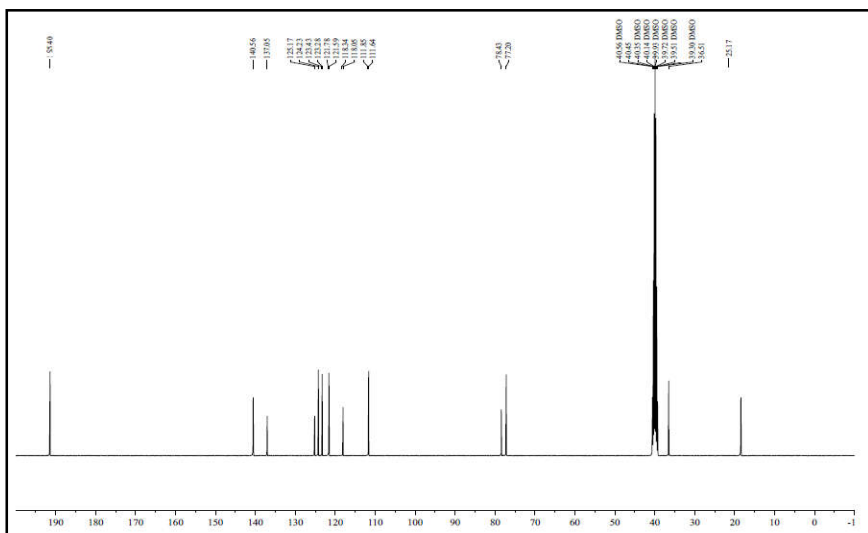


Fig. 4.7. ^{13}C NMR spectrum of compound **2.1b**

The structure of the compound is further confirmed by mass spectral analysis. The molecular ion peak at 221.0739 $[\text{M}+\text{Na}]^+$ obtained in MS (HRMS) further confirms the structure of the compound **2.1b** (Fig. 4.8).

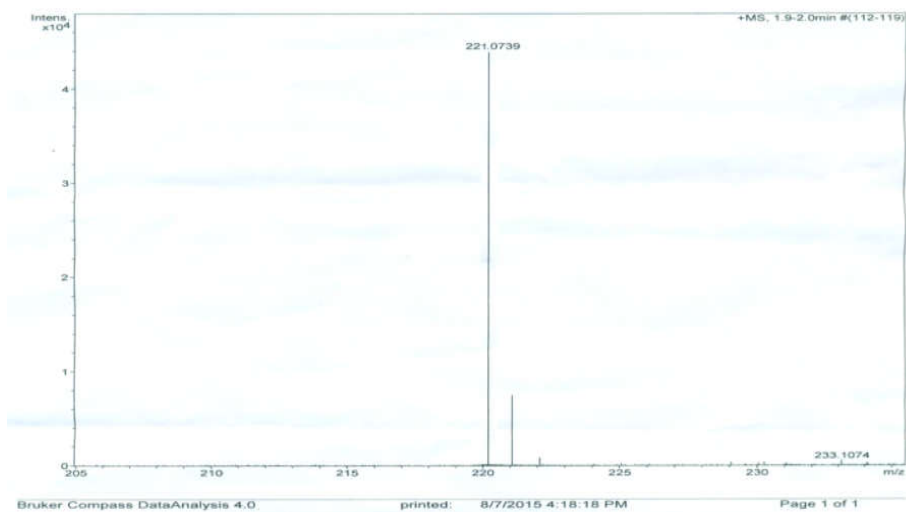


Fig. 4.8: HRMS of compound **2.1b**

3.4.2 Structure identification of 3-azido-N-(1-(4-methoxyphenyl)-3-oxo-3-(2-oxo-2H-Chromen-3-yl)propyl) propanamide 4.3c

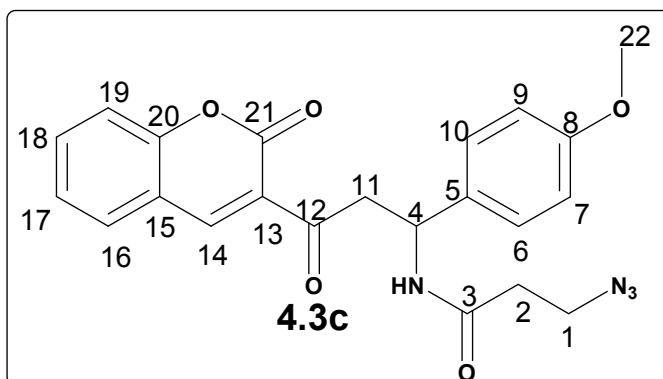


Fig.4.9. Structure of 4.3c

For a general discussion on the structure elucidation of azides, compound **4.3c** is taken as a representative example. The molecule is numbered as shown in Figure **4.9**. The FT-IR spectrum of the compound **4.3c** (figure **4.10**) give major absorptions at 3423, 2102, 1725, 1658, 1606 and 1563 cm^{-1} . The NH stretching vibration band of the acetamido group occurs at 3423 cm^{-1} . The band at 2102 cm^{-1} is the characteristic peak of the azide linked to the carbon at position 1. The peak at 1725 cm^{-1} is due to the lactone carbon at position C21. The amide I band, i.e., the band due to the C=O stretching vibration of (C2) occurs at 1658 cm^{-1} and the amide II band which arises from the interaction between the N-H bending and the C-N stretching of the C-N-H group is obtained at 1563 cm^{-1} .

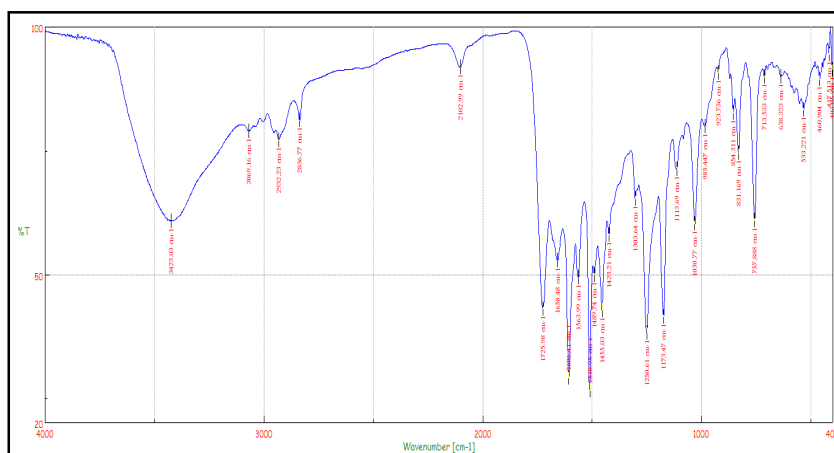


Fig. 4.10. FT-IR spectrum of the compound **4.3c**

The singlet obtained at δ 8.52 is due to the coumarin CH at position 14. Singlet obtained at δ 8.19 corresponds to the amido bond (NH). Triplet observed between δ 8.57-8.52 is attributed to the NH proton of the acetamido group. Other downfield resonances, a doublet between δ 7.93-7.92, triplet between δ 7.74-7.71 and a multiplet between δ 7.52-7.42 correspond to the aromatic protons at the coumarin part. The remaining aromatic protons on the aldehyde fragment appeared as two sets of two proton doublets between δ 7.07-7.05 and δ 6.49-6.48. Owing to the vicinal couplings, the CH proton at position 4 is obtained as a triplet between δ 5.08-4.94. The CH₂ protons at position 11 are obtained as a doublet of doublet between δ 3.62-3.57 and 3.26-3.21 with approximately equal coupling constants. The remaining two up field signals at δ 2.72-2.70 and 1.98-1.96 are due to the protons at position C2 and C1 respectively (Fig.4.11).

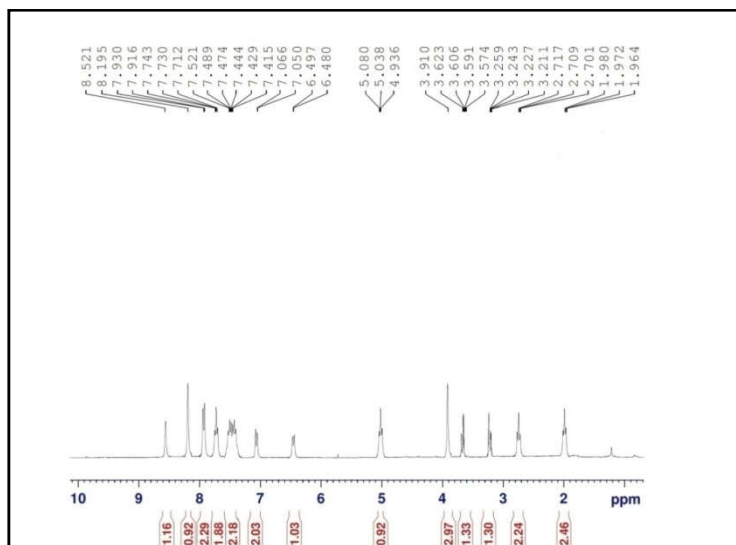


Fig.4.11: ¹H NMR spectrum of the compound 4.3c

In the ¹³C NMR spectrum, the ketone carbonyl carbon C12 and the amide carbonyl C3 are observed at δ 201 and 172 respectively (Fig.4.12). The lactone carbonyl peak at C21 is observed as a downfield peak at 160. The signals at δ 156, 153, 140, 134, 131, 130, 128, 125, 121, 120, 116 and 112 are due to the aromatic carbons. The peak at δ 56 is due to the methyl carbon at position 22. The other three up field resonances i.e., at δ 51, 47, 46 and 332 are attributed to C4, C11, C1 and C2 respectively.

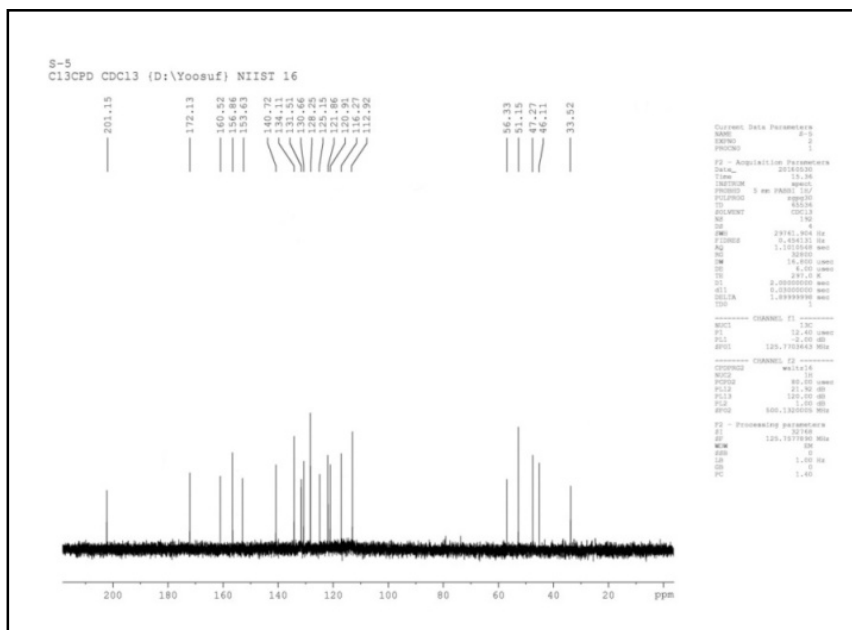


Fig. 4.12: ^{13}C NMR spectrum of the compound 4.3c

The structure is further confirmed by the mass spectral analysis. The M^+ peak is observed at m/z 420 (Figure 4.13).

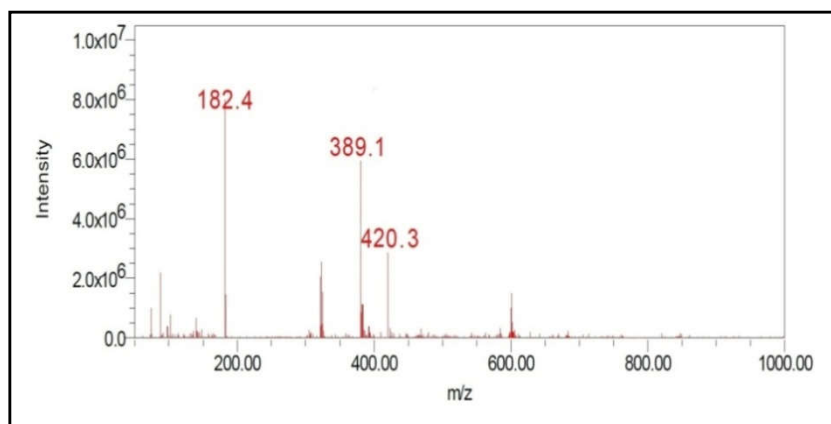


Fig. 4.13: The Mass spectrum of the compound 4.3c

3.4.3 Structure elucidation of 3-(4-((3-acetyl-1H-indol-1-yl)methyl)-1H-1,2,3-triazol-1-yl)-N-(1-(4-chlorophenyl)-3-oxo-3-(2-oxo-2H-chromen-3-yl)propyl)propanamide, 4.5b

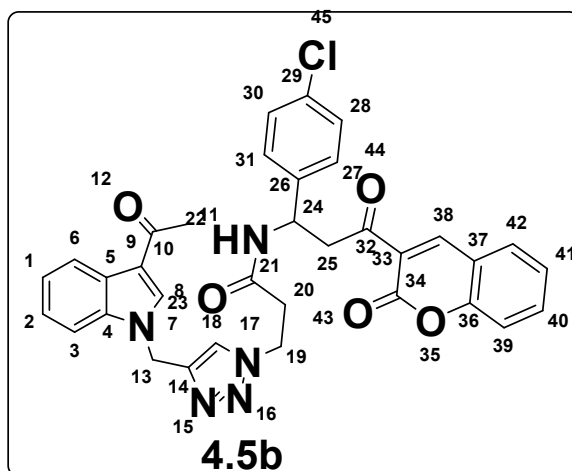


Fig.4.14.Structure of **4.5b**

For the structure elucidation of the click product, compound **4.5b** is taken as a representative and is numbered as in figure **4.14**. The FT-IR spectrum of the compound **4.5b** gave major absorptions at 3218,2923,1716,1680,1627,1609,1525,1488,1455,1388,1340,1275,1207,1090,1013,944,931,827,753,681,657 cm^{-1} . The band at 3218 cm^{-1} is due to the NH stretching vibration of the acetamido group. The amide I band, ie., band due to the C=O stretching vibration occurs at 1627 cm^{-1} and the amide II band which arises from the interaction between the N-H bending and the C-N stretching of the C-N-H group is obtained at 1525 cm^{-1} . The absorption at 1716 cm^{-1} is due to the C=O stretching vibration of the coumarin part. The absorption at 1680 cm^{-1} is due to the C=O stretching vibration of the indole part (Fig. **4.15**).

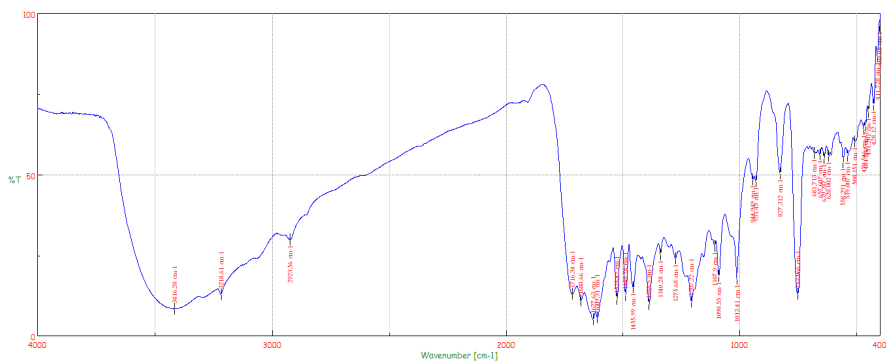


Fig.4.15. FTIR spectrum of compound **4.5b**

The singlet at δ 8.58 corresponds to CH proton at position 8. The coumarin CH proton at position 38 is observed as a singlet at δ 8.38. NH proton at position 22 was observed as a singlet at δ 8.30. The peaks from δ 8.21 to 7.26 correspond to the 11 aromatic protons. The Singlet obtained at δ =7.43 corresponds to the triazole proton. The peak at δ 5.24 corresponds to the CH₂ protons at position 13. The CH proton at position 24 and CH₂ proton at position 19 appears as a multiplet at δ 5.19-5.01 and δ 4.3-4.1 respectively. The CH₂ protons at position 25 are obtained as a doublet of doublet at δ 3.31-3.26 and 3.19-3.01 with approximately equal coupling constants. The three protons of the methyl group at position 11 appear as a singlet at δ 1.23 (Fig. **4.16**)

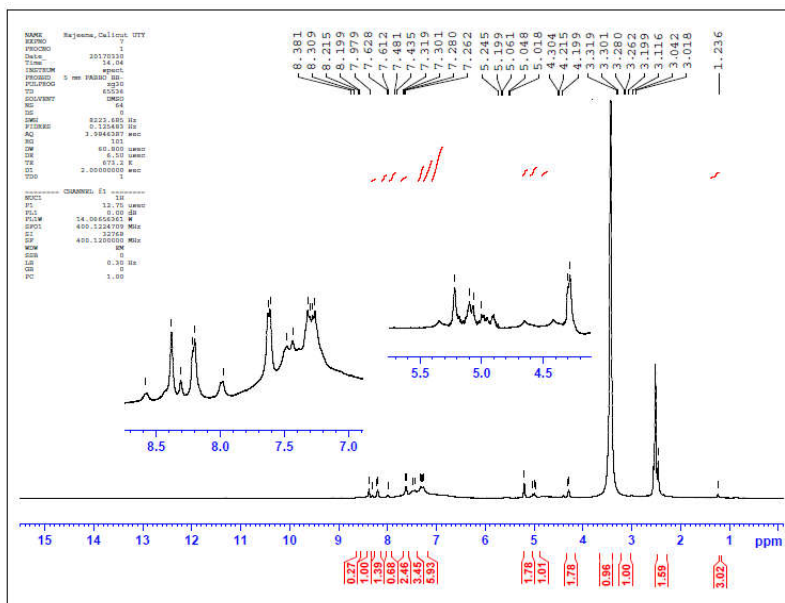


Fig.4.16. ¹HNMR spectrum of the compound **4.5b**

In the ¹³C NMR spectrum (Fig.4.17) the carbonyl carbon at C32, ketone carbonyl carbon at C10 and amide carbonyl at C21 are observed at their characteristic regions, at δ 195.1, 185.2 and 168.6 respectively. The lactone carbonyl at C₃₄ observed at 167.4. The carbons of the aromatic rings give the peaks at δ 141.0, 140.5, 139.8, 138.6,137.3,137.0,129.4,128.9,125.1,124.2,124.1,124.0,123.3, 123.2, 123.0,121.6,121.5,121.5,118.1,118.0,112.5,112.0,111.6,11.5,111.2. The remaining up field signals at δ 60.7, 51.6,50.9, 48.1, 28.5 and 28.3 are credited to the carbons C13,C24, C19, C25, C20 and C11 respectively.

4.4. Conclusion

In conclusion, we have demonstrated a three step process for the synthesis of a coumarin linked indole -triazole-coumarin hybrids by effectively employing the concept of multicomponent coupling strategy with click chemistry. 12 new hybrid structures were obtained in good to excellent yield and the compounds were characterized using FT-IR, ¹H NMR, ¹³C NMR and mass spectral techniques. The *in vitro* screening of the biological properties of the molecules via experimental and computational methods are discussed in chapter 5.

4.5. Experimental Section

4.5.1 Materials and methods

All solvents and reagents were of reagent grade quality brought from Aldrich Chemical Company, Fluka, or Merck and used without any further purification. The reactions were monitored by thin-layer chromatography (TLC) using plates prepared with Merck silica gel G by irradiation with UV light and/or treatment with iodine. Fourier transform infrared (FT-IR) spectra were recorded on a Jasco FTIR-4100 spectrometer. The ¹H- and ¹³C-nuclear magnetic resonance (NMR) spectra operating at the frequencies of 400 and 100 MHz respectively were measured with Varian NMR (VNMRS-400) spectrometer and the ¹H- and ¹³C-nuclear magnetic resonance (NMR) spectra operating at the frequencies of 300 and 75 MHz respectively were measured with Bruker ACF 300 MHz spectrometer in dimethylsulphoxide-*d* (DMSO-*d*₆). The ¹H NMR Chemical shifts are reported in parts per million (ppm) relative to TMS as internal standard ($\delta=0$ ppm). The coupling

constants are reported in hertz (Hz). Mass (FAB) spectra are recorded on a JEOL JMS600H spectrometer. The absorption spectra of the compounds were recorded on JASCO V 550 UV/Vis spectrophotometer and Fluorescence measurements were carried out on Perkin Elmer LS 55 spectrophotometer.

4.5.2. General procedure for the synthesis of coumarin functionalized azides 4.3a-4.3d.

A mixture of corresponding benzaldehyde (1 mmol), 3-acetylcoumarin (188 mg, 1mmol), and 3-bromopropionitrile (133 mg, 1 mmol) in acetonitrile (8 ml) were stirred in the presence of catalytic amount of CuSO₄ at room temperature for 4 h. Subsequently, the reaction mixture was poured into ice cold water and extracted with CH₂Cl₂ (15 mLx2). The evaporation of the solvent followed by purification on a silica gel column (100–200 mesh), by eluting with ethyl acetate/hexane (3:1) afforded the corresponding β -amidoketonebromide derivative **2**. **2** (1 mmol), K₂CO₃ (414 mg, 3 mmol), NaN₃ (65 mg, 1 mmol) were dissolved in dimethylacetamide and stirred for 6–8 h and then poured into ice cold water. The precipitate was filtered and dried under vacuum to afford the azides **4.3a-4.3d**.

3-bromo-N-(1-(4-chlorophenyl)-3-oxo-3-(2-oxo-2H-Chromen-3-yl)propyl) propanamide 4.2b. FT-IR (KBr) γ_{\max} : 3423, 3292 2923, 2852, 1725, 1676, 1608, 1560, 1527, 1455, 1349, 1225, 1174, 1108, 1024, 759 cm⁻¹; ¹H NMR (500 MHz, DMSO-*d*₆): δ H (ppm): 8.58 (s, 1H), 8.17 (s, 1H), 7.94-7.92(d, J = 7.5Hz, 1H), 7.77-7.74 (t, 1H), 7.52-

7.482 (m, 4H), 7.30-7.28 (t, 1H), 6.79-6.78 (d, 2H), 5.17-5.13 (t, 1H), 3.89-3.84 (dd, J = 8Hz, J = 16Hz, 1H), 3.45-3.40 (dd, J = 8Hz and J=20Hz, 1H), 3.19-3.17 (t, 2H), 2.36-2.30 (t, 2H); ¹³C NMR (100 MHz, DMSO-*d*₆)δC(ppm): 199.7, 175.3, 159.9, 153.6, 143.6, 139.0, 134.9, 129.7, 128.9, 125.4, 123.8, 121.8, 116.1, 113.2, 50.1, 47.5, 38.2, 29.4.

3-bromo-N-(1-(4-methoxyphenyl)-3-oxo-3-(2-oxo-2H-Chromen-3-yl)propyl) propanamide 4.2c. FT-IR (KBr) γ_{\max} : 3421, 3068, 2923, 2850, 1725, 1681, 1606, 1580, 1561, 1510, 1455, 1422, 1364, 1303, 1251, 1172, 1119, 1028, 922, 831 cm⁻¹; ¹H NMR (500 MHz, DMSO-*d*₆): δH (ppm): 8.31 (s, 1H), 8.04 (s, 1H), 7.78-7.76 (d, J = 8Hz, 1H), 7.50-7.49 (t, 1H), 7.44-7.41 (t, 1H), 7.01-7.08 (d, J=8Hz, 2H), 6.79-6.78 (d, J=7.5Hz, 2H), 5.23-5.21 (t, 1H), 3.98 (s, 3H), 3.78-3.74 (dd, J = 8Hz, J = 16Hz, 1H) 3.49-3.44 (dd, J = 8Hz and J=20Hz, 1H), 3.41-3.40 (t, 2H), 2.40-2.39 (t, 2H) ; ¹³C NMR (100 MHz, DMSO-*d*₆)δC(ppm): 200.5, 174.0, 160.8, 156.0, 153.6, 139.7, 134.2, 129.7, 128.9, 125.7, 123.7, 121.8, 118.2, 114.2, 109.2, 56.2, 51.0, 47.6, 39.5, 29.0; MS(ESI): m/z =459.3 [M +1]⁺

3-bromo-N-(1-(4-hydroxy-3-methoxyphenyl)-3-oxo-3-(2-oxo-2H-Chromen-3-yl)propyl) propanamide 4.2d. Yellowish solid ; 396.46mg (yield 86%); FT-IR (KBr) γ_{\max} : 3429, 2923, 2853, 1760, 1724, 1677, 1607, 1560, 1509,, 1489, 1455, 1422, 1370, 1269, 1199, 1123, 1083, 1031, 914, 862 cm⁻¹; ¹H NMR (500 MHz, DMSO-*d*₆): δH (ppm): 8.29 (s, 1H), 8.07 (s, 1H), 7.81-7.80 (d, J = 8Hz, 1H), 7.59-7.57 (t, 1H), 7.50-7.48 (t, 1H), 7.15-7.14 (d, J=8Hz, 2H), 6.89-6.87 (d, J=7.5Hz, 2H), 5.12-5.11 (t, 1H), 3.96 (s, 3H), 3.79-3.75 (dd, J = 8Hz, J = 16Hz, 1H) 3.49-3.44 (dd, J = 8Hz and J=20Hz, 1H), 3.27-3.25 (t, 2H), 2.21-

2.20 (t, 2H), 2.17 (s, 3H) ; ^{13}C NMR (100 MHz, $\text{DMSO-}d_6$) δC (ppm): 199.5, 172.7, 168.0, 159.0, 155.7, 150.8, 142.7, 139.0, 134.9, 129.9, 128.9, 125.0, 122.7, 120.8, 119.2, 114.2, 110.2, 106.2, 56.1, 52.6, 49.6, 47.6, 37.6, 29.9.

3-azido-N-(1-(4-chlorophenyl)-3-oxo-3-(2-oxo-2H-Chromen-3-yl)propyl) propanamide 4.3b. Brown solid ; 348.37mg (yield 82%); FT-IR (KBr) γ_{max} : 3423, 2107, 1720, 1655, 1606, 1489, 1456, 1407, 1267, 1213, 1121, 1037, 857, 755, 712 cm^{-1} . ^1H NMR (500 MHz, $\text{DMSO-}d_6$): δH (ppm): 8.581 (s, 1H), 8.40 (s, 1H), 7.94-7.92 (d, J = 8Hz, 2H), 7.77-7.74 (t, 2H), 7.52-7.48 (m, 2H), 7.30-7.28 (t, 1H), 6.79-6.78 (d, J=8Hz, 2H), 5.14-5.13 (t, 1H), 3.60-3.55 (dd, J = 8Hz, J = 16Hz, 1H) 3.18-3.13 (dd, J = 8Hz and J=20Hz, 1H), 2.12-2.11 (t, 2H), 1.31-1.30 (t, 2H) ; ^{13}C NMR (100 MHz, $\text{DMSO-}d_6$) δC (ppm): 199.7, 175.3, 159.8, 153.6, 143.7, 139.7, 134.9, 129.7, 128.9, 125.7, 123.7, 121.8, 116.2, 113.2, 51.1, 47.6, 45.9, 34.2.

3-azido-N-(1-(4-methoxyphenyl)-3-oxo-3-(2-oxo-2H-Chromen-3-yl)propyl) propanamide 4.3c FT-IR (KBr) γ_{max} : 3423, 3069, 2932, 2836, 2102, 1725, 1658, 1606, 1563, 1510, 1489, 1303, 1250, 1173, 1113, 1030, 985, 923, 854, 831 cm^{-1} ; ^1H NMR (500 MHz, $\text{DMSO-}d_6$): δH (ppm): 8.52 (s, 1H), 8.19 (s, 1H), 7.93-7.92 (d, J = 7Hz, 1H), 7.74-7.71 (t, 1H), 7.52-7.42 (m, 2H), 7.07-7.05 (d, J=8Hz, 2H), 6.49-6.48 (d, J = 8.5Hz, 1H), 5.08-4.94 (t, 1H), 3.91 (s, 3H), 3.62-3.57 (dd, J = 8Hz, J = 16Hz, 1H) 3.26-3.21 (dd, J = 8Hz and J=20Hz, 1H), 2.72-2.70 (t, 2H), 1.98-1.96 (t, 2H) ; ^{13}C NMR (100 MHz, $\text{DMSO-}d_6$) δC (ppm): 201.2, 172.0, 160.5, 156.8, 153.6, 140.7, 134.1, 131.5, 130.6, 128.2,

125.1, 121.8, 120.9, 116.2, 112.9, 56.3, 51.1, 47.2, 46.1, 33.5;
MS(ESI): m/z = 420.3.

3-azido-N-(1-(4-hydroxy-3-methoxyphenyl)-3-oxo-3-(2-oxo-2H-Chromen-3-yl)propyl)propanamide 4.3d. Brownish solid ; 382.76mg (yield 80%); FT-IR(KBr) γ_{\max} : 2936, 2834, 2108, 1729, 1607, 1510, 1455, 1415, 1384, 1270, 1202, 1122, 1030, 872, 757, 524 cm^{-1} ; ^1H NMR (500 MHz, DMSO- d_6): δH (ppm): 8.57 (s, 1H), 8.39 (s, 1H), 7.94-7.92 (d, J = 8Hz, 1H), 7.76-7.73 (t, 1H), 7.59-7.49 (m, 2H), 6.97-6.96 (d, J = 7Hz, 1H), 5.14-4.95 (t, 1H), 3.73 (s, 3H), 3.63-3.58 (dd, J = 8Hz, J = 16Hz, 1H), 3.38-3.34 (dd, J = 8Hz and J=20Hz, 1H), 2.46-2.44 (t, 2H), 2.04 (s, 3H), 1.68-1.66 (t, 2H); ^{13}C NMR (100 MHz, DMSO- d_6) δC (ppm): 200.5, 173.0, 169.0, 160.8, 156.6, 149.6, 139.7, 137.0, 134.9, 129.7, 128.9, 125.7, 123.7, 121.8, 119.2, 114.2, 110.0, 106.2, 56.1, 52.5, 48.6, 47.6, 35.6, 29.2.

3.5.3. General procedure for the Cu (I) 1, 3-dipolar cycloaddition reaction for the formation of indole-triazole-coumarin.

An equimolar amount 1-(prop-2-yn-1-yl)-1H indole-3-carbaldehyde **1a** (91.5342 mg, 0.5 mmol) and the coumarin azide **4.3b** (239.0744 mg, 0.5 mmol) were dissolved in minimum amount of DMSO. To this, 2 ml of *t*-BuOH, 1 ml of water, $\text{CuSO}_4 \cdot 5\text{H}_2\text{O}$ (200 mg) and sodium ascorbate (150 mg) were added and stirred in room temperature for 12 h. and then poured in to cold water. The precipitated click product was filtered, washed with water and dried under vacuum to afford **3.4d** in pure form (555.79 mg, 84%).

N-(1-(4-chlorophenyl)-3-oxo-3-(2-oxo-2H-chromen-3yl)propyl)-3-(4-((3-formyl-1H-indol-1-yl)methyl)-1H-1,2,3-triazol-1-yl)propanamide 4.4b. Brownish solid; 522.92mg (yield 86%); IR (KBr) ν_{max} : 3309, 2935, 2745, 2676, 2491, 1641, 1580, 1528, 1452, 1393, 1315, 1241, 1196, 1030, 750, 428 cm^{-1} ; ^1H NMR (400 MHz, DMSO- d_6): δH (ppm): 9.88(s, 1H), 8.41-8.36(d, $J=20$ Hz, 1H), 8.36-8.34(d, $J=8$ Hz, 1H), 8.30-8.27(d, $J=8$ Hz, 1H), 8.21(s, 1H), 8.12(s, 1H), 7.73-7.71(d, $J=7$ Hz, 1H), 7.66(s, 1H), 7.63-7.17(m, 8H), 6.36-6.34(m, 1H), 6.22(s, 2H), 5.93-5.87(dd, $J=8$ Hz and $J=16$ Hz, 1H), 5.48-5.43(dd, $J=8$ Hz and $J=20$ Hz, 1H), 5.06-5.01(m, 2H), 1.35-1.23(t, 2H); ^{13}C NMR (100 MHz, DMSO- d_6) δC (ppm): 199.9, 185.4, 177.7, 166.5, 159.3, 141.1, 139.8, 137.0, 131.9, 129.5, 125.3, 124.3, 124.1, 123.3, 123.2, 123.1, 121.6, 121.5, 121.5, 117.8, 112.5, 111.5, 112.5, 111.6, 111.2, 90.9, 77.2, 48.1, 46.1, 36.5; HRMS m/z ; 608.1699 (calc. 608.1701)

N-(1-(4-hydroxy-3-methoxyphenyl)-3-oxo-3-(2-oxo-2H chromen-3-yl) propyl)-3-(4-((3-formyl-1H-indol-1-yl) methyl)-1H-1,2,3-triazol-1-yl) propanamide 4.4d.

Brownish solid ; 555.79 mg (yield 84 %); IR (KBr) ν_{max} : 2922, 1719, 1655, 1608, 1530, 1488, 1465, 1401, 1384, 1321, 1269, 1201, 1170, 1123, 1032, 752 cm^{-1} ; ^1H NMR (400 MHz, DMSO- d_6): δ 9.93 (s, 1H), 8.90-8.87 (d, $J=12$ Hz, 1H), 8.40 (s, 1H), 8.40 (t, 1H), 8.35(s, 1H), 8.21(s, 1H), 8.11-7.11 (9H, m), 7.64(s, 1H), 6.37(s, 2H), 6.34-6.22(t, 1H), 5.92-5.90 (d, $J=8$ Hz, 1H), 5.75-5.71(d, $J=16$ Hz, 1H), 5.06-5.01(t, 2H), 5.06-5.01(t, 2H), 3.98(s, 3H), 1.23(s, 3H); ^{13}C NMR (100 MHz, DMSO- d_6) δC (ppm): 199.9, 185.4, 177.7, 166.5, 159.3, 156.2, 141.1, 139.8, 137.0, 131.9, 129.5, 125.3, 124.3, 123.3, 123.1, 121.6, 117.8, 112.5,

111.2,90.9,77.2,51.1,46.1,29.4; HRMS m/z ; 662.2232 (calc. 662.2251).

3-(4-((3-acetyl-1H-indol-1-yl)methyl)-1H-1,2,3-triazol-1-yl)-N-(1-(4-chlorophenyl)-3-oxo-3-(2-oxo-2H-chromen-3-yl)propyl)propanamide 4.5b. Brownish solid; 516.32mg (yield 83%); IR (KBr) ν_{max} : 3218, 2923, 1716, 1680, 1627, 1609, 1525, 1488, 1455, 1388, 1340, 1275, 1207, 1090, 1013, 944, 931, 827, 753, 681, 657 cm^{-1} ; ^1H NMR (400 MHz, DMSO- d_6): δH (ppm): 8.58(s, 1H), 8.38(s, 1H), 8.30(s, 1H), 8.21-8.19(d, $J=6\text{Hz}$, 1H), 8.21(s, 1H), 7.97(s, 1H), 7.62-7.61(d, $J=6\text{Hz}$, 1H), 7.48(s, 1H), 7.43(s, 1H), 7.31-7.26(m, 6H), 5.24(s, 2H), 5.19-5.01(m, 1H), 4.30-4.19(m, 2H), 3.31-3.26(dd, $J=8\text{Hz}, 16\text{Hz}$, 1H), 3.19-3.01(dd, $J=10\text{Hz}$, 1H), 2.46-2.35(m, 2H), 1.23(s, 3H); ^{13}C NMR (100 MHz, DMSO- d_6) δC (ppm): 195.1, 185.2, 168.6, 167.4, 160.7, 141.0, 140.5, 139.8, 138.6, 137.3, 137.0, 129.4, 128.9, 125.1, 124.2, 124.1, 124.0, 123.3, 123.2, 123.0, 121.6, 121.5, 121.5, 118.1, 118.0, 112.5, 112.0, 111.6, 11.5, 111.2, 60.7, 51.6, 50.9, 48.1, 28.5, 28.3; HRMS m/z ; 622.1854 (calc. 622.1857).

3-(4-((3-acetyl-1H-indol-1-yl)methyl)-1H-1,2,3-triazol-1-yl)-N-(1-(4-hydroxy-3-methoxyphenyl)-3-oxo-3-(2-oxo-2H-chromen-3-yl)propyl)propanamide 4.5d. Brownish solid ; 540.55 mg (yield 80%); IR (KBr) ν_{max} : 2927, 2851, 1718, 1681, 1608, 1513, 1488, 1455, 1428, 1387, 1364, 1319, 1271, 1215, 1123, 1084, 1031, 933, 859, 822, 756, 611, 559 cm^{-1} ; ^1H NMR (400 MHz, DMSO- d_6): δH (ppm): 9.93 (s, 1H), 8.38(s, 1H), 8.30(s, 1H), 8.21 (s, 1H), 7.65-7.63 (d, $J=8\text{Hz}$, 1H), 7.49-7.48 (d, $J=6\text{Hz}$, 1H), 7.41(s, 1H), 7.32-7.26(m, 7H), 6.37(s, 2H), 6.34-6.22(t, 1H), 5.19-5.04(t, 2H), 4.30(s, 3H), 3.93-3.87(dd, $J=10\text{Hz}$ and $J=12\text{Hz}$, 1H), 3.86-3.83(dd, $J=8\text{Hz}$, 1H), 2.43-2.41(t, 2H), 1.91(s, 3H), 1.23(s, 3H)

); ¹³CNMR(100MHz,DMSO-d₆) δ C(ppm):195.2,185.4,168.0,162.3, 160.7,148.1,147.8,141.0,140.5,139.8,138.6,137.3,129.4,128.9,125.1,124.2,123.3,121.6,118.1,112.5,111.6,111.2,78.4,77.2,51.7,44.9,31.7,28.3,20.0; HRMS m/z; 676.2400 (calc. 676.2407).

(1-(3-((1-(4-chlorophenyl)-3-oxo-3-(2-oxo-2H-chromen-3-yl)propyl)amino)-3-oxopropyl)-1H-1,2,3-triazol-4-yl)methyl 1H – indole-3-carboxylate 4.6b.

Brownish solid ; 505.47 mg (yield 81 %); ¹H NMR (400 MHz, DMSO-d₆):IR(KBr) ν max: 2974,2932,2738, 2676,2490,1748,1655, 1591,1528,1456,397,1360,1337, 1314, 1243, 1170,1243,1170,1122, 1089,1036,989,939,821,754cm⁻¹; δ H(ppm):9.91(s, 1H),8.29(s,1H),8.24(s, 1H), 8.13(s, 1H), 7.99(s, 2H), 7.76(s, 2H), 7.76-7.63(m, 2H), 7.49-7.04(m, 6H), 5.40(s, 2H), 5.32(t, 1H), 5.06-4.92(t, 2H), 4.83-4.71(dd, J= 20 Hz ,1H), 3.93-3.87(dd, J= 10 Hz and 12 Hz, 1H), 1.29-1.23(m, 2H); ¹³CNMR(100MHz,DMSO-d₆) δ C(ppm):194.0,185.1,168.2, 167.6, 147.8,141.0,140.0,140.6,140.5,139.8,137.3,137.0,125.1,124.2,124.2,124.1,124.0,123.3,123.2,123.0,121.6,121.5,121.5,112.5,112.0,111.6,111.6,111.5, 85.3, 60.9, 51.6, 48.1, 28.5;HRMS m/z; 624.1650 (calc. 624.1650).

1-(3-((1-(4-hydroxy-3-methoxyphenyl)-3-oxo-3-(2-oxo-2H-chromen-3-yl)propyl)amino)-3-oxopropyl)-1H-1,2,3-triazol-4-yl)methyl 1H – indole-3-carboxylate 4.6d. Brownishsolid;542.13mg(yield 80%); IR(KBr) ν max:2923,1704,1608,1532,1509,1488, 1456, 1394, 1268, 1199,1122, 1034,1031, 861,754, 606,518 cm⁻¹; ¹H NMR (400 MHz, DMSO-d₆): δ H (ppm): 9.87(s, 1H), 8.30-8.24(d, J=22 Hz , 1H), 8.13(s,

1H), 8.04(s, 1H), 8.02(s, 1H), 7.71-7.66(d, J=22 Hz , 1H), 7.49(s, 1H),7.45(s, 1H),7.42(s, 1H), 7.33-7.22(m, 6H), 5.22(s, 2H), 5.11-4.87(t, 1H), 4.66-4.64(t, 3H), 4.23(s, 3H), 3.75-3.65(dd, J=16Hz, 1H), 3.45-3.36(dd,J=10Hz,1H),1.47-1.44(t,2H), 1.239(s,3H);¹³ CNMR (100MHz, DMSO-d₆)δC(ppm): 194.3,185.4,167.6, 163.0,160.7, 148.1, 147.8,140.5,139.9,137.0,135.3,133.0,130.0,129.2,128.5,128.2,127.4,125.1,124.2,123.2,121.5,118.0,117.0,111.6,78.4,77.1,63.2,44.5,36.5,31.8, 29.4; HRMS m/z; 678.2194(calc. 678.2200).

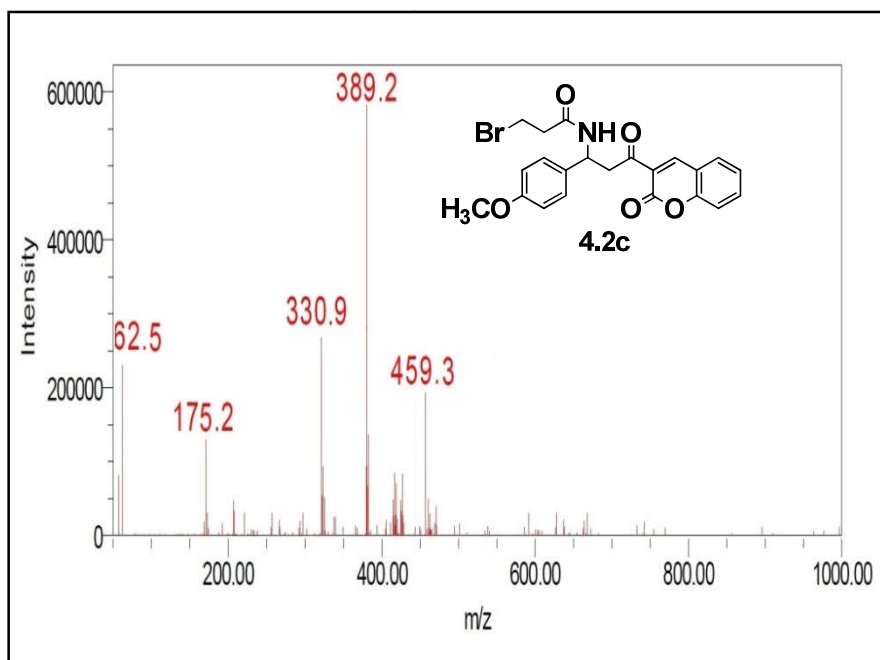
References

1. O. Kayser and H.Z. Kolodziej, *Naturforsch.*, 1999, **54c**, 169–174.
2. R.C.Sharma and R. K. J. Parashar, *Inorg. Biochem.*, 1988, **32**, 163.
3. Y.L.Garazd, E.M. Kornienko, L.N. Maloshtan, M.M. Garazd and V.P. Khilya, *Chem. Nat. Prod.* 2005, **41**, 508.
4. E.B.Ong, N. Watanabe, A. Saito, Y. Futamura, A. Koito, N. Najimudin, and H. Osada, *J. Biol. Chem.*, 2011, **286**, 14049.
5. J.A. Burlison, L. Neckers, A. B. Smith, A. Maxwell and B. S. J. Blagg, *J. Am. Chem., Soc.* 2006, **128**, 15529
6. S. Gurrapu, S. K. Jonnalagadda , M. A. Alam , C. T. Ronayne , G.L. Nelson L. N. Solano, E. A. Lueth, L. R. Drewes and V. R. Merreddy, *Bioorg. Med. Chem.Lett.*, 2016, **26** , 3282–3286.
7. (a)H. C. Kolb, M.G. Finn and K. B. Sharpless, *Angew Chem Int Ed.* 2001, **40** ,2004–2021; (b) K. M. Sreeman and M.G. Finn, *Chem Soc Rev.* 2010, **39**, 1252–1261; (c) V. Ganesh, S. Sudhir , T. Kundu and S. Chandrasekharan *Chem Asian J.*,2011, **6** ,2670–2694; (d) K. Ladomenou, V. Nikolaou, G. Charalambidis and A. G. Coutsolelos , *Coord Chem Rev.* 2016, **306**, 1–42; (e) Chen Xi et al. , *Chem Rev.*,2016, **116** ,3086–3240.

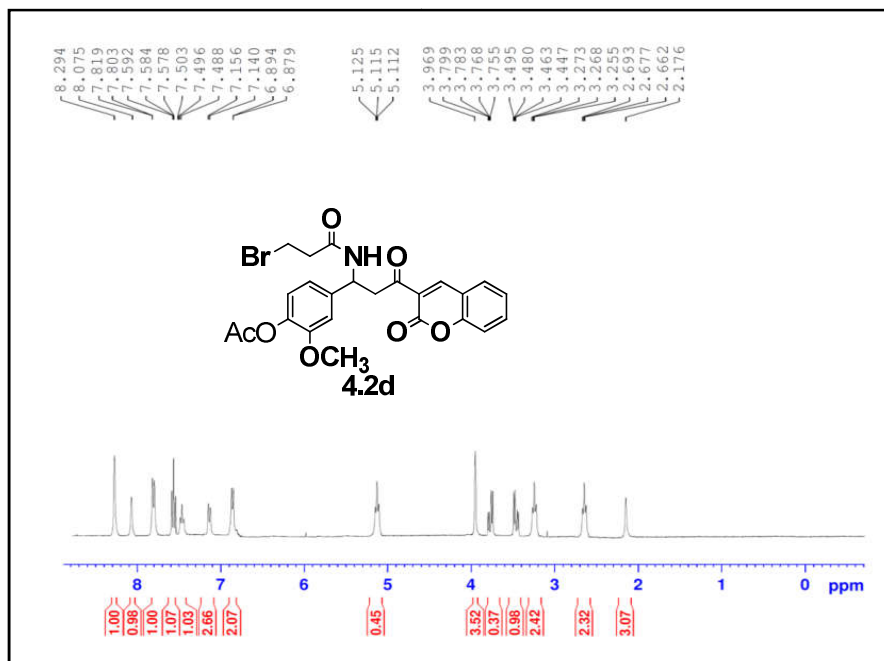
Supplementary Material

Copies of ^1H NMR, ^{13}C NMR and Mass spectra of selected
compounds

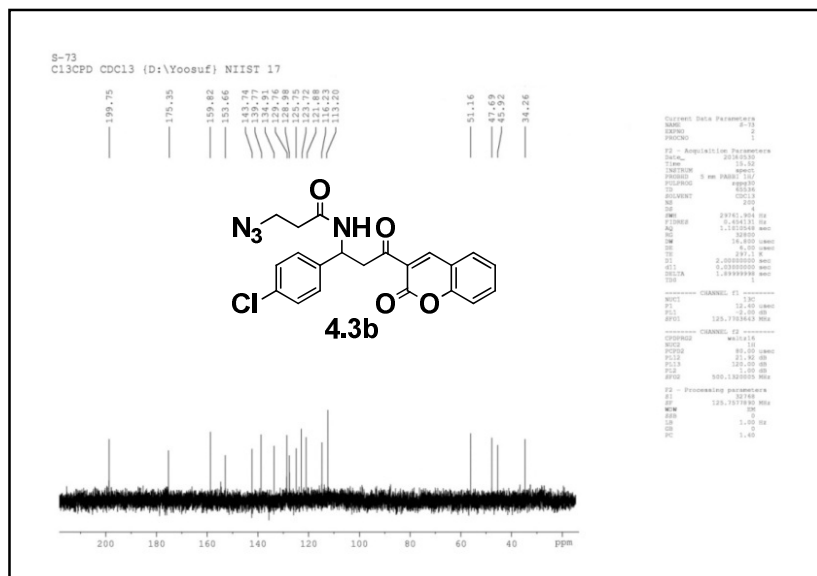
Mass spectrum of the compound **4.2c**



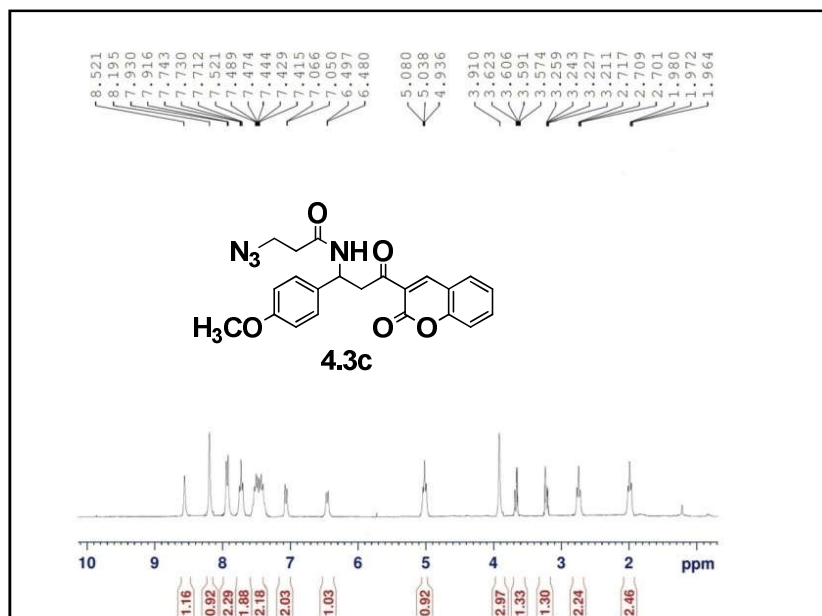
^1H NMR spectrum of the compound **4.2d**



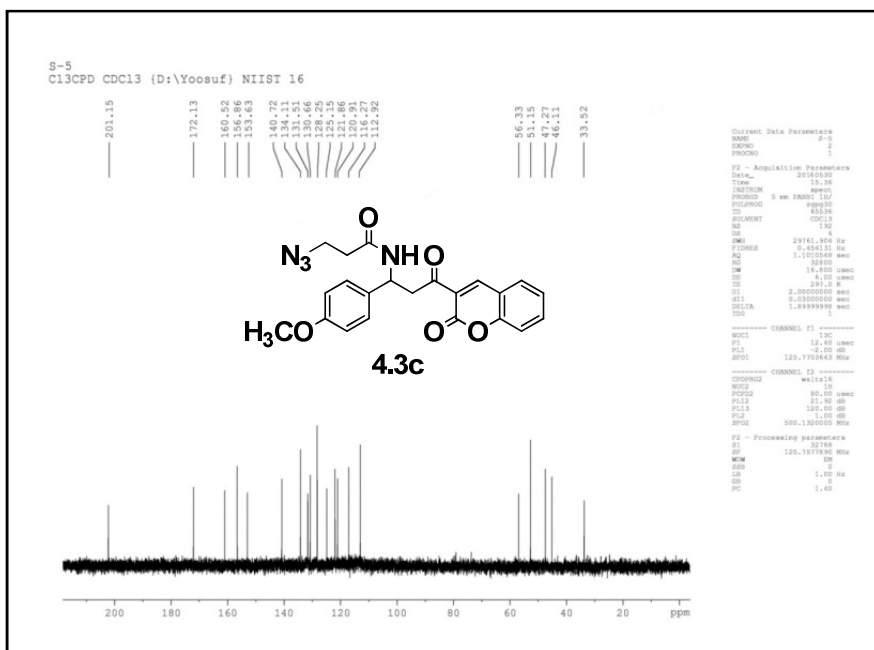
¹³C NMR spectrum of the compound **4.3b**



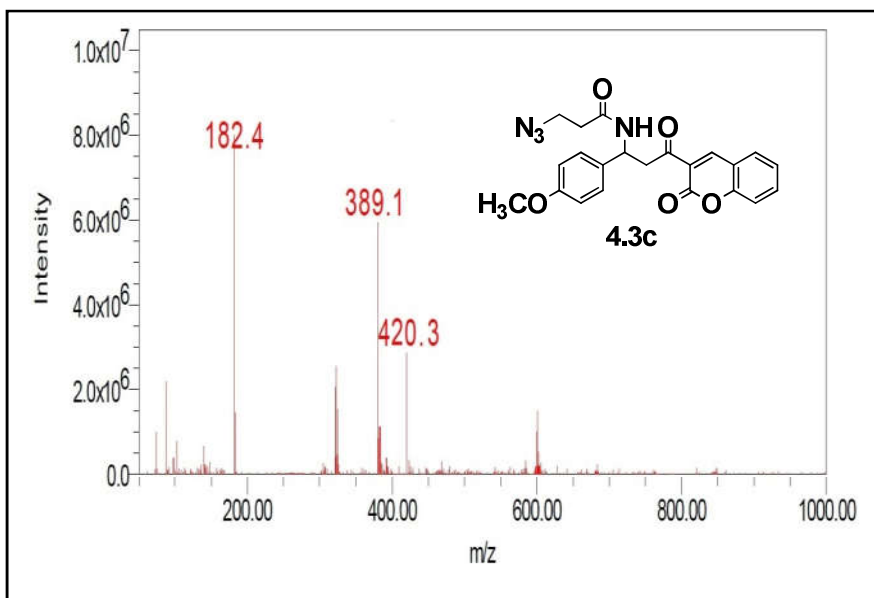
¹H NMR spectrum of the compound **4.3c**



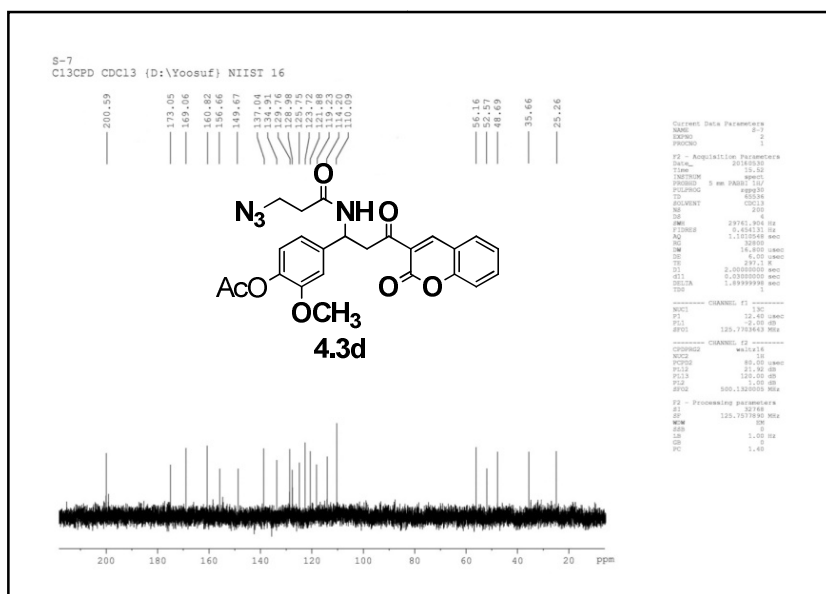
¹³C NMR spectrum of the compound **4.3c**



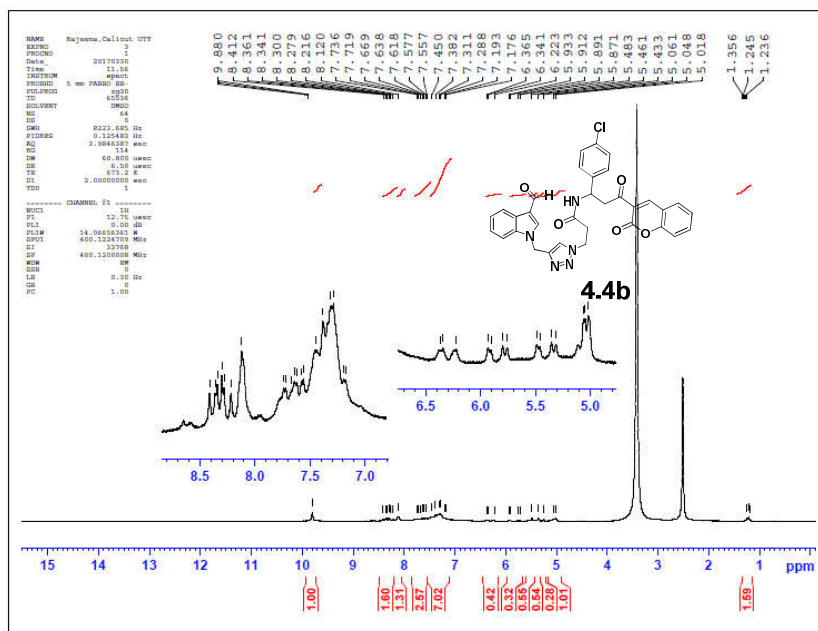
Mass spectrum of the compound **4.3c**



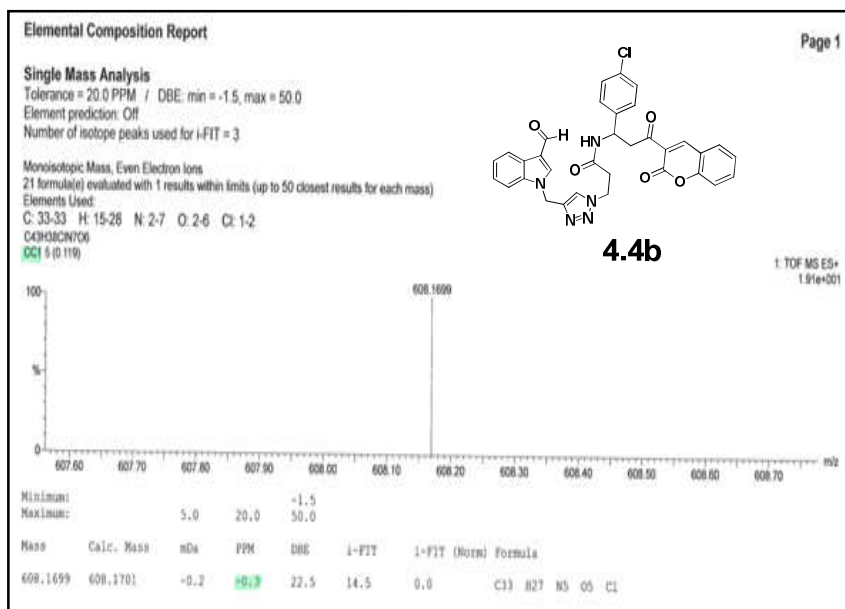
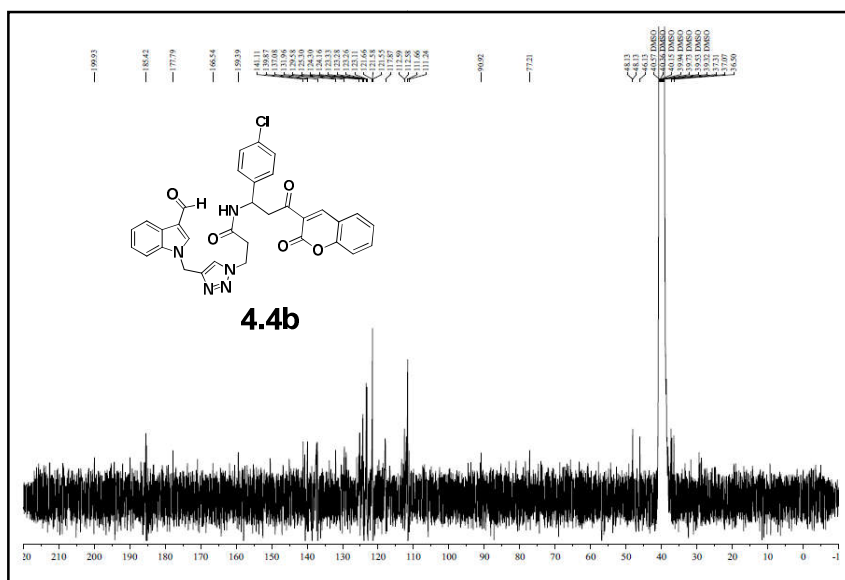
¹³C NMR spectrum of the compound 4.3d



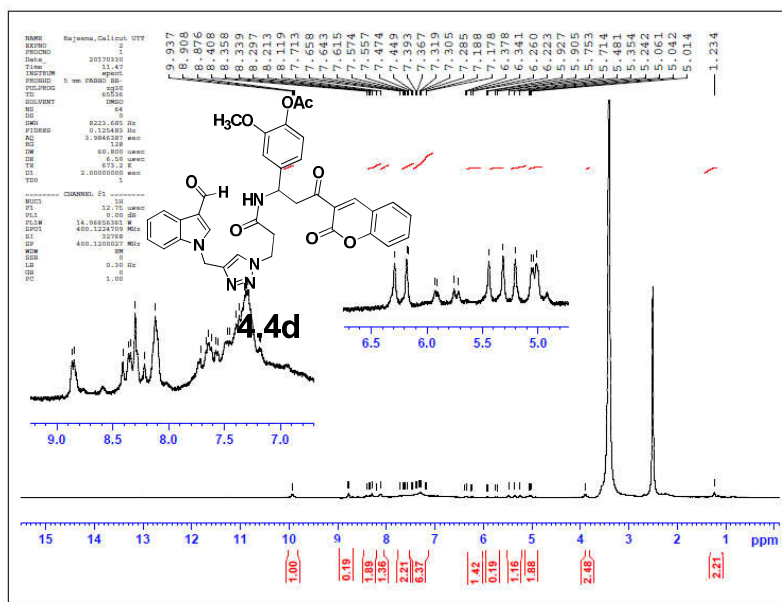
¹H NMR spectrum of the compound 4.4b



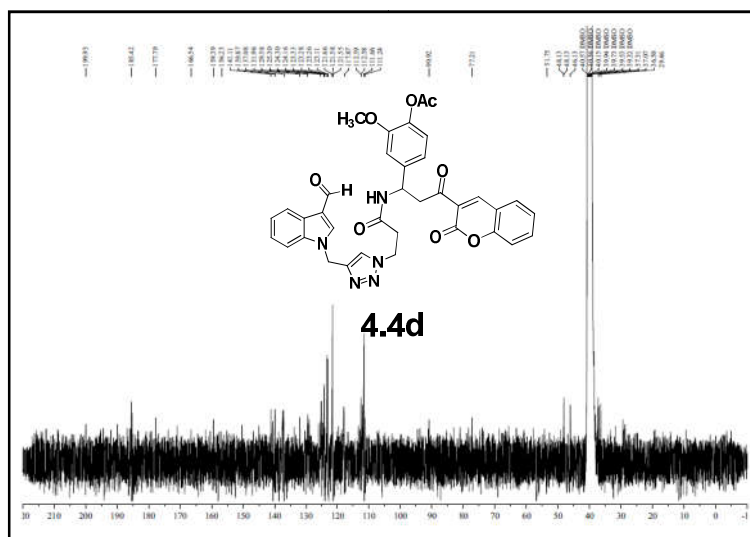
^{13}C NMR spectrum of the compound **4.4b**



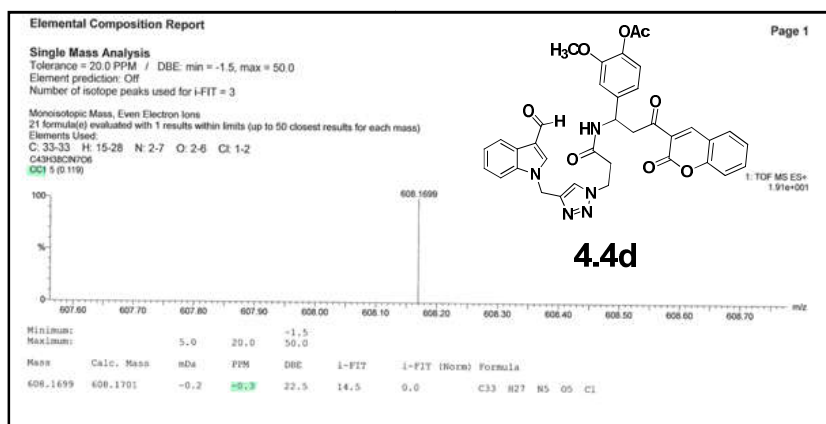
¹H NMR spectrum of the compound **4.4d**



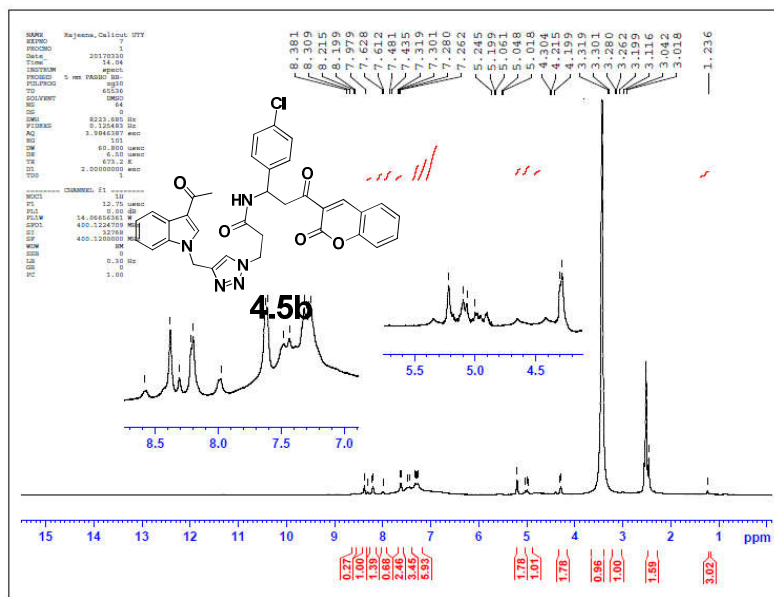
¹³C NMR spectrum of the compound **4.4d**



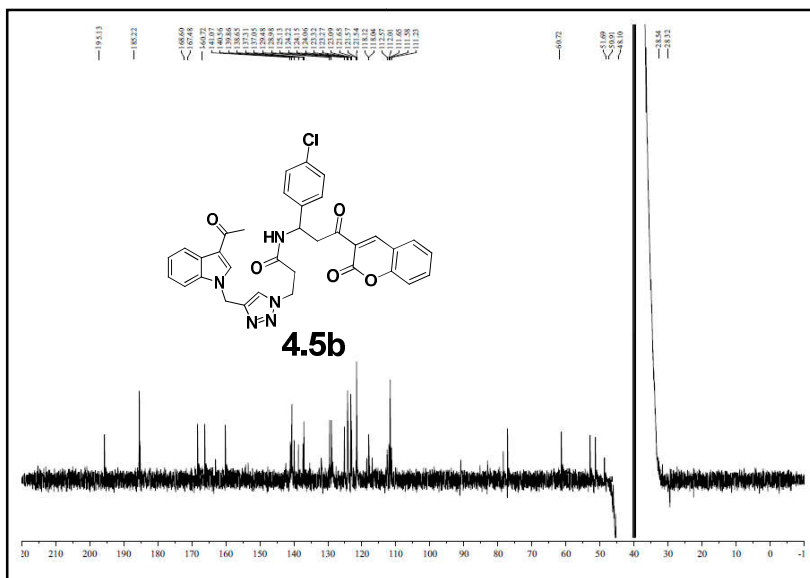
Mass spectrum of the compound 4.4d



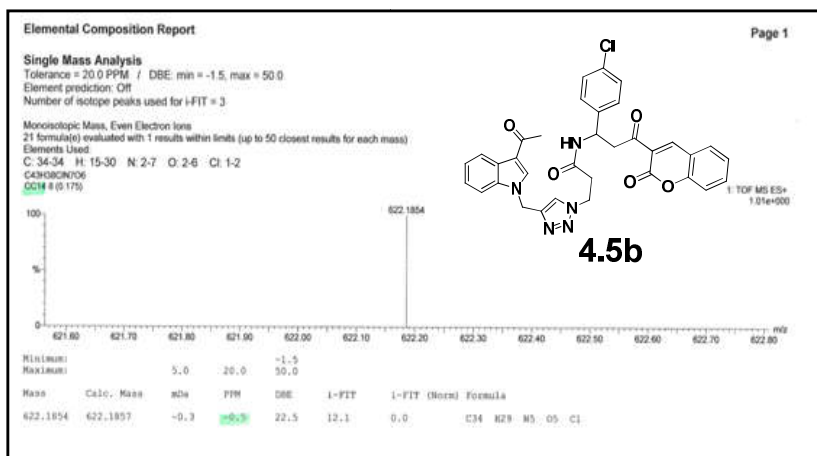
¹H NMR spectrum of the compound 4.5b



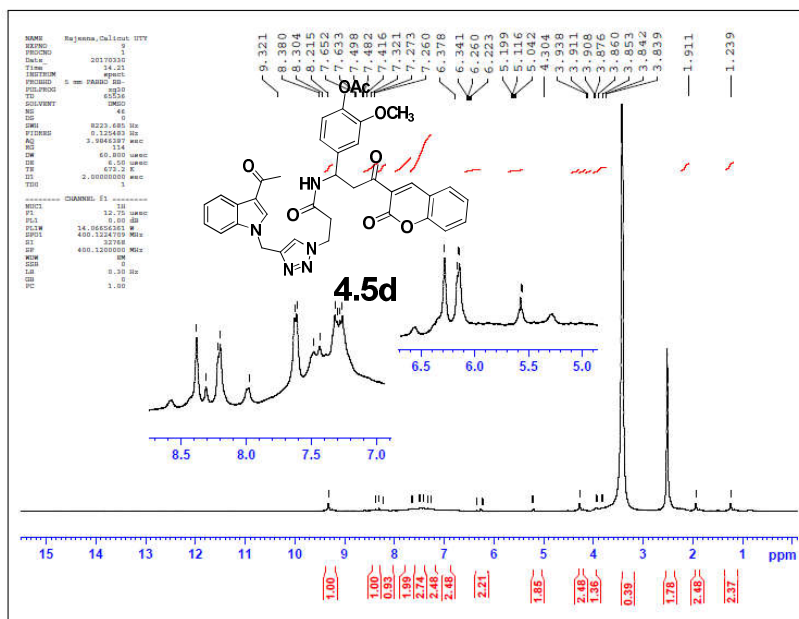
^{13}C NMR spectrum of the compound **4.5b**



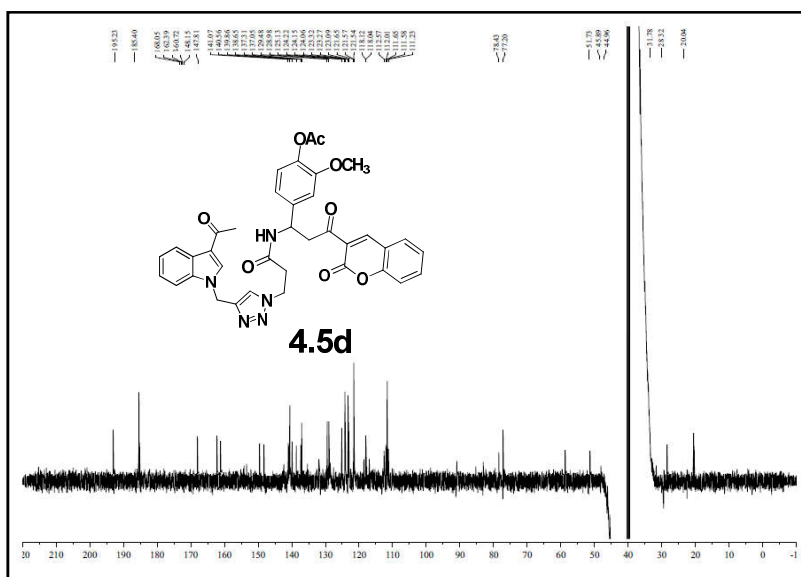
Mass spectrum of the compound **4.5b**



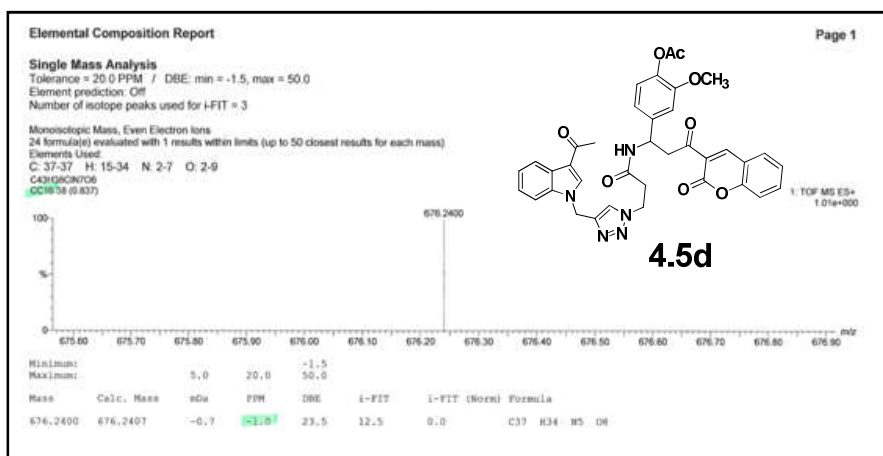
¹H NMR spectrum of the compound **4.5d**



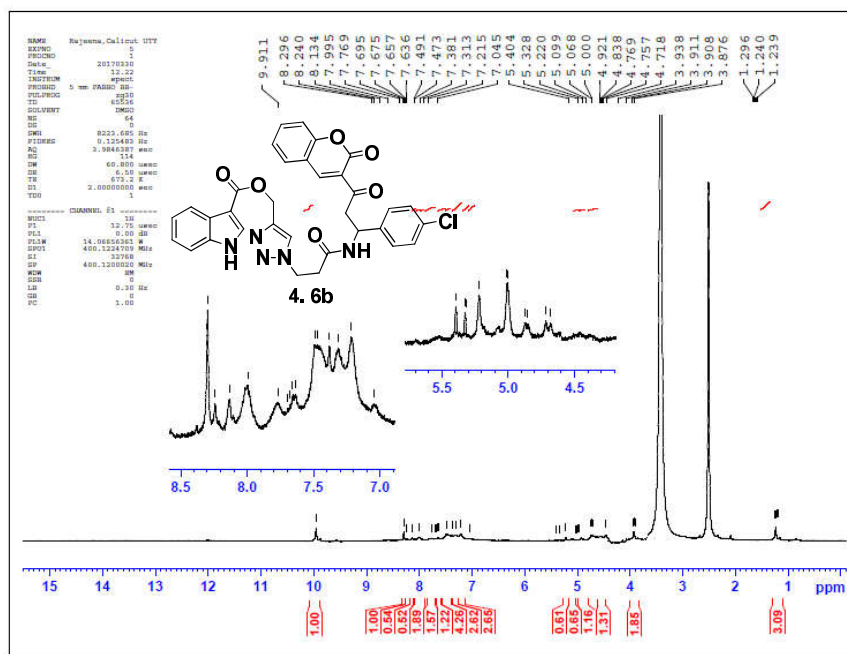
¹³C NMR spectrum of the compound **4.5d**



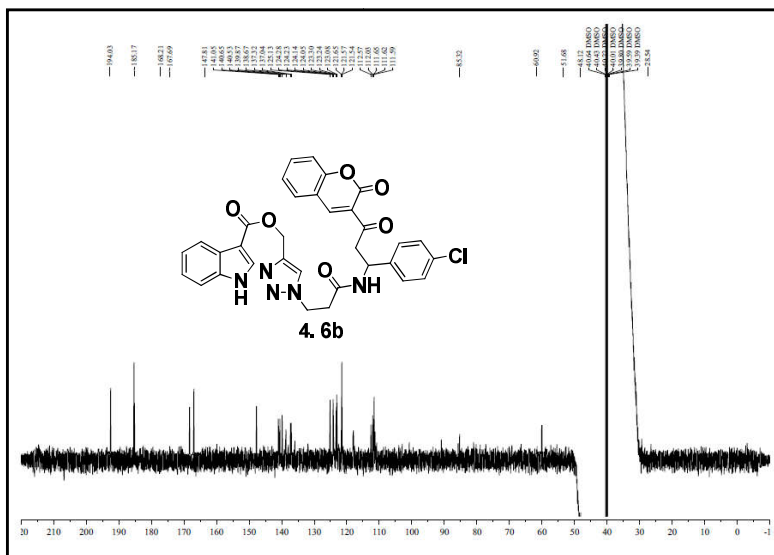
Mass spectrum of the compound 4.5d



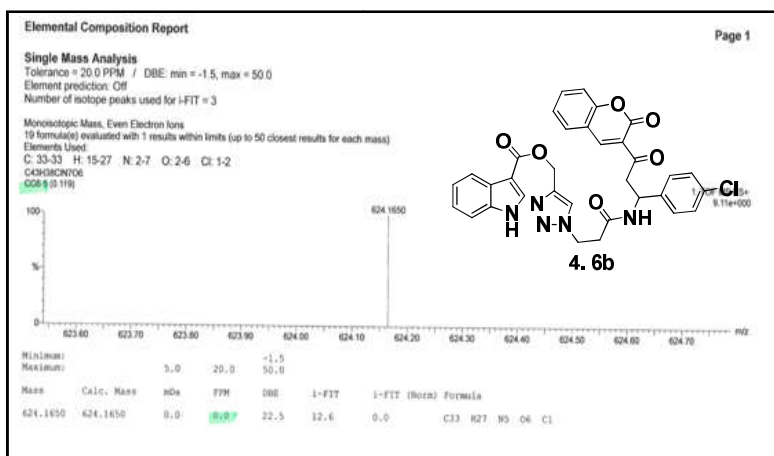
¹H NMR spectrum of the compound 4.6b



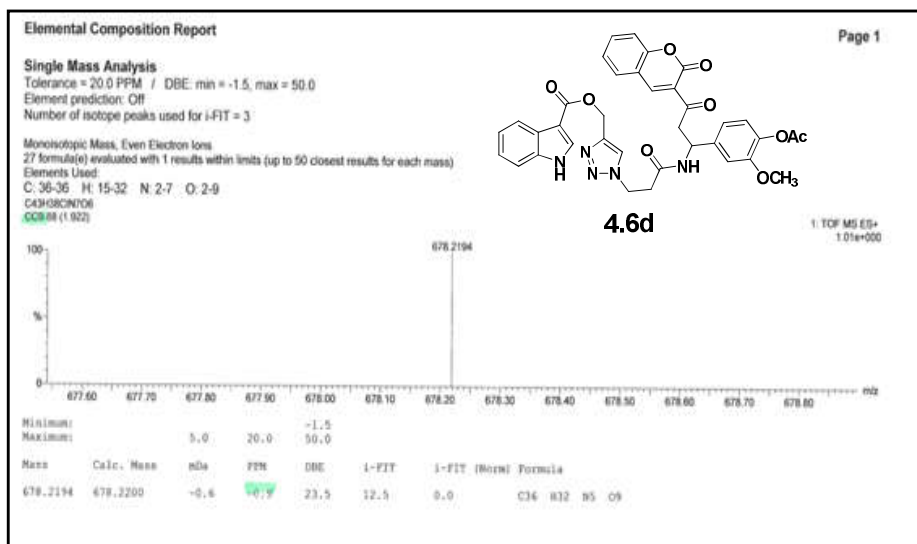
^{13}C NMR spectrum of the compound **4.6b**



Mass spectrum of the compound **4.6b**



Mass spectrum of the compound 4.6d



CHAPTER 5

**Biological evaluation of Indole-Triazole-
Coumarin hybride peptidomimetics**

Contents

5.1. Introduction.....	187
5.2. Result and discussion.....	187
5.3. Conclusion.....	201
References	202

5.1. Introduction

In the fourth chapter, we have discussed the synthesis of 12 indole –triazole-coumarin peptidomimetics by structure alterations of indole-triazole-carboxamide peptidomimetics discussed in chapter 2. This chapter presents the computational and invitro biological evaluation of these molecules against human breast cancer cell line MCF-7 and their selectivity towards CDK 2 proteins in MCF-7. The schematic representation of the work discussed in this chapter is shown in figure 5.1.

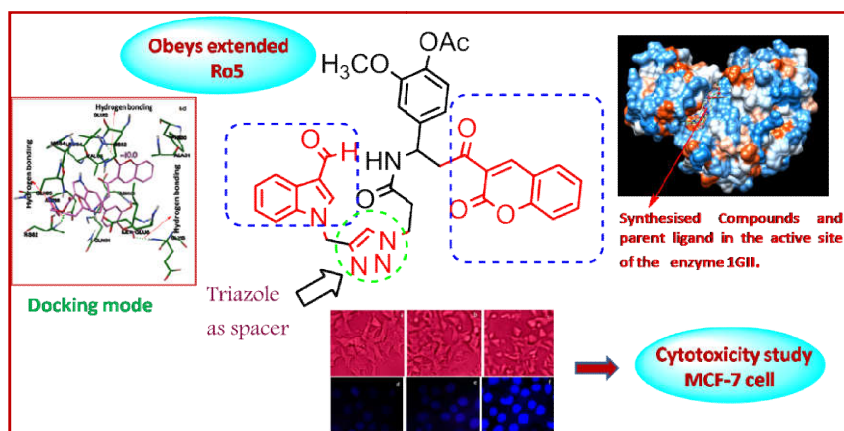


Fig. 5.1. A schematic representation of the computational and biological evaluation of Indole-Triazole-Coumarin peptidomimetics

5.2. Result and discussion

5.2.1. Primary evaluation of drug-likeness using molinspiration property study

Having synthesized the peptidomimetics, we then moved on to the calculation of the drug property descriptors of these new molecules using molinspiration property calculation service.¹ The values obtained

are slightly higher than that allowed by Lipinski's rule of 5 (Ro5) and are best suited to extended Ro5 space (table 5.1). Recent analysis of extended Ro5 molecules has revealed that such molecules have significant possibilities as orally bioavailable and cell permeable drug candidates for undruggable targets.²

Table 5.1. Drug property descriptors of the compounds from molinspiration property calculation service

Compound	Molecular weight	miLog p	TPSA	NO. of atoms	n O	N	n OHNH
4.4a	608.05	3.80	129.10	44	10		1
4.4b	608.05	3.85	129.10	44	10		1
4.4c	603.63	3.23	138.34	45	11		1
4.4d	619.63	2.51	158.56	46	12		2
4.5a	622.08	3.91	129.10	45	10		1
4.5b	622.08	3.96	129.10	45	10		1
4.5c	617.66	3.34	138.34	46	11		1
4.5d	633.66	2.62	158.56	47	12		2
4.6a	608.05	3.68	139.96	44	10		2
4.6b	608.05	3.73	139.96	44	10		2
4.6c	603.63	3.10	149.19	45	11		2
4.6d	619.63	2.39	169.42	46	12		3

5.2.2. Molecular docking of 4.4a-4.6d for studying CDK-2 binding interaction

Promising results obtained from the drug-likeness calculations prompted us to perform the virtual screening of our molecules against CDK 2 based on molecular docking.³ CDK-2 binders generally interact with CDK-2 proteins via hydrogen bonding, hydrophobic and Pi-cation interactions with various amino acid residues present in their active

sites. Protein target with PDB id 1GII was downloaded from web source.⁴ The active site of CDK2-1GII is comprised of amino acid residues such as 31Alanine, 144Alanine, 132Asparagine, 86Aspartic acid, 145Aspartic acid, 85Glutamin, 131Glutamine, 81Glutamic acid, 84Histidin, 10Isoleucine, 134Leucine, 33Lysine, 80Phenylalanine, 18Valine, 64Valine and 83Valine.⁵ Since most of the amino acid residues in the active site are hydrophobic and hence they are the main contributors for the receptor ligand interaction. PDB id 1GII was docked with **4.4a-4.6d** using the docking program Auto Dock Vina 1.1.2 and the binding energies and docking modes were derived. The docking scores obtained are listed in table **5.2**.

From the docking studies we observed that, similar to the parent ligand, the synthesized compounds can also be well embedded in the binding pocket of CDK2 (fig. **5.3**). The binding affinity of the parent or inbuilt ligand with CDK2-1GII is -9.5kcal/mol. Compound **4.4a** sits in the active site of the receptor protein (no H bonding) with a docking score of -10.9Kcal/mol whereas compound **4.4b** interacts with CDK-2 by forming two hydrogen bonds with the carbonyl part of the indole and His 82 with a docking score of -9.7Kcal/mol. **4.4c** does not form any hydrogen bonds with CDK-2 but well embedded in its active site with a binding score of -10.1Kcal/mol. **4.4d** interacts with receptor protein by forming two H-bonds, one between carbonyl group of the indole with HIS82 and the other one between the acetyl group of the indole with THR14 residue of the α -helical part of the enzyme with a binding affinity -9.8 kcal/mol. **4.5a**

interact with the receptor protein by forming one hydrogen bond with the carbonyl group of indole with HIS82 with a binding score of -10.6Kcal/mol, whereas **4.5b**, **4.5c** and **4.5d** were found to interact with the receptor protein with binding scores -10.8 Kcal/mol, -10.0 Kcal/mol and -10.1Kcal/mol respectively, and without forming any hydrogen bonds. This trend was followed in compounds **4.6a** and **4.6b** and these molecules were also interacted with CDK-2 with binding scores -11.2Kcal/mol and -10.3Kcal/mol respectively and without forming any hydrogen bonds. **4.6c** and **4.6d** were also interacted with CDK-2 with binding scores of -9.3Kcal/mol and -10.0Kcal/mol respectively. **4.6c** formed one hydrogen bond with the amide NH of the ligand whereas **4.6d** formed three hydrogen bonds with a) ester oxygen of indole with HIS82, b) carbonyl oxygen of the coumarin ring with GLU12 and c) NH group with GLY13 residue of the protein. Among the 12 compounds studied, **4.6a** showed the highest binding score of -11.2Kcal/mol (Fig.5.2). In addition to this, all the molecules showed a Pi-cation interaction with the receptor and ligand where the coumarin core and other aromatic rings act as Pi system and the NH_3^+ (zwitter ion) of the CDK-2 protein act as the cation(fig.5.4).

Table 5.2. Docking Score of compounds **4.4a-4.6d**.

Compound	Docking score / binding affinity (Kcal/mol)	Interactions with receptor
4.4a	-10.9	ALA 31, PHE 80, ASP145, VAL 18, LYS 20 ALA 144, ASP 86, LEU 1, HIS 84, VAL 64
4.4b	-9.7	VAL 64, PHE 80, ALA 31, ALA 144, GLY 13, LYS 129, LEU 134, HIS 82,(HB), LYS 20, ASN 132, ILE 10.
4.4c	-10.1	VAL 64, PHE 80, HIS 82, ASP 145, ALA 144 LYS 20, VAL 18, GLU 12, GLU 8, GLY 11 ILE 10, LEU 134, GLN 85, ASP 86, THR 89
4.4d	-9.8	THR 14(HB), GLY 13, GLU 12, GLY 11, ILE 10, HIS 82(HB), LEU 134, ALA 31, PHE 80, LYS 120
4.5a	-10.6	ALA 31, VAL 18, GLU 12, GLY 13, GLY 11 ILE 10, HIS 82(HB), ASN 132, LYS 129, GLN 131, LEU 134
4.5b	-10.8	PHE 80, VAL 18, GLU 8, LYS 20, ASP145 VAL 64, ALA 144, HIS 82, ILE 10, GLN 131 LEU 134, ASP 86, THR 89
4.5c	-10.0	LYS 20, ILE 10, ASN 132, LYS 129, GLN 131, LEU 134, GLN 85, ASP 86, LEU 298, LEU 134
4.5d	-10.1	LYS 120, THR 14, GLY 13, GLU 12, GLY 11, ILE 10, HIS 82, ALA 31, LEU 134, ALA 144
4.6a	-11.2	PHE 80, ALA 31, LYS 20, HIS 82, VAL 64, GLU 81, GLY 11, GLU 8, ILE 10, VAL 83 LEU 134, HIS 84, ASP 86
4.6b	-10.3	ALA 31, PHE 80, LYS 20, GLU 8, ILE 10, VAL 64, GLU 81, VAL 83, LEU 134, ASP 86 THR 89
4.6c	-9.3	VAL 18, ILE 10(HB), LYS 20, ALA 31, ASP 145, HIS 82, VAL 83, PHE 80, LEU 134
4.6d	-10.0	LYS 120, GLY 13(HB), GLU 12(HB), ILE 10, VAL 18, THR 89, HIS 82(HB), PHE 80, LEU 134, ALA 144, ASP 145

^aHB= Hydrogen bonding

In order to study the effect of water molecules in the binding interaction of the ligands, the molecules were also docked against the target in presence of water molecules in the crystal structure. However, water molecules did not form any hydrogen bonds with the ligands and also did not influence the binding energy of the molecules we obtained in the absence of the water molecules.

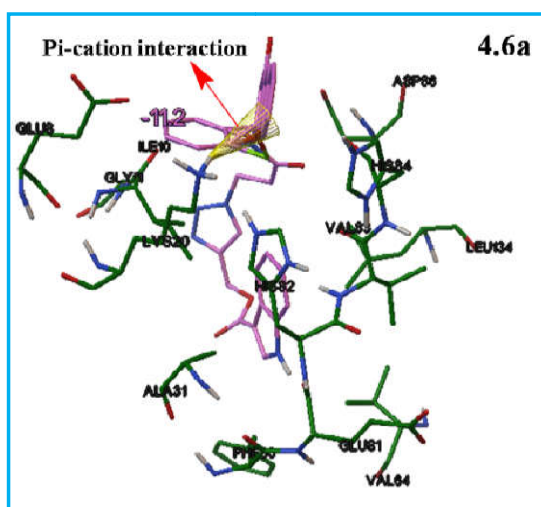
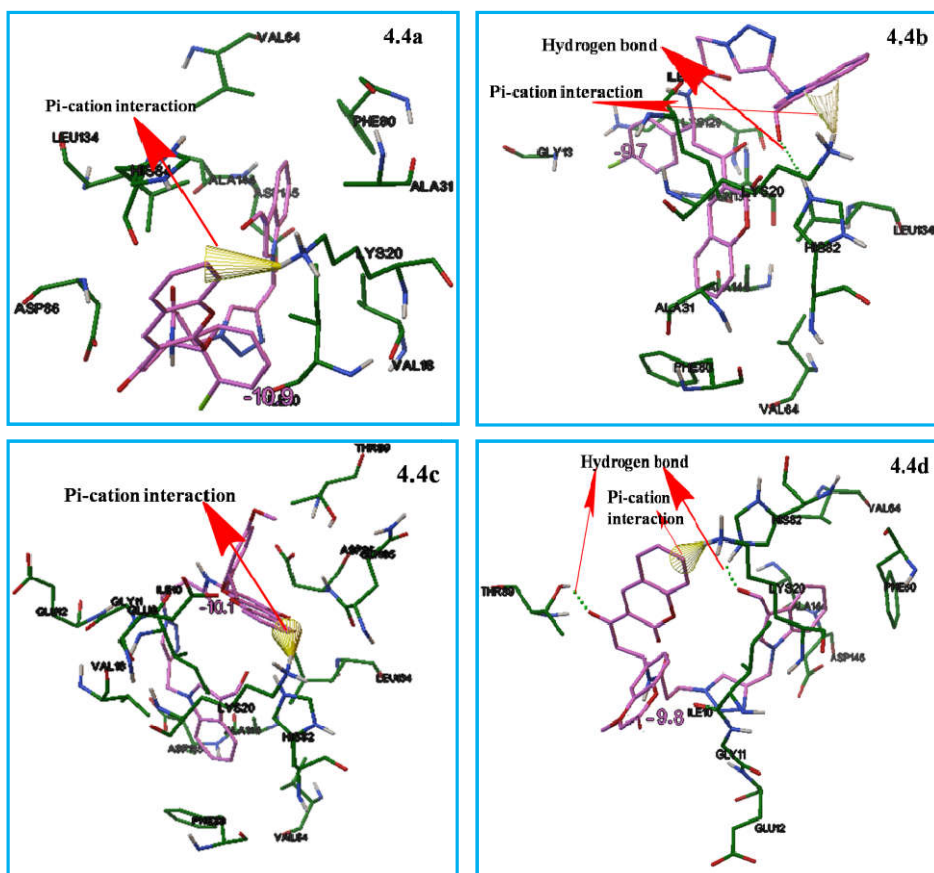


Fig. 5.2. The binding mode of compound 4.6a (high docking score) in the active site of CDK2-1GII



Fig. 5.3. The super imposition of the representative compounds **4.6d** (Red), **4.5d** (Green) , **4.4d**(Pink) and (B) **4.6a** (red) with parent ligand (blue) in the active site of CDK2-1GII



5.2.3. In vitro cytotoxic activity against MCF-7 cell lines

The cytotoxicity of **4.4d**, **4.5d**, **4.6a** and **4.6d** against human breast cancer cell lines (MCF-7) were evaluated using MTT assay for validating the results obtained from molecular docking.⁶ The molecules showed IC₅₀ in the range of 17.5-40 μ M (Fig.5.5-5.8). The molecules **4.6a** which showed the highest binding affinity has also showed the lowest IC₅₀ (17.5 μ M) against MCF-7 cell lines followed by **4.4d** which showed an IC₅₀ of 20 μ M against MCF-7 cells. However, we didn't observe any trend in IC₅₀ with respect to the binding energy obtained from computational method.

The presence of strong electronegative or electron donating groups at the core aromatic ring has a strong influence on the lipophilicity of molecules which can alter the cytotoxicity of the drug candidates. In compound **4.4d**, an electron withdrawing -CHO group is present at the third position of the indole ring and which could be the reason for the enhanced cytotoxicity observed for **4.4d**. In the case of **4.5d**, instead of the aldehyde functionality, a keto group is present at the 3-carbon of the indole which is less electron withdrawing compared to the aldehyde group and therefore the compound afforded a slightly high value for the IC₅₀ (30 μ M). While comparing **4.6a** and **4.6d**, both compounds have the same substitution at the third position of indole ring, but **4.6a** showed the least IC₅₀ value (17.5 μ M) and **4.6d** showed the highest IC₅₀ (40 μ M) . This could be due to the influence of the high electron releasing ability of the -OH and -OCH₃ groups in **4.6d** compared to the electronegative character of chlorine in **4.6a**.

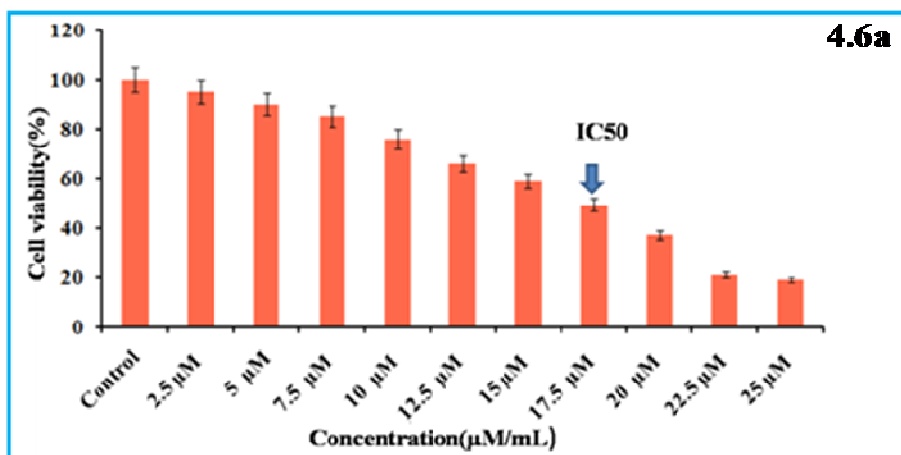


Fig. 5.5 MTT assay results confirming the in vitro cytotoxicity effect of **4.6a** against the MCF-7 cells. The detected IC₅₀ concentration was 17.5 µM

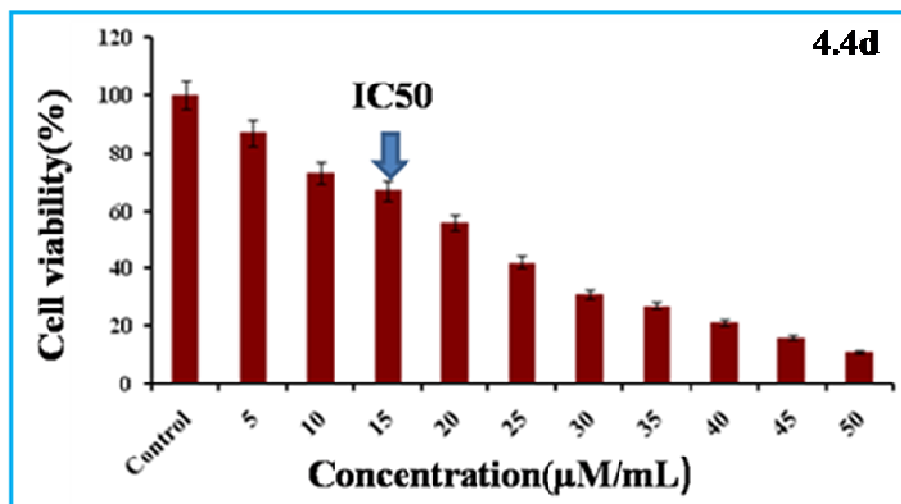


Fig. 5.6 MTT assay results confirming the in vitro cytotoxicity effect of **4.4d** against the MCF-7 cells. The detected IC₅₀ concentration was 20 µM.

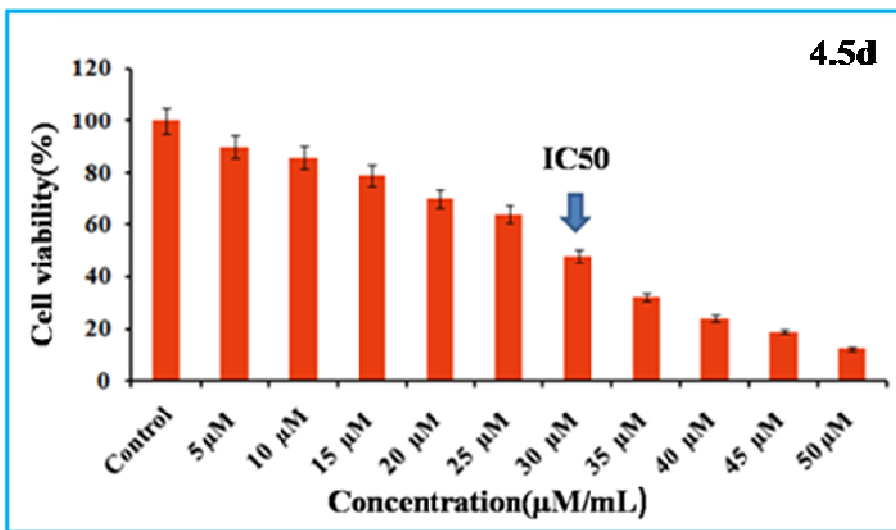


Fig. 5.7 MTT assay results confirming the in vitro cytotoxicity effect of **4.5d** against the MCF-7 cells. The detected IC₅₀ concentration was 30µM.

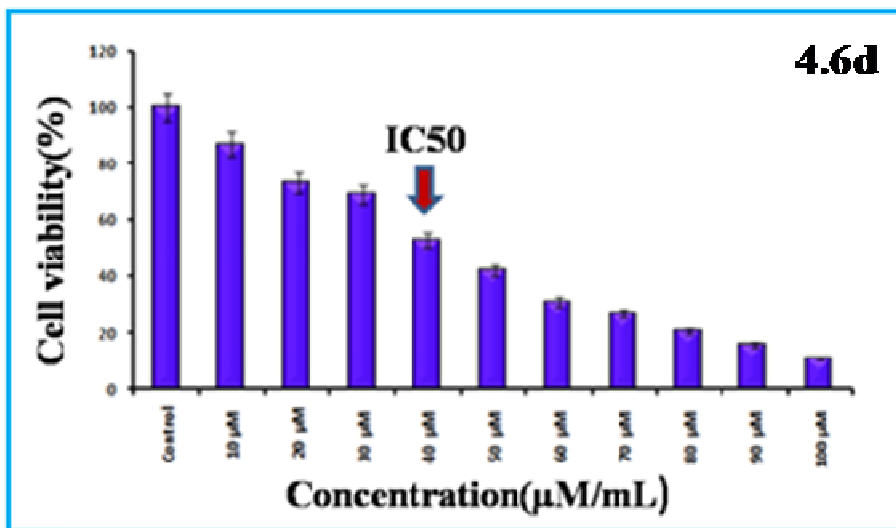


Fig. 5.8 MTT assay results confirming the in vitro cytotoxicity effect of **4.6d** against the MCF-7 cells. The detected IC₅₀ concentration was 40µM

5.2.4 Cell morphology studies

The morphology of the cells after treatment with **4.4d**, **4.5d**, **4.6d** and **4.6a** was also studied. For this, the MCF-7 cells were incubated with **4.4a**, **4.5a**, **4.6a** and **4.6a** at their IC₂₅ and IC₅₀ concentrations and were analyzed under a Nikon (Japan) bright field inverted light microscope at 40 magnification followed by DAPI (4,6-diamidino-2-phenylindole dihydrochloride) staining. The bright field and fluorescence microscopic images of **4.4d**, **4.5d**, **4.6d** and **4.6a** are also shown in Figure **5.9** & **5.10**. As shown in Figure **5.9** and Figure **5.10**, the control cells have a normal morphology with intact round nucleus emitting weak fluorescence. However, on treatment with **4.4d**, **4.5d**, **4.6a** and **4.6d**, a significant nuclei fragmentation with condensed and apoptotic nuclei was observed and the total number of apoptotic cells were increased with the increase in the incubation concentration. It has been reported that, the anti-cancer drug doxorubicin interacts with DNA topoisomerase II (topo II) causing the accumulation of enzyme –DNA leading to the rupture of the double-strand and cell death via apoptosis.⁷ Similar patterns of nuclei fragmentations were observed here also, when breast cancer cells MCF-7 were treated with **4.4d**, **4.5d**, **4.6a** and **4.6d**.

The MTT stained molecules were also observed under a Nikon (Japan) bright field inverted light microscope at 40 magnification. The bright field inverted light microscopy taken at various concentrations are shown in Figure **5.9** & **5.10**. As shown in Figure **5.9** & **5.10** (a, b, c), the cells incubated with **4.4d**, **4.5d**, **4.6a** and **4.6d** at their IC₅₀

concentrations showed maximum fluorescence whereas the control cells without **4.4d**, **4.5d**, **4.6a** and **4.6d** did not show any detectable fluorescence which indicates the potential of these molecules for developing in bio-imaging agents based on them.

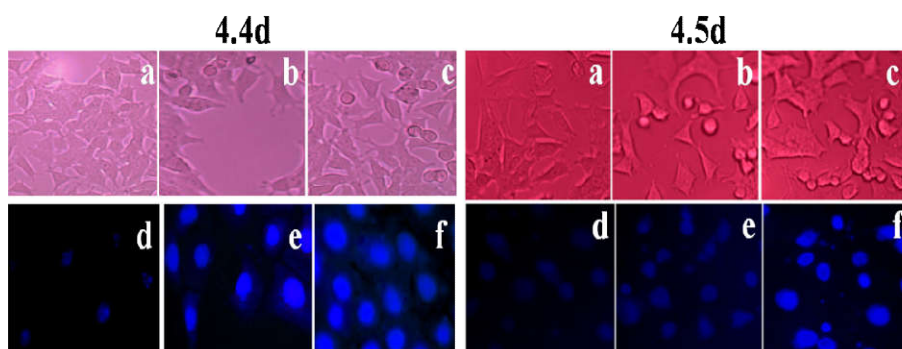


Fig. 5.9. Bright field inverted light microscopy images of MCF-7 treated with **4.4d** and **4.5d** (a) control cells, (b) cells treated with **4.4d** and **4.5d** at IC 25, (c) cells treated with **4.4d** and **4.5d** IC50. The Fluorescence microscopy images of: (d)control cells, (e) cells treated with **4.4d** and **4.5d** at IC25, and (f) cells treated with **4.4d** and **4.5d** at IC 50.

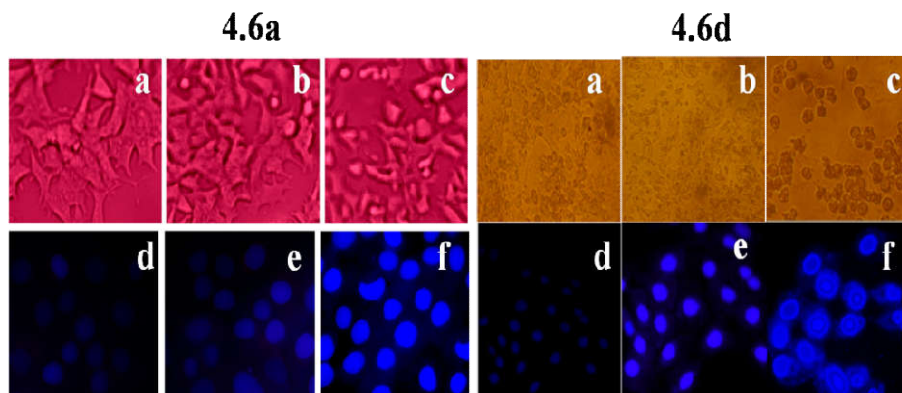


Fig. 5. 10. Bright field inverted light microscopy images of MCF-7 treated with **4.6a** and **4.6d** (a) control cells, (b) cells treated with **4.6a** and **4. 6d** at IC 25, (c) cells treated with **4.6a** and **4.6d** IC 50. The Fluorescence microscopy images of: (d)control cells, (e)cells treated with **4.6a** and **4.6d** at IC25, and (f) cells treated with **4.6a** and **4.6d** at IC 50.

5.2.5. Western Blot Analysis of 6a to study CDK-2 selectivity in MCF-7 cells

Since **4.6a** afforded highest binding affinity and lowest IC₅₀, we decided to study its CDK2 selectivity via western blot analysis.⁷ For this, the MCF-7 cells (1×10^6) were seeded into 100-mm culture dishes in the presence and absence of **4.6a** and kept for 48 h. The Cells were then washed twice with ice-cold PBS and incubated in lysis buffer. The lysates were centrifuged at $10,000 \times g$ for 5 min (at 4°C) and were used as the cell protein extracts. The extracts were then subjected to 12% SDS polyacrylamide gel electrophoresis after which the proteins were transferred in to a nitrocellulose membrane, and then blocked for 1 h using 10% skim milk in water. After washing in a PBS containing 0.1% tween 20 for 3 times, the primary antibodies were added at a v/v ratio of 1:1000. After overnight incubation at 4°C, the primary antibodies were washed away and the secondary antibodies were added for 1 h incubation at room temperature. Finally, the enhanced chemiluminescence detection reagents were used to develop the signal of the membrane. As shown in Figure **5.11** the protein level of CDK2 are significantly down-regulated in the **4.6a** treated cells compared to the control when β -actin was used as the internal standard.

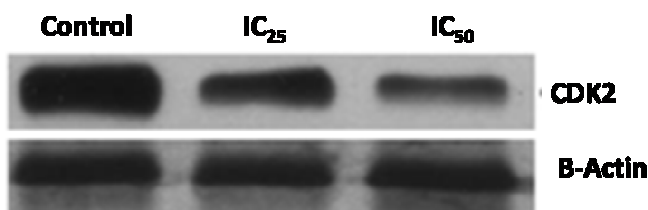


Fig. 5.11. Western blot Analysis of **4.6a** against CDK 2 in MCF-7 cell lines

5.3. Conclusion

In the previous chapter, we have demonstrated the design and synthesis of twelve indole-triazole-coumarin hybrids using a click-multicomponent strategy. In this chapter we have presented the studies on the invitro anticancer activity of the molecules via both theoretically and experimentally. Molecular docking studies with **4.4a-4.6d** against CDK2 revealed that, among the twelve molecules, **6a** has the highest binding affinity towards CDK2. In vitro cytotoxicity study with **4.4a-4.6d** against human breast cancer cell line MCF-7 were also conducted and here also **4.6a** showed the lowest IC₅₀ (17.5 μ M). The selectivity of **4.6a** towards CDK2 was further confirmed via western blot analysis using β -actin as standard. The ease in high yield synthesis, ease in library expansion via structure alterations, the cost effectiveness and the results obtained from theoretical and experimental anticancer studies are promising for undertaking high level computational and chemical/biochemical experiments to develop cost effective antitumor agents based on these molecules.

References

- 1 <http://www.molinspiration.com>.
- 2 B.C. Doak, J. Zheng and D. Dobritzsch, *J. Med. Chem.*, 2016, **59**, 2312-2327.
- 3 (a)V.S. Heena, H.G. Sunil and P. Rama, P, *J Comput Sci syst Biol.* 2012, **5**, 12–15; (b) P.F. Lamie, W.A.M. Ali, V. Bazgier and R. Lucie, *Eur. J. Med. Chem.*, 2016, **123**, 803-813.
- 4 (a)<http://www.rcsb.org/pdb/home/home.do> ; (b) M. Ikuta, K. Kamata, K. Fukasawa, T. Honma, T. Machida and H. Hirai, *J. bio. chem.*, 2001, **276**, 27548–27554.
- 5 S. Ke, T. Barata, T. Solmajer, J. Antic, Z. Juranic, S. Eric, M. Zloh and V. Savic, *Bioorg. Med. Chem. Lett.*, 2012, **20**, 5220–5228.
- 6 J.S. Dimitrios, K.K. Panagiotis, G.K. Eumorphia, *Int.J. Oncology.*, 2009, **34**, 137-160.
- 7 K. Vimala, S. Sundarraj, M. Paulpandi, S. Vengatesan, S. Kannan, *Process Biochem.*, 2014, **49**, 160-172

CHAPTER 6

Structure alterations of Indole-Triazole-Carboxamides with a Pyrimidine sub unit: Synthesis and cytotoxicity evaluation of a new series of Indole-Triazole-Pyrimidinone Hybride.

Contents

6.1. Introduction.....	203
6.2. Result and discussion.....	204
6.3. Structure elucidation by spectroscopy	217
6.4. Conclusion.....	218
6.5. Experimental Section	219
References	227
Supplementary Material	229

6.1. Introduction

In chapters 4 and 5, we have discussed the synthesis of indole-triazole –coumarin peptidomimetics and their *in vitro* cytotoxicity against MCF-7 cell lines as well as also their selectivity towards CDK-2 in MCF-7 cell lines. Based on the promising results obtained from the functionalization of indole core with different peripheral attachments such as simple carboxamide moieties and coumarin acetamides, we became curious to know the outcome of replacing coumarin with a pyrimidine unit. Hence we continued our structure alteration studies. This chapter presents the synthesis of a new series of Indole-triazole-pyrimidine peptidomimetics and their *in vitro* biological activity screening via computational and experimental methods. A graphical representation of the progress of the study from chapter 4 to chapter 6 is presented in figure 6.1.

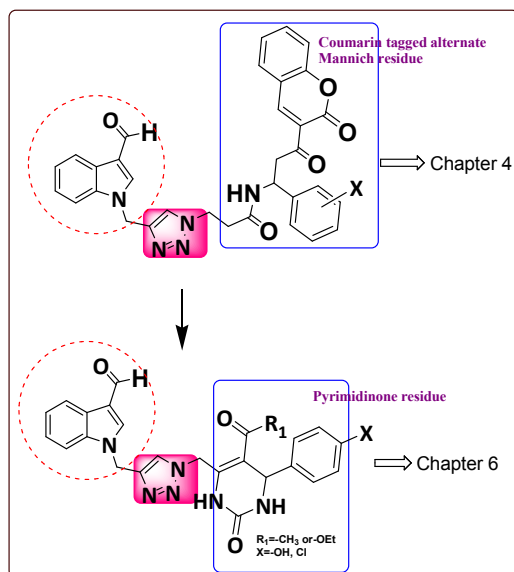


Fig. 6.1. The Structure alterations of Indole-Triazole-Coumarin peptidomimetics from Indole-triazole-coumarin peptidomimetics

Our rationale for selecting pyrimidine as a scaffold part to integrate with indole basically stemmed from the versatility of pyrimidines in the biological world. Pyrimidine derivatives are widely present in large number of therapeutics including calcium channel blockers, ¹antiviral², anticancer³, anti-inflammatory⁴ and anti-hypertensive⁵ agents. They have also been used as potent inhibitors of HIV integrase⁶ and poly (ADP-ribose) polymerase-1 (PARP-1).⁷ In addition to this, these class of compounds were proven to have significant activities against different types of human cancers, such as leukemia, lung, liver, colon, CNS, melanoma, ovarian, renal, prostate, and breast cancer⁸.

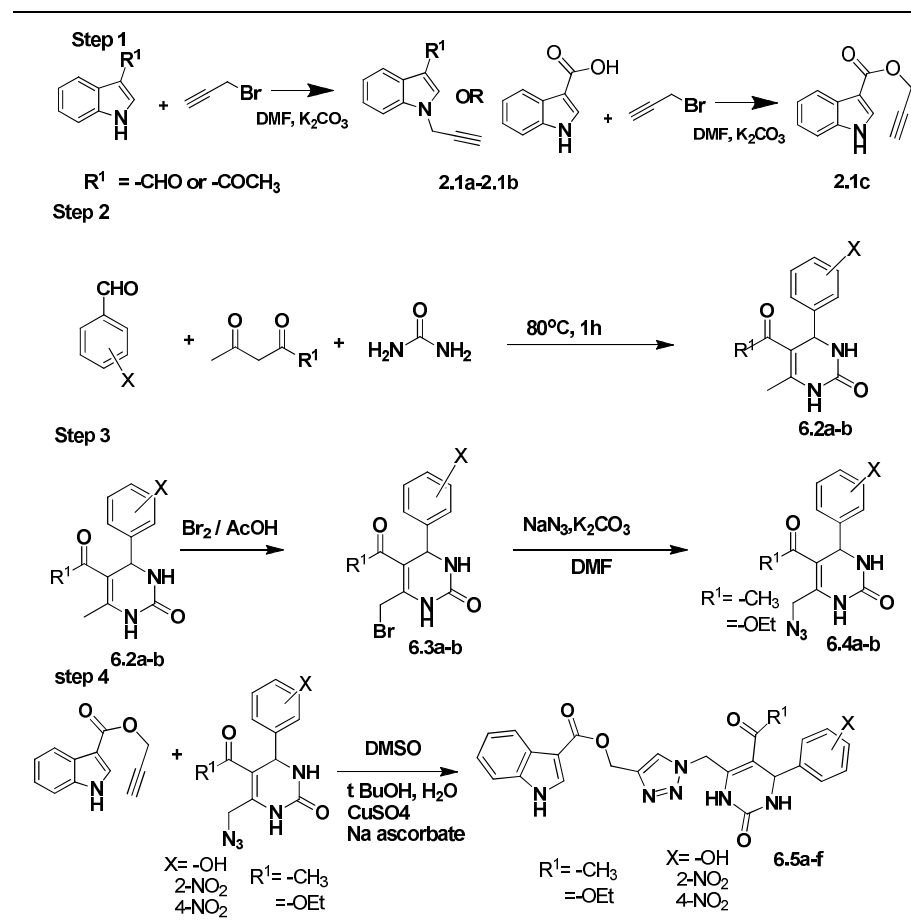
6.2. Result and discussion

6.2.1. Synthesis of Indole-pyrimidinone peptidomimetics via CuAAC reaction.

The overall synthetic procedure for the preparation of indole-triazole- pyrimidinone hybrids is shown in scheme **6.1**. The study began with the alkylation of indole derivatives under basic condition to obtain **2.1a-2.1c** which has also been discussed in chapter 2. The second task was to synthesize the pyrimidine derivative in the form of an azide and for this we have followed the well-known Biginelli reaction protocol.⁹ In a representative synthesis, a non-enolizable carbonyl compound (substituted aldehyde), enolizable carbonyl compound (acetyl acetone/ ethyl acetoacetate) and urea were mixed in the ratio 1:1:1.5. The mixture was then heated without any solvent at 80°C in an oil bath under constant stirring for 1h and subsequent

aqueous workup afforded corresponding 3,4-dihydro pyrimidinone **6.2a-6.2b** in pure form. The conversion of these molecules into the corresponding azide derivatives was achieved in two steps via an initial bromination of the C-6 methyl group to obtain the bromomethyl dihydropyrimidinones. Bromination was carried out by the slow addition of a mixture of bromine in glacial acetic acid to a solution of dihydropyrimidinone in glacial acetic acid. After the addition of the brominating mixture, the reaction mixture was kept at room temperature for 30 minutes followed by aqueous work up and subsequent filtration and recrystallization afforded pure bromomethyl DHPM. (All the DHPMs **6.2a-6.2b** were brominated using the same procedure to obtain the brominated DHPMs **6.3a-6.3b**). These brominated DHPMs were then converted to the corresponding azide derivative **6.4a-6.4b** by reacting them with sodium azide in DMF at 55 °C. The aqueous work up of the reaction mixture afforded the pyrimidinone azide **6.4a-6.4b** in good to excellent yield (Table 6.1)

The indole alkyne fragment and the pyrimidinone azides were then assembled by performing CuAAC reaction to obtain the indole-triazole-pyrimidinone hybrids **6.5a-6.5f**. The click reactions were done at room temperature in a mixed solvent system containing *t*-butanol, water and DMSO in the ratio 4:2:1 using CuSO₄ as Cu (I) source and sodium ascorbate as the reducing agent. All the click reactions afforded excellent yield for **6.5a-6.5f** as shown in table 6.2 and the structures were characterized by FT-IR, ¹H NMR, ¹³C NMR and HRMS.



Scheme 6.1. The overall protocol for the synthesis of Indole- Triazole-Pyrimidinone peptidomimetics

Table 6.1. List of Brominated DHPMs& Azido DHPMs

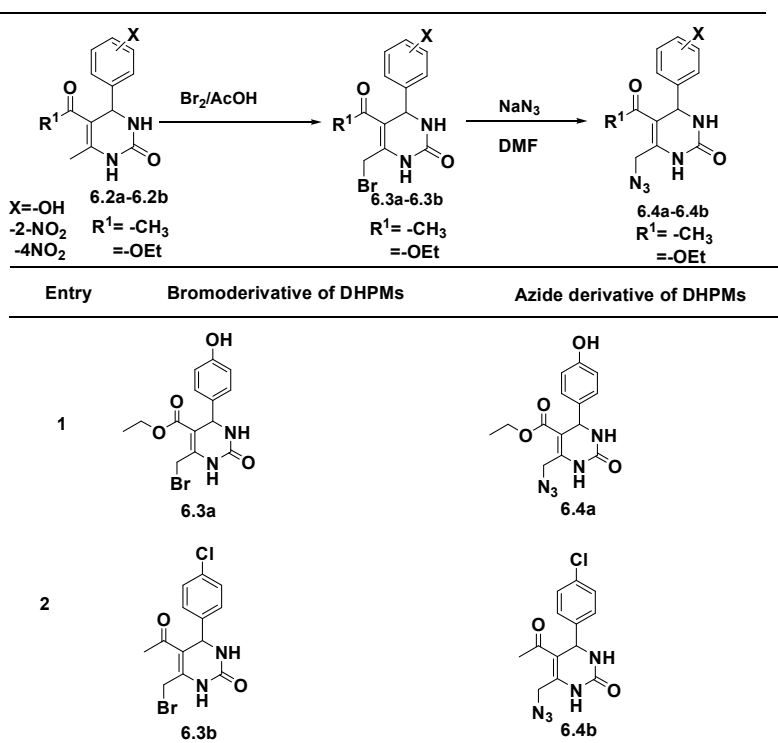
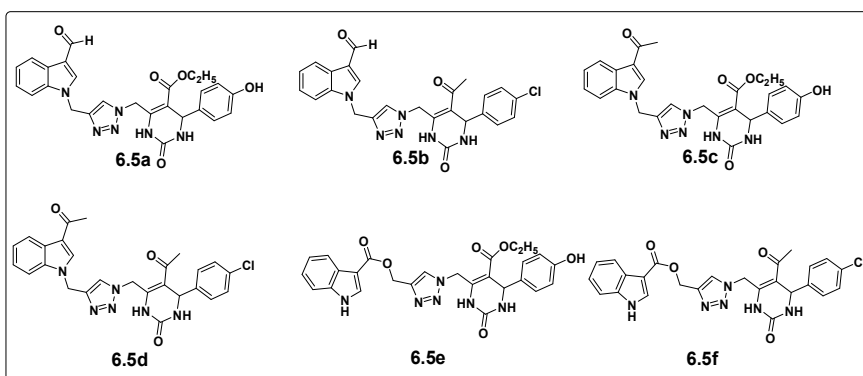


Table 6.2. The List of Indole-Triazole-Pyrimidone hybrids synthesized via CuAAC reaction.



6.2.2. Primary evaluation of drug-likeness by the calculation of drug property descriptors.

The indole pyrimidinone dyads **6.5a-6.5f** were then analyzed based on their drug property descriptors. The Log P and topological surface area (tPSA) values of the compounds were obtained from an online calculation service at www.molinspiration.com. The values obtained are well within the limit of rule of five and are presented in table **6.3**. The molecular weight of **6.5a-6.5f** lies between 500 and 535 and their LogP is between 2.87 and 4.05. This suggests that the indole-triazole- pyrimidinone hybrids **6.5a-6.5f** are good lead scaffolds for further structure activity studies directed to the development of the drug classes mentioned above.

Table 6.3. The calculated drug-property descriptors of Indole- Triazole-pyrimidinone peptidomimetic series.

compound	MW	natoms	miLogP	TPSA	nON	nOH NH	nrotb
6.5a	518.96	37	4.05	120.15	10	2	9
6.5b	500.51	37	2.90	140.38	11	3	9
6.5c	532.99	38	4.16	120.15	10	2	9
6.5d	514.54	38	3.01	140.38	11	3	9
6.5e	534.96	38	4.03	140.24	11	3	10
6.5f	516.51	38	2.87	160.47	12	4	10

6.2.3. Molecular docking of 6.5a-6.5f for studying CDK-2 binding interaction.

As the next step, we calculated the binding affinity of the molecules towards CDK2. The 3-dimension (3D) coordinates of cancer

target protein CDK2 with PDB id 2vv9 were selected and obtained from protein data bank (PDB) and was docked with **6.5a-6.5f** using the docking program AutoDockVina 1.1.2.

On analysing the docking interactions, it was found that all the synthesised compounds showed high binding affinity than the parent ligand (parent ligand binding affinity=-8.7Kcal/mol). Of the synthesised compounds, **6.5d** showed high binding affinity of -10.5 Kcal/mol. **6.5e** and **6.5f** forms hydrogen bonds with receptor protein. **6.5e** sits in the active site of protein and forms one hydrogen bond via NH of indole with VAL64. Similarly, **6.5f** also forms one hydrogen bond via the carbonyl group of pyrimidinone with GLN residue of protein with a binding affinity -9.8kcal/mol. All the compounds also showed Pi-cation interaction with the receptor except **6.5f**. On analysing the docking interaction, it was found that protein exists in zwitter ionic form and cationic part (NH_3^+) of protein forms a non covalent interaction with the pi system of the ligand. The binding mode of compounds **6.5a-6.5f** and types of interactions are represented in figure **6.2**. The docking score of the synthesised compounds are listed in table **6.4**

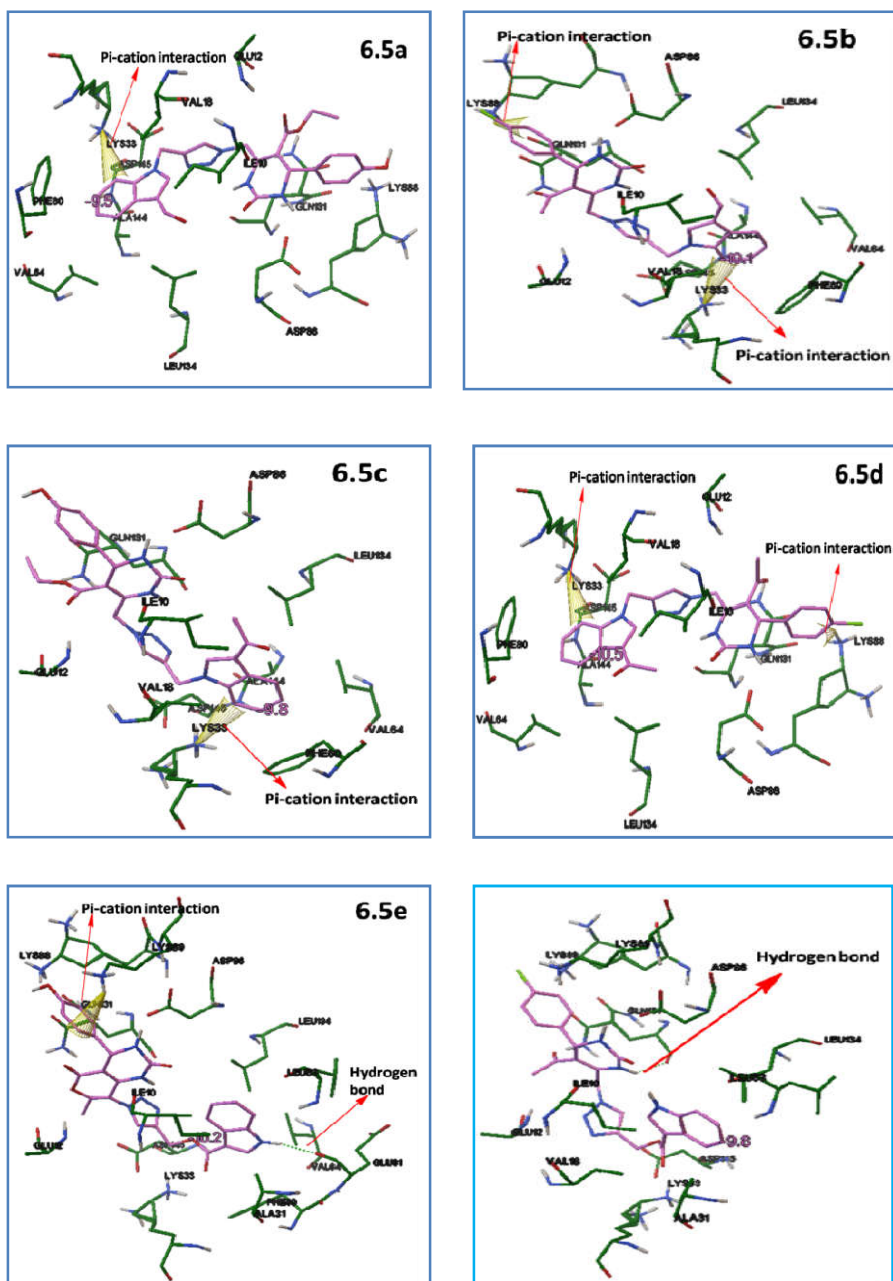


Fig. 6.2 .The binding mode of compounds 6.5a-6.5f respectively in the active site of CDK2-2vv9. The dotted lines represent the Hydrogen bonding.

Table 6.4. Docking scores of compounds **6.5a-6.5f**

Compound	Docking score / binding affinity (Kcal/mol)
6.5a	-9.5
6.5b	-10.1
6.5c	-9.8
6.5d	-10.5
6.5e	-10.2
6.5f	-9.8

6.2.4. Evaluation of cytotoxicity

6.2.4.1. Trypan blue exclusion method

The selected compounds were screened for short term in vitro cytotoxicity using Dalton's lymphoma ascites cells (DLA) or Ehrlich Ascites Carcinoma (EAC) cells. The tumor cells aspirated from the peritoneal cavity of tumour bearing mice were washed thrice with PBS or normal saline. The cell viability was determined by trypan blue exclusion method. The viable cell suspension (1×10^6 cells in 0.1ml) was added to tubes containing various concentrations of the test compounds and the volume was made up to 1 ml using phosphate buffered saline (PBS). The control tube contained only cell suspension. These assay mixtures were incubated for 3 hour at 37°C. Further, the cell suspension was mixed with 0.1 ml of 1% trypan blue and kept for 2-3minutes and loaded on a haemocytometer. The dead cells took up the blue colour of trypan blue, while the live cells did not take up the dye. The number of stained and unstained cells was counted separately for calculating the % cytotoxicity.¹⁰

$$\% \text{ cytotoxicity} = \frac{\text{No. of dead cells}}{\text{No. of live cell} + \text{No. of dead cell}} \times 100$$

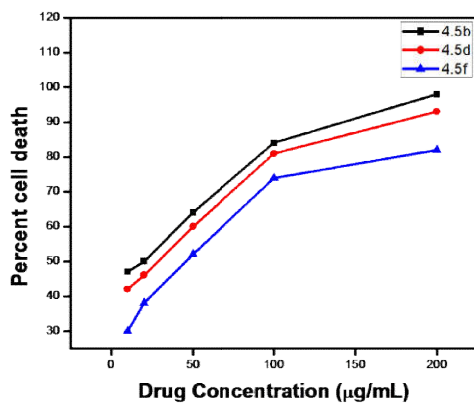


Fig. 6.3. Cytotoxic effects of **6.5b**, **6.5d** and **6.5f** on EAC cells.

Table: 6.5: IC₅₀ Value of **6.5b**, **6.5d** and **6.5f** from Trypan blue exclusion method

Compound	IC ₅₀
6.5b	14µg/mL
6.5d	26 µg/mL
6.5f	44 µg/mL

IC₅₀ values (concentration that inhibited cell growth in 50% compared to untreated controls) were obtained from the graph (Fig.6.3) and the IC₅₀ values are given in table.6.5. Of the three tested compounds, **6.5b** showed IC₅₀ value of 14µg/ml, **6.5d** showed 26 µg/mL and **6.5f** shows 44µg/mL. While comparing these three results, the compound **6.5b** caused fifty percent cell death at very low concentration of the compound. While analyzing the structure of the compounds, we can see that all the three compounds are bearing

almost the same functionalities except the substitution at the third position of indole. In **6.5b**, at the third position of indole, an aldehyde group is present which can form covalent interaction with the receptor and that could be the reason for the highest cytotoxicity observed compared to other two compounds.

6.2.4.2. Cytotoxicity against human breast cancer cell lines MCF-7: MTT Assay

(A): In vitro cytotoxicity of synthesized 6.5d

MCF-7 cells were seeded in 96-well plates at a concentration of 1.0×10^4 cells/well and were incubated overnight at 37°C in a 5% CO₂ humidified environment. Then the cells were treated with different concentrations of the sample **6.5d** like 10, 20, 30, 40, 50, 60, 70, 80, 90, and 100 μM/mL (dissolved with RPMI medium 1640), respectively. The controls were cultivated under the same conditions without addition of **6.5d**. The treated cells were incubated for 48 hrs for cytotoxicity analysis. The cells were then subjected to MTT assay. The stock concentration (5 mg/mL) of MTT-(3-(4,5-dimethylthiazol-2-yl)-2,5-diphenyltetrazolium bromide, a yellow tetrazole) was prepared and 100 μL of MTT was added in each wells and incubated for 4 hrs. The purple color formazan crystals were observed and these crystals were dissolved with 100 μL of dimethyl sulphoxide (DMSO), and read at 620 nm in a multi well ELISA plate reader (Thermo, Multiskan). The dose-dependent cytotoxicity was observed in the case of indole-triazole-pyrimidinone peptidomimetic **6.5d** which was treated with MCF-7 cells. Fifty percentage of cell death, which determines the

inhibitory concentration (IC₅₀) value of **6.5b** against MCF-7 cells, holds at **15 μ M** in 48 h (Fig.6.4). This indicates that these molecules exhibit increased bioavailability and have tremendous anticancer potential.

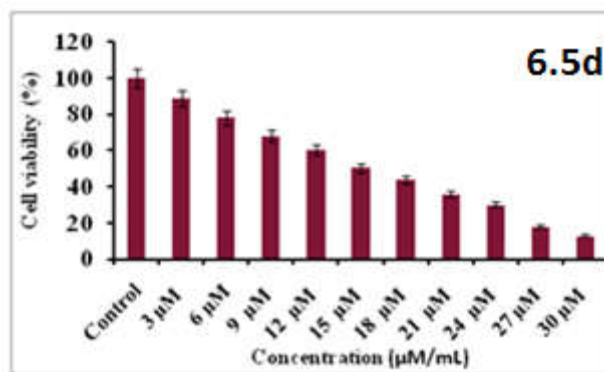


Fig. 6.4. MTT assay results confirming the in vitro cytotoxicity effect of **6.5d** against the MCF-7 cells. The detected IC₅₀ concentration was **15 μ M/mL**.

(B): DAPI (4, 6-diamidino-2-phenylindole, dihydrochloride) staining for morphological studies:

MCF-7 cells were treated with **6.5d** at its IC₅₀ concentration (15 μ M) for 48 h, and then fixed with methanol: acetic acid (3:1, v/v) prior to washing with PBS. The washed cells were then stained with 1 mg/mL DAPI (4, 6-diamidino-2-phenylindole dihydrochloride) for 20 minutes in dark atmosphere. The stained images were recorded with fluorescent microscope with appropriate excitation filter. The bright field and fluorescence microscopic images are shown in **Fig.6.5**. As shown in this, the strong bluish fluorescence and cellular uptake observed in the imaging studies with **6.5d** reveal that these molecules have high potency against breast cancer cell lines (MCF-7).

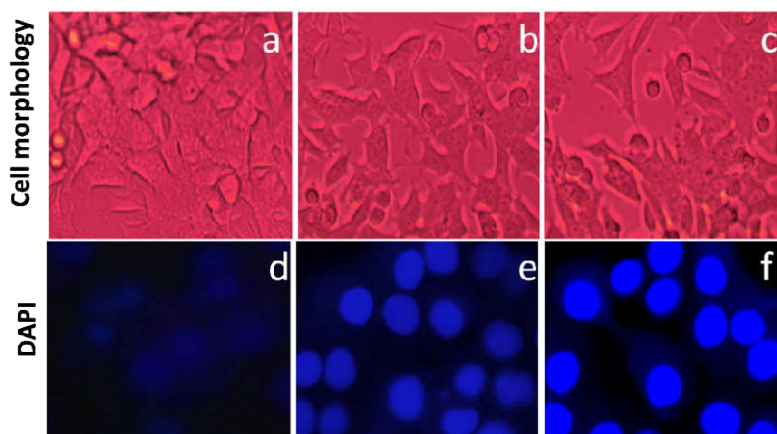


Fig. 6.5. Bright field inverted light microscopy images (a, b, c) and the DAPI nuclear staining (d, e, f) of control cells and **6.5d** treated cells. The DAPI images exhibits condensed form of nuclear materials in apoptotic cells.

6.2.4.3. Western blot Analysis to study the selectivity of the molecules towards CDK2

To study the expression of CDK2 protein in **6.5d** exposed in MCF-7 breast cancer cells, we have carried out western blot analysis (Fig. 6.6) using beta-actin as internal standard.

The MCF-7 cells (1×10^6) were seeded on to 100-mm culture dishes in the presence or absence of **6.5d** and were treated for 48 h. The cells were then washed twice with ice-cold PBS and incubated in lysis buffer. The lysates were centrifuged at $10,000 \times g$ for 5 min at 4 °C, and were used as the cell protein extracts. Each of the extracts was applied to 12% SDS polyacrylamide gel electrophoresis after which the proteins were transferred onto a nitrocellulose membrane, and then blocked for 1 hr using 10% skim milk in water. After washing in a PBS containing 0.1% Tween 20 for 3 times, the primary antibodies were added at a v/v ratio of 1:1000. After overnight incubation at 4 °C,

the primary antibodies were washed away and the secondary antibodies were added for 1 h incubation at room temperature. Finally, the enhanced chemiluminescence detection reagents were used to develop the signal of the membrane. Our findings demonstrate that the protein level of CDK2 is significantly down-regulated in the treated cells when compared to control and the results obtained are in well agreement with the recent results of Finn et al.¹¹

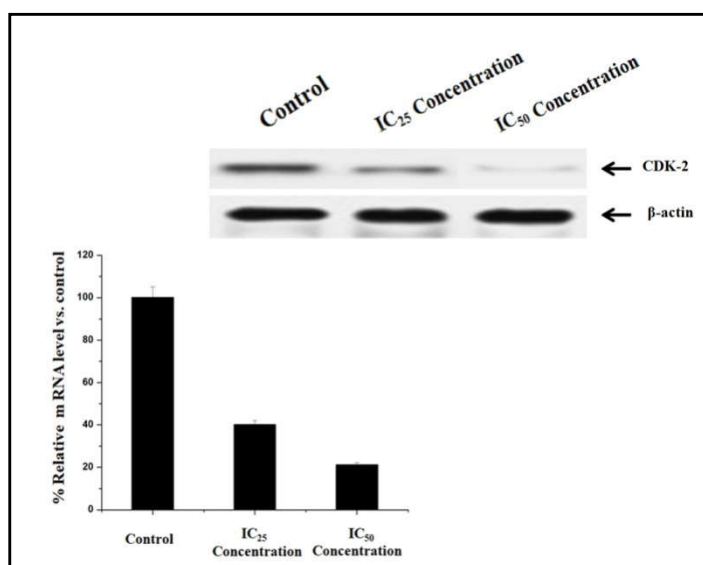


Fig. 6.6. Western blot Analysis of **6.5d** from MCF-7 cell line

6.3. Structure elucidation by spectroscopy

Structure identification of 6-((4-((3-formyl-1H-indol-1-yl)methyl)-1H-1,2,3-triazol-1-yl)methyl)-4-(4-hydroxyphenyl)-2-oxo-1,2,3,4-tetrahydro Pyrimidine-5-carboxylate. 6.5a.

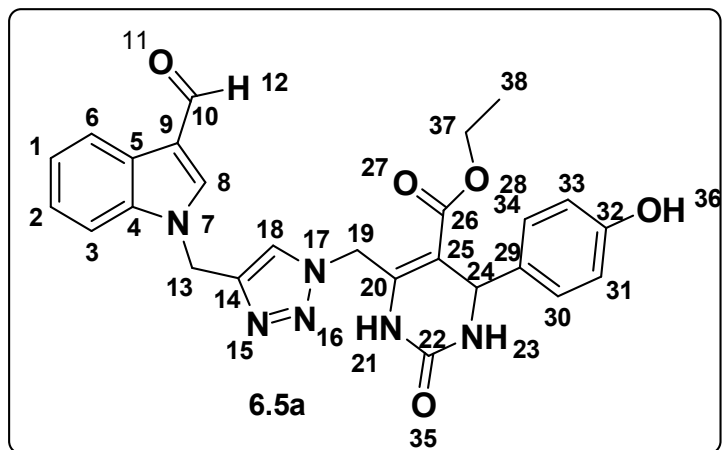


Fig. 6.7. structure of 6.5a

For the structure elucidation of the click product, compound **6.5a** is taken as a representative and is numbered as in figure **6.7**. The FT-IR spectrum of the compound **6.5a** gave major absorptions at 3218, 1785, 1644 cm^{-1} (Fig. **6.8**). The band at 3218 cm^{-1} is due to the NH stretching vibration of the pyrimidinone. The absorption at 1785 cm^{-1} is due to the C=O stretching vibration of the ester carbonyl. The absorption at 1644 cm^{-1} is due to the C=O stretching vibration of the indole carbonyl.

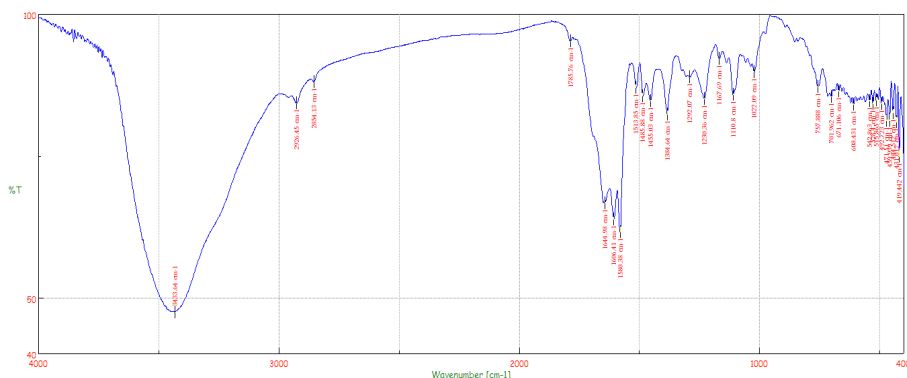


Fig. 6.8. FTIR spectrum of compound 6.5a

The singlet at δ 9.92 corresponds to aldehydic proton at position 11. The indole CH proton at position 8 is observed as a singlet at δ = 8.39. The peaks from 8.15 to 7.03 correspond to the 8 aromatic protons. The Singlet obtained at δ =7.72 corresponds to the triazole proton. The CH₂ proton at position 13 appears as a singlet at δ 5.61 and CH proton at position 24 appears as a doublet at δ 5.58-5.56. The singlet at δ 5.40 corresponds to CH₂ proton at position 19. The quartet at δ 3.96-3.92 corresponds to CH₂ proton at position 37 and triplet at δ 1.01-0.99 corresponds to CH₃ proton at position 38 (Fig. 6.9).

6.4. Conclusion

To conclude, in this chapter we have discussed the design, synthesis and *in vitro* cytotoxicity evaluation of a new series of Indole-Triazole-Pyrimidinone hybrids by systematic structure alterations of Indole-Triazole-Carboxamides described in chapter 2 and Indole-Triazole-Coumarin hybrids described in chapter 4 with a pyrimidine moiety. Here also the multicomponent coupling strategy and click chemistry were effectively utilized to obtain the new multi heterocycle

based peptidomimetics in good to excellent yield. The structure modification by pyrimidine substitution is more promising compared to the other two entities such as carboxamides and coumarin and that is well reflected in the IC₅₀ value obtained from cytotoxicity evaluation against human breast cancer cell line MCF-7. Most importantly, the molecules also possess excellent CDK 2 inhibition property compared to the molecules described in previous chapters and which is clearly seen in figure 6.7.

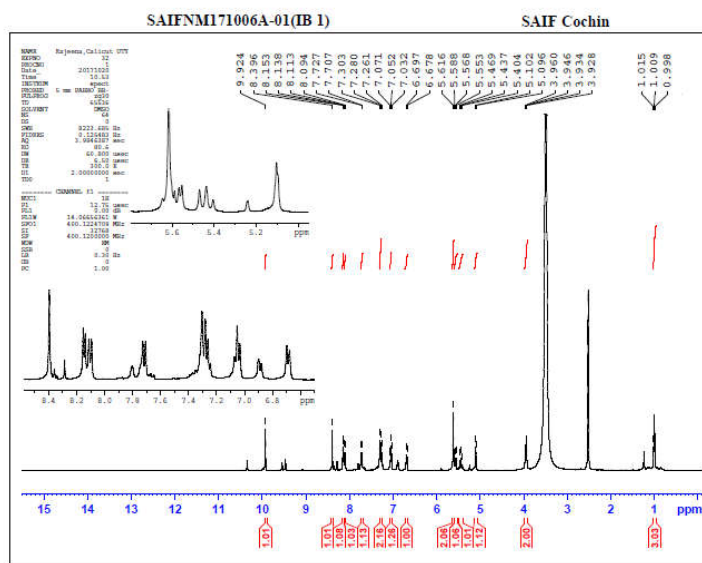


Fig. 6.9. ¹H NMR spectrum of the compound 6.5a

6.5. Experimental Section

General

All reactions were carried out with oven-dried glassware. The starting materials were purchased from Aldrich and Merck. IR spectra were recorded on a JASCO-FT/IR-4100 Fourier transform infrared

spectrometer by making KBr pellets of the samples. ^1H and ^{13}C NMR spectra were determined in DMSO using a Bruker amx 500MHz spectrometer. The high resolution mass spectra were measured with a Thermo Exactive Orbitrap with MeOH as solvent. The chemical shifts (δ) are given relative to tetramethylsilane (TMS) and the coupling constants (J) are reported in hertz (Hz). Absorption spectra of the compounds were recorded on a JASCO V-550 UV/Vis Spectrophotometer and fluorescence measurements were carried out with a Perkin Elmer LS55 Fluorescence Spectrometer.

General experimental procedure for the synthesis of 1-(prop-2-yn-1yl)-1H-indole-3-carbaldehyde 2.1a:

Indole-3-carbaldehyde (145.16mg, 1mmol) and potassium carbonate (414.63mg, 3mmol) were dissolved in minimum amount of DMF, and stirred at 50°C for 10 min. After cooling the reaction mixture to room temperature, propargyl bromide (118.96mg, 1mmol) was added to the reaction mixture and stirred for 4 h. and mixture was then poured into ice cold water. The solid product obtained was filtered and dried under vacuum to afford 1-(prop-2-yn-1yl)-1H-indole-3-carbaldehyde 2.1a.

White solid; 159mg (yield 87%); Mp $90-93^\circ\text{C}$; IR (KBr) ν max :3198, 2121, 1656, 1644, 1615, 1579, 1528, 1471, 1441, 1308, 1244, 1163, 1041, 770, 741, 562 cm^{-1} . ^1H NMR (DMSO- d_6 , 400 MHz) δ_{H} (ppm): 9.94 (1H,s), 8.37-8.35(1H, d=8Hz), 8.15-8.12(1H, m),7.66-7.64(1H,m),7.38-7.28(2H,m),5.24(2H,s),3.43(1H,s). ^{13}C NMR (DMSO-

d_6 , 100MHz) δ_C (ppm): 185.4, 140.5, 137.0, 125.1, 124.2, 123.4, 121.7, 118.3, 111.8, 78.4, 77.2, 40.4; MS(ESI): m/z = 184 [M + 1]⁺.

1-(1-(prop-2-yn-1-yl)-1H-indol-3-yl)ethanone 2.1b: White solid ; 167mg (yield 85%); Mp 103-105°C ; IR (KBr) ν max : 3218, 2125, 1676, 1628, 1578, 1523, 1388, 1211, 932, 762, 747 cm^{-1} ; ¹H NMR (DMSO- d_6 , 500 MHz) δ_H (ppm): 8.40(1H,s); 7.91(1H,s); 7.35-7.32 (1H,m); 7.26(2H,s); 4.92(2H,s); 2.17(1H,s); 1.56(3H,s); ¹³CNMR(DMSO d_6 , 125MHz) δ_C (ppm): 195.4, 140.5, 137.0, 125.1, 124.2, 123.2, 121.59, 118.0, 111.6, 78.4, 77.2, 40.4, 25.1; MS(HRMS) m/z = 221.0739[M+Na]⁺.

Prop-2-yn-1-yl 1H-indole-3- carboxylate 2.1c : White solid ; 163mg (yield 82%) ; Mp 80-82°C; IR (KBr) ν max : 3298, 3282, 2120, 1698, 1698, 1619, 1539, 1271, 1245, 1183, 1149, 1095, 916, 774, 749, 626 cm^{-1} . ¹H NMR (DMSO- d_6 , 400 MHz) δ_H (ppm): 12.00 (1H,S); 8.05-8.00 (2H, m); 7.66-7.64 (1H, d j=8Hz); 7.35-7.27 (2H,m), 5.23 (2H,S); 3.56 (1H,S). ¹³C NMR (DMSO- d_6 , 100 MHz) δ_C (ppm): 163.8, 136.8, 126.6, 122.9, 121.9, 121.1, 120.7, 112.9, 111.7, 79.6, 76.9, 51.4 ; MS(ESI): m/z = 222 [M + Na]⁺.

General procedure for the synthesis of 3, 4-dihydropyrimidinones (6.2a-6.2b): A mixture of benzaldehyde (1 mmol), ethyl acetoacetate or acetyl acetone (1mmol), and urea (1.5 mmol) was heated at 80 °C (oil bath). After few minutes, with the progress of reaction, the solid began to separate out. The mixture was kept at the same condition for 1h and the solid obtained was crushed, washed with cold water, filtered, and dried under vacuum to give the crude product.

Recrystallization of the solid product from hot ethanol provided the analytically pure product.

Ethyl 4-(4-hydroxyphenyl)-6-methyl-2-oxo-1, 2, 3, 4-tetrahydropyrimidin-5-carboxylate 6.2a: Yellow solid; Mp 222-224⁰C. FT-IR (KBr) ν_{\max} 3509,3368 , 3279, 3123, 2070,1683, 1644, 1598, 1517, 1460, 1381, 1368, 1316, 1294, 1288, 1230, 1171, 1090, 870, 820, 753, 651, 633, 589, 544, 522, 473, 418 cm^{-1} ; ¹H-NMR(500 MHz, DMSO) δ : 1.161-1.13(t, 3H), 2.31(s, 3H), 4.30-4.26(q, 2H), 5.13(s, 1H), 5.54(s, 1H), 6.77 (s, 1H), 6.76(s, 1H), 7.31-7.25(m, 4H) ppm; HRMS (EI) m/z calcd for C₁₄H₁₆N₂O₄ [M+H]⁺: 277.11984, found: [M+H]⁺ 277.11453

5-acetyl-4-(4-chlorophenyl)-6-methyl-3,4-dihydropyrimidin-2(1H)-one 6.2b. Yellow solid.Mp 228-230⁰C. FT-IR (KBr) ν_{\max} 3439, 3289,3121,2929,1806,1701,1644,1618,1542,1489,1468,1425,1402,1386,1363,1329,1294,1262,1236,1191, 1141,1091, 1032,1014,966, 791,736, 714, 681, 645, 600, 562, 423 cm^{-1} ; ¹H-NMR(500 MHz, DMSO) δ : 2.24(s, 3H), 2.25(s, 3H), 5.16(s, 1H), 6.60(s, 1H), 6.617(s, 1H), 6.82-7.35(m, 4H) ppm; HRMS (EI) m/z calcd for C₁₃H₁₃ClN₂O₂ [M+H]⁺: 265.07439, found: [M+H]⁺: 265.06898.

General procedure for the synthesis of brominated 3, 4-dihydro pyrimidinones (6.3a- 6.3b): A solution of 3, 4-dihy dropyrimidinone (10 mmol) was placed in 20 mL glacial acetic acid in a 500 mL flask. 1.598 g (0.4982 mL, 10 mmol) of bromine in 10 mL glacial acetic acid was added to the flask very slowly (about 30 min.) from a dropping funnel. The mixture was stirred vigorously during the addition of

bromine and kept the temperature at 0-5⁰C. When the addition was completed, it was allowed to stand at room temperature for another 30 min. The mixture was then poured into 400 mL water and stirred well. The precipitate was filtered, washed with cold water and recrystallised from dilute ethanol.

Ethyl 6-(bromomethyl)-4-(4-hydroxyphenyl)-2-oxo-1, 2, 3, 4 tetrahydro pyrimidine-5-carboxylate 6.3a: Yellow solid; Mp 235-237⁰C. FT-IR (KBr) ν_{\max} : 3568, 3381, 3234, 3105, 2971, 2819, 1683, 1645, 1612, 1595, 1513, 1464, 1431, 1389, 1366, 1325, 1304, 1281, 1232, 1169, 1144, 1118, 1103, 1046, 1019, 977, 934, 887, 872, 854, 828, 816, 784, 719, 678, 657, 633, 606, 570, 552, 531, 499, 464, 432, 417 cm^{-1} ; ¹H-NMR(500 MHz, DMSO) δ : 1.132-1.16(t, 3H), 4.25(s, 2H), 4.27-4.29(t, 3H), 5.16(s, 1H), 5.46(s, 1H), 6.87(s, 1H), 6.89(s, 1H), 7.22-7.93(m, 4H)ppm; HRMS (EI) m/z calcd for C₁₄H₁₅BrN₂O₄ [M+H]⁺: 355.02935, found [M+H]⁺: 355.03010.

5-acetyl-6-(bromomethyl)-4-(4-chlorophenyl)-3, 4-dihydropyrimidin-2(1H)-one 6.3b: Yellow solid. Mp 237-239⁰C. FT-IR(KBr) ν_{\max} 3410, 2923, 1687, 1490, 1446, 1408, 1272, 1230, 1157, 1091, 1014, 952, 833, 754, 727, 508, 486, 458, 435, 415 cm^{-1} ; ¹H-NMR(500 MHz, DMSO) δ : 2.29(s, 3H), 4.05(s, 2H), 5.22(s, 1H), 5.48(s, 1H), 5.54(s, 1H), 7.00-7.35(m, 4H) ppm; HRMS (EI) m/z calcd for C₁₃H₁₂BrClN₂O₂ [M+H]⁺: 342.98490, found: 342.04521.

General procedure for the synthesis of azide derivatives of dihydropyrimidinones (6.4a-6.4b): Bromoderivative of dihydropyrimidinone (1 mmol), K₂CO₃ (3 mmol) and sodium azide (1 mmol)

were stirred at room temperature in DMF. After completion of the reaction, the reaction mixture was poured into ice cold water. The solid product obtained was filtered and dried under vacuum to afford the dihydropyrimidinoneazide.

Ethyl 6-(azidomethyl)-4-(4-hydroxyphenyl)-2-oxo-1, 2, 3, 4-tetrahydro pyrimidine-5-carboxylate 6.4a: Yellow solid, Mp 165-167⁰C. FT-IR (KBr) ν_{\max} 3442, 2922, 2852, 2057, 1638, 1529, 1418, 1350, 1212, 1157, 1113, 1020, 873,664, 553, 511,481, 409 cm^{-1} ; ¹H-NMR(500 MHz, DMSO) δ : 1.13-1.15(t, 3H); 2.24-2.25(d, 2H); 4.01(s, 1H), 4.05(s, 1H); 5.22(s, 1H); 5.54(s, 1H); 6.82(s, 1H); 6.84(s, 1H); 7.00-7.35(m, 4H) ppm; HRMS (EI) m/z calcd for C₁₄H₁₅N₅O₄ [M+Na]⁺:340.10217, found: [M+Na]⁺: 340.10574

5-acetyl-6-(azidomethyl)-4-(4-chlorophenyl)-3,4-dihydropyrimidin-2(1H) one 6.4b: Yellow solid. Mp 164-166⁰C. FT-IR (KBr) ν_{\max} 3413, 2923, 2108, 2036, 1761, 1685, 1490, 1437, 1407, 1257, 1229, 1156, 1091, 1014, 833, 759, 627, 534, 512, 460, 416 cm^{-1} ; ¹H-NMR(500 MHz, DMSO) δ : 1.98(s, 2H), 2.19(s, 3H), 5.17(s, 1H), 6.34(s, 1H), 6.36(s, 1H), 7.26-7.362(m, 4H)ppm; HRMS (EI) m/z calcd for C₁₃H₁₂ClN₅O₂ [M]⁺:305.06795, found [M]⁺: 305.06762

General procedure for the synthesis of 1, 4-disubstituted triazolyl DHPMs tethered with indole derivative via Cu (I) catalyzed Huisgen cycloaddition (6.5a-6.5f). An equimolar mixture of azide and alkyne was mixed with 0.2 equiv. of CuSO₄ and 0.4 equiv. of sodium ascorbate in a mixed solvent system containing *t*-butanol, water, and

DMSO (4:2:1) at room temperature. After 12 h, the reaction mixture was diluted with cold water to afford the click product in solid form.

Ethyl 6-((4-((3-formyl-1*H*-indol-1-yl)methyl)-1*H*-1,2,3-triazol-1-yl)methyl)-4-(4-hydroxyphenyl)-2-oxo-1,2,3,4-tetrahydro Pyrimidine-5-carboxylate 6.5a: whitish solid; 455mg(yield 91%); IR (KBr) ν_{\max} :3433,3218, 2926, 1785, 1644, 1606, 1580, 1513, 1485, 1455, 1384,1292,1230,1167,1110, 1022, 757, 701, 671, 608, 542, 492, 471, 431,419 cm^{-1} ; $^1\text{H-NMR}$ (400 MHz, DMSO) δ : 1.01-0.99(t,3H), 3.96-3.92(q, 2H), 5.10(s, 2H), 5.40(s, 2H), 5.58-5.56(d, 1H),5.61(s, 1H), 6.69-6.67(d, 1H), 7.70-7.03(m, 4H), 7.72(s, 1H), 8.15-8.09(m, 4H), 8.39(s, 1H), 9.92(s, 1H).

1-((1-((5-acetyl-6-(4-chlorophenyl)-2-oxo-1,2,3,6 tetrahydropyrimidin-4-yl) methyl) methyl)-1*H*-1,2,3-triazol-4-yl)methyl)-1*H*-indole-3-carbaldehyde6.5b: whitish solid; 435mg (yield 89%); IR (KBr) ν_{\max} : 3426, 2926, 1665 1648, 1604, 1580, 1530, 1486, 1453, 1384, 1350, 1326, 1305, 1219, 1168, 1138, 1111, 1058, 1022, 889, 856, 754, 700, 614, 467, 431, 413 cm^{-1} ; $^1\text{H-NMR}$ (400 MHz, DMSO) δ : 1.81(s,3H), 4.37(s, 2H), 4.99-4.86(d, 2H), 5.15(s, 1H), 5.44(s, 1H), 7.42-7.06(m, 8H), 7.87(s, 1H), 8.04(s, 1H), 9.44(s, 1H)

Ethyl 6-((4-((3-acetyl-1*H*-indol-1-yl)methyl)-1*H*-1,2,3-triazol-1-yl)methyl)-4-(4-hydroxyphenyl)-2-oxo-1,2,3,4-tetrahydro Pyrimidine-5-carboxylate 6.5c: whitish solid; 473 mg (yield 92%);IR (KBr) ν_{\max} : 3421,2924, 1790, 1668, 1648, 1603, 1580, 1515, 1488, 1451, 1384, 1325, 1293, 1213, 1168, 1110, 1092, 1014, 854, 754, 700, 618, 509, 473, 464, 437, 428, 419, 411 cm^{-1} ; $^1\text{H-NMR}$ (400 MHz,

DMSO) δ : 1.01-1.00(t, 3H), 2.44(s, 3H), 3.95-3.92(q, 2H), 5.32(s, 1H), 5.38(s, 1H), 5.45-5.42(ds, 1H), 5.54(s, 1H), 5.57(s, 2H)5.59(s, 2H), 6.69- 6.67(d, 1H), 6.89-6.87(d, 1H), 7.06-7.02(t, 1H), 7.26-7.19(m, 2H), 7.30(s,1H), 7.67-7.65(d, 1H), 8.12-8.11(d, 1H), 8.18-8.16(d, 1H), 8.44(s, 1H), 9.44(s, 1H).

(1-((5-(ethoxycarbonyl)-6-(4-hydroxyphenyl)-2-oxo-1,2,3,6-tetrahydropyrimidin-4-yl)-1H-1,2,3-triazol-4-yl)methyl 1H-indole-3-carboxylate 6.5e: whitish solid; 464mg(yield 90%); IR (KBr) ν_{\max} : 3425, 3310, 2925, 1783, 1766, 1646, 1603, 1582, 509, 1490, 1453, 1429, 1382, 1315, 1297, 1255, 1185, 1160, 1106, 1023, 984, 887, 862, 622, 564, 533 515, 481, 472, 434,421, 408 cm^{-1} ; $^1\text{H-NMR}$ (400 MHz, DMSO) δ : 1.23-1.04 (t, 3H), 3.97-3.93(q, 2H), 5.12(s, 1H), 5.21-5.19(d, 1H), 5.44(s, 2H), 5.67(s, 2H), 6.69(s, 1H), 6.90-6.88(d, 1H), 7.19-7.03(m, 1H), 7.33-7.21(m, 3H), 7.75-7.48(M, 1H), 7.81(s, 1H), 7.99-7.96(m, 1H), 8.24-8.01(m, 1H), 8.29-8.26(d, 1H), 8.30(s, 1H), 9.46(s, 1H)

(1-((5-acetyl-6-(4-chlorophenyl)-2-oxo-1, 2, 3, 6-tetrahydropyrimidin-4-yl) methyl)-1H-1, 2, 3-triazol-4-yl)methyl 1H-indole-3-carboxylate 6.5f: whitish solid; 449mg (yield 89%); IR (KBr) ν_{\max} : 3433, 3310, 2926, 1783, 1766, 1646, 1603, 1584, 1557, 1530, 1509, 1490, 1453, 1429, 1378, 1350, 1325, 1315, 1297, 1255, 1185, 1106, 1070, 1023, 984, 887, 862, 832, 803, 776, 698, 683, 622564, 419 cm^{-1} ; $^1\text{H-NMR}$ (400 MHz, DMSO) δ :1.00(s, 3H),4.69-4.68(d, 1H), 5.16(s, 2H), 5.29(s, 2H), 6.98(s, 1H),7.00-6.99(d, 1H), 7.08-7.02(m, 2H), 7.20-7.10(m, 1H), 7.28-7.24(m, 3H), 7.42-7.40(d, 1H),7.80-7.76(m, 1H), 7.89(s, 1H), 8.01(s, 1H), 8.06(s, 1H).

Reference

1. K. Singh, D. Arora, E. Poremsky, J. Lowery and R. S. Moreland, *Eur. J. of Med.Chem.*, 2009,**44**, 1997–2001.
2. a) R. Saladino, U. Ciambecchini, G. Maga, P. Mastromarino, C. Conti and M. A. Botta, *Bioorg. Med. Chem. Lett.*, 2002, **10**, 2143–2153. b) A. E. Rashad, A. H. Shamroukh, R. E. Abdel-Megeid, A. Mostafa, A. Kandil, R. Elshesheny, M. A. Ali and K. Banert, *Eur. J. Med. Chem.*, 2010, **45**, 5251–5257.
3. a) R. Dudhe, P. K. Sharma, P. Verma and A. Chaudhary, *J. Adv. Sci. Res.* 2011, **2 (3)**, 10–17. b) A. E. Rashad, A. E. Mahmoud and M. M. Ali, *Eur. J. Med. Chem.*, 2011, **46**, 1019–1026.
4. J. V. dos Anjos, R. M. Srivastava, J. H. Costa-Silva, L. Scotti, M. T. Scotti, A. G. Wanderley, E. S. Leite, S. J. de Melo, and F. J. B. M. Junior, *Molecules*, 2012, **17**, 809–819.
5. a) C. A. Bernhart, F. B. Haudricourt, J. L. Assens, J. Gougat, C. Lacour, A. Roccon, C. Cazaubon, J. C. Brelie`re, G. Le Fur and D. Nisato, *Bioorg. Med. Chem. Lett.*, 1994, **4**, 157–162. b) A. Salimbeni, R. Canevotti, F. Paleari, D. Poma, S. Caliarì, F. Fici, R. Cirillo, A. R. Renzetti, A. Subissi, L. Belvisi, G. Bravi, C. Scolastico and A. Giachetti, *J. Med. Chem.*, 1995, **38**, 4806–4820.
6. a) M. Markowitz, J. Q. Morales-Ramirez, B. Y. Nguyen, C. M. Kovacs, R. T. Steigbigel, D. A. Cooper, R. Liporace, R. Schwartz, R. Isaacs, L. R. Gilde, L. Penning, J. Zhao and H. Teppler, *J. Acquir. Immune Def. Syndr.*, 2006, **43**, 509; b) D. J. Hazuda, P. Felock, M. Witmer, A. Wolfe, K. Stillmock, J. A. Grobler, A. Espeseth, L. Gabryelski, W. Schleif, C. Blau and M. D. Miller, *Sci.*, 2000, **287**, 646;
7. J. Ishida, K. Hattori, H. Yamamoto, A. Iwashita, K. Miharab and N. Matsuoka, *Bioorg. Med. Chem. Lett.*, 2005, **15**, 4221.
8. A. E. Rashad, A. E. Mahmoud and M. M. Ali, *Eur. J. Med. Chem.* 2011, **46**, 1019–1026. b) E. Nassar, *J. Am. Sci.*, 2010, **6 (8)**, 463–471. c) K. M. Amin, M. I. El-Zahar, M. M. Anwar, M. M. Kamel and M. H. Mohamed, *Acta Pol. Pharm. Drug Res.*, 2009, **66**, 279–291
9. (a) K.M. Sreeman and M.G. Finn, *Chem. Soc. Rev.*, 2010, **39**, 1252; (b) C. L. Droumagueta, C. Wang and C, Q. Wang, *Chem. Soc. Rev.*, 2010, **39**, 1233; (c) A. H. El-Sagheer and T. Brown, *Chem.Soc.*

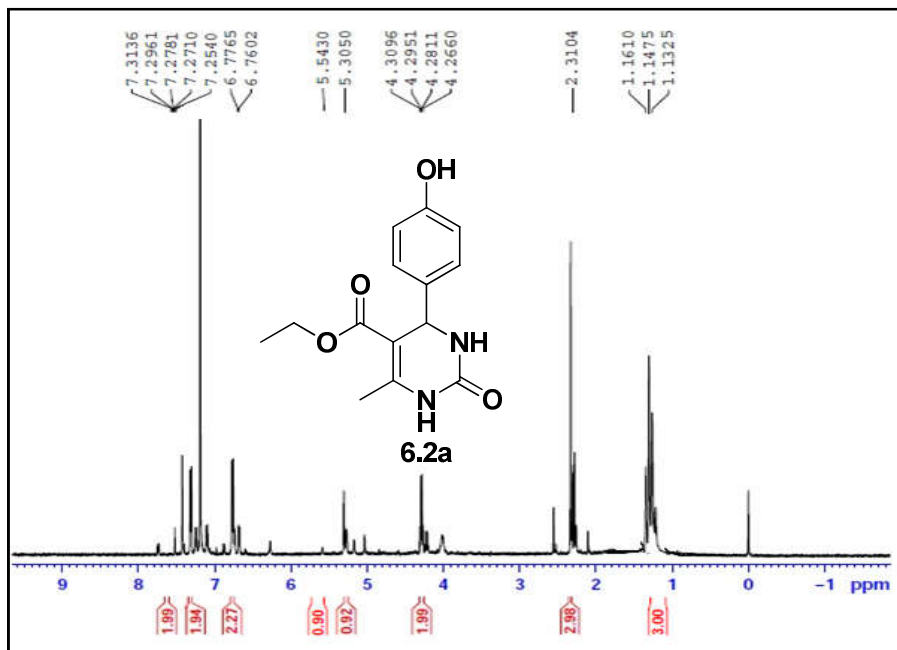
Rev., 2010, **39**, 1388; (d) F. Manzenrieder, R. Luxenhofer, M. Retzlaff, R. Jordan and M.G.Finn, *Angew. Chem., Int. Ed.*, 2011, **50**, 2601; (e) T. Suzuki, Y. Ota, Y. Kasuya, M. Mutsuga, Y. Kawamura, H. Tsumoto, H. Nakagawa, M.G. Finn, and N. Miyata, *Angew. Chem., Int. Ed.*, 2010, **49**, 6817.

10. M. F. D. Mota, P. L. Benficia, A. C. Batista, F. S. Martins, J.R.D. Paula, M.C. Valadares, *J. Ethnopharmacol.*, 2012, **139**, 319-329.
11. R. S. Finn, A. Aleshin and D. J. Slamon, *Breast Cancer Res.*, 2016, **18**, 17.

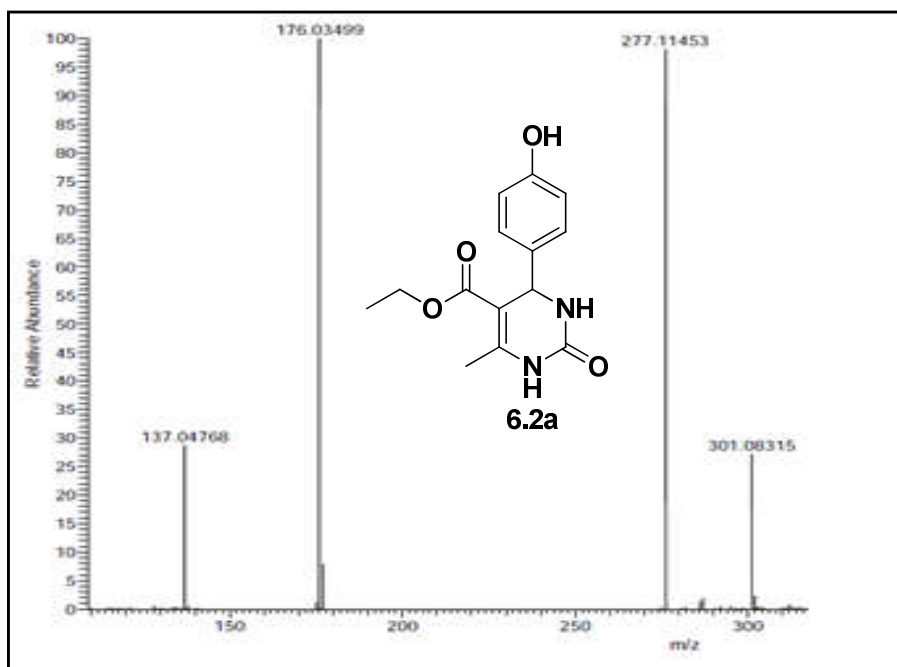
Supplementary Material

Copies of ^1H NMR and Mass spectra of selected compounds

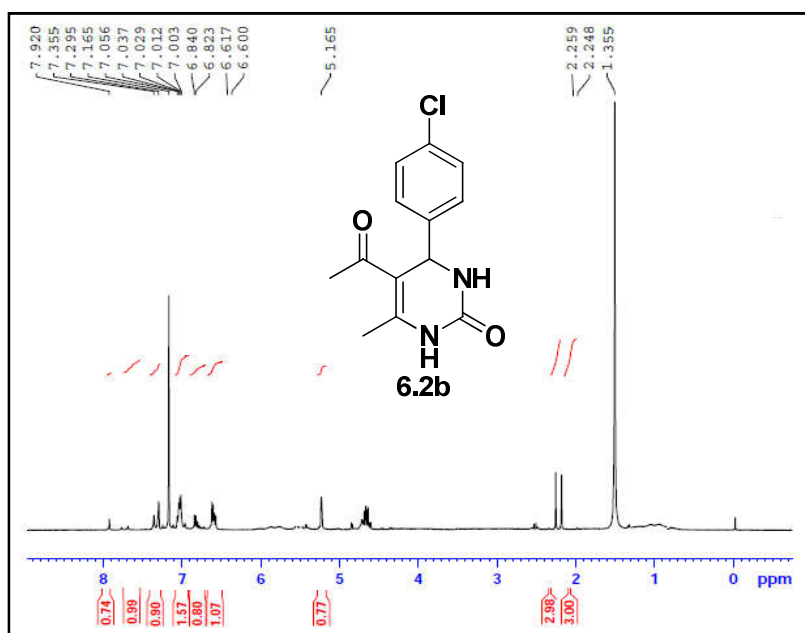
¹H NMR spectrum of the compound **6.2a**



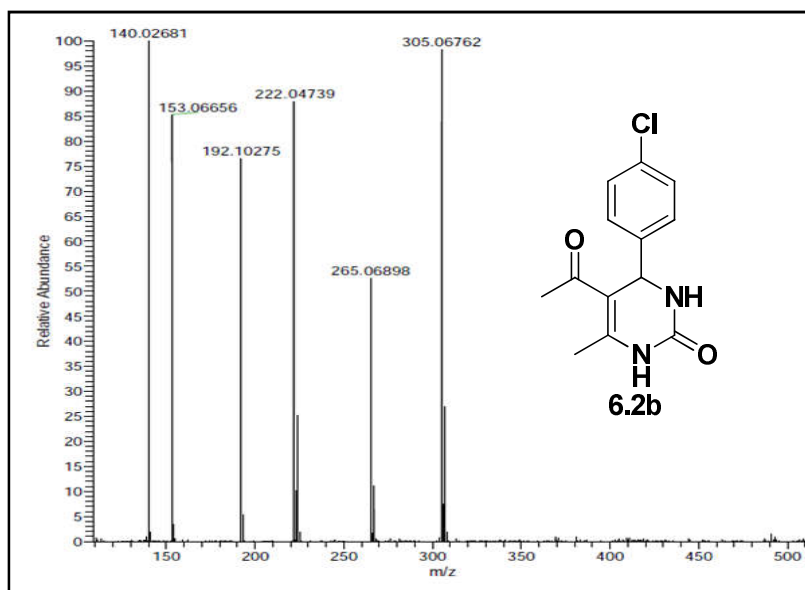
Mass spectrum of the compound **6.2a**



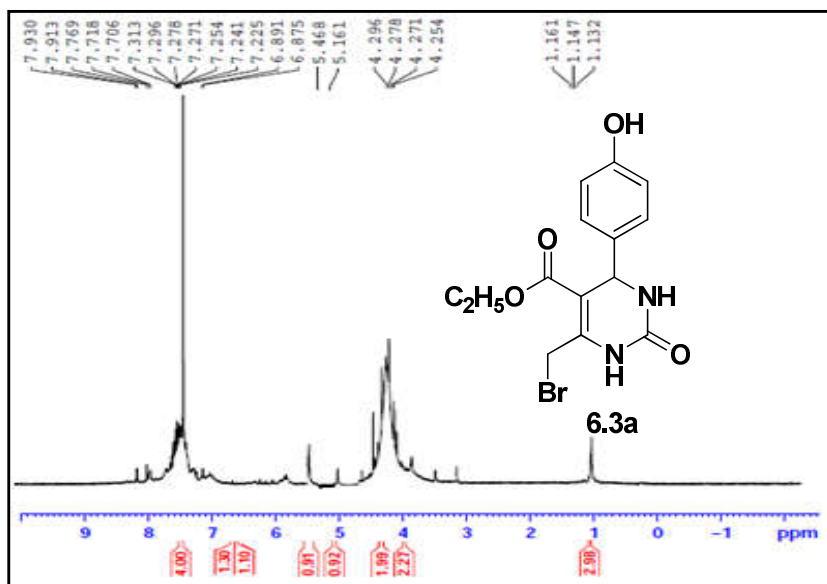
^1H NMR spectrum of the compound **6.2b**



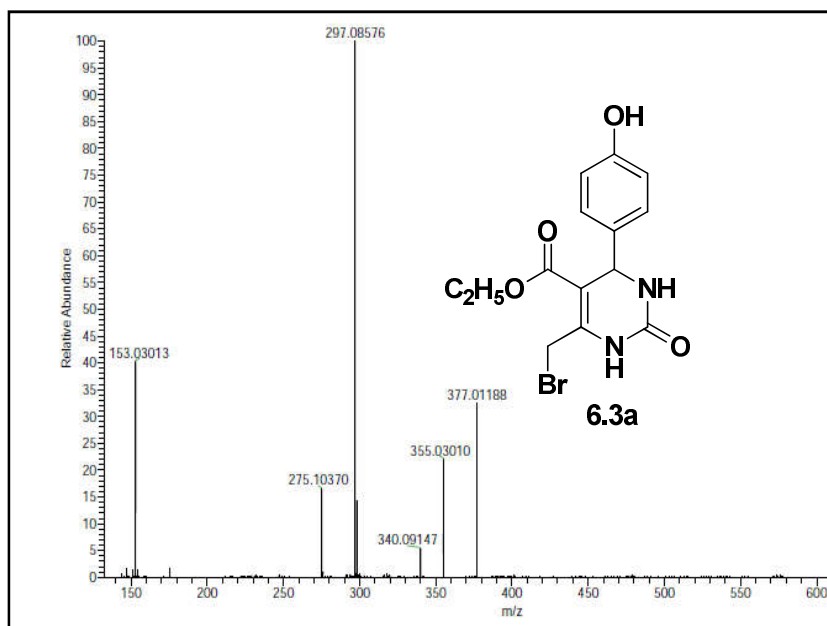
Mass spectrum of the compound **6.2b**



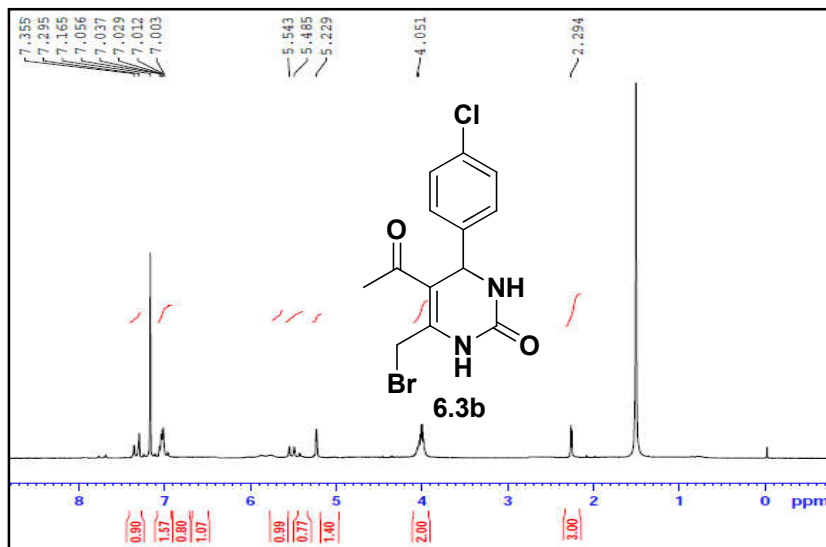
^1H NMR spectrum of the compound **6.3a**



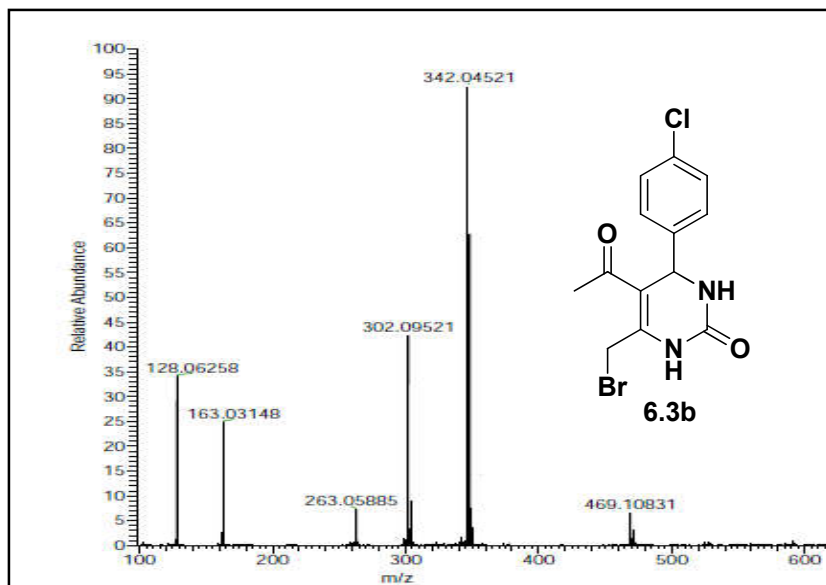
Mass spectrum of the compound **6.3a**



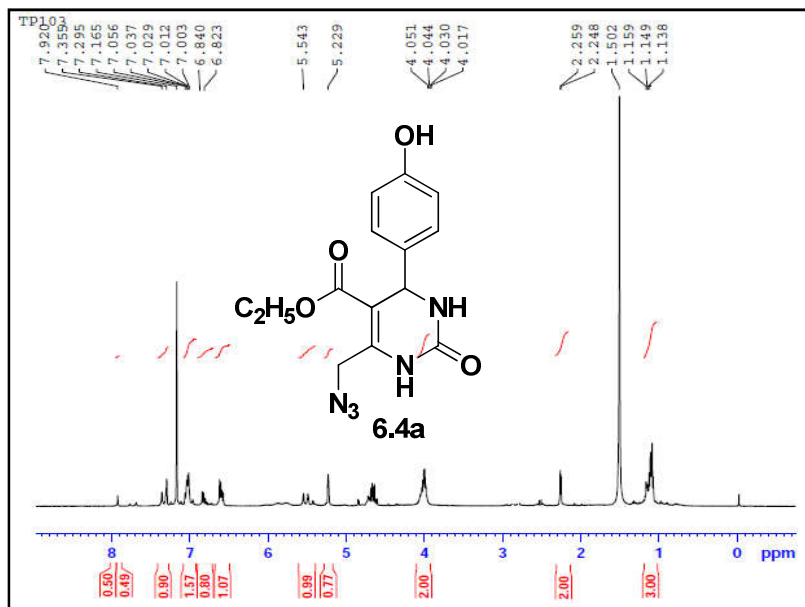
^1H NMR spectrum of the compound **6.3b**



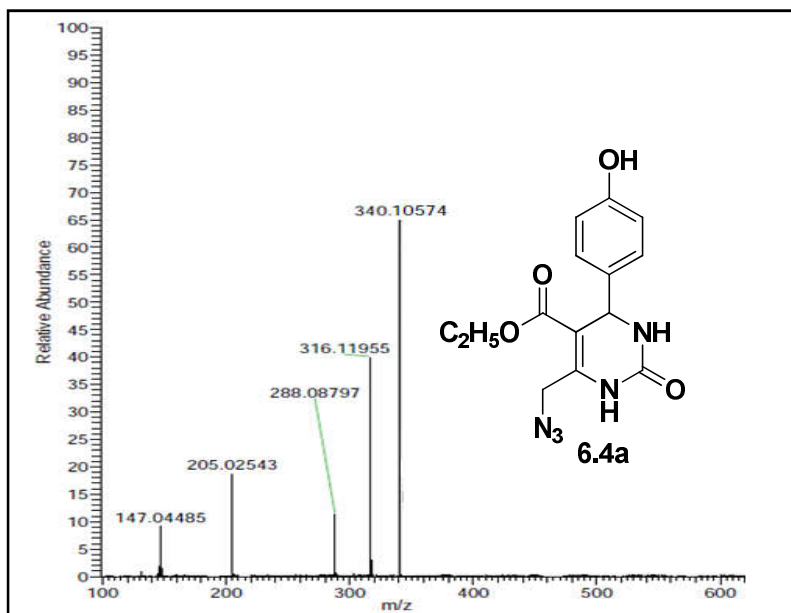
Mass spectrum of the compound **6.3b**



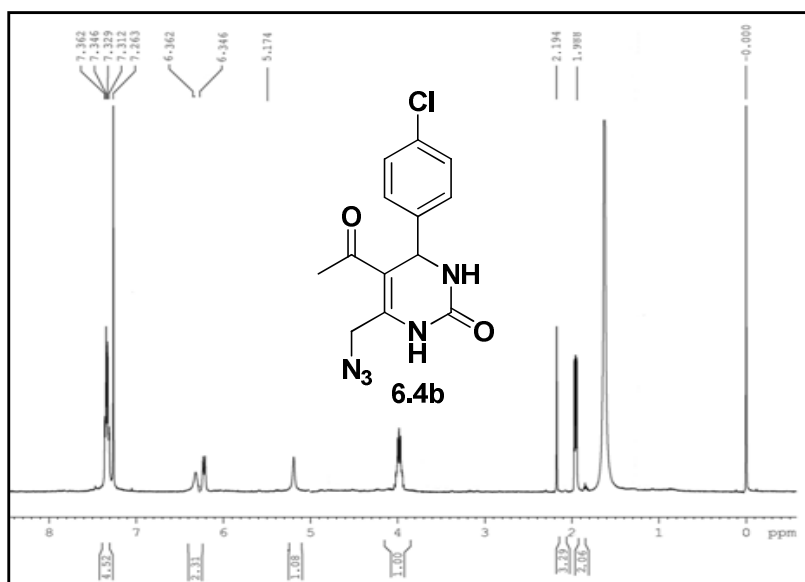
^1H NMR spectrum of the compound **6.4a**



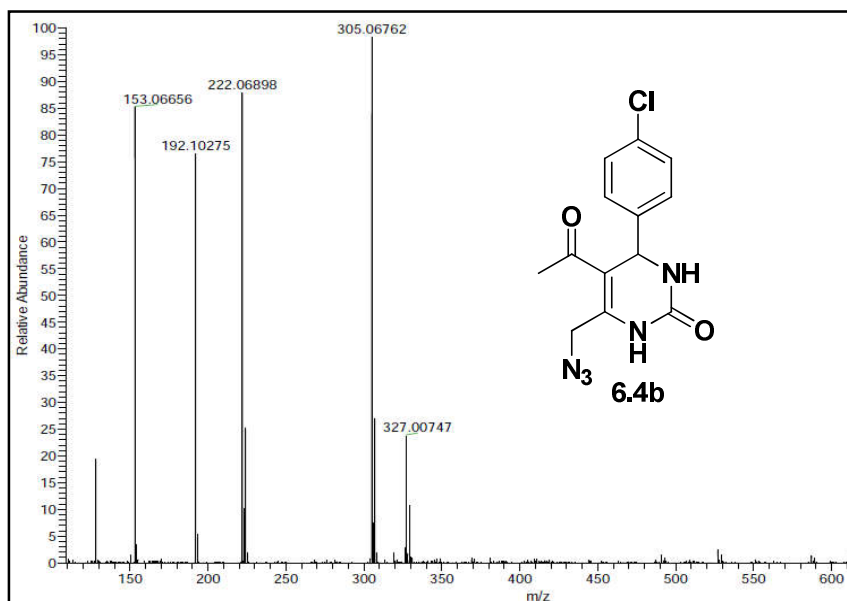
Mass spectrum of the compound **6.4a**



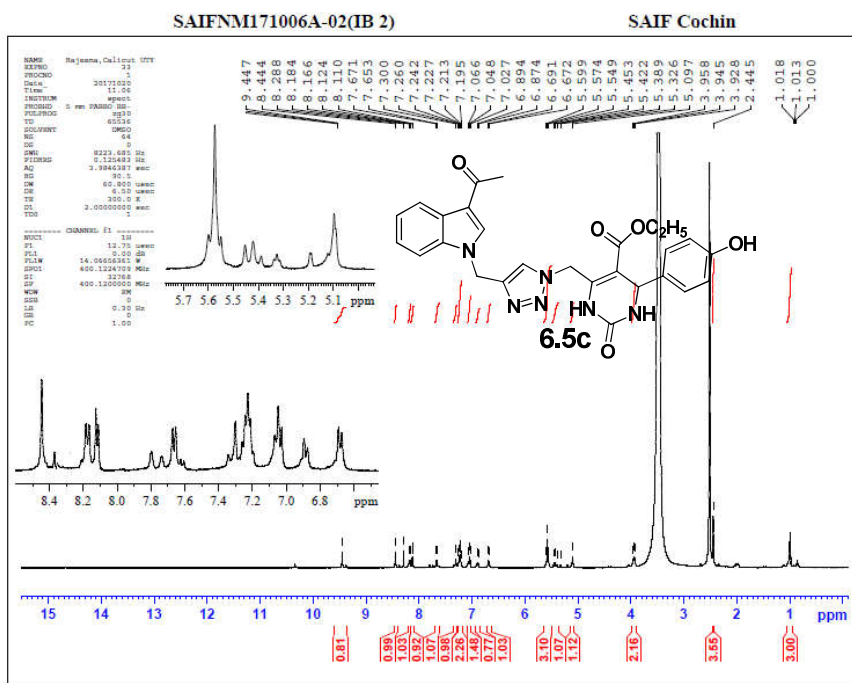
^1H NMR spectrum of the compound **6.4b**



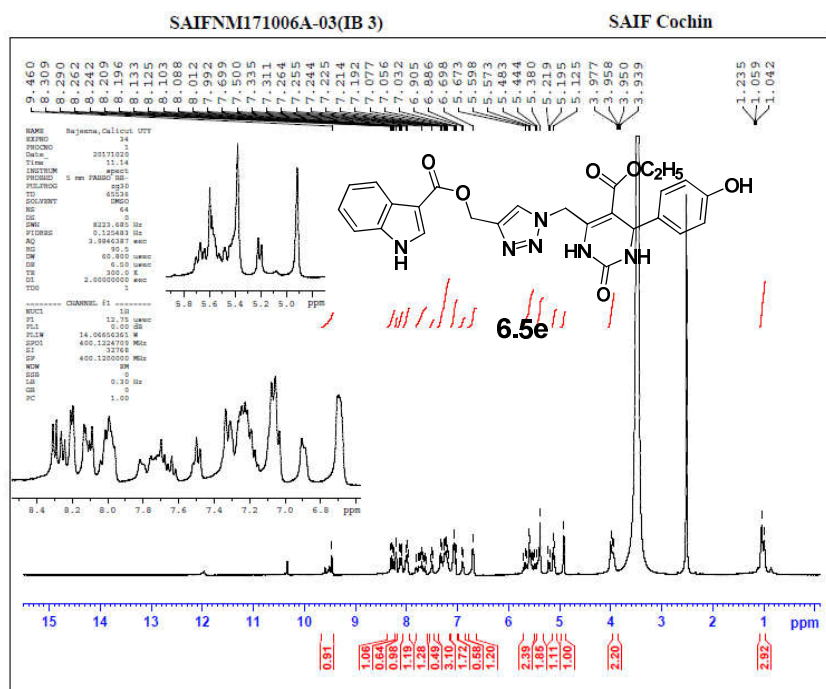
Mass spectrum of the compound **6.4b**



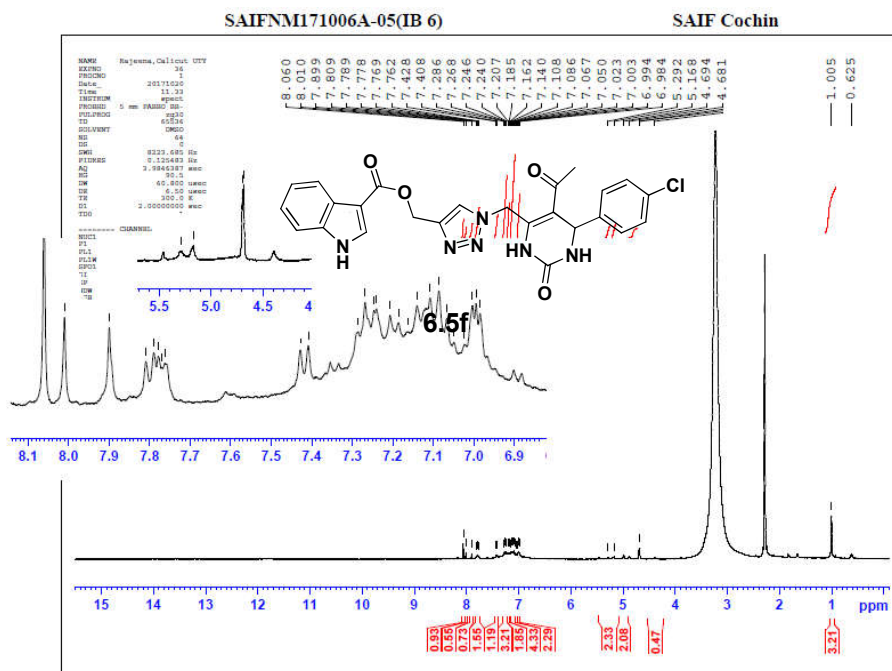
¹H NMR spectrum of the compound 6.5c



¹H NMR spectrum of the compound 6.5e



¹H NMR spectrum of the compound 6.5f



CHAPTER 7

Structure alteration of Indole-Triazole-Carboxamides via Macrocyclization: Synthesis and in vitro cytotoxicity evaluation of Indole-Triazole-Amide macrocycles

Contents

7.1. Introduction.....	238
7.2. Result and discussion.....	240
7.3. Structure elucidation by spectroscopy	255
7.4. Conclusion.....	258
References	265
Supplementary Material	267

7.1. Introduction

Macrocyclic compounds are abundant in nature. They have unique physicochemical and topological properties that allow them to exhibit unusual biological properties.¹ Generally, macrocyclic molecules contain at least one large ring composed of 8 or more atoms. They are more conformationally restricted (due to the presence of the decreased number of rotatable bonds) than their linear analogues and have the ability to exhibit high target binding affinity, selectivity, and improved oral bioavailability.² In addition, the more rigid structures can potentially exhibit excellent pharmacokinetic profile, such as increased metabolic stability and better membrane permeability.³ The impact of macrocyclic structures on modern medicinal chemistry is demonstrated by the diverse structures that exhibit significant biological properties. Natural products are one of the main source of macrocycles, such as erythromycin, rapamycin, vancomycin, cyclosporine, and epothilone.² The difficulties involved in extracting these natural products have compelled researchers to develop strategies such as diversity oriented synthesis (DOS) of macrocyclic compounds with known bioactive privileged scaffolds.⁴ The prevalence of macrocyclic structures in natural products and synthetic derivatives has paved way for the development of elegant and efficient syntheses, particularly when applied to the search for new drugs.

The indole heterocyclic system is found in several natural and synthetic macrocyclic structures and many of them have excellent biological functions. Nowadays, Indole-based macrocyclic systems attract increasing interest because of their conformational and self-

association properties, stacking interactions, spectroscopic features, cavity shape, and performance as ligands or ion-sensing scaffolds. The indole heterocyclic system is also frequently found in alkaloid compounds, especially in those compounds that regulate biological functions.⁵ These natural alkaloids were synthesized from the amino acid tryptophan and/or its decarboxylated derivative tryptamine.⁶ One of the indole based macrocycle is Ruboxistaurin which is a synthetic bis-1,3- disubstituted indole macrocyclic molecule, and it can selectively inhibit protein kinase C beta (PKC- β) and has been recommended for the treatment of diabetic retinopathy and macular edema.⁷ Some of the reported Indole based macrocycles are presented in Figure 7.1.

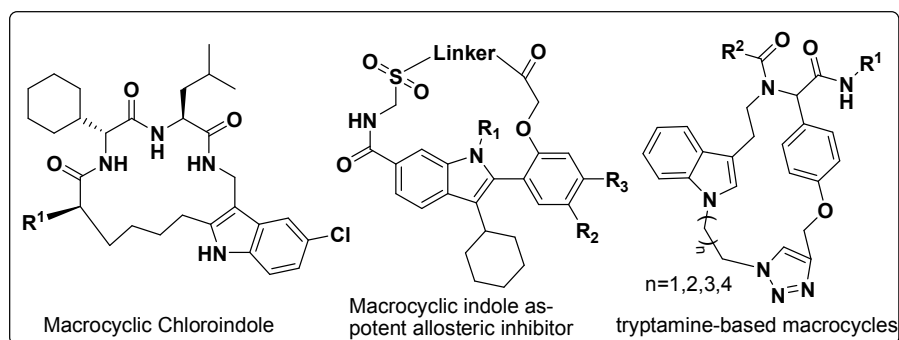


Fig. 7.1. Some of the Reported Indole based Macrocycles.

A variety of synthetic approaches for the synthesis of macrocycles has been reported. Of these, copper-catalyzed azide–alkyne cycloadditions embed the bioactive triazole moiety within the macrocyclic framework. These triazoles mimic the structure of peptide hormones in more stable analogs with higher pharmacokinetic properties, improved stability, bioavailability, and selectivity toward a

particular target. In recent years, both the alternate Mannich type reaction (4-CR)⁸ and the copper(I)-catalyzed azide alkyne cycloaddition (CuAAC)⁹ have emerged as efficient methodologies for the construction of a range of different macrocyclic structures for different purposes.

In continuation of the structure alteration studies on Indole-triazole-carboxamides (ITC) with other potential privileged scaffolds such as coumarin and pyrimidine discussed in chapters 2-6, we decided to move on the synthesis of the macrocyclic version of the ITC as shown in figure 7.2. This chapter reports the synthesis and *in vitro* biological property evaluation of 13 and 14 membered macrocyclic peptidomimetics comprising of indole, triazole and carboxamides as the macrocyclic ring system.

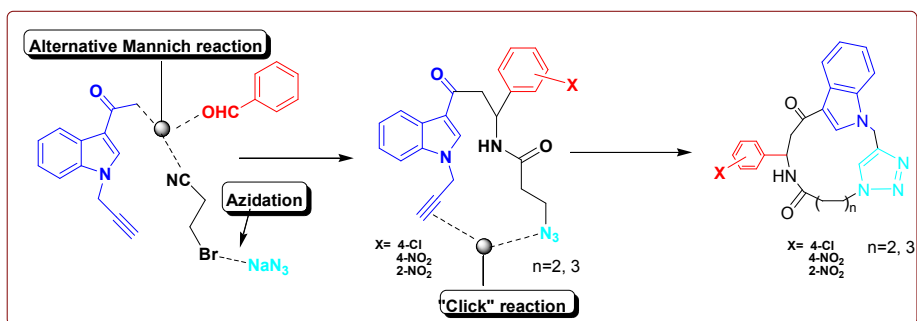


Fig. 7.2. Schematic representation of macrocycle formation.

7.2. Result and discussion

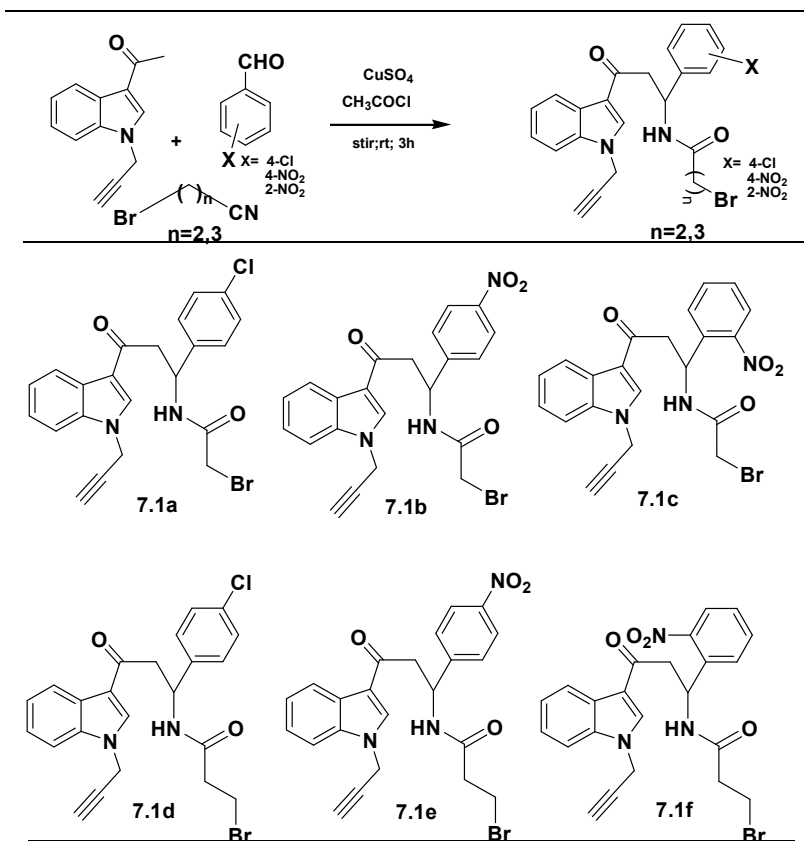
The overall synthetic procedure involves three steps. The first step is an alternate Mannich type reaction of an aromatic aldehyde and an N-propargylated 3-acetyl indole with a nitrile component in the

presence of an acid chloride to form an Indole acetamido alkyne **7.1a-7.1f**. In the second step, a base catalyzed azidation reaction replaces the bromine with an azide moiety to form azido alkyne **7.2a-7.2f**. The third step is the copper catalyzed intramolecular [3+2] azide-alkyne click cycloaddition to afford the respective macrocycles.

7.2.1. Synthesis of bromoamidoalkyne precursor 7.1a-7.1f

The studies were initiated with the synthesis of 13 and 14 membered macrocycles. For that, we initially synthesized N-alkylated 3-acetyl indole via the base catalyzed propargylation of 3-acetyl indole and which was then subjected to a three component Mannichtype reaction with 2-bromoacetonitrile (for 13 membered macrocycle) or 3-bromohexanenitrile (for 14 membered macrocycle) as the nitrile component as shown in table **7.1**. The four-component reaction was conducted as a solvent free reaction by stirring the alkyne functionalized 3-acetyl indole, substituted aldehyde (Chloro benzaldehyde, 3-Nitro benzaldehyde or 4- nitrobenzaldehyde) and bromoalkanenitrile with slight excess of acetyl chloride in the presence of catalytic amount of copper sulphate at room temperature for 3h. The subsequent aqueous workup followed purification, afforded the bromoamidoalkynes **7.1a-7.1f** in good to excellent yield. The general synthetic strategy and structure of the molecules are shown in table **7.1**.

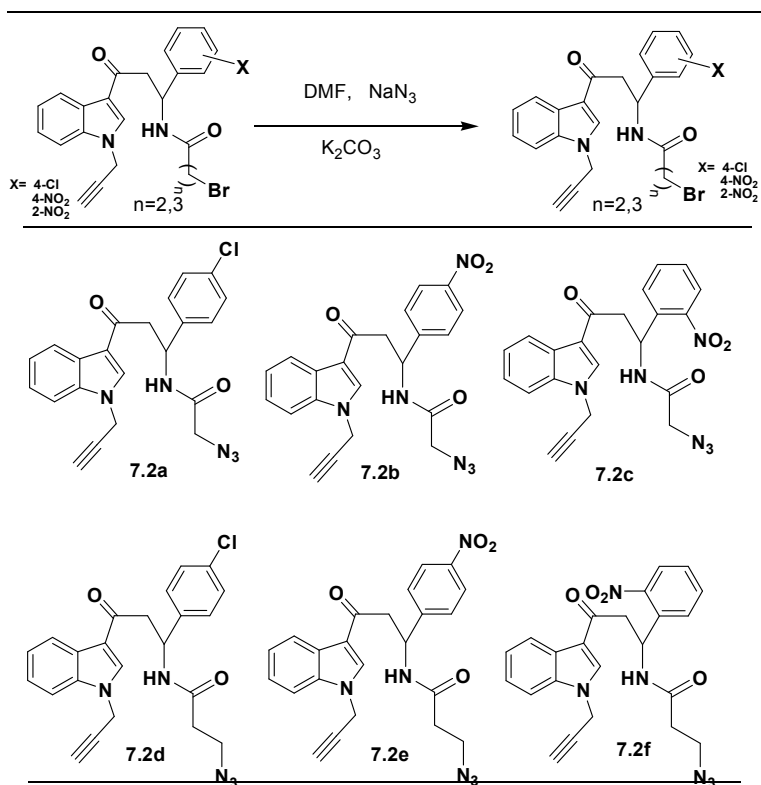
Table 7.1. List of bromoamidoalkynes 7.1a-7.1f



7.2.2. Synthesis of azidoamidoalkyne precursor 7.2a-7.2f

The next step was the replacement of bromine in 7.1a-f with an azide moiety to afford the azidoamidoalkynes 7.2a-f and this was accomplished by a base catalyzed reaction of 7.1a-f with sodium azide in DMF at room temperature. The aqueous work of this reaction mixture afforded the azidoamidoalkynes 7.2a-f in good to excellent yield. The general synthetic strategy and the structure of the synthesized molecules are shown in table 7.2.

Table 7.2. List of Azidoamidoalkynes 7.2a-7.2f

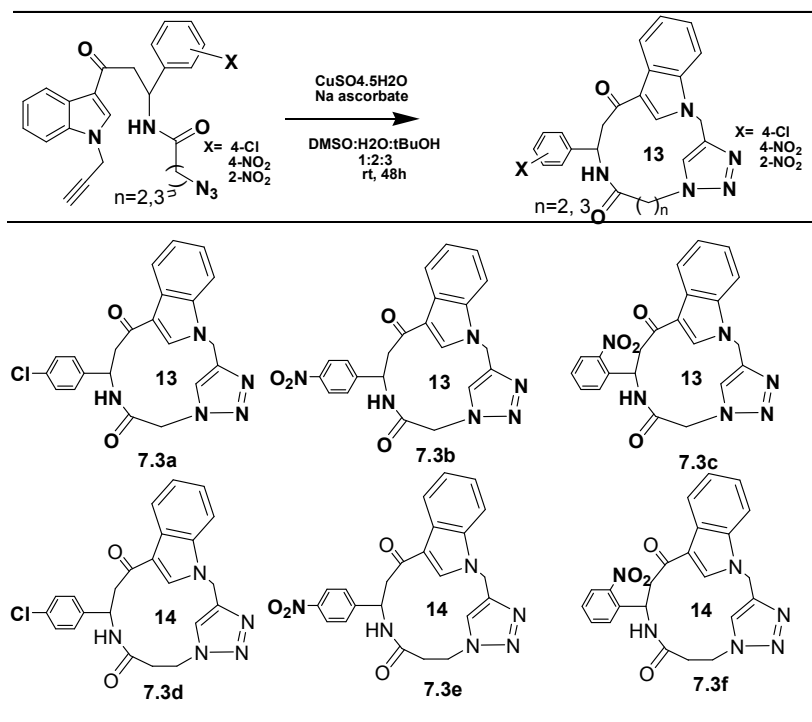


7.2.3. Synthesis of 13 or 14 membered indole based macrocycles

The third and the final step was the macrocyclization. For that, the azidoamidoalkynes **7.2a-7.2f** were subjected to ring closure by an intramolecular copper catalyzed [3+2] azide-alkyne click cycloaddition in a solvent mixture comprising of *t*-BuOH/ H_2O /DMSO in the ratio 4:2:1 to afford the 13 and 14 membered peptidomimetic macrocycles **7.3a-f** in good to excellent yield. The general synthetic strategy and the scope of these indole-based macrocycles are shown in table 7.3. Structurally, these macrocycles are decorated with an amide bond isosteres such as 1, 2, 3-triazole and an indole ring within the cycle.

These features are promising for exhibiting excellent binding affinity towards both core as well as peripheral sites of a broad spectrum of therapeutic targets. The list of macrocycles obtained are shown in table 7.3

Table 7.3. Final CuAAC synthetic step for the development of 13 and 14 membered macrocycles **7.3a–7.3f** and their diversity scope



7.2.4. Primary evaluation of drug-likeness by the calculation of drug property descriptors

The drug property descriptors of the macrocycles **7.3a–7.3f** were then calculated (table 7.4). The Log P and topological surface area (tPSA) values of the compounds were obtained from www.molinspiration.com. Generally, the macrocyclic drug-like molecules doesn't obey the

rule of five. But these synthesized macrocycles are well within the limit of rule of five. The molecular weight of **7.3a–7.3f** lies between 433 and 458 and their Log P values are between 1.11 and 2.12. It was reported that most of the anti-inflammatory, anti-depressant, anti-physicotic, hypnotic and anti-infective drugs usually have Log P values between 2 and 3 with molecular weight less than 400. This suggests that the macrocycles **7.3a–7.3f** are good lead scaffolds for further structure activity studies directed to the development of the drug classes mentioned above.

Table 7.4. Calculated drug-property descriptors of Indole based macrocycles **7.3a–7.3f**.

compound	MW	natoms	miLogP	TPSA	nON	nOH NH	nrotb
7.3a	433.90	31	1.85	81.82	7	1	1
7.3b	444.45	33	1.13	127.64	10	1	2
7.3c	444.45	33	1.11	127.64	10	1	2
7.3d	447.93	32	2.12	81.82	7	1	1
7.3e	458.48	34	1.40	127.64	10	1	2
7.3f	458.48	34	1.38	127.64	10	1	2

7.2.5. Molecular docking of 7.3a-7.3f for studying CDK-2 binding interaction.

We then performed the virtual screening of our molecules against CDK 2, based on molecular docking since CDK2 plays a key role in cell cycle regulation such as cell cycle propagation, neuronal function, differentiation and apoptosis. The protein target with PDB id

2VV9 was downloaded from <http://www.rcsb.org/pdb/home/home.do>. The active site of CDK2-2vv9 comprises of amino acid residues such as 31 Alanine, 144 Alanine, 145 Asparagine, 64 Valine, 83 Leucine, 134 Leucine, 101 Isoleucine, 85 Glutamine, 131 Glutamine, 89 Lysine and 80 Phenylalanine.¹⁰ CDK2 protein receptor was docked against the intermediate azide-alkyne complex and with macrocycles using the docking program AutoDockVina 1.1.2. The intermediate and the macrocycles sit in the active site of the receptor with a high binding affinity for the macrocycles compared to the intermediate. This clearly indicates the role of the triazoles unit in increasing the binding affinity towards CDK 2 (table 7.5 & 7.6). Similarly, we also noticed a decrease in binding affinity with an increase in ring size. The 13 membered macrocycles showed high binding affinity than the 14 membered macrocycles. All the compounds sit in the active site of the receptor and forms different modes of interactions (**fig 7.3**). While analyzing the structure-binding energy relationships, it was found that the nitro substituted macrocycles show high binding energy than chloro substituted macrocycles. Of the nitro substituted macrocycles, ortho nitro substituted macrocycles, showed high binding affinity than para-nitro substituted macrocycles. The compound **7.3d** forms one hydrogen bond via the triazole nitrogen of the ligand with ASP 86 of the protein and in the case of compound **7.3f**, there is one hydrogen bond through the amide NH of the ligand with the ASP 86 of the protein. Compound **7.3e** interacted with the receptor via pi cation interaction, in which the NH_3^+ of the protein acts as cation part and indole ring acts as the pi system.

Table 7.5. The Docking score for the compounds **7.2a-7.2f**.

compound	Docking score/ binding affinity (Kcal/mol)	Interaction with receptor
7.2a	-9.4	LEU 134,LEU 83, PHE 82, ALA 144, ALA 31, ASN 145, GLN 131(HB), ILE 10, VAL 18,ASP 86, LYS 33
7.2b	-9.5	ALA 31, PHE 82, LEU 83,LYS 129, LEU 134, LYS 33, ASP 145(HB), GLN 131(HB) ALA 144, VAL 18, ILE 10, ASN 145
7.2c	-9.5	LYS 83, PHE 80, ASP 145, ILE 10,ALA 144, VAL 64, LEU 134, ASP 86
7.2d	-7.4	LYS 83, PHE 80, ASP 145, ILE 10, ALA 144, VAL 64, LEU 134, ASP 86
7.2e	-7.6	LYS 89(HB), ILE 10, ASP86, GLN 131,LEU 134, ALA 144, ASP 145, PHE 80
7.2f	-8.8	LYS 89, LYS 129, ILE 10, GLY 13, LEU 134, ALA 144, ALA 31, PHE 80

Table 7. 6. Docking score for the compound **7.3a-7.3f**

compound	Docking score/ binding affinity (Kcal/mol)	Interaction with receptor
7.3a	-9.5	GLU 12, GLY 11, VAL 18, ILE10,ASP 145,GLN 131 ASP 145, ASNI32,LYS 89,ASP 86,ALA 31
7.3b	-9.7	GLU 12, GLN 131, GLY 11, ASP 145, VAL 18,ILE 10 ASN 132, ALA 31, LEU 134, ASP 86, LYS 89
7.3c	-10.1	GLU 12, GLU 13, GLY 11, ILE 10, GLN 131,VAL 18, LYS 33, ASP 145, LEU 83, LEU 134
7.3d	-9.0	ILE 10, LEU 134, ASP 86(HB), LYS 129, LYS 89, GLN 131,
7.3e	-9.1	ILE 10, LEU 134, GLN 131, ASP 86, LYS 89
7.3f	-9.2	LEU 134, ASP 86 (HB), LYS 89, ILE 10, GLY 11, GLN 131, GLU 12

The docking modes of the macrocycles are presented in figure 7.3.

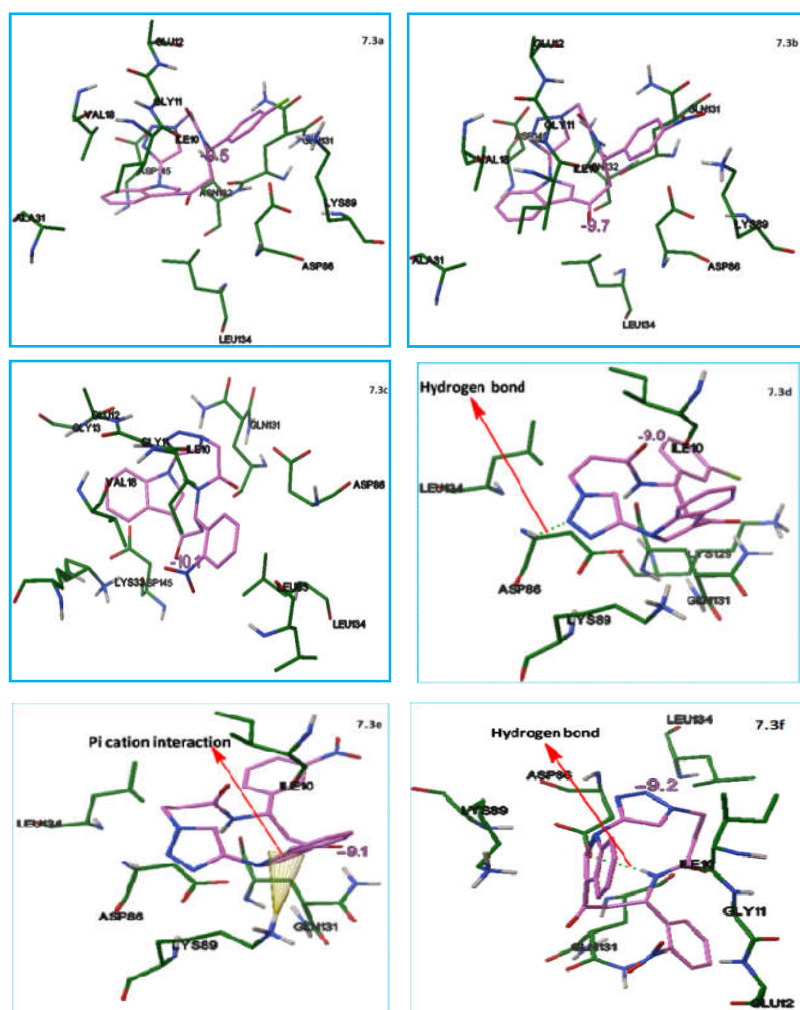


Fig. 7.3. The binding mode of compounds 7.3a-7.3f respectively in the active site of CDK2-2vv9. Hydrogen bonds are represented in dotted lines.

7.2.6. *In vitro* biological assay

7.2.6.1. Trypan blue exclusion method

Selected macrocycles were studied for short term *in vitro* cytotoxicity using Dalton's lymphoma ascites cells (DLA) or Ehrlich Ascites Carcinoma (EAC) cells. The tumour cells aspirated from the peritoneal cavity of tumour bearing mice were washed thrice with PBS or normal saline. Cell viability was determined by trypan blue exclusion method. Viable cell suspension (1×10^6 cells in 0.1 ml) was added to tubes containing various concentrations of the test compounds and the volume was made up to 1 ml using phosphate buffered saline (PBS). Control tube contained only cell suspension. These assay mixture were incubated for 3 hour at 37°C . Further cell suspension was mixed with 0.1 ml of 1% trypan blue and kept for 2-3 minutes and loaded on a haemocytometer. The dead cells took up the blue colour of trypan blue while the live cells did not take up the dye. The number of stained and unstained cells was counted separately for determining the % cytotoxicity.¹¹

$$\% \text{ cytotoxicity} = \frac{\text{No. of dead cells}}{\text{No. of live cell} + \text{No. of dead cell}} \times 100$$

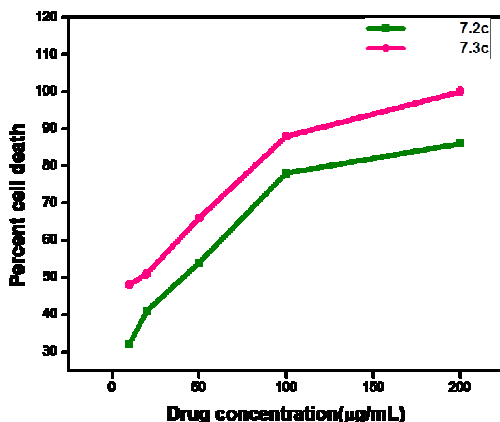


Fig.7.4. Cytotoxic effects of 7.2c and 7.3c on EAC cells.

Table.7.7. IC₅₀ Value of 7.2c and 7.3c from Trypan blue exclusion method

Compound	IC ₅₀
7.2c	38 µg/mL
7.3c	11 µg/mL

From the plot (**fig.7.4**) of percentage cell death against drug concentration, we determined the IC₅₀ values (concentration that inhibited cell growth in 50% compared to untreated controls), and the IC₅₀ values are given in table.7.7. Of the two tested compounds, **7.2c** exhibit IC₅₀ value of 38 µg/mL, whereas **7.3c** showed 11 µg/mL. This is in clear agreement with the binding energy values obtained from docking studies described in section 7.2.5. There also compound **7.3c** have highest binding energy.

7.2.6.2. In vitro cytotoxicity evaluation against human breast cancer cell line MCF-7: MTT assay

(A): Cell culture and maintenance

Human breast cancer MCF-7 (purchased from National Centre for Cell Science, Pune, India) cells were maintained in RPMI medium 1640 supplemented with 10% fetal bovine serum as well as 100 µg/mL streptomycin, 100 U/mL penicillin, 2 mM L-glutamine and Earle's BSS adjusted to contain 1.5 g/l Na bicarbonate, 0.1 mM non-essential amino acids, and 1.0 mM of Na pyruate in a humidified atmosphere containing 5% CO₂ at 37 °C.

(B): In vitro cytotoxicity of synthesized 7.3c

Cell viability was determined by MTT assay. MCF-7 cells were seeded in 96-well plates at a concentration of 1.0×10^4 cells/well and incubated overnight at 37°C in a 5% CO₂ humidified environment. Then the cells were treated with different concentrations of the sample **7.3c** like 10, 20, 30, 40, 50, 60, 70, 80, 90, and 100 µM/mL (dissolved with RPMI medium 1640), respectively. The controls were cultivated under the same conditions without addition of **7.3c**. The treated cells were incubated for 48 h for cytotoxicity analysis. The cells were then subjected for MTT assay. The stock concentration (5 mg/mL) of MTT-(3-(4,5-dimethylthiazol-2-yl)-2,5-diphenyltetrazolium bromide, a yellow tetrazole) was prepared and 100 µL of MTT was added in each wells and incubated for 4 h. Purple color formazan crystals were observed and these crystals were dissolved with 100 µL of dimethyl sulphoxide (DMSO), and read at 620 nm in a multi well ELISA plate

reader (Thermo, Multiskan). The dose dependent cytotoxicity was observed in the case of indole-triazole peptidomimetics **7.3c** treated MCF-7 cells. Fifty percentage of cell death, which determines the inhibitory concentration (IC₅₀) value of **7.3c** against MCF-7 cells holds at 12 μ M in 48h (Fig.7.5 which indicates that these molecules exhibit increased bioavailability and have tremendous anticancer potential.

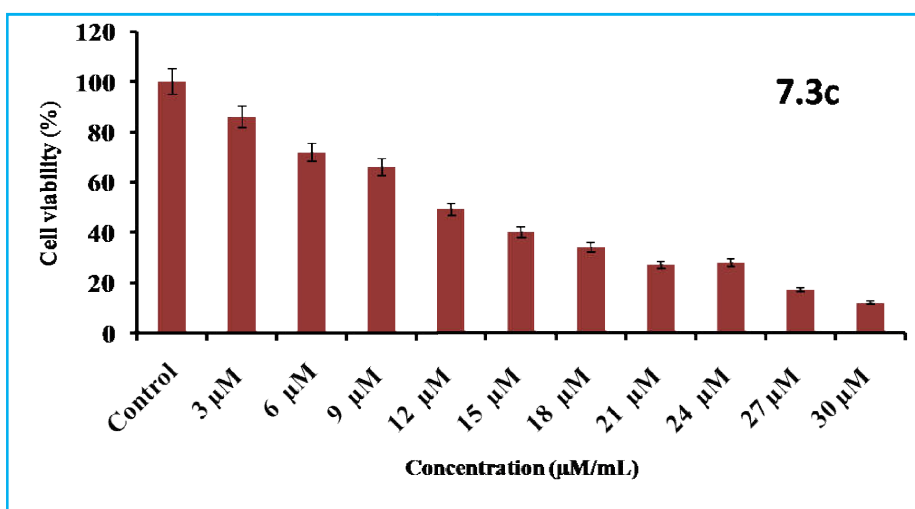


Fig. 7. 5. MTT assay results confirming the in vitro cytotoxicity effect of **7.3c** against the MCF-7 cells. The detected IC₅₀ concentration was 12 μ M/mL.

(C). Cell morphology study using DAPI (4, 6-diamidino-2-phenylindole, dihydrochloride) staining

MCF-7 cells were treated with **7.3c** at its IC₅₀ concentration (12 μ M) for 48 h, and then were fixed with methanol: acetic acid (3:1, v/v) prior to washing with PBS. The washed cells were then stained with 1 mg/mL DAPI (4, 6-diamidino-2-phenylindole dihydrochloride) for 20 min in the dark atmosphere. The stained images were recorded

with fluorescent microscope with appropriate excitation filter. The bright field and fluorescence microscopic images are shown in Fig.7.6. As shown in Fig.7.6, the strong bluish fluorescence and cellular uptake were observed in the imaging studies with **7.3c** which reveals that these molecules have high potency against breast cancer cell lines (MCF-7).

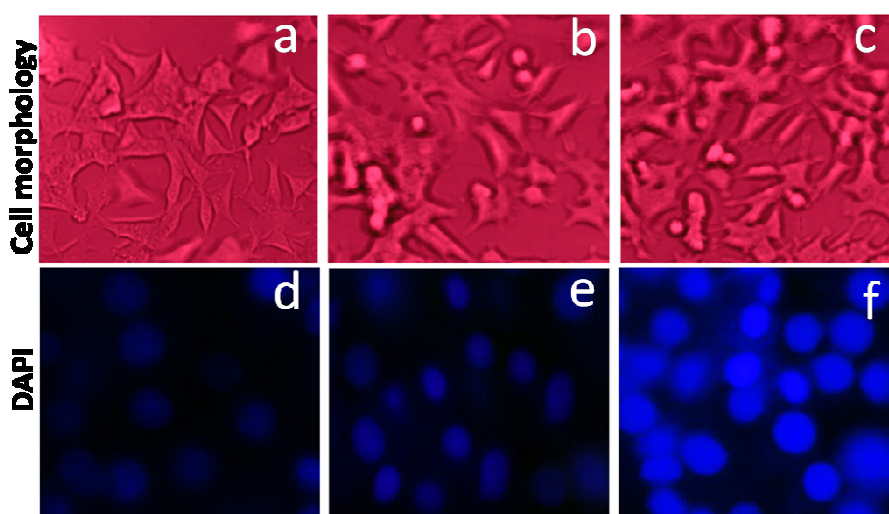


Fig. 7.6. Bright field inverted light microscopy images (a, b, c) and the DAPI nuclear staining (d, e, f) of control cells and **7.3c** treated cells. The DAPI images exhibit condensed form of nuclear materials in apoptotic cells

7.2.6.3. CDK 2 selectivity of the macrocycles via Western blot Analysis

Western blotting was performed to detect the proteins of CDK2 in MCF-7 with compound **7.3c** using beta-actin as the standard. The MCF-7 cells (1×10^6) were seeded onto 100-mm culture dishes in the presence or absence of **7.3c** and were treated for 48hrs. Cells were then washed twice with ice-cold PBS and

incubated in lysis buffer. The lysates were centrifuged at $10,000 \times g$ for 5 min at $4^\circ C$, and were used as the cell protein extracts. Each of the extracts was applied to 12% SDS polyacrylamide gel electrophoresis after which the proteins were transferred onto a nitrocellulose membrane, and then blocked for 1 h using 10% skim milk in water. After washing in a PBS containing 0.1% Tween 20 for 3 times, the primary antibodies were added at a v/v ratio of 1:1000. After overnight incubation at $4^\circ C$, the primary antibodies were washed away and the secondary antibodies were added for 1h incubation at room temperature. Finally, the enhanced chemiluminescence detection reagents were used to develop the signal of the membrane.

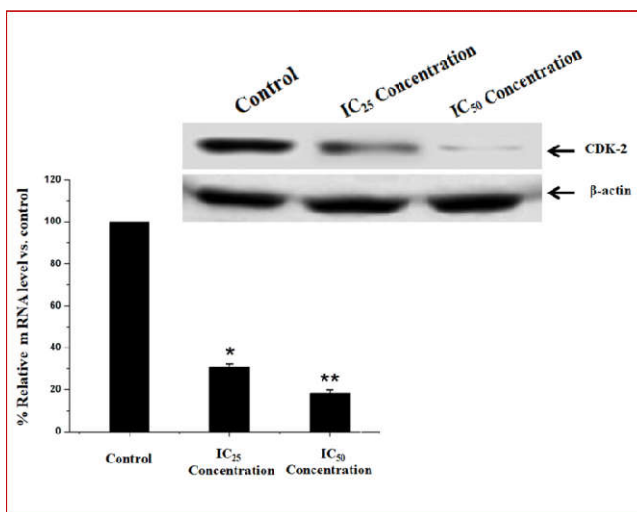


Fig.7.7. Western blot Analysis of 7.3c from MCF-7 cell line

As shown in figure 7.7. Our findings demonstrate that the protein level of CDK2 are significantly down-regulated in the treated cells when compared to control.

7.3. Structure elucidation by spectroscopy

Structure identification of macrocycle 7.3a.

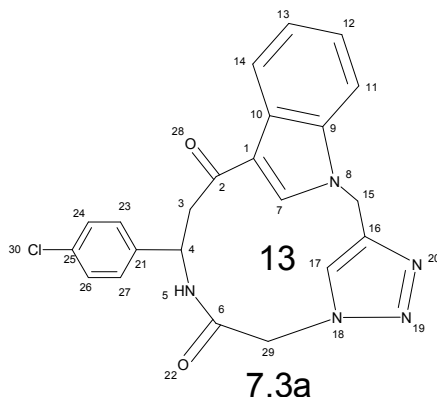


Fig.7.8. The structure of **7.3a**

For a general discussion on the structure identification of the macrocyclic compounds **7.3a-d**, **7.3a** is taken as the representative and the molecule is numbered as shown in figure **7.8**. The FT-IR spectrum of the compound **7.3a** showed major absorptions at 3435, 1660, 1629, 1547 cm^{-1} (fig. **7.9**). The band at 3435 cm^{-1} is due to the N-H stretching vibration of the acetamido group and that at 1629 cm^{-1} is due to amide C=O stretching vibration. The amide II band which arises from the interaction between the N-H bending and the C-N stretching of the C-N-H group is obtained at 1547 cm^{-1} and the ketone C=O stretching vibration is obtained as a strong band at 1660 cm^{-1} . The disappearance of the peak of N_3 stretching vibration at 2091 cm^{-1} gives the initial confirmation for the triazole formation.

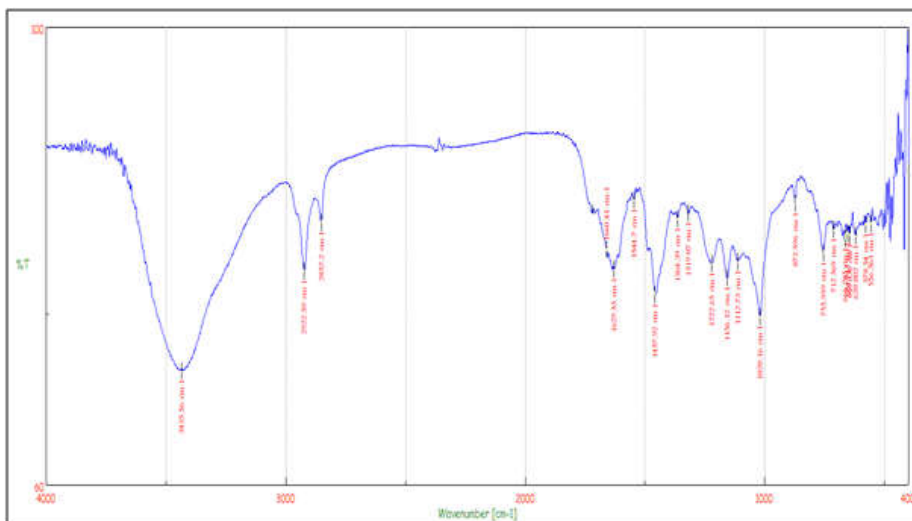


Fig.7.9. FTIR spectrum of compound **7.3a**

These results are further validated by NMR analysis. In the ^1H NMR spectrum, the singlet observed at δ 9.92 corresponds to aromatic proton at position 7. The singlet at δ 8.09 represent the NH proton. Peaks from δ 6.98 to 7.16 correspond to the 8 aromatic protons. Singlet obtained at δ 7.39 corresponds to the triazole proton. The CH_2 proton at position 15 appears as a singlet at δ 5.47 and CH proton at position 4 appears as a multiplet at δ 5.38-5.56. The CH_2 proton at position 29 appears as a singlet at δ 4.81. The doublet of doublet at δ 4.77-4.56 and at δ 3.64-3.59 corresponds to CH_2 proton at position 3 (Fig.7. 10).

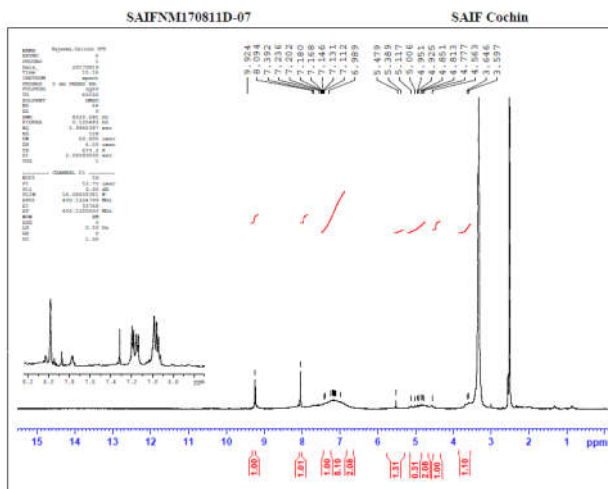


Fig. 7. 10. ^1H NMR spectrum of the compound **7.3a**

The structure was further confirmed by the mass spectral analysis. HRMS m/z ; 420.17089 $[\text{M}+1]^+$ (Figure 7.11).

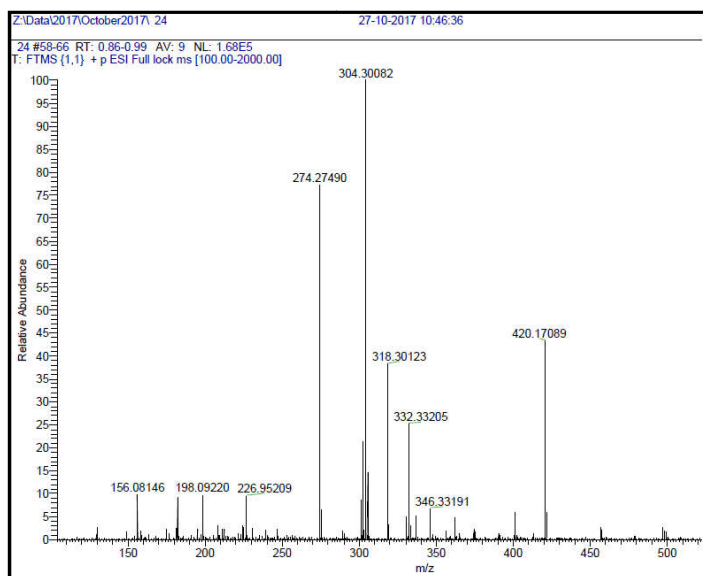


Fig. 7.11. Mass spectrum of the compound **7.3a**

7.4. Conclusion

This chapter has demonstrated the development of a convenient methodology for the synthesis of a series of medium ring size (13 or 14) macrocycles using MCR and Click strategy with substantial molecular diversity and structural diversity. The results are also showing that, we are in the right direction in our structure alteration studies and the evolutionary IC 50 values obtained from the linear indole-triazole-carboxamides (ITC) to the macrocyclic ITCs showed a gradual enhancement in the anticancer properties. As expected, the macrocycles showed substantial potential as anti-cancer agents and it is worth to undertake further studies on their chemistry (for example optimization of ring size) and chemical biology (studies with a range of enzymes). The cytotoxicity study with macrocycles has also shed light on the influence of the triazole ring in the biological properties of these molecules.

7.5. Experimental section

General

All reactions were carried out with oven-dried glassware. The starting materials were purchased from Aldrich and Merck. Alkyne-functionalised azides were synthesized based on literature procedure. IR spectra were recorded on a JASCO-FT/IR-4100 Fourier transform infrared spectrometer by making KBr pellets of the samples. ^1H and ^{13}C NMR spectra were determined in DMSO using a Bruker amx 500 MHz spectrometer. High resolution mass spectra were measured with a Thermo Exactive Orbitrap with MeOH as solvent. The chemical shifts

(δ) values are given relative to tetramethylsilane (TMS) and the coupling constants (J) are reported in hertz (Hz). The absorption spectra of the compounds were recorded on a JASCO V-550 UV/Vis Spectrophotometer and fluorescence measurements were carried out with a Perkin Elmer LS55 Fluorescence Spectrometer.

General experimental procedure for the synthesis of 7.1a:

A mixture of p-chlorobenzaldehyde (140.567 mg, 1 mmol), N-propargylated 3-acetyl indole (197.2325 mg, 1mmol), and 3-bromoacetonitrile (119.948 mg, 1 mmol) in acetonitrile (8 ml) were stirred in the presence of catalytic amount of CuSO₄ at room temperature for 4 h. After completion of the reaction as indicated by TLC, the reaction mixture was poured into ice cold water and extracted with CH₂Cl₂ (15 ml). Evaporation of the solvent followed by purification on silica gel (100–200 mesh), ethyl acetate/hexane (3:1) afforded 3-bromo-N-(1-(4-chlorophenyl)-3-oxo-3-(1-(prop-2-yn-1-yl)-1H-indol-3-yl)propyl)acetamide 1a.

2-bromo-N-(1-(4-chlorophenyl)-3-oxo-3-(1-(prop-2-yn-1-yl)-1H-indol-3-yl)propyl)acetamide 7.1a: FT-IR (KBr) ν_{\max} 3414, 3287, 3067, 2927, 2861, 2120, 1725, 1679, 1607, 1560, 1490, 1455, 1420, 1383, 1366, 1292, 1224, 1178, 1109, 1051, 1024, 977, 923, 885, 861, 838, 670, 641, 588, 547cm⁻¹;

2-bromo-N-(1-(4-nitrophenyl)-3-oxo-3-(1-(prop-2-yn-1-yl)-1H-indol-3-yl)propyl) acetamide 7.1b: FT-IR(KBr) ν_{\max} 3437, 3287, 2924, 2854, 2120, 1671, 1607, 1559, 1509, 1490, 1455, 1394, 1225,

1178, 1111, 1075, 1022, 923, 831, 808, 757, 673, 642, 602, 555, 537cm⁻¹.

2-bromo-N-(1-(2-nitrophenyl)-3-oxo-3-(1-(prop-2-yn-1-yl)-1H-indol-3-yl)propyl)acetamide 7.1c: FT-IR(KBr) ν_{\max} 3381, 3285, 3067, 2934, 2863, 2120, 1664, 1607, 1559, 1511, 1491, 1455, 1424,1367,1263, 1221, 1175, 1142, 1109, 1083, 1021, 923, 860, 808, 676, 610, 558, 494cm⁻¹.

3-bromo-N-(1-(4-chlorophenyl)-3-oxo-3-(1-(prop-2-yn-1-yl)-1H-indol-3-yl)propyl)propanamide 7.1d: FT-IR (KBr) ν_{\max} 3425, 3284, 3067, 2956, 2925, 2870, 2121, 1685, 1607, 1560, 1489, 1455, 1365, 1292, 1223, 1178, 1109, 1051, 1024, 977, 922, 885, 861, 838, 756, 670, 641, 588, 547cm⁻¹.

3-bromo-N-(1-(4-nitrophenyl)-3-oxo-3-(1-(prop-2-yn-1-yl)-1H-indol-3-yl)propyl)propanamide 7.1e: FT-IR (KBr) ν_{\max} 3385, 3286, 3062, 2923, 2854, 2120, 1605,1608, 1560, 1509, 1489, 1455, 1365, 1304, 1223, 1172, 1109, 1083, 1023, 923, 873, 831, 759, 671, 641,600, 539cm⁻¹.

3-bromo-N-(1-(3-nitrophenyl)-3-oxo-3-(1-(prop-2-yn-1-yl)-1H-indol-3-yl)propyl)propanamide 7.1f: FT-IR (KBr) ν_{\max} 3424, 3288, 3077, 2927, 2854, 2120, 1665, 1608, 1560, 1509, 1489, 1455, 1365, 1305, 1222, 1172, 1109, 1083, 1023, 923, 873, 831, 759, 671, 641, 600,539cm⁻¹.

General procedure for the synthesis of 7.2a: The bromide **7.1a** (457mg, 1 mmol), K₂CO₃ (414 mg, 3 mmol) and NaN₃ (65 mg, 1

mmol) were dissolved in dimethylformamide and stirred for 6–8 h. After completion, the reaction mixture was poured into ice cold water and the precipitate was filtered, dried under vacuum to afford the azide **7.2a**.

2-azido-N-(1-(4-chlorophenyl)-3-oxo-3-(1-(prop-2-yn-1-yl)-1H-indol-3-yl)propyl)acetamide 7.2a: FT-IR (KBr) ν_{\max} 3425, 3289, 2923, 2857, 2097, 1659, 1606, 1556, 1509, 1455, 1402, 1219, 1178, 1118, 1024, 957, 926, 873, 830, 758, 672, 645, 597, 542 cm^{-1} .

2-azido-N-(1-(4-nitrophenyl)-3-oxo-3-(1-(prop-2-yn-1-yl)-1H-indol-3-yl)propyl)acetamide 7.2b: FT-IR (KBr) ν_{\max} 3439, 2924, 2856, 2098, 1708, 1648, 1608, 1489, 1455, 1419, 1221, 1155, 1022, 874, 856, 757, 697, 638, 598, 555, 504 cm^{-1} .

2-azido-N-(1-(2-nitrophenyl)-3-oxo-3-(1-(prop-2-yn-1-yl)-1H-indol-3-yl)propyl)acetamide 7.2c: FT-IR (KBr) ν_{\max} 3404, 3287, 2925, 2853, 2097, 1652, 1608, 1497, 1456, 1263, 1220, 1172, 1140, 1022, 924, 871, 857, 809, 757, 710, 695, 672, 643, 588, 548 cm^{-1} .

3-azido-N-(1-(4-chlorophenyl)-3-oxo-3-(1-(prop-2-yn-1-yl)-1H-indol-3-yl)propyl)propanamide 7.2d: FT-IR(KBr) ν_{\max} :3423, 3293, 2922, 2852, 2117, 1654, 1607, 1560, 1489, 1455, 1421, 1383, 1222, 1111, 1021, 875, 754, 669, 638, 546 cm^{-1} .

3-azido-N-(1-(4-nitrophenyl)-3-oxo-3-(1-(prop-2-yn-1-yl)-1H-indol-3-yl)propyl)propanamide 7.2e :FT-IR (KBr) ν_{\max} 3405, 3288, 2922, 2102, 2036, 1651, 1608, 1509, 1455, 1425, 1264, 1223, 1178, 1112, 1025, 873, 855, 831, 758, 694 cm^{-1} .

3-azido-N-(1-(3-nitrophenyl)-3-oxo-3-(1-(prop-2-yn-1-yl)-1H-indol-3-yl)propyl)propanamide 7.2f: FT-IR (KBr) ν_{\max} 3423, 3287, 2924, 2854, 2615, 2116, 2036, 1718, 1666, 1507, 1455, 1411, 1384, 1334, 1255, 1156, 1021, 926, 892, 873, 808, 757, 639, 555, 504 cm^{-1} .

General procedure for the Cu (I) 1, 3-dipolar cycloaddition reaction for the formation of macrocycle 7.3a: 2-azido-N-(1-(4-chlorophenyl)-3-oxo-3-(1-(prop-2-yn-1-yl)-1H-indol-3-yl)propyl)acetamide **7.2a** (209 mg, 0.5 mmol) was dissolved in minimum amount of DMSO. To this, 2 ml of *t*-BuOH, 1 ml of water, CuSO₄·5H₂O (200 mg) and sodium ascorbate (150 mg) are added and stirred in room temperature for 12 h. and then poured in to cold water. The precipitated click product was filtered, washed with water and dried under vacuum to afford **7.3a** in pure form.

Macrocycle 7.3a: FT-IR (KBr) ν_{\max} 3435, 2922, 2852, 1660, 1629, 1544, 1457, 1364, 1319, 1222, 1156, 1112, 1020, 873, 755, 712, 666, 620, 578, 556 cm^{-1} ; ¹H NMR (DMSO-*d*₆, 400 MHz) δ_{H} (ppm):3.64-3.59 (1H,d); 4.77-4.56(1H, d);4.813(S, 2H), 5.38-4.85(m, 1H), 5.47(S, 2H), 7.14-6.98(m, 4H), 7.23-7.16(m, 4H), 7.39(S, 1H), 8.09(S, 1H), 9.92(S, 1H);HRMS (EI) *m/z* calcd for C₂₂H₁₈ClN₅O₂ [M+H]⁺: 420.1149, found : [M+H]⁺ 420.17089.

Macrocycle 7.3b: FT-IR (KBr) ν_{\max} 3443, 2924, 1658, 1608, 1509, 1455, 1364, 1319, 1264, 1213, 1153, 1079, 1022, 951, 862, 822, 762, 740, 709, 665, 637 cm^{-1} ; ¹H NMR (DMSO-*d*₆, 400 MHz) δ_{H} (ppm):2.12-2.11(d, 1H),2.27-2.26(d, 1H), 3.52(S, 2H), 4.99-4.84(m, 1H), 5.00(S, 2H), 7.02-7.02(d, 2H), 7.14-7.10(m, 4H), 7.20(S, 1H),

8.29-8.26(d, 2H), 8.30(S, 1H), 9.20(S, 1H); HRMS (EI) m/z calcd for $C_{22}H_{18}N_6O_4$ $[M+H]^+$: 431.1390, found : $[M+H]^+$: 431.14826.

Macrocycle 7.3c: FT-IR (KBr) ν_{max} 3415, 2921, 2852, 1664, 1634, 1607, 1560, 1456, 1380, 1219, 1178, 1110, 1080, 1021, 950, 872, 831, 758, 670, 644, 620, 578, 533cm^{-1} ; ^1H NMR (DMSO- d_6 , 400 MHz) δ_{H} (ppm):2.56-2.52(d, 1H), 2.63-2.593(d, 1H), 4.55(S, 2H), 5.39-4.95(m, 1H), 5.47(S, 2H), 7.80-7.42(m, 6H), 7.89(S, 1H), 8.26-8.24(d, 2H), 8.29(S, 1H), 9.12(S, 1H); HRMS (EI) m/z calcd for $C_{22}H_{18}N_6O_4$ $[M+Na]^+$: 453.1390, found : $[M+Na]^+$: 453.2234.

Macrocycle 7.3d: FT-IR (KBr) ν_{max} 3435, 2922, 2852, 1653, 1629, 1544, 1364, 1319, 1222, 1156, 1112, 1020, 873, 755, 712, 666, 620, 578, 556cm^{-1} ; ^1H NMR (DMSO- d_6 , 400 MHz) δ_{H} (ppm):2.27-2.08(t, 2H), 3.56-3.52(d, 1H), 3.63-3.59(d, 1H), 4.69-4.66(t, 2H), 5.49-5.41(m, 1H), 5.63(S, 2H), 7.26(S,1H), 7.65-7.27(m, 7H), 8.21(S, 1H), 8.38-8.35(d, 1H), 9.32(S, 1H);HRMS (EI) m/z calcd for $C_{23}H_{20}ClN_5O_2$ $[M+Na]^+$: 456.1306, found : $[M+Na]^+$: 456.33749

Macrocycle 7.3e: FT-IR (KBr) ν_{max} 3423, 2923, 2852,1655, 1608, 1498, 1453, 1408, 1383, 1365, 1254, 1211, 1154, 1082, 1023,860,757,631 cm^{-1} ; ^1H NMR (DMSO- d_6 , 400 MHz) δ_{H} (ppm):2.08-2.04(d, 1H), 2.27-2.25(d, 1H), 3.00-3.02(t, 2H), 4.69-4.63(t, 2H), 5.21-5.12(m, 1H), 5.44(S, 2H), 7.16(S, 1H), 7.33-7.26(m, 4H),7.63-7.61(d, 2H), 8.22-8.20(d, 2H), 8.38(S, 1H), 9.10(S, 1H);HRMS (EI) m/z calcd for $C_{23}H_{20}N_6O_4$ $[M+Na]^+$: 467.1546, found : $[M+Na]^+$: 467.1729.

Macrocycle 7.3f: FT-IR (KBr) ν_{\max} 3426, 2923, 2854, 1712, 1671, 1644, 1556, 1531, 1504, 1487, 1455, 1434, 1402, 1384, 1352, 1322, 1294, 1223, 1192, 1109, 1082, 1051, 1020, 939, 876, 855, 754, 680, 656 cm^{-1} ; ^1H NMR (DMSO- d_6 , 400 MHz) δ_{H} (ppm): 2.08-2.06(d, 1H), 2.12-2.11(d, 1H), 2.28-2.26(t, 2H), 3.64-3.52(t, 2H), 4.81-4.75(m, 1H), 5.20(s, 2H), 6.94-6.92(d, 3H), 7.18-7.16(d, 3H), 7.74(s, 1H), 8.22-8.20(d, 2H), 8.38(s, 1H), 9.12(s, 1H); HRMS (EI) m/z calcd for $\text{C}_{23}\text{H}_{20}\text{N}_6\text{O}_4$ $[\text{M}+\text{Na}]^+$: 467.1546, found : $[\text{M}+\text{Na}]^+$: 467.1678.

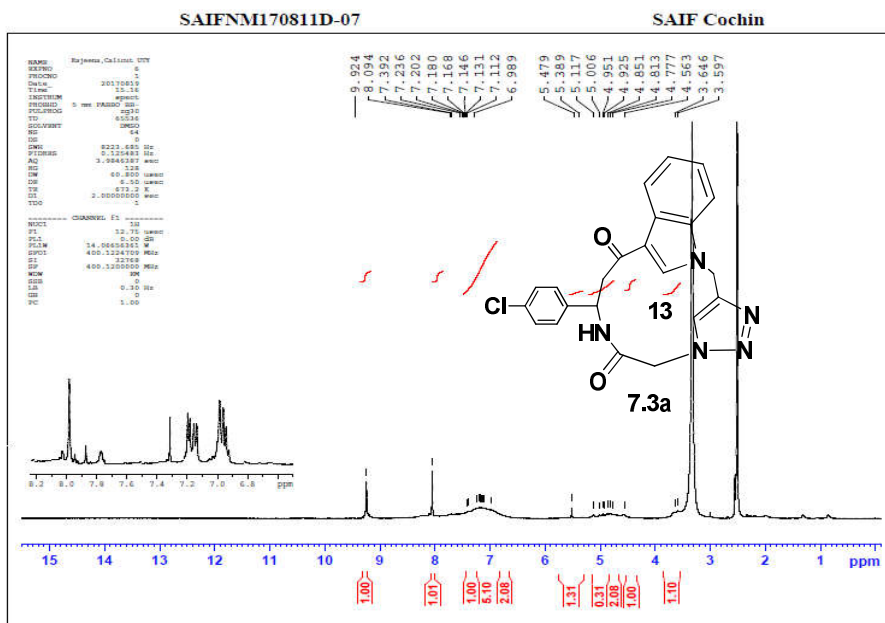
References

1. (a) E. Marsault and M. L. Peterson, *J. Med. Chem.* 2011, **54**, 1961–2004; (b) C. M. Madsen and M. H. Clausen, *Eur. J. Org. Chem.*, 2011, 3107–3115.
2. E. M. Driggers, S. P. Hale, J. Lee and N. K. Terrett, *nature reviews.*, 2008, **7**, 609.
3. (a) J. D. A. Tyndall and D. P. Fairlie, *Curr. Med. Chem.*, 2001, **8**, 893; (b) E. M. Driggers, S. P. Hale, J. Lee and N. K. Terrett, *Nat. Rev. Drug Discov.*, 2008, **7**, 608.
4. (a) D. Gottschling, J. Boer, A. Schuster, B. Holzmann, H. Kessler, *Angew. Chem., Int. Ed.*, 2002, **41**, 3007–3011; (b) M. Pawlikowski and G. Melen-Mucha, *Curr. Opin. Pharmacol.*, 2004, **4**, 608–613; (c) P. Grieco, M. Cai, L. Liu, A. Mayorov, K. Chandler, D. Trivedi, G. Lin, P. Campiglia, E. Novellino, V. J. Hruby, *J. Med. Chem.*, 2008, **51**, 2701–2707.
5. (a) R. Álvarez, V. Lopez, C. Mateo, M. Medarde and R. Pelaez, *J. Org. Chem.*, 2014, **79**, 6840–6857; (b) M.-Z. Zhang, Q. Chen and G.-F. Yang, *Eur. J. Med. Chem.*, 2015, **89**, 421–441; (c) H. Zhang, L. V. R. Boñaga, H. Ye, C. K. Derian, B. P. Damiano and B. E. Maryanoff, *Bioorg. Med. Chem. Lett.*, 2007, **17**, 2863–2868.
6. R. B. Herbert, *Alkaloids.*, 1982, **12**, 1–34
7. S. Bartlett, G. S. Beddard, R. M. Jackson, V. Kayser, C. Kilner, A. Leach, A. Nelson, P. R. Oledzki, P. Parker, G. D. Reid and S. L. Warriner, *J. Am. Chem. Soc.*, 2005, **127**, 11699–11708.
8. (a) V. S. Shinu, B. Sheeja, E. Purushothaman and D. Bahulayan, *Tetrahedron Lett.*, 2009, **50**, 4838–4842; (b) V. S. Shinu, P. Pramitha and D. Bahulayan, *Tetrahedron Lett.* 2011, **52**, 3110–3115; (c) D. Bahulayan, V. S. Shinu, P. Pramitha, S. Arun and B. Sheeja, *B. Synth. Commun.*, 2012, **42**, 1162–1176.
9. (a) H. C. Kolb, M. G. Finn and K. B. Sharpless, *Angew. Chem. Int. Ed.*, 2001, **40**, 2004.
10. M. R. V. Finlay, D. G. Acton, D. M. Andrews, A. J. Barker, M. Dennis, E. Fisher, M. A. Graham, C. P. Green, D. W. Heaton, G. Karoutchi, S. A. Loddick, R. C. Morgentin, A. Roberts, J. A. Tucker, M. Hazel Weir, *Bioorg. Med. Chem. Lett.*, 2008, **18**, 4442–4446.
11. M. F. D. Mota, P. L. Benfícaa, A. C. Batista, F. S. Martins, J. R. D. Paula, M. C. Valadares, *J. Ethnopharmacol.*, 2012, **139**, 319–329.

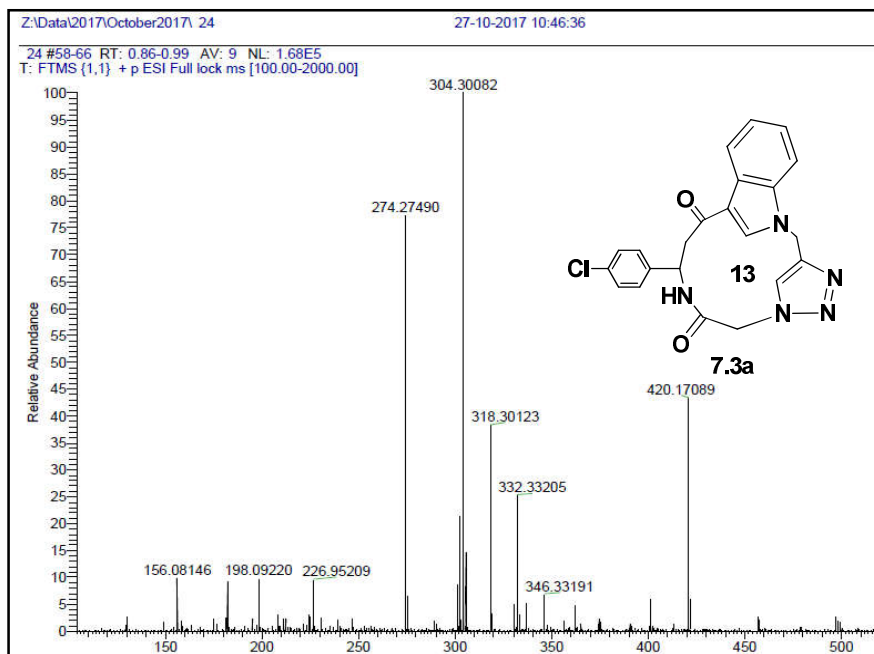
Supplementary Material

Copies of ^1H NMR and Mass spectra of selected compounds.

¹H NMR spectrum of the compound 7.3a



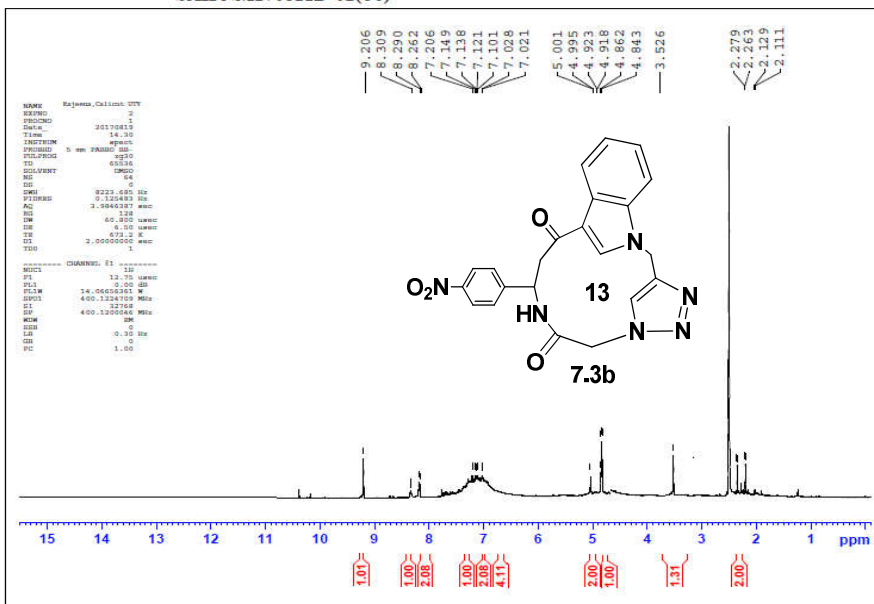
Mass spectrum of the compound 7.3a



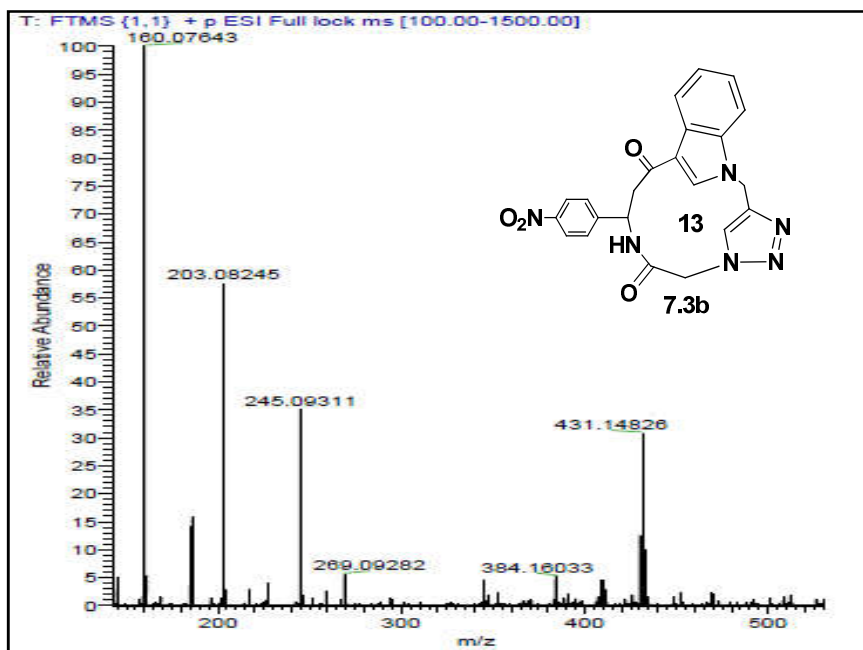
¹H NMR spectrum of the compound 7.3b

SAIFNMI70811D-02(36)

SAIF Cochin



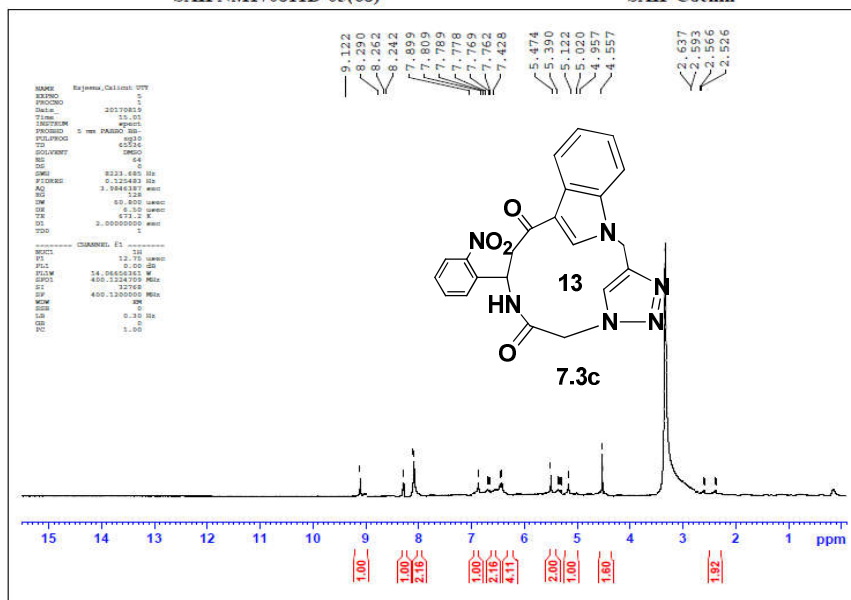
Mass spectrum of the compound 7.3b



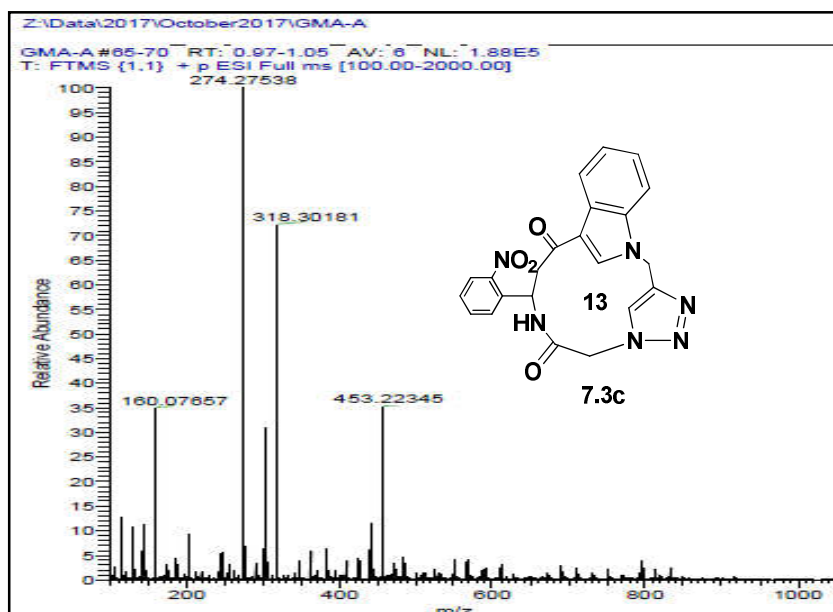
¹H NMR spectrum of the compound 7.3c

SAIFNM170811D-05(68)

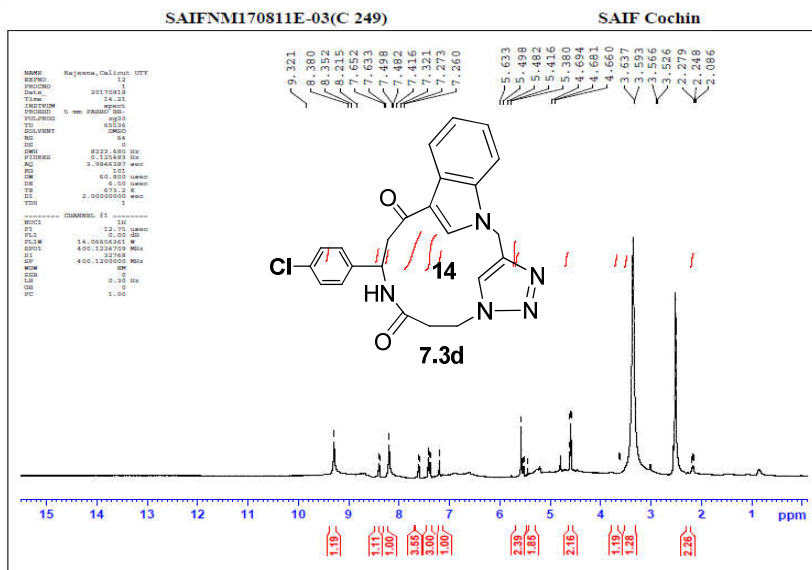
SAIF Cochin



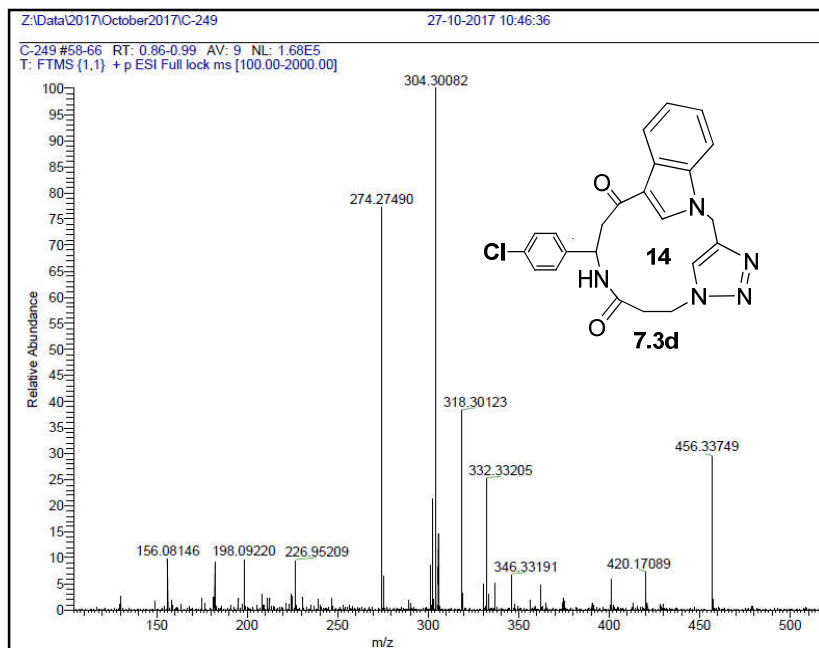
Mass spectrum of the compound 7.3c



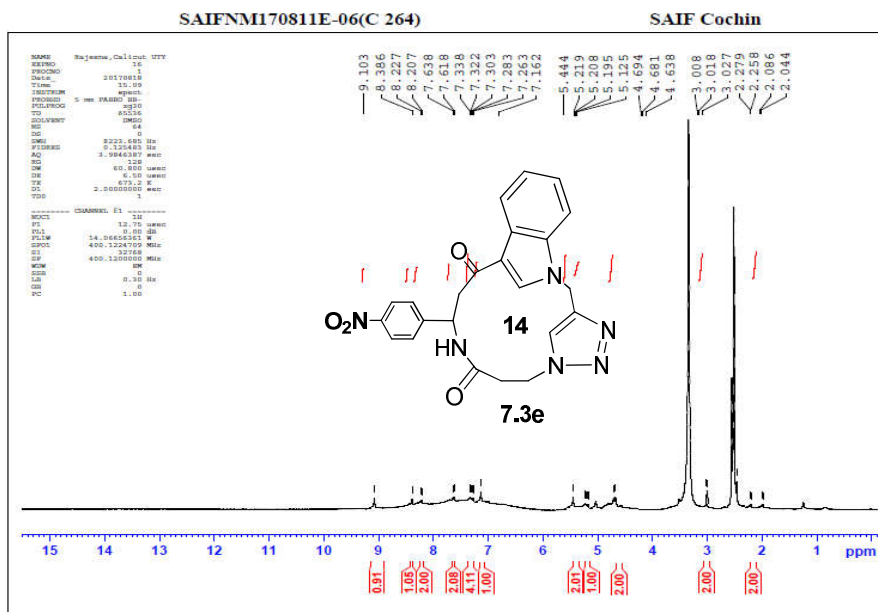
¹H NMR spectrum of the compound 7.3d



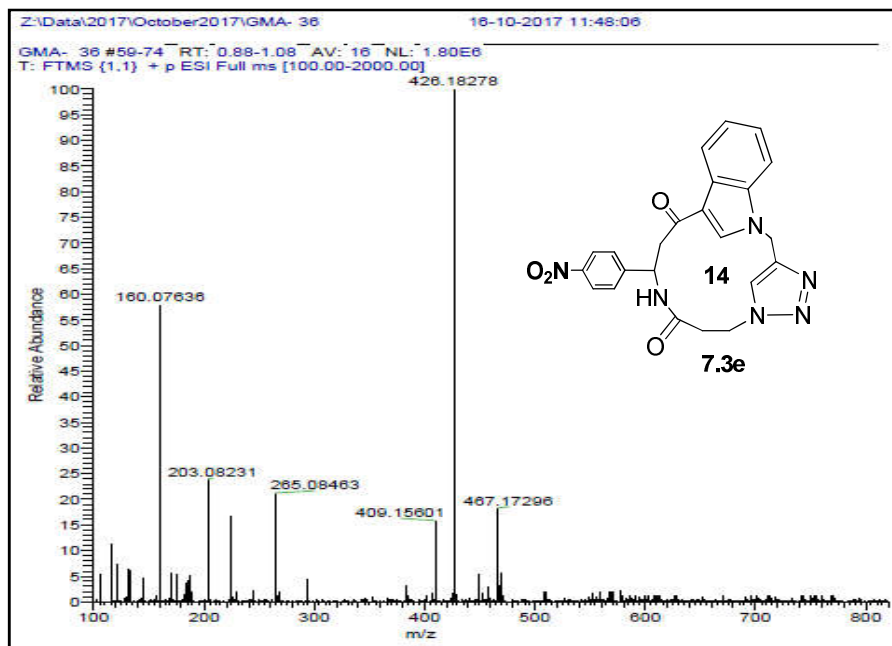
Mass spectrum of the compound 7.3d



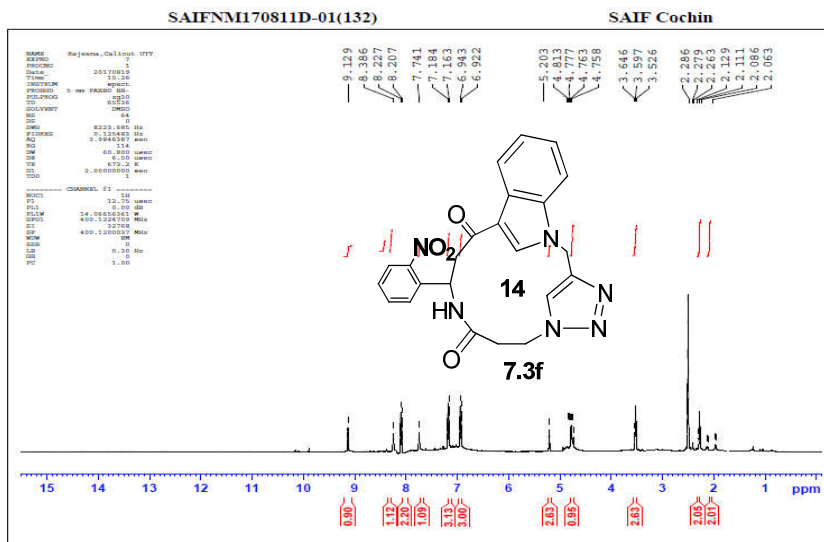
¹H NMR spectrum of the compound 7.3e



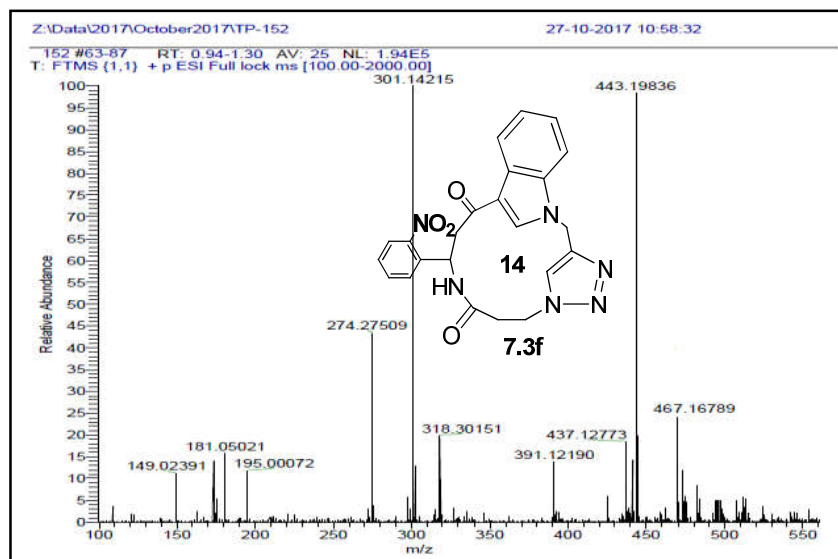
Mass spectrum of the compound 7.3e



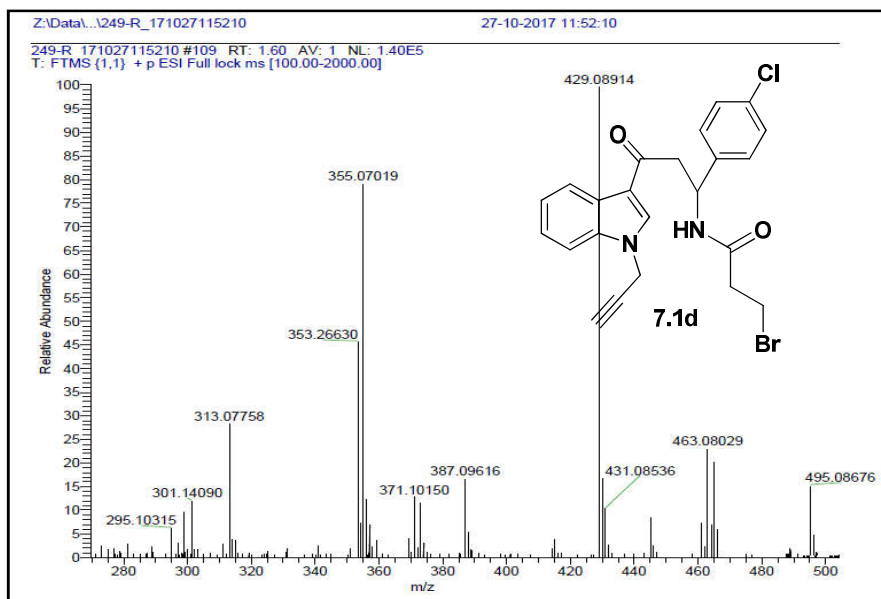
¹H NMR spectrum of the compound 7.3f



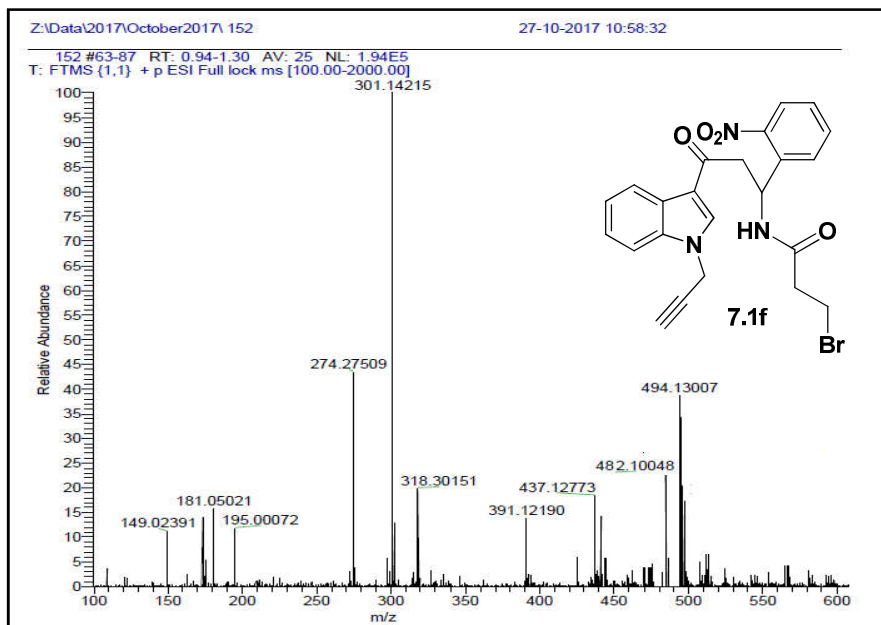
Mass spectrum of the compound 7.3f



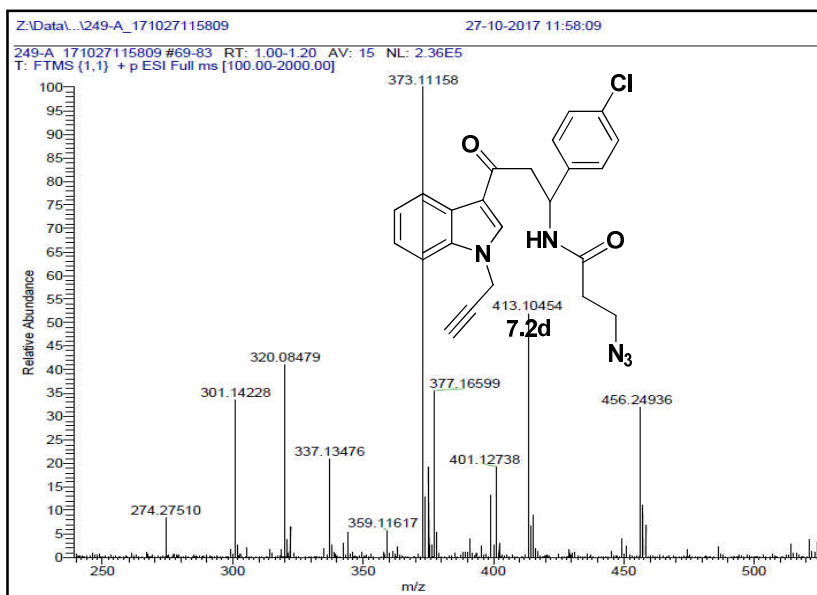
Mass spectrum of the compound 7.1d



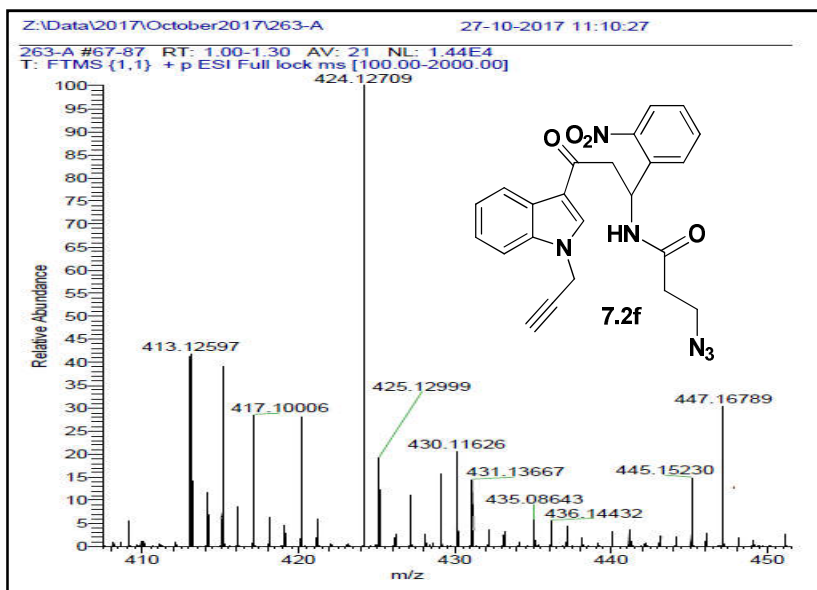
Mass spectrum of the compound 7.1f



Mass spectrum of the compound 7.2d



Mass spectrum of the compound 7.2f



CHAPTER 8

**Photophysical and chemosensing
behavior of Indole peptidomimetics**

Contents

8.1. Introduction.....	275
8.2. Result and Discussion.....	276
8.3. Conclusion	291
8.4. Experimental section.....	291
References	293

8.1. Introduction

Fluorescent labeling of biologically active molecules is widely employed to study their functions within cells and whole organisms.¹ For the intracellular perception and recognition of the potential targets, the fluorescent tagging of a pharmacophore is very important in drug discovery.² One of the methods to achieve this goal is to explore the chemical space around the known fluorophore cores to search for fluorescent drug like molecules with specific recognition properties.³ Likewise, the fluorescent chemosensors can sense biologically important analytes by different signal transduction mechanisms. In this regard, sensing of certain alkaline earth metal ions (such as Ca^{2+} and Mg^{2+} etc) and transition metal ions (such as Cu^{2+} , Fe^{2+} , Fe^{3+} etc) are important because of their involvements in different biological processes.

Magnesium and iron are among the most important elements that affect innumerable processes inside our body. In biochemical reactions that occur in our body, magnesium plays a momentous role, which, in turn, is responsible for various chemical reactions. It plays a crucial role in the production of energy within the cells. Magnesium ion is responsible for the stability and proper functioning of DNA and it is one of the most vital mineral that maintain a healthy electrolytic balance in our body. The deficiency of this ion results in the improper functioning of sodium-potassium pump, besides leading to a number of chronic diseases such as diabetes, osteoporosis, hypertension and coronary heart disease.⁴ Similarly iron is another vital element in the biological system. It is very important to the functioning human body

as it is the main constituent of hemoglobin, cytochrome and other component of respiratory enzyme system. The deficiency of iron leads to anemia, fatigue, frequent infections, and restless legs syndrome.⁵ There is also a lack of easy and ready availability of methods for assessing these ions. Hence it is important to develop efficient sensors of these ions that can detect the very low concentration of ions. Keeping these facts in mind, these studies so far have been extended to the evaluation of the photophysical properties of all the 4 libraries of compounds discussed in chapters from 2 to 7. The study has also conducted the metal ion sensing studies with the indole-triazole-coumarin hybrids.

8.2. Result and discussion

The absorption-emission properties of all the peptidomimetics were evaluated in DMSO (50 ppm) at neutral pH to study the changes in stokes shift with respect to the structural features of the molecules.

8.2.1. Photophysical studies of Indole-triazole carboxamide peptidomimetics.

The absorption maxima, emission maxima and stokes shift values of indole –triazole –carboxamide peptidomimetics measured and are documented in table **8.1**.

Table 8.1. Abs_{max}, Emn_{max} and Stokes shift values of the Indole-triazole-carboxamide peptidomimetics.

Compound	Abs _{max} (nm)	Emn _{mas} (nm)	Stokes shift (nm)	Compound	Abs _{max} (nm)	Emn _{mas} (nm)	Stokes shift (nm)
2.3a	296	364	68	2.4e	309	434	125
2.3b	296	364	68	2.4f	308	404	96
2.3c	295	394	99	2.4g	305	386	81
2.3d	297	376	79	2.4h	308	394	86
2.3e	297	360	63	2.5a	284	386	102
2.3f	294	404	110	2.5b	286	356	70
2.3g	298	375	77	2.5c	286	386	100
2.3h	297	402	105	2.5d	283	335	52
2.4a	304	414	110	2.5e	282	354	72
2.4b	308	402	94	2.5f	281	330	49
2.4c	308	385	77	2.5g	285	334	49
2.4d	309	394	85	2.5h	275	332	57

Similar to tryptophan probes,⁶ the new peptidomimetics **2.3a-2.5h** showed absorption in the wavelength region between 275 to 309 nms and emission in the blue region between 330 and 434 nm. Most of these peptidomimetics showed intense narrow blue emission with high Stokes shift ranging from 46 to 125 nms. Among the 24 peptidomimetics, **2.3h**, **2.4a**, **2.4e** and **2.5h** showed stokes shift values > 100 nm from which **2.4e** showed the maximum stokes shift of 125 nm. However, a generalization based on the structural features is inappropriate at this stage. A normalized absorption-emission spectra of the peptido-mimetics showing high stokes shift is given in figure **8.1**.

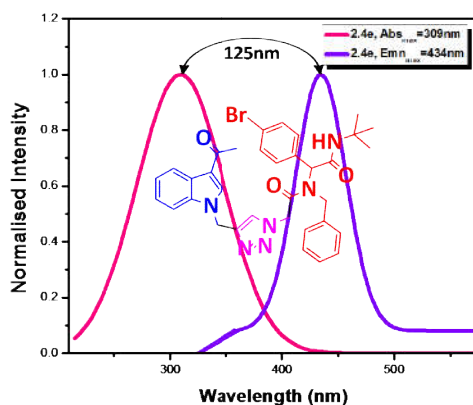


Fig. 8.1. The normalised absorption and emission spectra of indole-triazole peptidomimetics **2.4 e** in DMSO at room temperature.

8.2.2. Photophysical studies of Indole-triazole Coumarin hybrids

To study the photophysical properties, the absorption and emission spectra of all the compounds **4.4a-4.6d** were recorded in DMSO at neutral pH. The absorption maxima, emission maxima and stokes shift values are documented in table **8.2**. The new peptidomimetics **4.4a-4.6d** showed absorption in the wavelength region between 290 to 308nm and emission in the blue region between 472 and 490nm. All the synthesized compounds showed emission in the blue region with large stokes shift values, 178-188nm. The compound **4.6d** exhibits highest emission maxima and **4.6a** exhibits highest stokes shift. These values are higher than those of the Indole-Triazole-Coumarin hybrids discussed in chapter 2. The increase in fluorescence property may be due to the presence of coumarin fluorophore. The normalized absorption and emission spectrum representative compound **4.6a** is shown in figure **8.2**.

Table 8. 2. Abs_{max}, Emn_{max} and Stokes shift value of the Indole-triazole-Coumarin peptidomimetics.

sample code	Absn nm	Emission nm	stoke shift value
4.4a	290	472	182
4.4b	298	476	178
4.4c	299	480	181
4.4d	297	484	187
4.5a	295	474	179
4.5b	290	476	186
4.5c	295	479	184
4.5d	298	482	184
4.6a	290	478	188
4.6b	294	476	182
4.6c	298	481	187
4.6d	308	490	182

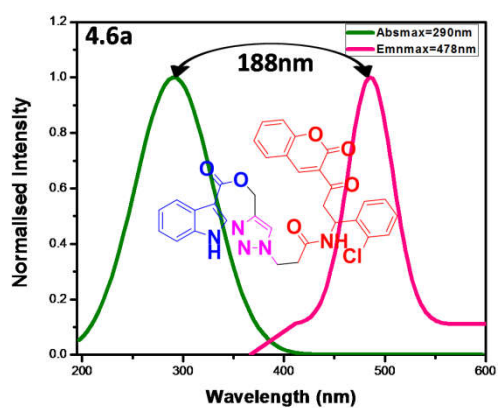


Fig. 8.2. The normalized absorption and emission spectrum of the compound 4.6a

8.2.3. Photophysical studies of Indole-triazole-Pyrimidinone peptidomimetics

Indole-Triazole-Pyrimidinone hybrids **4.5a-4.5f** were also showed absorption in the wavelength region between 304 to 310 nms and emission in the blue region between 445 and 474 nm. All the synthesized compounds showed emission in the blue region with large stoke shift values in the range 141-164 nm. The compound **6.5d** showed the highest emission maxima. These values are higher than those of the Indole-Triazole-peptidomimetics discussed in chapter 2. The increase in fluorescence property may be due to the presence of pyrimidinone fluorophore. The normalized absorption and emission spectrum of **6.5d** is shown in figure **8.3**. The absorption maxima, emission maxima and stokes shift values are documented in table **8.3**.

Table 8.3. Abs_{max}, Emn_{max} and Stokes shift values of the Indole-triazole-Pyrimidine peptidomimetics.

compound	Abs _{max} (nm)	Emn _{mas} (nm)	Stokes shift (nm)
6.5a	304	455	151
6.5b	308	466	158
6.5c	305	462	157
6.5d	310	474	164
6.5e	304	445	141
6.5f	305	458	153

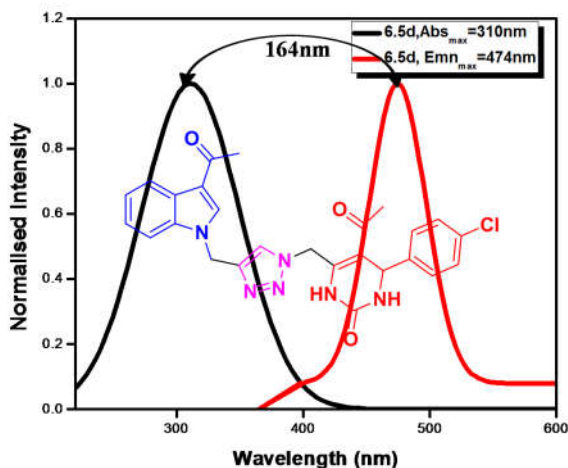


Fig. 8.3. The normalized absorption and emission spectrum of the compound **6.5d**

8.2.4. Photophysical studies of Indole based macrocycles.

The photophysical studies of the indole based macrocycles were evaluated in DMSO at neutral pH. The absorption maxima, emission maxima and stokes shift values of Indol macrocycles **7.3a-7.3f** are documented in table **8.4**. The new indole based macrocycles **7.3a-7.3f** showed absorption in the wavelength region between 270 to 281 nm and emission in the blue region between 480 and 498nm with large stokes shift values, 206-226nm. The compound **7.3a** exhibits the highest emission maxima while the compound **7.3b** shows the highest stokes shift value. A decrease in Stokes shift value was observed with an increase in the ring size of the macrocycles. The indole based macrocycles exhibits higher stokes shift value than the all other peptidomimetics discussed in the previous chapters. The normalized absorption and emission spectrum of Indol based macrocycle **7.3b** is shown in figure **8.4**.

Table 8.4. Abs_{max}, Emn_{max} and Stokes shift values of the Indole based macrocycles.

Compound	Abs _{max} (nm)	Emn _{max} (nm)	Stokes shift (nm)
7.3a	280	498	218
7.3b	270	496	226
7.3c	270	494	224
7.3d	289	495	206
7.3e	281	492	211
7.3f	271	480	209

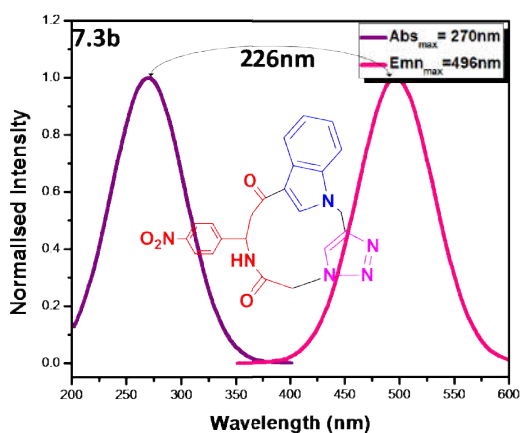


Fig. 8.4. The normalized absorption and emission spectra of the compound **7.3b**

From the photophysical study, we can conclude that all the indole based peptidomimetics shows high stoke shift values. The absorption/ emission properties and the high stokes shift observed for these molecules are strongly supporting the possibility of these molecules for applications such as bioimaging, flow cytometry and targeted cell imaging.

8.2.5. Chemosensor behavior of Indole- Triazole Coumarin peptidomimetics towards Mg^{2+} and Fe^{3+} ions.

Of the synthesised indole based peptidomimetics, indole-triazole-coumarin peptidomimetics were selected for evaluating the chemosensing behavior. We have tested all the indole based peptidomimetics with different ions (cations and anions) to evaluate the chemosensor behavior of the synthesised compounds. It was found that the indole-triazole coumarin peptidomimetics showed a drastic change in the emission colour under UV light in the presence of Mg^{2+} or Fe^{3+} ions. Hence, we decided to conduct further studies using indole-triazole-coumarin peptidomimetics.

8.2.5.1. Cation sensing study

The chemosensor behavior of Indole-triazole-coumarin peptidomimetics were evaluated by mixing it with different metal ions (3 equi.) namely Fe^{3+} , Ba^{2+} , Co^{2+} , Cu^{2+} , Hg^{2+} , Mg^{2+} , Fe^{2+} , K^+ , Pb^{2+} , Na^+ , Ni^{2+} and Cd^{2+} in bulk water. There was a naked eye response under UV lamp to Mg^{2+} and Fe^{3+} while mixing with compound solution, i.e. with Mg^{2+} there was an enhancement of blue colour to bright blue at the same time the Fe^{3+} quenches the blue colour to colourless. To confirm this drastic colour change under UV, the fluorescence emission behavior of representative compound (**4.6d**) upon addition of various metal ions has been investigated in DMSO (Fig.8.5).

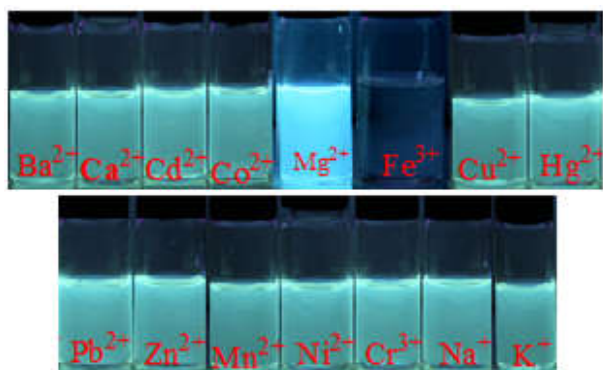


Fig. 8.5. The fluorescence emission responses of the compound **4.6d** with different metal ions under UV irradiation.

4.6d showed a single emission band at 490nm with an excitation of 308 nm. The sequential addition of Mg^{2+} ions from 0 to $50\mu\text{L}$ to the solution of **4.6d** showed a gradual increase in emission intensity. Under a UV lamp, the solution of **4.6d** in the presence of Mg^{2+} showed a dramatic colour change from dull fluorescence blue to bright fluorescent blue. The experiment was repeated by adding Fe^{3+} ions from 0 to $50\mu\text{L}$ to the solution of **4.6d** which showed a colour change from blue to colour less, without any shift in wavelength, which could easily be detected under UV lamp (fig.8.6).

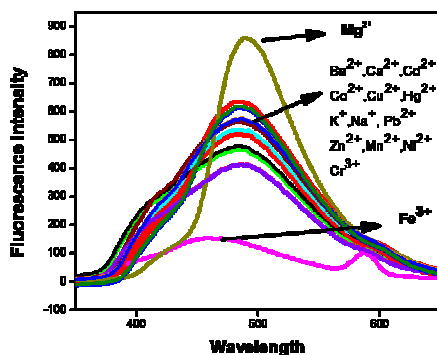


Fig. 8.6. The fluorescence emission spectra of the compound **4.6d** with different metal ions.

To obtain more insight into fluorescence, fluorescence titration curve of **4.6d** towards Mg^{2+} and Fe^{3+} were investigated. With increasing concentration of Mg^{2+} the fluorescence intensity of **4.6d** showed a drastic increase and in the mean time with increasing concentrations of Fe^{3+} , the fluorescence intensity of **4.6d** shows a drastic decrease. The fluorescence intensity of **4.6d** increases with Mg^{2+} like an off-on sensing response and with Fe^{3+} decreased like an on-off sensing response

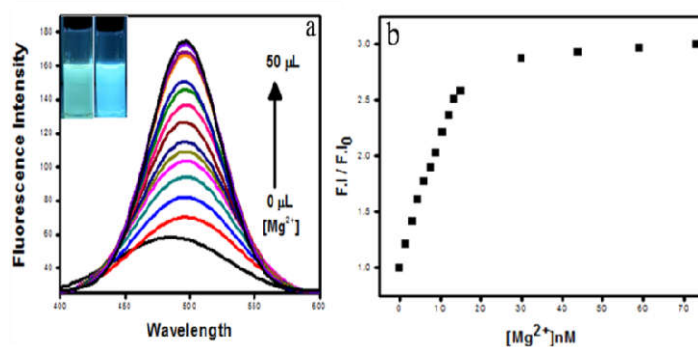


Fig. 8.7. a) Changes in the fluorescence spectra of compound **4.6d** as a function of Mg^{2+} concentration b) Fluorescence ratio changes (I/I_0) of compound **4.6d** upon gradual addition of Mg^{2+} ion.

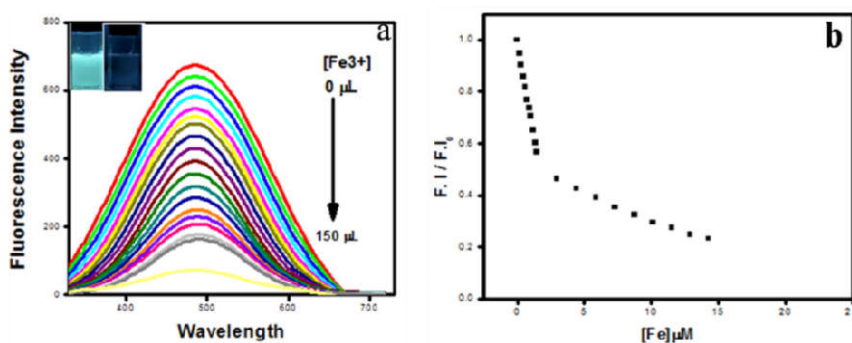


Fig. 8.8. a) Changes in the fluorescence spectra of compound **4.6d** as a function of Fe^{3+} concentration b) Fluorescence ratio changes (I/I_0) of compound **4.6d** upon gradual addition of Fe^{3+} ion.

8.2.5.2. Fluorescence life time study

To further understand the enhancement and quenching mechanism, we have performed fluorescence life time measurements of compound **4.6d** in the presence of different concentrations of Mg^{2+} and Fe^{3+} . The fluorescent decay data are collected at $\lambda_{\text{ex}}=308\text{nm}$ and $\lambda_{\text{em}}=490\text{nm}$ and they are given in table **8.5**. The fluorescence decay curve of **4.6d** and with varying the concentration of Mg^{2+} and Fe^{3+} are shown in figure **8.9**, respectively. It can be seen that the decay time of compound **4.6d** increases with increasing concentration of Mg^{2+} ion, whereas it decreases with increasing concentration of Fe^{3+} ions. In the absence of metal ions, the excited state lifetime of **4.6d** was 3.7ns. While adding Mg^{2+} ions, the excited state life time changes to 4.28 and with Fe^{3+} it changes to 2.7ns(table **8.5**).

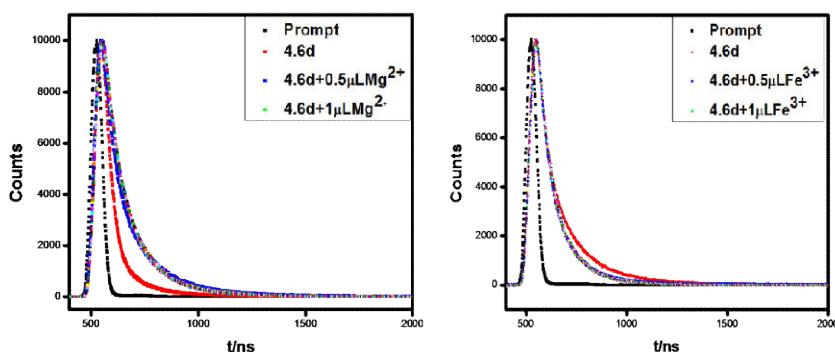


Fig. 8.9: Fluorescence decay curve of compound **4.6d** in DMSO with Mg^{2+} and Fe^{3+} concentration measured by time-correlated single photon counting and fluorescence monitored at corresponding emission maxima ($\lambda_{\text{ex}}=308\text{nm}$ for **4.6d**)

Table 8.5. Variation in life time of compound **46d** with respect to Mg^{2+} and Fe^{3+} .

Compound code	Life time	Compound code	Life time
4.6d	3.7ns	4.6d	3.7ns
4.6d+0.5μL Mg^{2+}	4.09ns	4.6d+0.5μL Fe^{3+}	2.91ns
4.6d+1μL Mg^{2+}	4.28ns	4.6d+1 μL Fe^{3+}	2.76ns

8.2.5.3. Quantum yield calculation.

The fluorescence quantum yield was calculated from the area of total fluorescence emission over the whole spectral range. The variation in quantum yields was studied before and after the gradual addition of metal ions to the sensor solution. For this, 1.0 μ M solution of the sensor **4.6d** and 10 μ M solution of metal ions were prepared. Before the addition of any metal ions, the sensor **4.6d** had a fluorescence quantum yield 0.54 and it changed in the presence of various concentrations of ion solutions. The quantum yields were measured for 2 different concentrations of Mg^{2+} and Fe^{3+} ions and values are listed in table **8.6**. In the case of Mg^{2+} , an increase in quantum yield with the increase in concentration of metal ions were observed whereas, in the case of Fe^{3+} there is a decrease in quantum yield with the increase in concentration of metal ions was observed.

Table 8.6. Variation in Quantum yield with respect to Mg^{2+} and Fe^{3+}

Compound code	Quantum yield	Compound code	Quantum yield
4.6d	0.54	4.6d	0.54
4.6d+10μL Mg^{2+}	0.59	4.6d+10 μL Fe^{3+}	0.50
4.6d+20μL Mg^{2+}	0.61	4.6d+20 μL Fe^{3+}	0.48

8.2.5.4. Job's plot

Furthermore, to explore the binding mechanism or the stoichiometric ratio between the receptor **4.6d** and cation metal ions, the Job's plot (the method of continuous variation) of fluorescence emission titration with Mg^{2+} and Fe^{3+} were used (Fig. **8.10**). The total concentration of receptor **4.6d** and cations Mg^{2+} and Fe^{3+} was kept constant (1.0×10^{-4} M) with continuous variation of mole fraction of **4.6d**. The maximum emission was observed when the molar fraction reached 0.5, which is indicative of a 1:1 stoichiometry complexation for the newly formed species of **6d**- Mg^{2+} and **6d**- Fe^{3+} . The plausible complexation of **4.6d** with Mg^{2+} and Fe^{3+} are given in figure **8.11**.

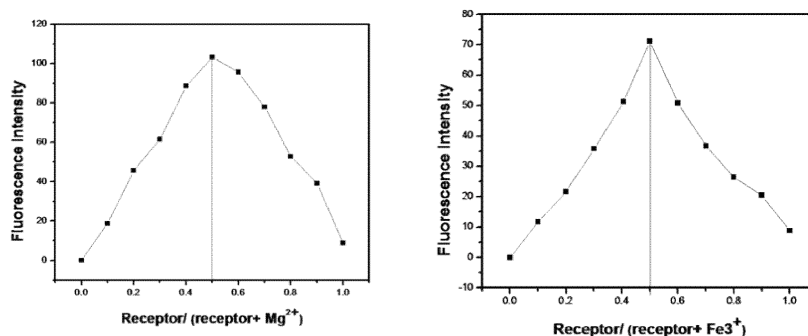


Fig. 8.10. Job's plot for **4.6d**- Mg^{2+} and **4.6d**- Fe^{3+} respectively.

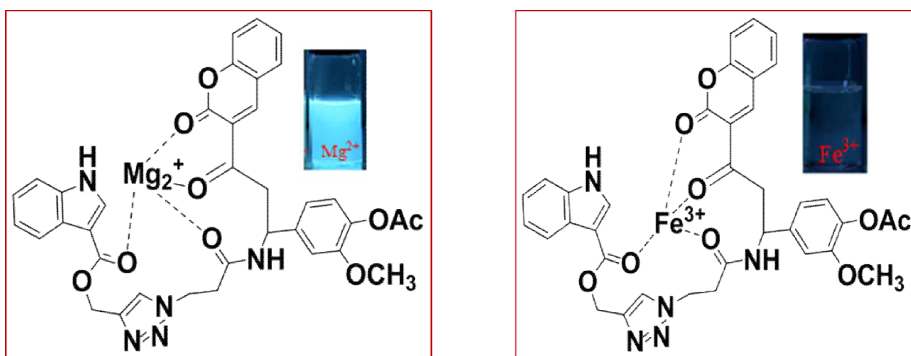


Fig. 8.11. Plausible complexation for Mg^{2+} and Fe^{3+} complex with **4.6d**.

8.2.5.5. The Limit of detection

In order to probe the sensitivity of compound **4.6d** towards Mg^{2+} and Fe^{3+} , we examined the change in the fluorescence intensity of the solution in the presence of different concentrations of Mg^{2+} and Fe^{3+} (0- 15nM for Mg^{2+} and 0-1.5 μM for Fe^{3+}), maintaining all other experimental parameters the same. The variation in the intensity of the emission maximum at 490 nm was carefully investigated to ascertain the sensitivity and detection limit of the compound **4.6d**, with Mg^{2+} and Fe^{3+} . The intensity of fluorescence of indole triazole coumarin derivatives varied linearly with increase in the concentration of Mg^{2+} and decrease with Fe^{3+} ion, enabling the use of the system for quantitative analysis. The lowest detection limit ($3\delta/\text{slope}$, where ‘ δ ’ is the standard deviation) was observed to be 0.069 nM for Mg^{2+} and 0.044 μM for Fe^{3+} (fig.8.12), which is highly significant when compared to similar systems reported previously for trace detection of Mg^{2+} and Fe^{3+} ions.

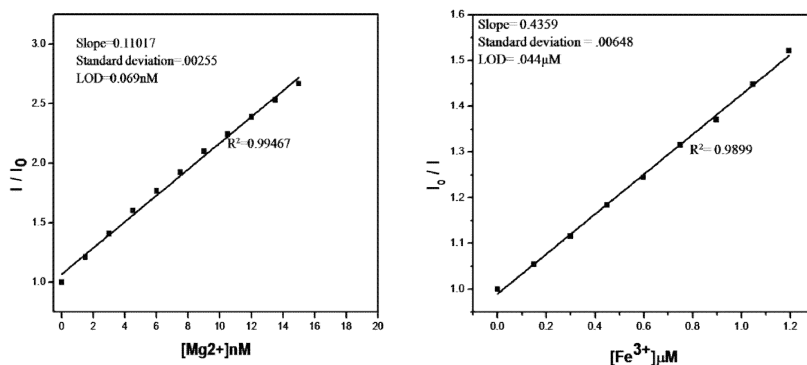


Fig.8.12. Variation in fluorescence intensity of compound **4.6d** with Mg^{2+} and Fe^{3+} ion respectively.

8.2.5.6. Real time analysis

To check the practical applicability of the synthesized compounds as a sensor of Mg^{2+} and Fe^{3+} ions, we carried out the real sample experiments by using distilled water, tap water and simulated waste water. For this, we used 1.0×10^{-6} M solution of **4.6d** with 3 equivalents of Mg^{2+} ion in waste water, tap water and distilled water and the results are shown in figure **8.13**. The experiments were repeated with 100×10^{-6} M solution of **4.6d** with 3 equivalent of Fe^{3+} ions in distilled water, tap water and simulated waste water and the results are shown in figure **8.13**. From this study, it is clear that, the fluorescence enhancement ability of Mg^{2+} and fluorescence quenching ability of Fe^{3+} with the synthesized compounds using distilled water shows good agreement with the same property obtained from tap water and waste water. These results indicate the practical and industrial applicability of the synthesized compounds.

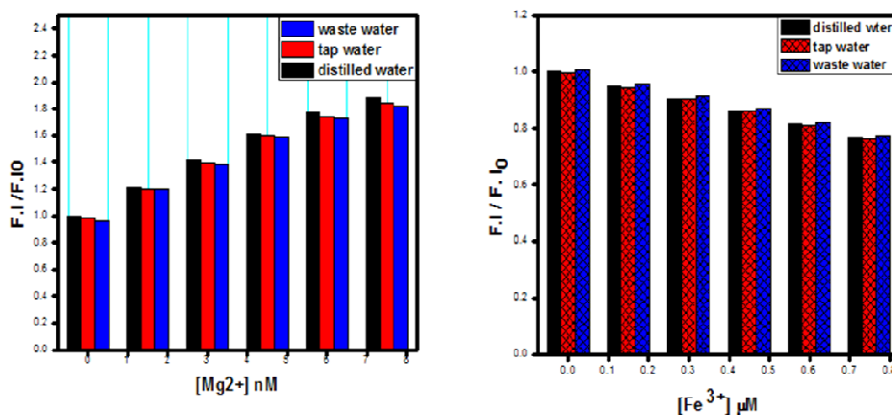


Fig. 8.13. The fluorescence signalling of Mg^{2+} and Fe^{3+} ions by compound **4.6d** in distilled water, waste water and tap water samples, In aqueous DMSO.

8.3. Conclusion

In conclusion, all the synthesized peptidomimetics showed fluorescence behavior with high stokes shift values. The sensing behavior of indole triazole coumarin peptidomimetics exhibits emission signals in the blue wavelength region and is highly sensitive to Mg^{2+} and Fe^{3+} . Since these ions are highly important in biological Process, these sensor molecules can be implemented in many biological fields. The real time analysis confirms the practical and industrial applicability of these sensor molecules.

8.4. Experimental section

8.4.1. Fluorescence quantum yield

Fluorescence quantum yield (ϕ_f) was computed using the below equation.

$$\phi_f = \phi_{fR} F_S A_R \eta_s^2 / F_R A_S \eta_R^2$$

Where F_S and F_R are the integrated fluorescence intensities of the sample and reference, A_S and A_R are the absorbance of the sample and reference at excitation wavelength, η_S and η_R are the refractive indexes of the solvents used for the sample and reference. Anthracene in ethanol solution was used as the reference ($\phi_{fR} = 0.27$) as standard.

8.4.2. Fluorescence lifetime

Fluorescence decay curves were recorded with a Horiba Fluorolog Fluorescence spectrometer with TCSPC and lifetime τ was calculated using the below equation using three exponentials, where T stands for Time and B stands for relative amplitude.

$$\tau = T_1B_1 + T_2B_2 + T_3B_3 \dots / 100$$

Reference

1. L. D. Lavis and R. T. Raines, *ACS Chem. Biol.*, 2008, **3**, 142.
2. O. N. Burchak, L. Mugheri, M. Ostuni, J. J. Lacap and M. Y. Balakirev. *J. Am. Chem. Soc.*, 2011, **133**, 10058–10061.
3. (a) G.R. Rosania, J. W. Lee, L. Ding, H.S. Yoon and Y.T. Chang, *J. Am. Chem. Soc.*, 2003, **125**, 1130. (b) M. Vendrell, J. S. Lee and Y.T. Chang, *Curr. Opin. Chem. Biol.*, 2010, **14**, 383.
4. W. J. Dechent and M. Ketteler, *Clin. Kidney J.*, 2012, **5**, i3–i14.
5. S. Devaraj, Y. Tsui, C. Chiang and Y. Yen, *Acta, Part A.*, 2012, **96**, 594–599.
6. P. Talukder, S. Chen, C. T. Liu, E. A. Baldwin, S. J. Benkovic and S. M. Hechi, *Bioorg Med Chem Lett.*, 2014, **24**, 5924.

CONCLUSION AND FUTURE PERSPECTIVES

The concept of employing privileged scaffolds is a new paradigm in drug discovery as these structures can quickly provide potential chemotypes by modifying the central core structure in many ways including side chain modifications. Such molecular scaffolds can provide potent and selective ligands for a range of diverse biological targets through rational structure optimizations. Among the various scaffolds that have been investigated or reinvestigated, indole ring is represents one of the most prominent one for the discovery of multipurpose drug candidates. Indole subunit is an integral part of a large variety of therapeutic agents including anticancer agents, enzyme inhibitors and bioreceptor modulators. A careful literature survey has revealed that most of the drug candidates that have been developed so far with indole as core unit are being made mainly based on the structure alterations of indole core or through the side chain modifications. However, the concept of developing hybrid scaffolds by the fusion of two or more privileged scaffolds to obtain a drug candidate that can interact with multiple binding sites of an enzyme is still in its infant stage. This thesis presents such a concept of developing hybrid scaffolds of indole by linking it with a secondary scaffold through a 1,2,3-triazole spacer by the skillful use of green synthetic methodologies such as multicomponent coupling reactions (MCRs) and Cu(I) catalyzed [3+2] azide-alkyne cycloaddition (CuAAC). The secondary scaffolds used in this study are carboxamides, coumarins, pyrimidines and macrocyclic acetamides.

The thesis has been divided into nine chapters. The introductory chapter presents a brief perspective mainly on indole

along with coumarin and pyrimidine in the field of medicinal and materials chemistry. A concise discussion on synthetic methodologies such as multicomponent reactions (MCRs) and Cu (I) catalyzed [3+2] azide-alkyne cycloaddition (CuAAC) are also presented in this chapter.

Chapters 2-7 present the systematic structure alterations of indole scaffold starting with a small peptide like carboxamide, followed by coumarin, pyrimidine and a cyclic acetamide (macrocycle) in a sequential way to study the variations in their anticancer activity against human breast cancer cell line MCF-7 and specificity towards CDK 2. A recently reported indoline-2- carboxamide derivative as potential therapeutic for stage 1 human African trypanosomiasis (HAT) has been taken as the reference indole structure to make structure alterations.

In chapter 2, the derivatization of the indole with a carboxamide moiety spaced with a 1,2,3-triazole linker is discussed. Indole alkynes were synthesized and were linked with carboxamideazides (synthesized by following Ugi 4 component reaction) by following CuAAC reaction to obtain the indole-triazole-carboxamides (ITC).

Chapter 3 presents the results and discussion of the CDK 2 binding affinity of the ICT molecules presented in chapter 2. The results obtained from the computational studies are also validated by performing anticancer activity evaluation of these molecules against various malignant cell lines such as Ehrlich Ascites Carcinoma (EAC) cells (Trypan blue exclusion method), human breast cancer cell lines (MCF-7 cell lines, MTT assay) and finally selectivity of these

molecules towards CDK-2 protein by western blot analysis is also presented.

Chapter 4 presents the structure alterations of indole with a coumarinacetamide scaffold spaced with a 1,2,3-triazole. The synthesis was performed mainly through conducting a reaction of the indole alkynes with coumarin acetamideazides (obtained from a two-step process comprising of a key Mannich type reaction) by following CuAAC.

The 5th chapter presents the molecular docking studies with indole-triazole-coumarin hybrids to obtain the binding affinity of these molecules towards CDK-2 proteins followed by experimental validation of the results obtained from molecular docking via screening the molecules against human breast cancer cell lines. The western blot analysis was also performed to validate the selectivity towards CDK 2 protein and the results are also discussed in this chapter.

Chapter 6 presents the structure alterations of indole derivative with a pyrimidine scaffold to obtain the indole-triazole- pyrimidinone hybrids. The indole-triazole-pyrimidinone hybrids were then evaluated for their binding affinity towards CDK 2 and cytotoxicity against MCF-7 cell lines. The representative compounds showed the highest docking score against CDK 2 and the lowest IC₅₀ (15 μ M) against MCF-7 cells. The western blot analysis to confirm the selectivity towards CDK 2 protein is also discussed.

Chapter 7 presents the progress of the work from the linear indole scaffolds to macrocyclic versions and the evaluation of the

binding affinity of these macrocycles against CDK 2 and anti-cancer activity against MCF-7 cells. The macrocycles are obtained from an intramolecular CuAAC reaction and their anti-cancer activity against MCF-7 cells were also discussed.

Chapter 8 presents the photophysical properties of all the four libraries of compounds reported in chapters from 2-7. The Absorption and emission spectra of all the molecules are reported in this chapter along with a brief discussion on the variations in stokes shift of the molecules with respect to the changes in their structures. A detailed description on the sensor applications of indole-triazole-coumarin hybrids are also presented in this chapter. The physicochemical and biological property evaluation data of all the four libraries are presented in tables 1-5. Based on the analysis of tables 1-5, a collection of molecules are selected and listed in table 6 which shows the highest binding affinity against CDK proteins and lowest IC₅₀ against human breast cancer cell line MCF-7.

Table 9.1. Representative compound from Indole-Triazole-Carboxamide peptidomimetic series with their properties

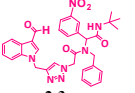
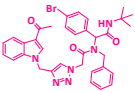
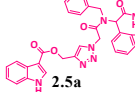
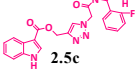
Structures	Properties
 <p>2.3a</p>	Binding affinity=-9.7 Kcal/mol LogP=4.25 n O N=12 nOH NH=1
 <p>2.4e</p>	Binding affinity=-10.1 Kcal/mol LogP=5.24 n O N=9 nOH NH=1
 <p>2.5a</p>	Binding affinity=-11.9 Kcal/mol LogP=4.92 n O N=10 nOH NH=2
 <p>2.5c</p>	Binding affinity=-10.0 Kcal/mol IC50=25µM LogP=4.41 n O N=10 nOH NH=2

Table 9.2. Representative compound from Indole-Triazole- Coumarin peptidomimetic series with their properties.

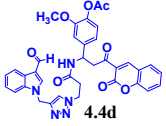
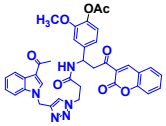
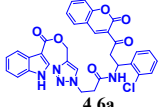
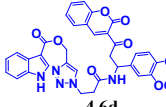
Structures	Properties
 <p>4.4d</p>	Binding affinity=-9.8 Kcal/mol IC50=20µM LogP=2.51 n O N=12 nOH NH=2
 <p>4.5d</p>	Binding affinity=-10.1 Kcal/mol IC50=30µM LogP=2.62 n O N=12 nOH NH=2
 <p>4.6a</p>	Binding affinity=-11.2 Kcal/mol IC50=17.5µM LogP=3.68 n O N=10 nOH NH=2
 <p>4.6d</p>	Binding affinity=-10.0 Kcal/mol IC50=40µM LogP=2.39 n O N=12 nOH NH=3

Table 9.3. Structure of indole-Triazole-Pyrimidinone peptidomimetics with their properties.

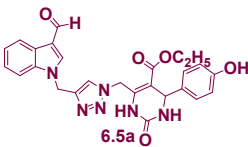
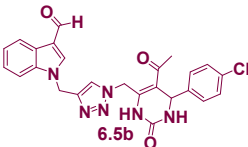
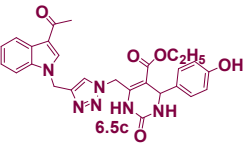
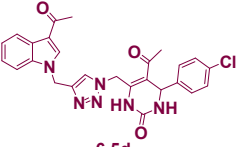
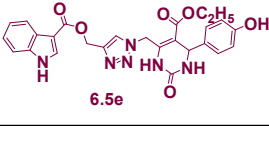
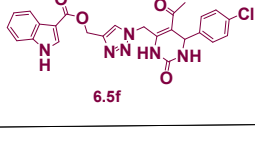
Structures	Properties
 <p>6.5a</p>	Binding affinity=-9.5 Kcal/mol LogP=4.05 n O N=10 nOH NH=2
 <p>6.5b</p>	Binding affinity=-10.1 Kcal/mol LogP=2.90 n O N=11 nOH NH=3
 <p>6.5c</p>	Binding affinity=-9.8 Kcal/mol LogP=4.16 n O N=10 nOH NH=2
 <p>6.5d</p>	Binding affinity=-10.5 Kcal/mol IC50=15μM LogP=3.01 n O N=11 nOH NH=3
 <p>6.5e</p>	Binding affinity=-10.2 Kcal/mol LogP=4.03 n O N=11 nOH NH=3
 <p>6.5f</p>	Binding affinity=-9.8 Kcal/mol LogP=2.87 n O N=12 nOH NH=4

Table 9.4. The Structure of Indole-macrocyclic peptidomimetics with their properties.

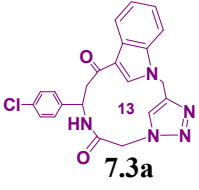
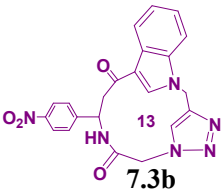
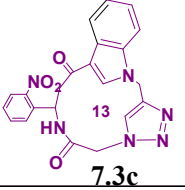
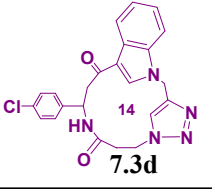
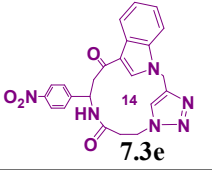
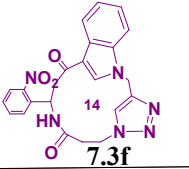
Structures	Properties
 <p>7.3a</p>	Binding affinity=-9.5 Kcal/mol LogP=1.85 n O N=7 nOH NH=1
 <p>7.3b</p>	Binding affinity=-9.7 Kcal/mol LogP=1.13 n O N=10 nOH NH=1
 <p>7.3c</p>	Binding affinity=-10.1 Kcal/mol IC50=12μM LogP=1.11 n O N=10 nOH NH=1
 <p>7.3d</p>	Binding affinity=-9.0 Kcal/mol LogP=2.12 n O N=7 nOH NH=1
 <p>7.3e</p>	Binding affinity=-9.1 Kcal/mol LogP=1.40 n O N=10 nOH NH=1
 <p>7.3f</p>	Binding affinity=-9.2 Kcal/mol LogP=1.38 n O N=10 nOH NH=1

Table 9.5. Structure of Indole-peptidomimetics with the highest stoke shift values.

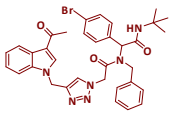
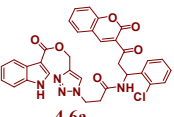
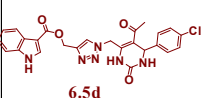
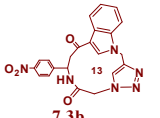
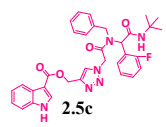
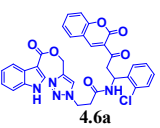
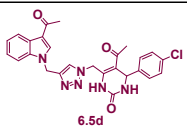
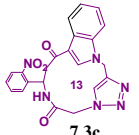
Structures	Properties
 <p>2.4e</p>	<p>Abs max=309nm Emn max=434nm Stoke shift value= 125nm</p>
 <p>4.6a</p>	<p>Abs max=290nm Emn max=478nm Stoke shift value=188nm</p>
 <p>6.5d</p>	<p>Abs max=310nm Emn max=474nm Stoke shift value=164nm</p>
 <p>7.3b</p>	<p>Abs max=270nm Emn max=496nm Stoke shift value=226nm</p>

Table 9.6. Compounds with highest binding affinity and the lowest IC50 value.

Structures	Properties
 <p>2.5c</p>	<p>Binding affinity=-10.0Kcal/mol IC50=10μM</p>
 <p>4.6a</p>	<p>Binding affinity=-11.2Kcal/mol IC50=17.5μM</p>
 <p>6.5d</p>	<p>Binding affinity=-10.5Kcal/mol IC50=15μM</p>
 <p>7.3c</p>	<p>Binding affinity=-10.1Kcal/mol IC50=12μM</p>

Overall, the thesis presents the step economic and cost effective synthesis of 4 different classes of indole-triazole-carboxamide/coumarin/pyrimidine/macrocyclic hybrids and their early stage anticancer property evaluation based on computational and *in vitro* screening methods. The results presented are promising for undertaking further in-depth studies based on both computational techniques and screening methods to identify suitable scaffolds to move on to the next stage of lead discovery based on these molecules. Since some of the molecules showed excellent sensor properties, further in-depth studies that can relate this with anti-cancer property of the same molecules is also a possible future goal.

RESEARCH PAPER PUBLISHED

P. Rajeena and D. Bahulayan, Synthesis of large Stokes shift and narrow emission indole–triazole–carboxamidepeptidomimetics via MCR-click strategy, *Tetrahedron Letters*, 2016, **57**, 2360–2366.

Paper under evaluation:

P. Rajeena, D. Bahulayan, MCR-Click Synthesis, Molecular docking and Cytotoxicity evaluation of a new series of Indole-Triazole-Coumarin hybrid Peptidomimetics, *New journal of chemistry*, ACS.